
# Gold Nanoparticles: Synthesis, Surface Modification and Functionalization for Biomedical Applications

**Dissertation**

zur Erlangung des Doktorgrades
der Naturwissenschaften
(Dr. rer. nat.)

Dem
Fachbereich Physik
der Philipps-Universität Marburg

vorgelegt von

**Mahmoud Soliman**

**aus**

North Sinai, Ägypten

**Marburg, 2016**

Vom Fachbereich Physik der Philipps-Universität (Hochschulkennziffer 1180) als Dissertation angenommen am:

Erstgutachter: Prof. Dr. Wolfgang J. Parak
Zweitgutachter: Prof. Dr. Wolfram Heimbrodt
Prüfer: Prof. Dr. Norbert Hampp

Tag der mündlichen Prüfung:

Die vorliegende Arbeit wurde am Fachbereich Physik
der Philipps-Universität Marburg unter der Anleitung von

**Herrn Prof. Dr. Wolfgang J. Parak**

in der Zeit von April 2012 bis July 2016 angefertigt.

# Zusammenfassung

Die Oberfläche von Nanopartikeln (NP) spielt eine wichtige Rolle bei der Interaktion der Partikel mit ihrer Umgebung, definiert insbesondere ihr Schicksal in biologischen Medien und kann genutzt werden, um eine große Anzahl an funktionalen Gruppen aufzunehmen, die verschiedenste Anwendungsmöglichkeiten bieten.

Das Hauptthema dieser Thesis ist die Synthese, die Oberflächenmodifikation sowie die Charakterisierung von Gold NP (GNP). Die Nanopartikel wurden in den gängigsten Größen (bis hin zu 100 nm Durchmesser) und Formen (sphärisch und stabförmig) synthetisiert. Die verwendeten NP wurden ursprünglich in wässriger Lösung vorbereitet, stabilisiert mittels Zitrat-Ionen im Falle der sphärischen GNP (SGNP) und mittels Cetyltrimethylammoniumbromid (CTAB) während der Synthese der stabförmigen GNP (GNR). Diese Ligandenmoleküle sind jedoch nur schwach an die Oberfläche gebunden und daher ungeeignet für biomedizinische Anwendungen der Partikel. Die Stabilisation der GNP war das Hauptziel dieser Arbeit welches durch den Austausch der vorhandenen Liganden durch andere Moleküle mit höherer Affinität zum Kern der GNP und der Anwendung eines das Partikel umgebenden, amphiphilen Polymers (poly(isobutylene-alt-maleic anhydride) dodecylamine grafted, (PMA)) erreicht wurde. Die Technik der Polymer-Beschichtung wird bereits seit Jahren erfolgreich für die Beschichtung verschiedenster NP-Systeme verwendet, welche ursprünglich in organischen Lösungsmitteln synthetisiert werden müssen und auch nur dort stabil sind. Die NP, die mittels dieser Herstellungsvariante erhalten wurden, sind höchst stabil, auch in physiologischen Medien. Um dieser Methode auch für wasserlösliche Systeme nutzen zu können, wurde ein neuartiger Ansatz mittels eines so genannten Wechsels eingeführt, welcher einen Phasentransfer vor dem eigentlichen Beschichten einführt. Zuerst wurden die NP mit Hilfe von $\alpha$-metoxi-$\omega$-thiol-poly-(ethyleneglycol)- (PEG) Ketten (mPEG-SH ($M_w$= 750 Da)) stabilisiert, um dann mittels Dodecylamin (DDA) von wässriger Lösung in Chloroform überführt werden zu können. Diese solcher Art DDA-beschichteten NP wurden anschließend mit einem amphiphilen Polymer vermischt und beschichtet, ermöglicht durch die hydrophobe Interaktion der Liganden (Kohlenstoff Ketten) an der Oberfläche der NP sowie den hydrophoben Seitenketten des Polymers. Die resultierenden Polymer-beschichteten-NP wurden anschließend aufgereinigt mittels Gel-Elektrophorese, charakterisiert über UV-Vis Spektroskopie sowie Dynamische Licht Streuung (DLS), Laser Doppler Anemometrie (LDA) und Transmissions Elektronen Mikroskopie (TEM).

Ferner wurde die Oberfläche der NP mit PEG verschiedenster Größen modifiziert um die Bildung einer so genannten Protein-Korona zu verhindern sowie die kolloidale Stabilität zu erhöhen. Diese Stabilität wurde daraufhin in unterschiedlichen biologischen Medien mittels UV_VisSpektroskopie und DLS getestet. Außerdem wurde die Toxizität der hergestellten NP sowohl in Krebszelllinien als auch in standard-Zelllinien überprüft und als nicht toxisch eingestuft unterhalb einer Konzentration von 1 mg/mL.

Außerdemwurde der Einfluss von GrÖße, Geometrie sowie Oberflächenbeschaffenheit von Nanopartikeln auf deren Interaktion mit Proteinen und Blutzellen untersucht.

# Abstract

The nanoparticles (NPs) surface plays an important role in the interaction of the NPs with surrounding environments, defines their fate in the biological media and it can be engineered to provide a large number of functional groups for different applications.

The main topic of this thesis is the synthesis, the surface modification and the characterization of gold NPs (GNPs). The NPs were prepared with different sizes (up to 100 nm) and shapes (spherical and rods). The employed NPs were prepared originally in aqueous medium, stabilized by citric ions in case of spherical GNPs (SGNPs) and by hexadecyltrimethylammonium bromide (CTAB) in case of gold nanorods (GNRs). These ligand molecules are weakly bound to the NPs surface and thus, they are unsuitable for biomedical applications. Stabilizing of these NPs was the target of this work and then, it was achieved by exchange these ligands by other molecules with higher affinity and finally wrapping the NPs with an amphiphilic polymer (poly(isobutylene-*alt*-maleic anhydride) dodecylamine grafted, (PMA)). The polymer coating technique has been used over the past years for coating of NPs, which are synthesized originally, and only dispersible in organic media. The NPs obtained using this methodology are highly stable in physiological media. Aiming to use this technique in water-soluble NPs, a new round-trip process was developed using a phase transfer step before the polymer coating. The NPs were stabilized with $\alpha$-metoxi-$\omega$-thiol-poly-(ethyleneglycol)- (PEG) chains (mPEG-SH ($M_w$= 750 Da)) and then transferred from water to chloroform using dodecylamine (DDA). The DDA-capped NPs were coated with a modified amphiphilic polymer due to the hydrophobic interaction between the hydrophobic ligands (carbon chains) on the surface of the NPs and the hydrophobic side chains of the used polymer. The resulted polymer coated NPs were cleaned and characterized using different techniques, such as agarose gel electrophoresis, UV-Vis spectroscopy, dynamic light scattering (DLS), laser Doppler anemometry (LDA) and transmission electron microscopy (TEM).

Furthermore, the surface of the polymer-coated NPs was modified using different molecular weight of PEG to provide them with higher colloidal stability and prevent the formation of the so-called protein corona. The colloidal stability of all particles was assayed against different biological media *via* UV-Vis spectroscopy and DLS. The toxicity of these NPs was tested in cancer and non-cancer cells lines showing no-toxicity up to 1 mg/mL concentration levels.

Additionally, the effect of NPs size, shape, and surface coating on their interaction with plasma proteins and blood cells was studied.

## Acknowledgement

First and foremost, I would like to express my sincere gratitude and appreciation to Prof. Wolfgang J. Parak for giving me the opportunity to work and study in his group and supervising me during my PhD thesis. To prof. Parak, thanks so much for his support and encouragement during my PhD work. It was my pleasure to work and study at Philipps-Universität Marburg in the Biophotonics Group under supervision of Prof. Wolfgang J. Parak.

I would like to thank my good friends and co-supervisors Dr. Beatriz Pelaz and Dr. Pablo del Pino for their support, constructive discussions, continuous motivation and advices. I really appreciate their help.

I would like to thank all my current and old lab fellows for providing a stimulating and fun environment, to learn and grow.

Furthermore, I would like to thank Frau Stefanie Kramer for administrative work and many thanks go to Andreas Rentzos who helped for computer problems and other technical stuff.

I would like to thank Youssef Jameel Institute and FAZIT-Stiftung for financial support of PhD and staying in Germany.

Many thanks go to all my friends in Marburg, outside the University campus, especially, Mohammed Alasel and Ahmed Shokry (Mared Washweshny). The moments we spent together will not be forgotten.

I would like to thank my brothers and sisters, very specially my brothers Mohamed and Fady for their supporting and helping me. Also, I would like to thank my parents for their prayers and support during all these years.

Finally, I am deeply grateful to my beloved wife "Samar" for her great patient, support, encouragement and dedication, for being the person who shared with me all the moments, and for being a wonderful mother for our lovely daughters, Hana and Haidy.

# Table of Contents

# 1. Introduction

Nanotechnology is one of the most important fields of science, which includes physics, chemistry, engineering, biology, and medicine[1,2,3,4,5]. There are different perspectives between the researchers from different area of science about the definition of the nanotechnology but the most common definition as provided by the U.S. National Nanotechnology Initiative (NNI) is the formation and control of the matter on nanometer scale, which is commonly in the range of 1-100 nm[6,7]. However, in some cases, the nanomaterials have dimensions of hundreds of nanometers as in case of nanowires[8].

The manipulation of the materials at nanometer scale will face new different properties[9,10] compared with those for the same materials when they are in the bulk form. For instance, the silver is nontoxic in bulk form but the silver NPs (AgNPs) is very toxic and can be used as antimicrobial agents[11,12]. Many properties like color, weight, and strength changed and also in some cases the same metal becomes semiconductor or insulator when the nanometer scale is reached[10].

Nanomaterials can be fabricated in two ways by using the process which is called "bottom-up" (was first discussed in 1959 by Richard Feynman)[13]. The first one: by self-assembly in which the nanomaterials can be fabricated "atom by atom" ("bottom-up" approach). This concept of self-assembly can be observed in natural biological process where the molecules are assembled together to form a complex system as in case of formation of DNA double helix. By following this approach, the scientist can create nanomaterials with specific properties, controlled size and shape and designed to correspond specific function. The other way to produce nanomaterials is called "top-down" approach, which essentially depends on breaking down the system into its compositional sub-units (finer components)[14]. The work presented in this thesis falls within the approach of "bottom-up" and therefore aims to control the matter from the atomic to the nanometer scale.

NPs, have a huge number of applications in diagnosis, imaging, drug delivery and therapy (*i.e.* photothermal therapy (PTT)), due to the special physical and chemical properties of NPs in comparison with their bulk material counterpart. These applications and properties depend on the size and shape of the NPs. GNPs is the most common example of such NPs. For instance, SGNPs are not the best choice for PTT because they absorb light in the range 515-580 nm depending on the size; and the light in this range can be also absorbed by the body

constituents (water, hemoglobin, fat, *etc*.). On the other hand, the anisotropic NPs such as GNRs are more effective in the PTT because they can absorb the light in the range of 650-1100 nm and the body constituents have transmission window in this range[15,16].

Colloidal metallic NPs have a long history dated back to millennia. Colloidal gold was used in Chinese medicine for more than 5000 years as purported curative for a wide variety of diseases and also, it was used by Egyptian Pharaohs for health and beauty[17]. GNPs and AgNPs are known, or at least used since ancient in the Roman times for coloring the glass. They added the gold salt during glass preparation which was reduced to colloidal gold during annealing of the glass producing a transparent strong red-colored glass. This color was due to the nucleation and growth of small GNPs which have size in range of 4-60 nm[17, 18]. One of the common examples of colloidal metallic NPs is the famous Lycurgus Cup which is presented in British Museum as shown in Figure 1a. The presence of the GNPs and AgNPs in a glass matrix of this Cup is responsible for its color where the color of the glass is changed depending on the position of the light source. If litted from outside, it appears green and if litted form inside, it appears red. Another example is using the colloidal GNPs for staining the glass widows in old European cathedrals as shown in Figure 1b, due to the pretty red color of the GNPs[10,19]. The red color of the glass is due to the absorption of the light around 515 nm where small SGNPs usually appear red but with increasing the size and changing the shape, the color is changed. This phenomenon is due to optical properties of the noble metals (*e.g*. GNPs), which originate from the ability of the free conduction electrons to oscillate at the NPs surface, that called localized surface plasmon resonance (SPR), when they are excited by light of a certain wavelength.

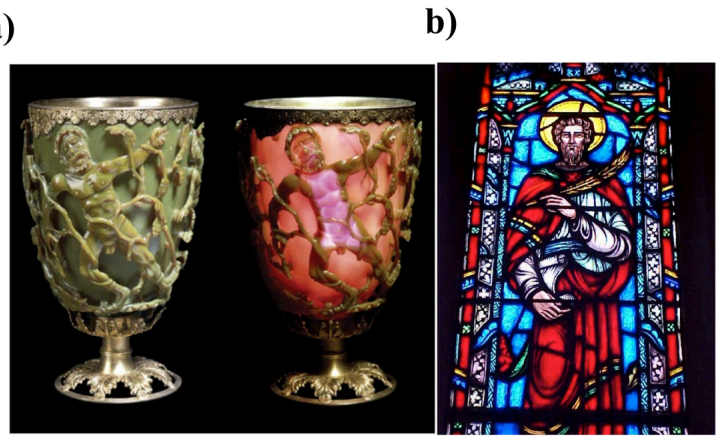


**Figure 1**. a) Lycurgus cup is presented in the British Museum and its color is due to the presence of GNPs inside the glass[17, 18]. b) Stained glass by GNPs used in medieval in churches [10,19].

## 1.1. Surface Plasmon Resonance (SPR) in NPs.

SPR was first described by Otto in 1968[20] and introduced commercially to bimolecular applications by Biacorin in 1990[21]. SPR is a unique characteristic optical phenomenon of metallic NPs. The incident photons can induce surface plasmon oscillations of the free conduction electrons of the NPs surface when they have the appropriate energy. The resonant energy will depend on the particle size, shape, material and environment[16]. The oscillation of these electrons induces an electric field inside the nanoparticle (NP) that can be much larger than and opposite to the incident light[22].

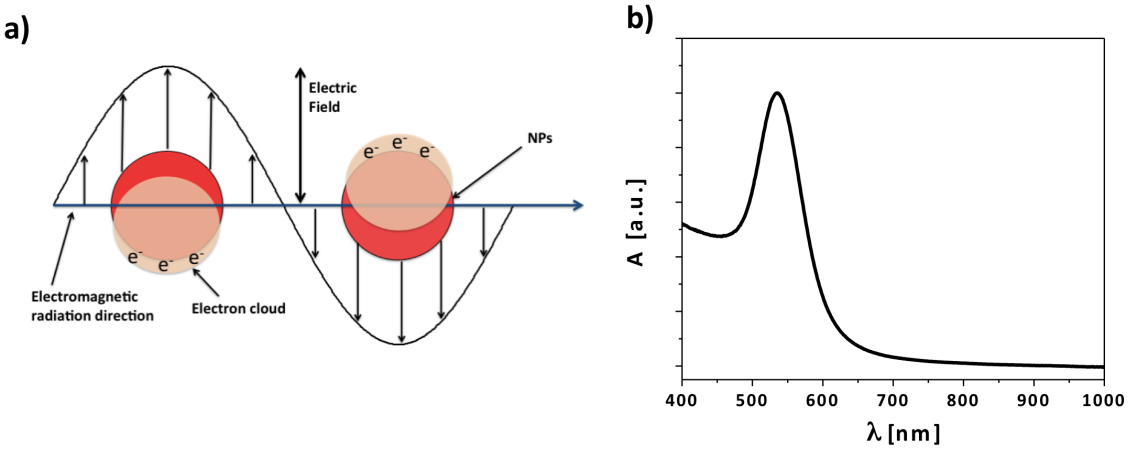


**Figure 2**. a) Scheme illustrating the interaction of polarized light with a metallic NP to form SPR. The electric field of the incident light induces collective oscillation of the conduction electrons moving them towards the NP surface with respect to the positively charged metallic core. b) Absorption spectrum for SGNPs, which have one SPR band in the visible region and its maximum absorption wavelength is around 520 nm depending on the size of NPs.

For the better understanding, let's imagine metallic NP is irradiated by light as shown in Figure 2a. The electromagnetic waves of the incident light (in resonance with the SPR) induce a collective coherent oscillation of the free conduction electrons moving them towards the NP surface. This oscillation will cause charge separation between the free electrons and the ionic metal core forming an electric dipole inside the NP[22,23]. This dipole will produce an electric field within the NP, which works to return the electrons to the equilibrium position once the electric filed of light is removed. These free conduction electrons oscillate alongside the NP surface with a specific frequency called SPR, since it is located at the surface. The SPR induce strong absorption of light, which is responsible for the observed color of metallic NPs[24,25,26]. The SPR band is much stronger, especially, for noble metallic NPs (Au and Ag)

than other metals and it is measuring for absorption of light by metallic NPs, as done by UV-Vis spectroscopy. The SPR band parameters (intensity and wavelength) depend on some factors such as metal type, capping material, particle size, shape and dielectric constant of surrounding medium, which affect on the electron charge density on the particle surface[25,27,28].

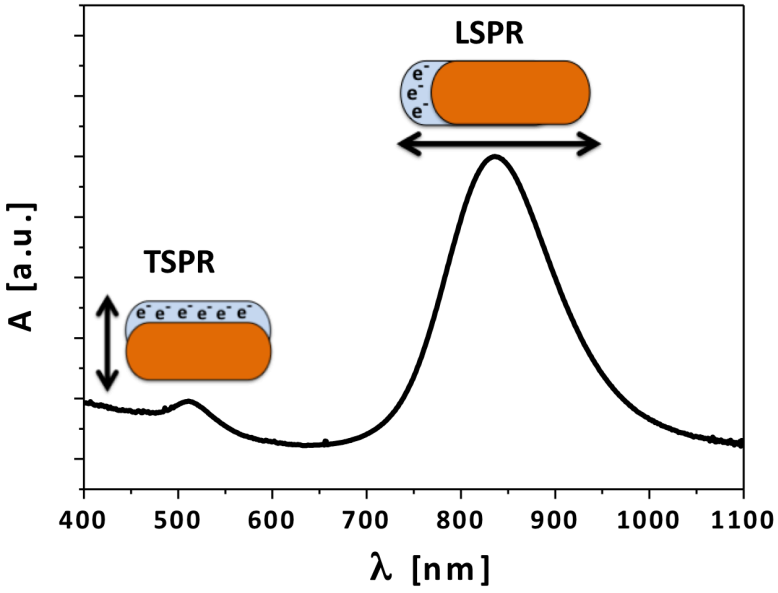


**Figure 3.** UV spectrum for GNRs showing two SPR bands; one of them is located in the visible region corresponding to electron oscillations along the short axis (transversal) and the second located is in the infrared region corresponding to electron oscillations along the long axis (longitudinal).

In case of SGNPs, the free conduction electrons can oscillate in just one symmetric mode showing strong SPR band in visible region around 520 nm (Figure 2b). The position of SPR band shifted to high wavelength and also the color of the colloidal solution changed from intense red to purple or blue with increasing the size of the NPs[29]. Usually, the SPR wavelength is located in visible region for SGNPs (and also for AgNPs) but when the shape of the nanospheres changed to nanorods, which have an anisotropic structure, two SPR bands will be resulted as shown in Figure 3[30]. First: Longitudinal SPR which is a strong band corresponding to the oscillation of the conduction electrons along the long axis and located in the near infarred region (NIR). Second: Transversal SPR which is a weaker band, corresponding to the oscillation of the conduction electrons along the short axis and located in the visible region similar to that of the SGNPs band but it is not sensitive to size of

spherical or rods. Increasing the aspect ratio (length/width) of rods will shift the position of the NIR band to a higher wavelengths and also the color of the solution will be changed from blue to red[10,23,25]. On the other hand, the transversal SPR does not depend on the aspect ratio. The aspect ratio of the rods can be controlled by optimizing the experimental parameters in the growth solution such as pH, seed solution volume or concentration, surfactant, silver ions and the strength of the reducing agent; typically weak redactants are producing anisotropic NPs (*i.e.* ascorbic acid (AA))[26,31,32].

Due to manipulating the light at nanometer scale, SPR technology can be used in different fields, including biomedical, energy, and sensing. Nowadays, the application of SPR increases quickly with the development of new nanomaterials fabrication techniques and manipulation.

## 1.2. Novel methods for preparation of NPs.

In general, several methods have been developed and reported in the literature for the synthesis of metallic NPs such as sol-gel method, chemical reduction of metallic salts, thermal decomposition of metallic compounds, *etc.*[33,34]. The metallic NPs are often prepared by either decomposition or reduction of the metal precursor to produce Zero-valent metal atoms [33], which are the main component of the metallic NPs. Preparation of colloidal metallic NPs in aqueous and/or organic solvent, which termed "wet chemical method", depends on the chemical reduction of metal salts in the presence of appropriate stabilizing agents to prevent the aggregation of NPs and improves their chemical stability[35,36]. In many cases, these stabilizing agents work as stabilizers and shape directing agents such as CTAB in synthesis of GNRs[37,38].

Significant efforts have been exerted during the last decade to fabricate monodisperse GNPs with controlled size and shape using chemical reduction method. In this part of the thesis I am going to talk only about the reduction method for preparation of the SGNPs and GNRs.

### 1.2.1. SGNPs.

Generally, SGNPs can be prepared in aqueous and organic media according to the following methods:

- ***Turkevich method***

In 1857, for first time, Michael Faraday prepared a ruby fluid of colloidal GNPs by reducing in aqueous solution chloroauric acid with phosphors in presence of carbon disulphide[39] as shown in Figure 4. In the period of 1906-1917, many attempts have performed by Richard Zsigmondy for preparing of GNPs and finally, obtained gold hydrosols by reducing chloroauric acid with formaldehyde in a weakly alkaline solution[40]. In 1951, Turkevich modified the Zsigmondy method by using the sodium citrate as reducing agent instead of formaldehyde[41]. The sodium citrate was used not only as reducing agent but also as a capping agent to keep the NPs separated by electrostatic repulsion. In 1973, G. Frens refined this work, by studying the effect of concentration ratio of sodium citrate to gold salt on the resulting particle diameter[42].

**Figure 4.** Colloidal gold NPs by Michael Faraday, which are reproduced by courtesy of the Royal Institution of Great Britain[43] .

Turkevich method still is the most common way for preparation of aqueous SGNPs with changing the stoichiometry of the reagents (precursor salt and reduction agent)[44,45,46], sequence of the reagents addition (inverse and direct)[47] and reaction conditions (temperature,

pH, stirring, *etc.*) to control the size distribution, particle shape and diameter[48,49]. The preparation of GNPs in aqueous solution involves consecutive steps. Once the gold salt is reduced, the gold atoms are formed and undergo for a fast nucleation process from the homogeneous solution which is followed by slow growth process leading to formation of NPs[17,33]]. The initial formation of GNPs can be observed by a change the color to brown, since the particles at the beginning are very small (>3 nm) and do not present plasmon band[50]. Then, a characteristic red color appears (that is, the plasmon band) which spectral position depends on the size of NPs. Depending on this mechanism, monodisperse GNPs can be synthesized up to 200 nm by separating the nucleation and growth stages and addition of some restrictions to prevent a secondary nucleation during the subsequent growth steps as reported by Bastus *et al*.[51]. They used the formed NPs (8 nm in diameter) as seed nuclei and by using hot-injection technique[33], *i.e.* injecting the gold salt solution to the hot reaction mixture, they can grow these NPs to 180 nm in diameter with a better size distribution than using the classical method.

- ***Brust Method***

Brust prepared GNPs in organic solvent in 1990[52]. The gold salt (in water) is transferred to the organic phase (toluene) using tetraoctylammonium bromide (TOAB) and reduced to GNPs using sodium borohydride ($NaHB_4$). Due to TOAB is a weak surfactant; additional ligand molecules such as dodecanethiol (DDT) are added to increase the stability of these NPs. The average particle diameter can be controlled between 3-6 nm changing the stoichiometry of the reagents, reaction condition and also by using different hydrophobic ligands.

- ***Martin Method***

In 2010[53], Martin prepared naked GNPs in water by reducing the gold salt using sodium borohydride in the presence of sodium hydroxide (NaOH) and hydrochloric acid (HCl). These particles are colloidally stable even without using other stabilizer like citrate due to their high charge from the excess ions in solution. The average particle diameter can be controlled between 3-6 nm. These particles can be transferred to non-polar solvents using hydrophobic ligands such as DDT.

## 1.2.2. GNRs.

- ***Seeded growth method***

It is the simplest method to synthesize GNRs[54]. The first seeded growth synthesis for GNRs was done by Jana in 2001[55] and developed by the groups of Murphy and El-Sayed[32,56,57]. This method depends on three steps as shown in Figure 5. i) using a strong reducing agent such as $NaBH_4$ to reduce the gold sat ($Au^{+3}$) to seed NPs (4 nm) in the presence of CTAB; ii) using a weak reducing agent such as AA to reduce more $Au^{+3}$ to $Au^{+1}$ in presence of silver nitrate ($AgNO_3$) and CTAB, and iii) using the seed particles to reduce the $Au^{+1}$ to $Au^0$ forming the GNRs[37,58,59]. CTAB is the most popular molecule for this synthesis which is used to direct the reaction for formation of the GNRs[38]. However, the mechanism of GNRs growth is still poorly understood. Recent modifications introduced to the GNRs synthesis method to control the dimensions of Au nanorods. These modifications include changing the synthesis conditions, such as the concentration of CTAB, seeds particles, ascorbic acid and silver nitrate and also, changing the pH of the growth solution[32,60,61,62]. In addition to, the effect of surfactants on the gold nanorods yield and aspect ratio using binary surfactant mixtures composed of CTAB and aromatic additives (*e.g.* 5-bromosalicylic acid or benzyldimethylhexadecylammonium chloride, *etc*.)[63] or composed of CTAB and sodium oleate (NaOL)[64] also were reported.

Although, it is easy to prepare GNPs with different sizes and shapes, there are still some impedimenta related to their colloidal stability and toxicity, especially in the case of GNRs. The ionic stabilization, which is produced from coating of the particles with molecules such as citrate or CTAB, is generally insufficient to prevent the aggregation of particles in biological media and then, the particles are unsuitable for biomedical applications. Therefore, many strategies have been developed to improve the colloidal stability and to decrease the toxicity of particles, as I will explain in section 1.3.

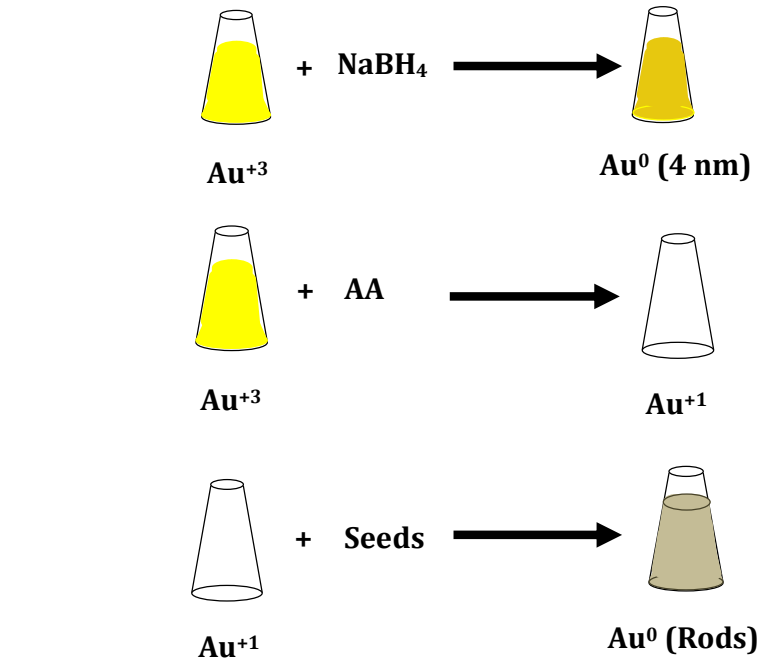


**Figure 5.** Scheme illustrates the mechanism of preparation of GNRs using seed mediated-growth method.

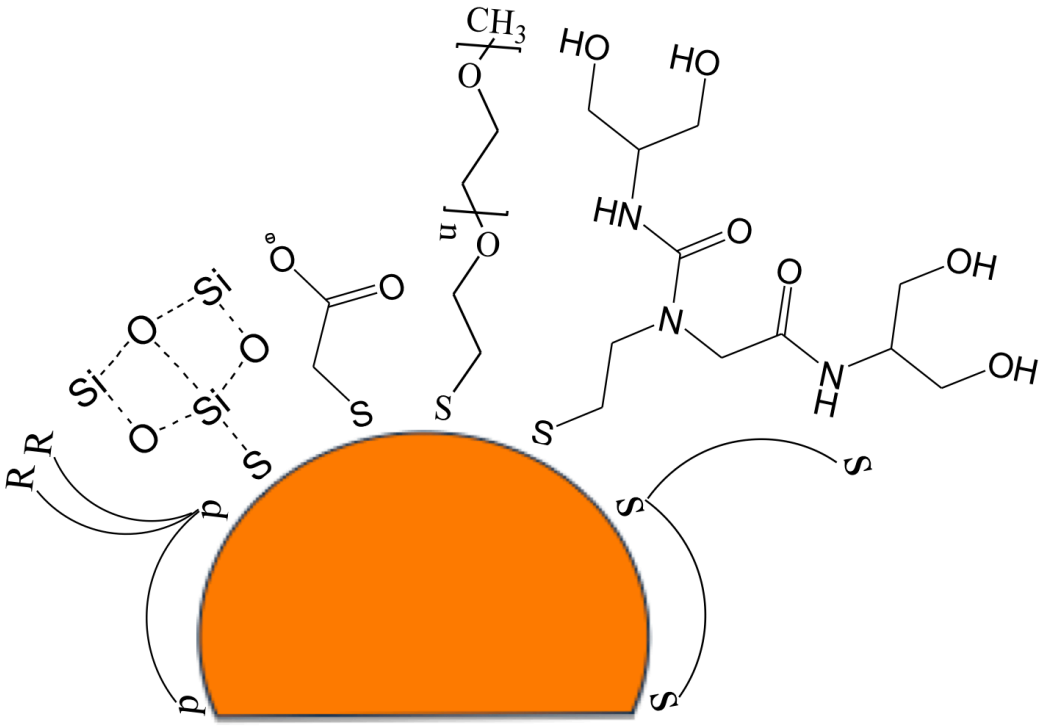


**Figure 6**. Spherical core NPs with different kinds of ligands which can be used to stabilize the NPs in both aqueous and organic solvent. The schematic molecule structures above are not to drawn to nano-scale. Left to right: Oligomeric phosphines, silica shell, monothiol terminated-alkyl carboxilic acids (e.g. MAA, MUA, *etc.*), PEG derivatives, dendrons, and peptides.

## 1.3. Stabilization of NPs against aggregation

Colloidal stability plays a very important role and determines the fate of the NPs in different applications. The capping molecules present in the synthesis of the NPs are not only used to control the growth of the NPs during the synthesis but also to prevent the aggregation by repulsion forces between the particles. These ligands are selected depending on the NPs core materials and the dispersion medium. As soon as their stability decreased (by changing the dispersion medium, the pH, the ionic strength, *etc*.), they will start to agglomerate and big aggregates of NPs will be formed. The agglomeration is the result of an attractive interaction between the surfaces of individual NPs and it can be prevented by surface modifications. These modifications can be done using different kinds of ligands (Figure 6), which bind to the NPs surface preventing the aggregation of the NPs by inducing repulsion forces among the individual NPs. These repulsion forces are either electrostatic repulsion (Figure 7a), which are originated due to the NPs are surrounded by a double layer of electric charges and the interaction between these charges is described by Van der Waals forces (equally "charged" particles repel each other); or steric repulsion (Figure 7b), which is originated between the molecules adsorbed on the surface of neighboring NPs. The size and the chemical nature of these molecules determine the stabilility degree. Also, it is worthy to mention that the surfactants can be attached to the particle surface by electrostatic attraction and/or hydrophobic interaction and/or covalent binding depending on their functional groups. There are chemical functional groups with higher affinity to metallic materials such as thiols which bind strongly to Au and Ag[65,66]. In many cases, thiolated ligands are added during the NPs synthesis and bound to the NPs core to provide colloidal stability[52,67]. Some of these ligands are only soluble in non-polar solvents (*i.e.* chloroform or hexane) such as DDT meanwhile others can be soluble in both of polar and non-polar solvents such as PEG and Mercaptohexanoic acid (MHA)[68]

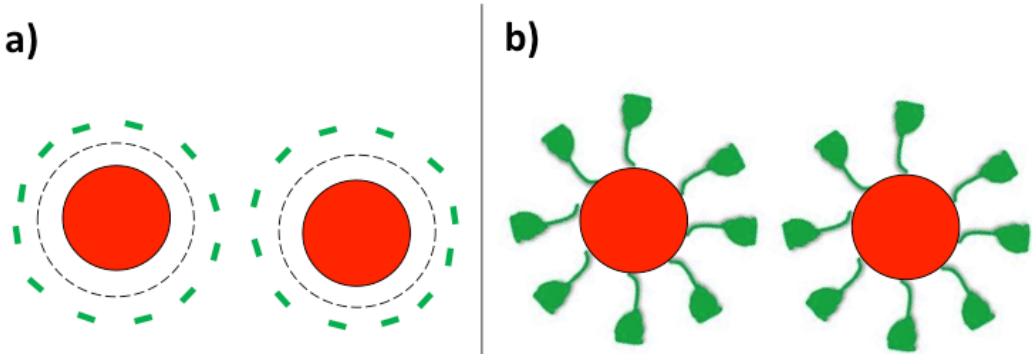


**Figure 7**. Shows NPs stabilized by a) electrostatic repulsion and b) steric repulsion.

As I mentioned in section 1.2.1, GNPs can be prepared in both organic and aqueous solvents. Again, GNPs in organic solvent are prepared in the presence of TOAB and stabilized with DDT.

As described above, GNPs in aqueous solution can be prepared in the presence of citrate (nanospheres) or in the presence of CTAB (nanorods). The resulting nanospheres are capped with citrate anions which are negatively charged (-COOH-). On the other hand, the nanorods are capped with CTAB bilayers that are highly positive charges due to the ammonium groups. In both cases, the particles are stabilized by electrostatic repulsion. However, once the ionic strength is changed and the resulting charge screening is large enough, the capped ligand molecules will ride out and the NPs will aggregate and subsequently, precipitate. Therefore, these synthesized-GNPs are not suitable for biomedical applications and they need for modifying their surface by exchange these capped ligand molecules to improve their colloidal stability and and also to decrease their toxicity, especially in case of GNRs due to the toxicity of CTAB itself[69]. There are many ligand molecules that can be used to exchange these original ligands from the particles synthesis and the incoming ligands bind more strongly to the NPs surface. The new ligand molecules should have high affinity to the inorganic core NPs to quickly replace the original (or old) ligands. For instance, mercaptoacids and thiolated-PEG are the most common ligands due to the high affinity of thiol/GNPs[65,66]. The mercaptoacids will provide electrostatic stabilization and the particles will be stable at higher salt concentrations. On the other hand, PEG molecules provide steric stabilization and if they have a pH reactive group in the other end (*e.g*. amine or carboxylic group) the particles will be charge stabilized as well. Therefore, PEGylated NPs are stable at longer times and at higher salt concentrations than electrostatically stabilized NPs[67].

In addition to, the GNPs in aqueous media can be stabilized using layer-by-layer (LBL) approach forming dense alternating shells of positive poly-allylamine hydrochloride (PAH) and negative polystyrene sulfonate (PSS) around the NPs[70,71]. The formed new shell can be modified with different molecules for different applications. Poly(vinylpyrrolidone) (PVP) can be used for preparation and stabilizing of SGNPs in aqueous media[17,72,73]. Citrate can be replaced in few hours by PVP providing high colloidal stability[74]. But in the case of GNRs, it is harder to exchange CTAB by PVP due to the strong binding of CTAB to the GNRs surface. However, an indirect way to stabilize the GNRs by PVP was reported[75]. Firstly, GNRs are wrapped by PSS and PAH layers using the LBL technique described above. Then,

the PVP is adsorbed to PAH coated NPs by electrostatic interaction. The PVP can slightly screen the surface charge from *ca*. +36 mV to +16 mV as described by Pastoriza-Santos *et al*.[75]. Remarkably, Wei and coworkers reported that GNRs could be stabilized by citrate. The GNRs were subjected to PSS and after three cycles of centrifugation and redispersion for removing the excess of unreacted CTAB. Then, the PSS capping the GNRs was replaced by citrate providing of citrate-capped GNRs with the typical colloidal stability of the citrate-capped NPs[76].

Another way to preform a ligand-exchange is transferring the particles from water to organic solvent by using phase-transfer reagents, such as surfactants (*e.g.* alkanethiol, alkylamine or other ligands), to improve the solubility of nanoparticles in organic solvent. For instance, GNPs can be transferred from water to organic solvent using cationic surfactants (*e.g.* 1-butyl-3-methylimidazolium hexafluorophosphate) in ionic liquids[77], C11-resorcinarene[78], DDT[79] and thiolated-PEG[80] as reported in the literature. Also, S. Emory and co-workers transferred the GNPs to chloroform using dicyclohexylamine (DCHA) in two steps: first, GNPs were functionalized with mercaptoacetic acid (MAA) and second, the DCHA was attached covalently to MAA immobilized on the NPs surface after activation of the carbonyl carbon of MAA by using dicyclohexylcarbodiimide (DCC)[81]. However, Transferring aqueous NPs, with different sizes (up to 100 nm) and different shapes to organic solvent still faces a big challenge because the stability of synthesized-GNPs is not enough to prevent the NPs aggregation when they are in contact with organic solvents. In 2015[82], W. Parak and co-workers solved this problem by using the PEG as mediator for stabilizing the particles at the phase transfer point. Then, the original ligands (citrate or CTAB) capped GNPs can be replaced by DDA to transfer these NPs from aqueous media to organic solvent. During this process, the amine group ($-NH_2$), which terminated the DDA at one side, binds strongly to the NPs surface in order to replace the original ligands and the other side (hydrophobic chains) have hydrophobic character to dissolve the particles in the organic phase. Also, additional components can be added, *e.g.* methanol or NaCl that decreases the surface tension at the interface to facilitate the contact of the NPs with the phase boundary.

In both cases, whether GNPs were prepared originally in organic solvent or prepared in aqueous media and transferred to organic solvent, they usually can't be used in biomedical applications because the biological process takes place only at aqueous environment. Therefore, it is necessary to transfer them to aqueous solution (water) before using them in

biomedicine. There are different methodologies for transferring the NPs from organic solvent to aqueous solution[68]. These methodologies should offer certain criteria: 1) They must offer good water solubility for the NPs, 2) they should provide with a colloidal stability to the NPs, 3) they should decrease the toxicity of NPs in some cases, 4) they should not affect the physic-chemical properties of the NPs, and 5) they can offer further functionalization options for the NPs modification with different purposes. Therefore, the most common methodology which can satify all these criteria is coating of particles with amphiphilic polymer (PMA) which consist of an anhydride rings backbone[83]. This polymer is synthesized by modifying its anhydride rings with aminated hydrocarbon chains (*e.g.* DDA) creating two domains in the polymer: one hydrophilic domain, which will bear a charge after the transference to water and a second hydrophobic domain consisted of the side aliphatic chains which will interact (hydrophobic multivalent interaction) with the hydrophobic surfactants of the NP surface. If the hydrophilic domains, unreacted anhydride rings, are exposed to basic aqueous buffer such as sodium borate (SBB pH 12), these anhydride rings will open providing carboxylates ($-CO_2^-$) and the polymer will forms a dense shell around the NP core providing colloidal stability by electrostatic repulsion of the charged groups. Typically, this polymer coating technique has been applied for the coating of small hydrophobic NPs (usually <20 nm), to transfer them from an organic solvent to aqueous solution as reported the first time by Pellegrino *et al*.[84]. Until 2015, the biggest size of polymer coated NPs was 35 nm in lenght (semiconductor CdSe/CdS nanorods) by Malvindi *et al*.[85].

In the work presented in this thesis, I used this methodology to coat GNPs with different sizes (up to 100 nm) and different shapes (spheres, rods and triangular nanoprisms) providing high colloidal stability in high ionic strength media. This strategy allow to the NPs to have a universal surface and then easily to functionalize them with different kinds of biomolecules. Figure 8 summarizes some kinds of molecules which used in the present work for stabilizing and functionalizing the surface of the NPs.

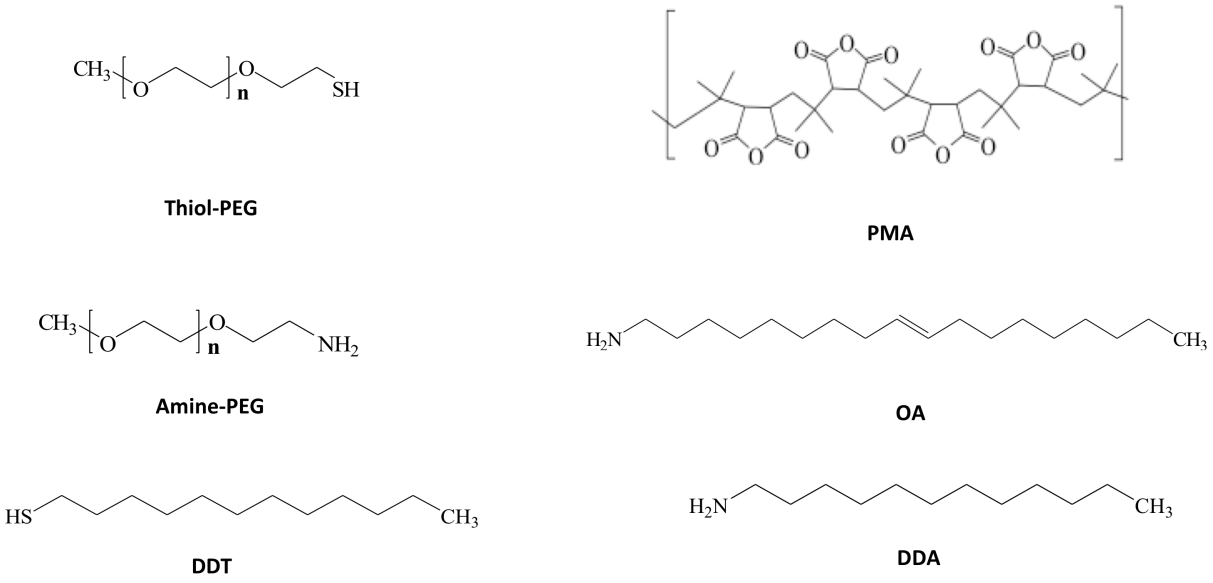


**Figure 8**. Scheme showing the different surfactants which can be used for NPs surface modification during the work presented in this thesis. OA is the abbreviation of oleylamine surfactant.

In the literature the stability of NPs using other ligand molecules has been extensively explored. These molecules include dimethylamino pyridine (DMAP)[86], peptides[87], Dithiocarbamate[88], dendrons[89] and dendrimers[90] among others. Also, the use of polymers such as poly(ethylene imine) (PEI)[91], and poly(acrylic acid) (PAA)[92] or silica encapsulation[93] have been reported.

## 1.4. Functionalization of NPs toward biomedical applications.

GNPs have suffered a significant increment in their biomedical applications, including diagnostic, optical imaging of cells and tissues[23], immunoassays and photothermolysis of cancer cells[15], as well as drug[22] and gene delivery[26]. For biomedical applications, surface functionalization of GNPs is very important to apply them to specific area of disease and allow them to selectively interact with cells[94,95]. The ligand molecules, which stabilize the NPs, often give functional groups for such a functionalization, *i.e.* NPs stabilized with the electrostatic repulsion of $-CO_2^-$. These functional groups are either part of individual surfactant molecules (like in PEG, MUA, etc.) or part of an amphiphilic polymer backbone and can be used to anchor biomolecules on the NPs. For this purpose, the water-soluble 1-Ethyl-3-(3-dimethylaminopropyl) carbodiimide (EDC) is commonly used as shown in Figure 9. EDC react with the carboxylic groups activating them to form an unstable intermediate

compound that easily reacts with primary amines. This primary amine will form an amide bond with the original –COOH and by this way, we can introduce to the NPs surface different kinds of biomolecules such as PEG, organic fluorophores, antibodies, DNA, *etc*. for different purposes[68,96].

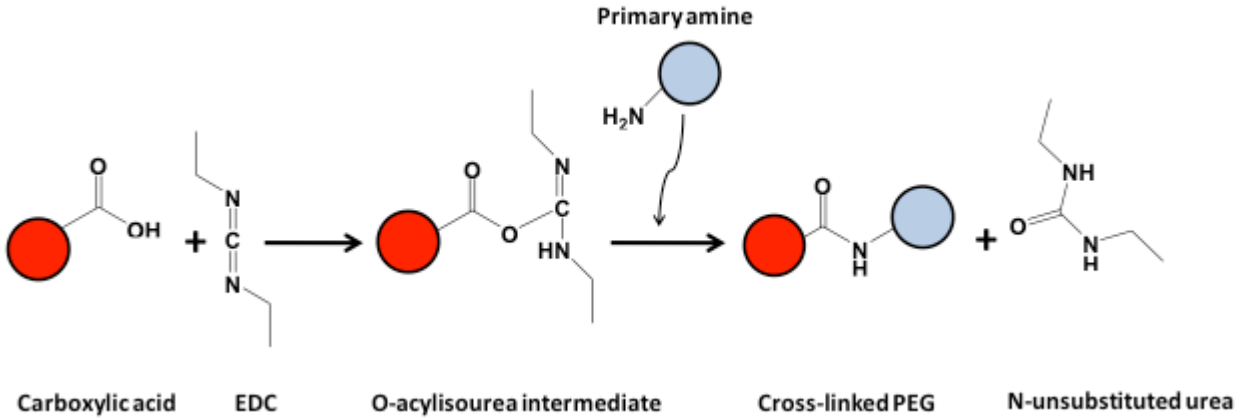


**Figure 9.** Scheme illustrating the conjugation reaction of –COOH groups from the NP surface with EDC. The water-soluble EDC activates the -COOH forming an unstable o-acylisourea intermediate. This can either be hydrolyzed or react with a primary amine group forming an stable amide bond.

Another possibility was reported[83] to introduce the biofunctional molecules (such as PEGs, dyes, sugars, *etc.*) to the NPs surface by embedding additional monomer in the amphiphilic polymer backbone after synthesis. The only limitation of this approach is that only molecules either soluble or stable in organic solvents are suitable for their insertion into the polymer.

A quick reaction to introduce the biomolecules to the surface of nanomaterial and to deliver an active pharmaceutical agent to specific organelles was developed through **click chemistry**, which defined and described by Sharpless in 2001 (Nobel Prize in Chemistry)[97]. The idea of click chemistry is based on the coupling of two reactive partners (covalently) that will react easily providing a very high yield. Typically, these click chemistry reactions can be performed in a variety of solvents and under mild conditions. The click processess are used for labeling of biomolecules such as proteins, nucleic acids, DNA, peptides and also can be used for introducing multiple functionalities onto NPs surface using different kinds of click reactions[98]. Such reactions involve certain functional groups presented on the NPs surface which will bind, in one step, to the functional group of the added molecules. The most common reaction within the click chemistry is Cu(I)-catalyzed azide alkyne cycloaddition (CuAAC). This reaction basically involves coupling of alkyneto an azide forming a 1,2,3-

Triazole ring under catalyst of Cu (I) at room temperature[99,100]. For example, using this reaction lipase was conjugated to SGNPs[101] (Figure 10a) and peptides were conjugated to GNRs[102]. Also, thiolated PEG chains have been linked to magnetic NPs through another click reaction called thiol–yne reaction under catalyst of UV light[103] (Figure 10b).

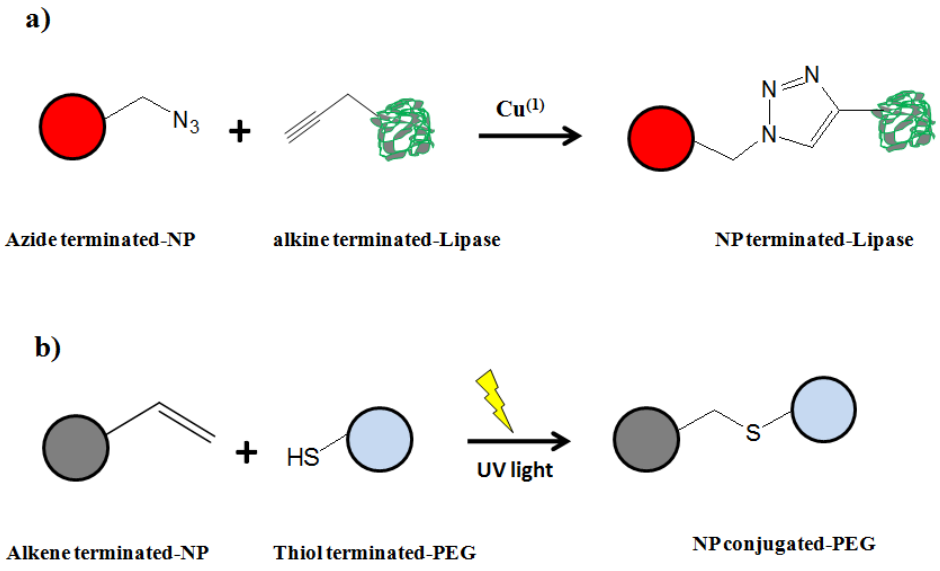


**Figure 10**. Scheme illustrating the conjugation mechanism of lipase and thiol-PEG to the gold and iron oxide NPs by using a) CuAAC reaction and b) Thiol-yne reaction respectively.

## 1.5. PEGylation

PEG is the common abbreviation for poly(ethylene glycol), which consist of repeated ethylene glycol units (-$CH_2$-$CH_2$-O-). Polyethylene glycols (PEGs) having different molecular weight are soluble in water and in many organic solvents forming random coils with diameters relatively larger than proteins of comparable molecular weight[68]. The attachment of the PEG chains to other molecules, normally a drug or a protein, called PEGylation, is one of the most successful techniques to enhance the therapeutic and biotechnological applications of these molecules[104]. The various applications of the PEG in chemistry and biological applications are explained by its simple structure, chemical stability, as well as its inert behaviour, non-toxicity, non-immunogenicity and highly solubility in water[68].

mPEG-SH as surfactants has the ability to interact directly with NPs core by place-exchange reactions providing the colloidal stability and to transfer the NPs from organic solvent to aqueous media or vice versa[68,80]. Also, bifunctional thiolated-PEG containing reactive groups such as -COOH or $NH_2$ can be used to introduce new functional groups to the NPs surface through conjugation chemistry as described above. In addition to, PEG can be either embedded in amphiphilic polymer before NPs coating or interact with NPs surface by covalent coupling (carboxylic-amine coupling or thiol-amine coupling) depending on the functional group on the NP surface[83]. In all cases, PEGs tend to form a dense shell around the NP that increases the NP hydrodynamic diameter ($d_h$) in order of a few to tens of nanometers depending on their molecular weights[105] and their graft desity as well[106], which provide the colloidal stability of the NPs by steric repulsion[107,108].

NPs are often functionalized with PEG to reduce the non-specific adsorption of proteins and to shield them from being recognized by immune system[109]. In addition to, the density of the PEG on the NPs surface can be controlled to increase the circulation time of NPs *in vivo*. However, the cell uptake PEGylated NPs[110,111] is reduced *in vitro*.

To fully understand the NPs behavior in physiological environments, we need to know in detail the protein corona formation, composition, topology and the particular conformation of the individual proteins inside the corona, which produced due to the interaction of NPs with the cells.

## 1.6. Interaction of the NPs with the cells

NPs-cells interaction is very critical in many applications such imaging, PTT and drug delivery. These applications require a steady control over this interaction, which are mainly depend on the surface properties of NPs. In the biological environment, there are more than 1000 different proteins, which are the main components of blood plasma[112]. Also, the lipids and nucleic acids are presented in the blood plasma. Once the NPs are injected to the biological media, they are going to interact with the different blood plasma components and a competition will happen between them to adsorb on the NPs surface. The non-specific adsorption of proteins on the NPs surface leads to the formation of a protein corona around the NP, as shown in Figure 11, conferring a new biological identity[113,114,115]. This corona changes the size and the composition of the NPs and determines the physiological responses

including cellular uptake, accumulation, toxicity, agglomeration and circulation lifetime[116]. Blood proteins are polypeptides with a particular structure and carry surface charge depending on the pH of the surrounding medium. The adsorption of the proteins on the surface of the NPs depends on the NPs surface and it is affected by its size, shape, surface charge, core material and surface functional groups. Also, it depends on the nature of the physiological environment (blood, tissue fluid, *etc*.) and the duration of interaction with NPs[117,118,119,120]. Therefore, there is no one "universal" plasma protein corona for all NPs and the composition of the adsorbed proteins does not depend on their relative abundances in plasma but with their affinity constant for the NPs surface [113]. As well, it is known that the protein corona is a dynamic entity which can be modified along the time.

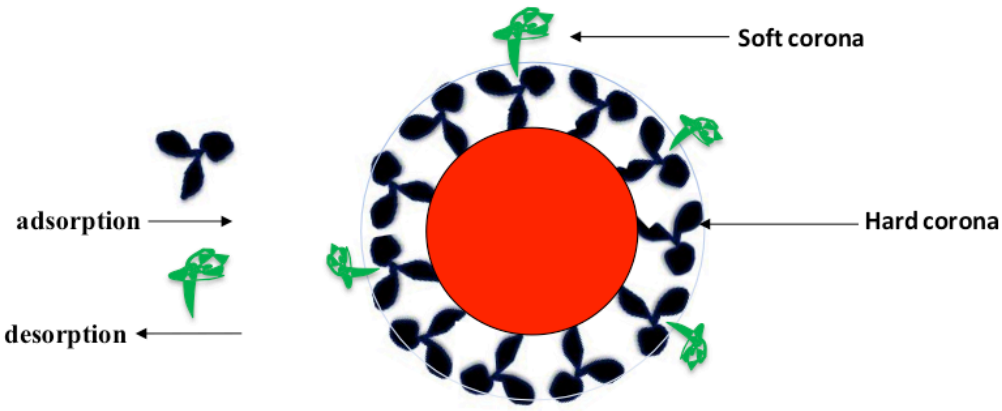


**Figure 11**. Scheme showing the desorption and adsorption of proteins on the NPs surface forming a protein corona. This corona is formed from hard and/or soft corona which are not formed only from a single protein. In this scheme, two types of proteins are drawn for the protein corona due to the difficulty drawing of different proteins.

At the initial stage of protein corona formation, most abundant proteins are adsorbed on the NPs surface and with time they will be replaced by higher affinity proteins (hard corona). The proteins which loosely bonded to the NPs or to the hard corona lead to the formation of "soft corona" which undergoes intensive exchange with the surrounding media. The formation of "hard corona" is due to the direct interaction of proteins with the surface of the nanoparticles (strongly attached) while the formation of "soft corona" is due to the protein-protein interaction (soft with hard corona)[115]. However, in some case of NPs like PEGylated NPs, there is no hard corona can be formed but only a weak corona adsorbed on the NPs surface[121].

Colloidal NPs often tend to agglomerate in the protein-free media in the presence of salts and/or big pH changes but when they are immersed in a biological media, the adsorption of proteins on the NPs surface improves their stability when they act as a spacer between the individual NPs and cause entropic or steric stabilization[122,123]. However, they are still having the tendency to agglomerate in the biological media when the proteins reduce the NPs surface charge[124] or directly bind to two NP and bridge them[125]; leading to changing the surface properties of NPs and the surface area for protein binding. However, the agglomeration of NPs induced by proteins in biologicl media is requried in some applications (*e.g.* immunoassays), where NP specifically binds antibodies[126]. The agglomeration of GNPs can be easily detected due to a strong shift in the SPR of the particles[127]. On the other hand, in many applications, the agglomeration of the particles is undesirable[128] and therefore, many studies have used different kinds of surfactants[82, 87,90] and polymer coating[83,91,92] to control the agglomeration of NPs in the biological medium.

## 1.7. Applications of GNPs

NPs have wide variety of applications in many areas including electronic and biomedical fields. One of these different kinds of NPs is the GNPs. The easy preparation, low toxicity, higher stability and unique optical properties make the GNPs widely studied and used in many applications[121]. For instance, GNPs can be used in electronics to connect the conductors, resistors and other elements of an electronic chip[129]. In biomedical fields, GNPs can be used in (i) PTT: Near-infrared absorbing GNPs (*e.g.* nanorods) can produce heat when excited with light leading to killing the tumors cells in treatment[23,130]; (ii) Drug delivery[131]: GNPs surface can be coated with different biomolecules (theraptic and target agents) and handle them to the desired place (*e.g.* cells, tissue, *etc.*); (iii) Diagnosis[132]: GNPs can be used to detect several diseases including cancer, heart disease, Alzheimer, *etc.* and (iv) Biomedical imaging: GNPs can scatter the light producing number of interesting color under the microscope which can be used in biological imaging[16,23,133].

# 2. Synthesis and characterization of GNPs

This chapter is assigned to the author's experimental work and presents the preparation and surface modification of GNPs with different sizes and shapes. All theses particles were characterized with different techniques including UV-Vis spectroscopy, TEM, gel electrophoresis, DLS and LDA. Furthermore, the stability of the particles with different surface coating of was studied in different media and also, the toxicity of these particles was tested in cancer and non-cancer cells. Additionally, the biodistribution of the different types of NPs in various organs was studied by inductively coupled plasma mass spectrometry (ICP-MS).

## 2.1. Synthesis of NPs

The GNPs with different sizes and shapes were prepared by using the seed-mediated growth method[51]. SGNPs with core diameter of 25 nm, 50 nm, and 60 nm were prepared and presented as 25-GNPs, 50-GNPs and 60-GNPs respectively. GNRs with SPR located at 850 and 1100 nm were prepared and presented as 850-GNRs and 1100-GNRs respectively.

### *2.1.1. Synthesis of SGNPs*

Preparation of Au seeds (AuNPs): were prepared by following a modified protocol of Bastús *et al.*[51] . This protocol depends on the reduction of gold salt using sodium citrate. To prepare AuNPs, 1.5 mL of tetrachloroauric acid (25 mM) was added to the boiling solution of sodium citrate (150 mL, 1.32 mM) in 250-flask connected to the condenser to prevent water evaporation. A color was immediately changed from yellow to blue and finally to soft red. After 10 min of boiling, the solution was cooled to room temperature. The resulted AuNPs have core diameter of 17.6 ± 3.4 nm, as shown in Figure 12.

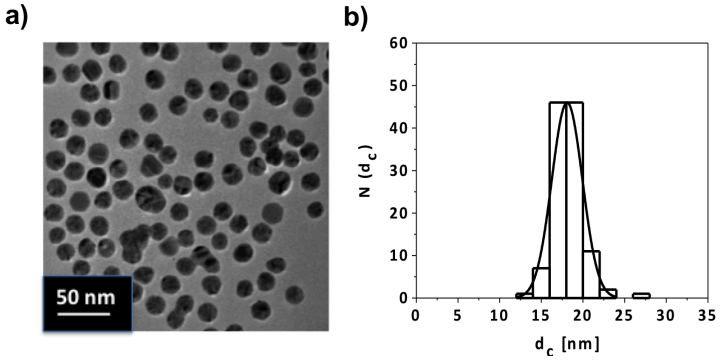


**Figure 12.** TEM picture of citrate capped AuNPs. b) Size distribution graph of the Au cores with diameter $d_c$ = 17.6 ± 3.4 nm. N ($d_c$) refers to the total counts and the scale bar corresponds to 50 nm.

Growing of AuNPs to 25-GNPs, 50-GNPs and 60-GNPs: After the seeds synthesis, the AuNPs solution was cooled down to 90 ºC to prevent the secondary nucleation during the growth period. Then, 1 mL of $HAuCl_4$ (25 mM) was injected to solution in the same vessel and stirred for 30 min. The last step was repeated twice and after that, the sample was diluted by extracting 55 mL of sample and adding 53 mL of MilliQ water and 2 mL of sodium citrate (60 mM). This process was repeated consecutively until we get particles with core diameters of 25, 50 and 60 nm. After each generation (*i.e.* $g_x$, x from 0 to 5), the UV spectrum was recorded using UV-Vis spectroscopy as shown in Figure 13.

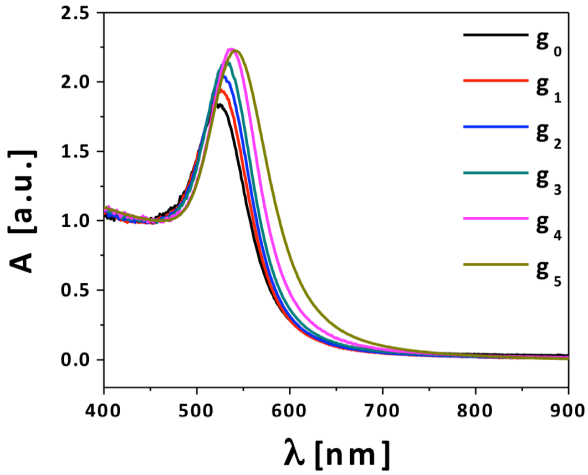


**Figure 13**. Shows normalized UV spectra for SGNPs after different growth steps. The SPR peaked at 524, 526, 528, 532 and 537 nm after 5 growth steps ($g_0$-$g_5$).

### *2.1.2. Synthesis of GNRs*

GNRs were prepared by using seed-mediated growth method based on two steps (seed and growth solution) as described below:

Seed solution preparation: This step was done using strong reducing agent, $NaBH_4$ to reduce ($Au^{+3}$) to ($Au^0$) in in the presence of CTAB. To produce seed solution of 4 nm Au NPs, in glass tube (40 mL), 5 mL of $HAuCl_4$ (0.5 mM) were mixed with 5 mL of CTAB (0.2 M). After that, 0.6 mL of freshly prepared $NaBH_4$ (0.01 M)) was diluted with 1 mL of cooled MilliQ water and injected to solution in the same tube with stirring. The solution color was changed immediately to brownish-yellow. The seed solution was strongly stirred for 2 min at 1200 rpm and kept at room temperature for 30 min before using[64].

Growth solution preparation: This step was done using a weak reducing agent, AA to reduce $Au^{+3}$ to $Au^{+1}$ in the presence of CTAB and $AgNO_3$. By following the protocol of Murray[64], the growth solution was prepared by dissolving, 7 g of CTAB and 1.234 g of NaOL in 250 mL of hot MilliQ water at 50 ºC. After dissolving, the solution was cooled down to 30 °C and then, a specific volume of $AgNO_3$ (4 mM) was added. The solution was kept at 30 °C for 15 min without any shaking. After that, 250 mL of $HAuCl_4$ (1 mM) was added to the solution with stirring at 700 rpm for 90 min. During this time, the solution color was changed from intense yellow to colorless. To control the aspect ratio of GNRs, a certain volume of HCl (37 wt.% in water, 12.1 M) was added to adjust the pH (Table 1) and stirred again at 400 rpm for 15 min. After that, 1.25 mL of AA (0.064 M) was added and the solution was vigorously stirred for 30 s. To reduce $Au^{+1}$ to $Au^0$, a small amount of seed solution (freshly prepared as described above) was injected into the growth solution (Table 1), stirred for 30 s and kept at 30 °C without stirring overnight for GNRs growth. The CTAB concentration in GNRs is 37 mM and the final products were isolated by centrifugation.

**Table 1**. Growth conditions for GNRs. $V_{HCl}$ refers to the volume of HCl which used to optimize the pH of growth solution, $V_{AgNO3}$ refers to the volume of $AgNO_3$ and $V_{seed}$ refers to the volume of seed solution

| Sample | $V_{HCl}$[mL] | pH | $V_{AgNO3}$ [mL] | $V_{seed}$ [mL] | $\lambda_{LSPR}$ [nm] |
|---|---|---|---|---|---|
| 1100-GNRs | 5 | 1.2 | 24 | 0.8 | 1100 |
| 850-GNRs | 2.9 | 1.6 | 18 | 0.4 | 850 |

## 2.2. Stabilizing and phase transfer of GNPs

Citrate-caped SGNPs and CTAB-caped GNRs are weak ligands and then, the particles are not stable for long time and further applications. So, I tried to exchange these ligands by transferring the particles from aqueous media to organic solution using different kinds of ligands such as DDA, DDT and OA. As shown in Table 2 but unfortunately, the particles were aggregated. Then, I tried to stabilize the particles at the critical point of phase transfer, which causes the particles to aggregate using mPEG-SH (750 Da). I used PEG because of its amphipatic nature it can be dissolved in both aqueous and organic solvent and then, expected to work as stabilizer and phase transfer helpers. The selected PEG contains a thiol group in one side, which has high affinity to the GNPs as it was mentioned in section 1.3, and a non-charged methoxy group in the other side.

The particles were coated with PEG for few hours and using a basic pH to promote the thiol group reactivity and after that a 0.4 M solution of DDA in chloroform was mixed strongly with particles using stirring until the particles were transferred to the chloroform as shown in Figures 14-15. Remarkably, this transference process can be done as well in a separation funnel upon the methanol addition to enhance the two phases interaction. After that, the particles were cleaned twice by centrifugation to remove the unreacted DDA and PEG, dispersed in chloroform and their concentration was determined by UV-Vis spectroscopy (section 2.5.1).

Two main advantages for the phase transfer approach have to be mentioned. First, the CTAB-capping the GNRs is cytotoxic[69] and it is binded strongly to the GNRs compared with citrate and is hardly removed through the ligand exchange using the same synthesized-solution. But the CTAB exchange will be faster by transferring the GNRs to another phase (organic solvent)[79] as it was previously described. Then the toxicity of the remaining CTAB, in case there is still some, is prevented by wraping the NPs core with the amphiphilic polymer as shown in section 4. Secondly, this technique is very versatile. It can be applied to any aqueous NPs just adjusting the reactivity of the PEG chains. This PEGylation will increase their stability and will produce a common surface to study the cell-NPs interactions.

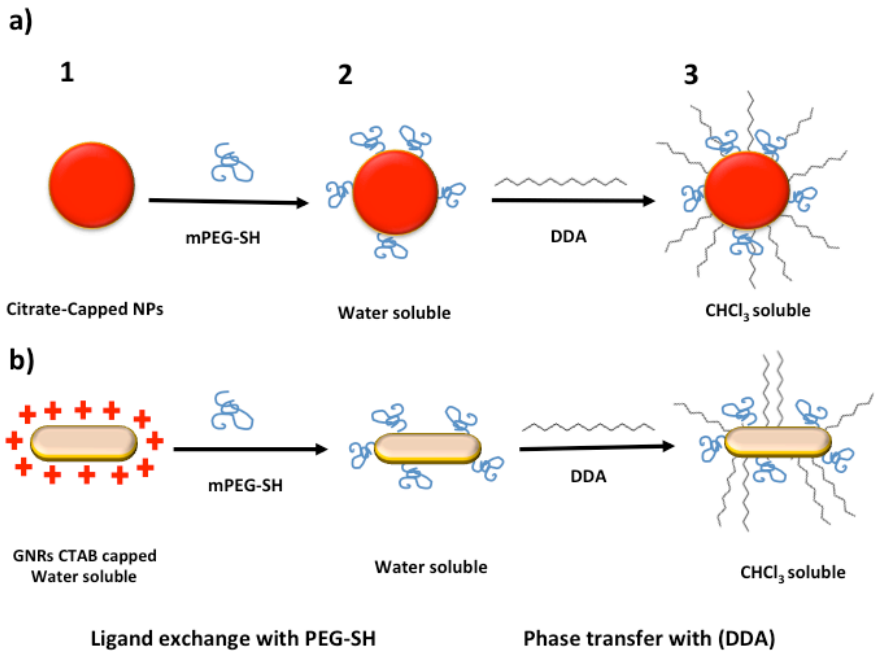


**Figure 14.** Schematic illustration of the PEGylation and phase transfer strategies for a) SGNPs and b) GNRs. 1) Particles in water after their synthesis, 2) PEGylated particles before the phase transfer and 3) in chloroform after the phase transfer using DDA.

a)

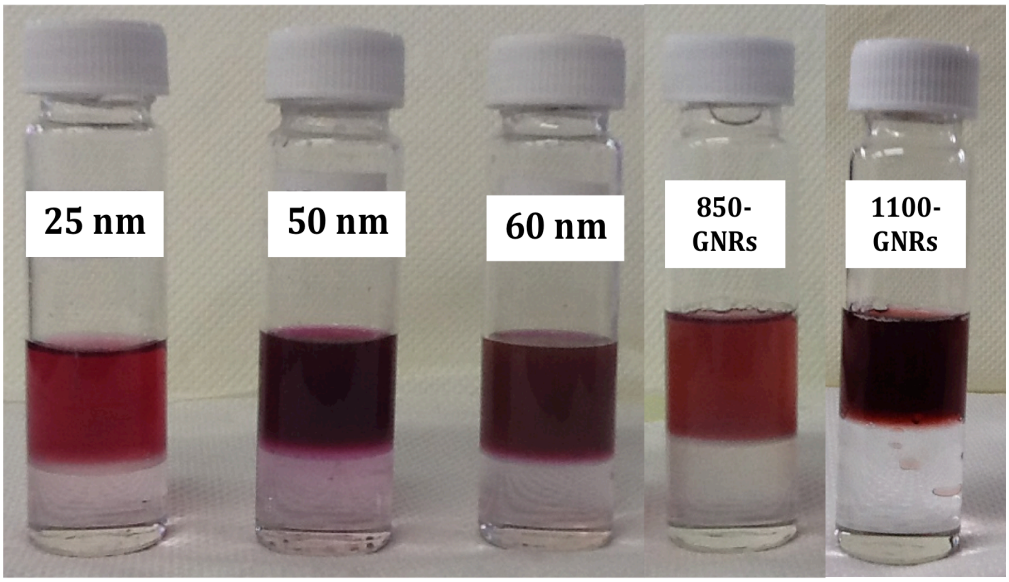


b)

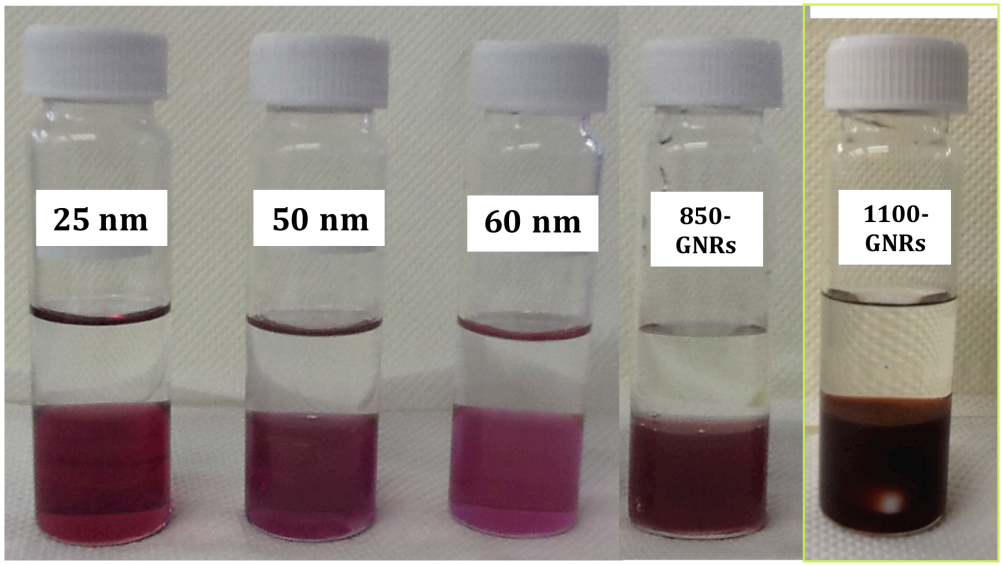


**Figure 15.** GNPs solutions. a) Left to right: 25-GNPs, 50-GNPs, 60- GNPs, 850-GNRs and 1100-GNRs after PEGylation and before phase transfer. b) The same order for the GNPs but after their transference to the chloroform by using DDA.

**Table 2**: Different reactions conditions that were tested for transferring the particles conjugated with or without PEG (mPEG-SH, $M_W$=750 Da) from aqueous media (water) to organic media. $C_{PEG}/C_{NP}$ refers to the ratio of added PEG (with concentration $C_{PEG}$) to NPs (with concentration $C_{NP}$); $C_{Ligand}$ refers to the concentration of the ligand molecules.

| Sample | $C_{PEG}/C_{NP}$ | Ligand | $L_{igand}$ [M] | Solvent | Results |
|---|---|---|---|---|---|
| 25-GNPs | $5 \cdot 10^3$ | OA | 0.25 | Chloroform | Didn't work |
| | $1 \cdot 10^5$ | OA | 0.25 | Hexane | Didn't work |
| | $1.5 \cdot 10^5$ | OA | 0.25 | Chloroform | Didn't work |
| | $2 \cdot 10^5$ | DDA | 0.25 - 0.4 | Chloroform | Didn't work |
| | $3 \cdot 10^4$ | DDA | 0.25 - 0.4 | Chloroform | Worked |
| | $6 \cdot 10^4$ | DDA | 0.25 - 0.4 | Chloroform | Worked |
| 50-GNPs | $3 \cdot 10^4$ | DDA | 0.25 | Chloroform | Didn't work |
| | $6 \cdot 10^4$ | DDA | 0.25 | Chloroform | Didn't work |
| | $1 \cdot 10^4$ | DDA | 0.4 | Chloroform | Didn't work |
| | $1.5 \cdot 10^5$ | DDA | 0.4 | Chloroform | Didn't work |
| | $3 \cdot 10^5$ | DDA | 0.4 | Chloroform | Worked |
| 60-GNPs | $3 \cdot 10^4$ | DDA | 0.4 | Chloroform | Didn't work |
| | $1 \cdot 10^5$ | DDA | 0.4 | Chloroform | Didn't work |
| | $2 \cdot 10^5$ | DDA | 0.4 | Chloroform | Didn't work |
| | $5 \cdot 10^5$ | DDA | 0.4 | Chloroform | Worked |
| 850-GNRs | - | OA | 0.4 | Chloroform | Didn't work |
| | - | OA | 0.1 | Chloroform | Didn't work |
| | - | DDT | 0.75 | Chloroform | Didn't work |
| | - | DDT | 0.75 | Acetone | Didn't work |
| | $1 \cdot 10^5$ | DDT | 0.75 | Chloroform | Didn't work |
| | $1 \cdot 10^5$ | DDT | 0.75 | Acetone | Didn't work |
| | $1 \cdot 10^5$ | OA | 0.4 | Chloroform | Worked |
| | $6 \cdot 10^4$ | DDA | 0.4 | Chloroform | Worked |
| 1100-GNRs | $1 \cdot 10^5$ | DDT | 0.4 | Chloroform | Didn't work |
| | $6 \cdot 10^4$ | DDT | 0.4 | Acetone | Didn't work |
| | $8 \cdot 10^4$ | DDA | 0.4 | Chloroform | Worked |

## 2.3. Polymer coating

Once the NPs were dissolved in chloroform, the polymer coating technique can be applied. The particles were coated with a modified amphiphilic polymer. This polymer was poly(isobutylene-alt-maleic) with molecular weight of 6 kDa and consist of anhydride rings backbone. The modification of the polymer was done according to Lin et *al.*,[83]. Briefly, 75 % of the polymer anhydride rings were modified with DDA in tetrahydrofuran (THF) at 70 $^0$C with stirring overnight (Figure 16). During reaction time, this anhydride rings were opened by the amine group of the DDA forming an amide bond. The other unreacted 25 % of

the polymer rings can be used for linking of other molecules like PEG, dye molecules, *etc*., through conjugation chemistry[83]. After modification process, the polymer was dried using a rotavapor under reduced pressure at 40 $^0$C and dispersed in 30 mL of chloroform to produce a stock solution with final concentration 0.75 M.

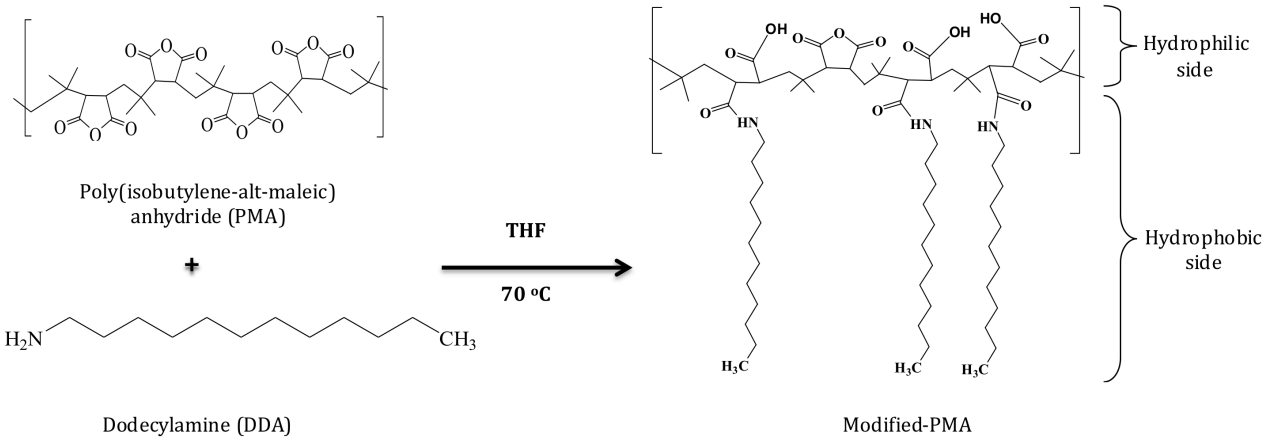


**Figure 16.** Schematic illustration of the the modification of poly(isobutylene-alt-maleicwith DDA in THF at 70 $^0$C, to obtain the amphiphilic polymer with a hydrophilic and a hydrophobic domain.

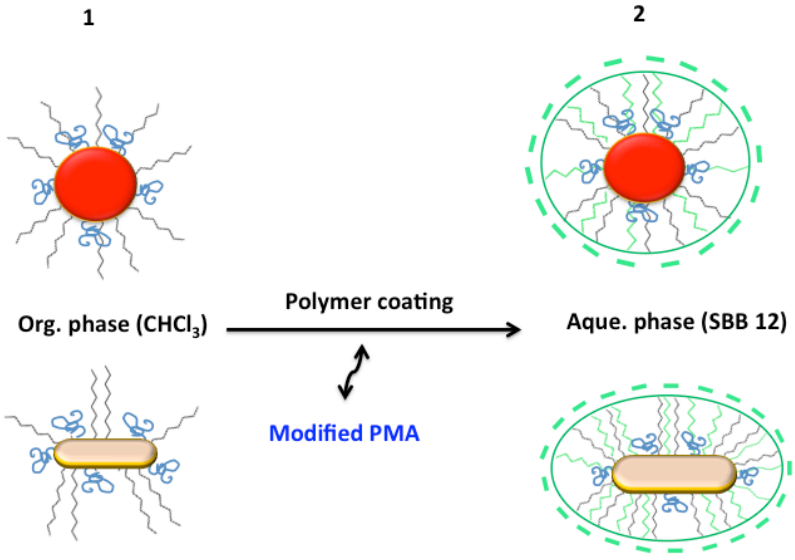


**Figure 17.** Scheme showing the polymer coating for both nanospheres and nanorods to transfer them from chloroform (1) to water (2).

The NPs were coated with a specific volume of polymer (PMA) as showns in Figure 17 accordingly to the following equations 1-4[83]. Nanorods were considered as cylinders to simplify the calculations. The surface of one NP can be calculated employing formulas 1 and 2 for SGNPs and GNRs, respectively.

$$A_0 = 4\pi \cdot ((d_c + 2d_L)/2)^2 = \pi \cdot d_{eff}^2 \quad (1)$$

$$A_0 = 2\pi \cdot \left(\frac{(d_c + 2d_L)}{2}\right) \cdot (L_c + 2d_L) \quad (2)$$

Where: $A_0$ is the surface area of one NP; $d_c$ is the diameter of SNPs or GNRs; and $L_c$ is the length of the GNRs as determined by TEM; $d_L$ corresponds with the thickness of the surfactant layer and $d_{eff}$ is the effective diameter and equal to the NP core value determined by TEM ($d_c$) plus two times the assumed thickness of the surfactant shell ($d_L$ = 1 nm).

The total surface area (A) of the NPs can be calculated by Formula 3.

$$A = C \times V \times N_A \times A_0 \quad (3)$$

Where: C is corresponding to the NPs concentration [M]; V refers to the volume of solution [L] of NPs and $N_A$ is the Avogadro constant.

Then, the amount of polymer needed to stabilize the NPs can be determined by formula 4.

$$V_P = \frac{N_P}{C_P} = \frac{A \cdot R_{P/Area}}{N_A \cdot C_P} \quad (4)$$

Where, $V_P$ is the volume of polymer needed to coat the NPs [L]; $N_P$ is the molar concentration of polymer [M]; $C_P$, concentration of polymer in stock solution [M]; A is total surface area of all the colloidal NPs [$cm^2$] in the solution and $R_{P/Area}$ is the ratio of monomer per $nm^2$ needed to stabilize efficiently the particles and $N_A$ is the Avogadro constant.

To increase the stability of the NPs the use of PEI (branched, $M_w$= 800 Da) as cross-linker was explored; and its volume can be calculated using the formula 5.

$$V_c = \frac{C_P \cdot V_P \cdot r_{c/p}}{C_c} \quad (5)$$

Where, $V_C$ is the volume of cross-linker solution added to the NPs solution [L]; $V_P$ is the volume of polymer needed to coat the NPs [L]; $r_{C/P}$ is the ratio of cross-linker added per polymer; $C_P$, $C_c$ are the concentration of polymer and cross-linker in stock solution, respectively.

As an example, for coating of 1 mL of 50-GNPs with concentration equal to 5 nM, 2.748 mL

of polymer ($C_p$= 0.05 M, $R_{p/Area}$ = 3000 monomers per $nm^2$) was added. The volume of NPs and polymer were placed together in a round flask, and diluted with chloroform. After 20-30 min, the chloroform was slowly evaporated[84] under reduced pressure using a rotavap at 40 °C in the bath until the solvent was completely evaporated. This procedure was repeated twice. In case of using the crosslinker, it was added at this point; 0.75% of PEI ($C_c$= 0.05 M, $V_c$= 20.61 µL) was added to the NPs and diluted with chloroform. After 20-30 min, the chloroform was slowly evaporated and the resulting solids were quickly dissolved in basic buffer solution (0.1 M NaOH or SBB pH 12) to drive the NPs to the aqueous phase. To remove any big aggregate, the solution was filtrated through a syringe membrane filter (0.22 $\mu$ m pore size). Then, the empty micelles generated by the excess of polymer were removed by precipitation of the NPs using centrifugation. The buffer was changed to water. See Table 3 for the centrifugation conditions depending on the NPs size and shape.

Three main advantages for polymer coating techniques have to be mentioned. First, the surface coating of inorganic NPs (semiconductor or metal oxide) by the polymer will not affect the physical properties of the core such as quantum yield, absorption, scattering or magnetism. Second, the NPs from different kinds of materials will be wrapped by a universal surface and then, the effect of the surface can be removed from the equation because they have the same surface coating. Third, this approach of NPs coating is not only used to transfer the NPs from an organic solvent to aqueous solution, but also serves as general platform which can be used for the attachment of biological molecules to the polymer surface through bioconjugation chemistry[83].

As reported by Murphy[64] , the CTAB in nanorods solution, directly after nanorods synthesis, has concentration of 37 mM. A specific volume of 850-GNRs, directly after synthesis, was diluted 15 times and the UV spectrum was recorded as shown Figure 19 (black spectra). In this sample, the concentration of CTAB is 3.3 mM due to the dilution of 15 times. Applying the round trip process of phase transfer and polymer coating will decrease the concentration of CTAB in the nanorods solution. This fact was tested recording the UV spectra for different CTAB concentrations in water in the region of the UV (Figure 18). Then, the absorbance in the same region of GNRs solutions after each step of surface modifications (from synthesis to PMA) was recorded (Figure 19). The results show that the concentration of CTAB in the GNRs solution decreased to less than 0.5 mM, which is the lowest concentration tested.

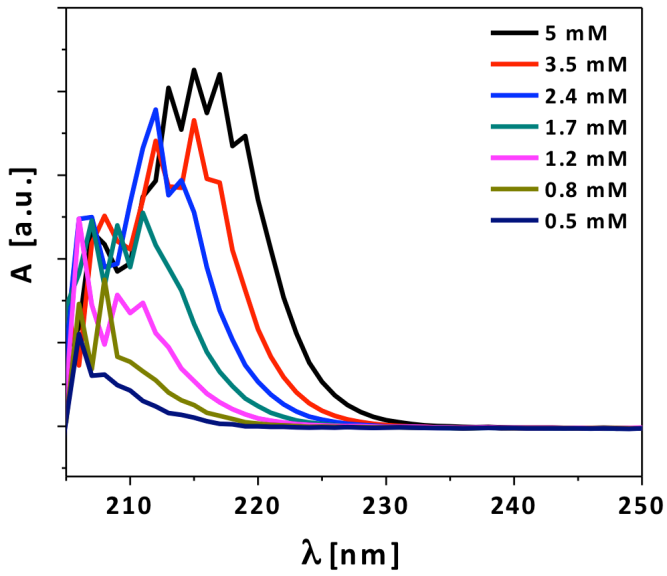


**Figure 18**. UV spectra for the different dilutions of CTAB dissolved in water.

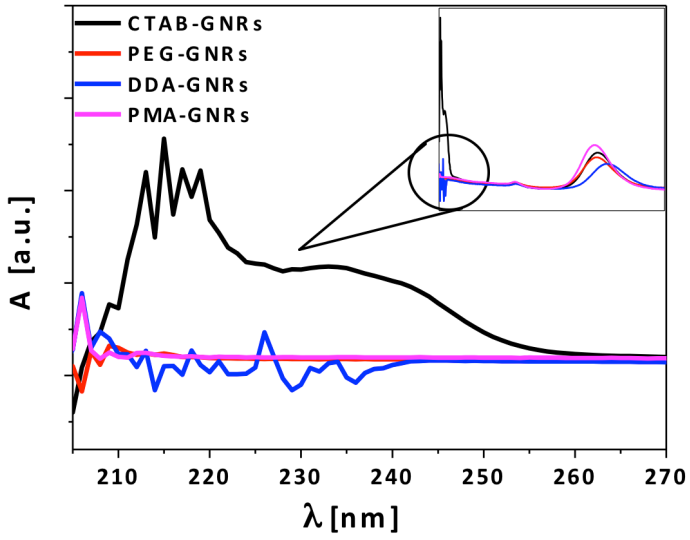


**Figure 19**. UV spectra for the 850-GNRs solution after each step of surface modification in the region of CTAB absorbance (200-270 nm range).

## 2.4. PEGylation of NPs

After polymer coating, the NPs surface is rich in –COOH groups. Therefore, using EDC chemistry[96] they can be activated and functionalized with different kind of molecules. In particular, NPs surfacewere modified with differnet mPEG-$NH_2$ (Figure 20). The molecular weight of the PEG chains was varied between the different samples (from 0.75 to 10 kDa) as

shown in Table 3. The interaction mechanism of the EDC with –COOH and -$NH_2$ was reported in section 1.4. The reaction was left overnight and after that, the NPs were cleaned using dialysis for 1 h and concentrated by centrifugation.

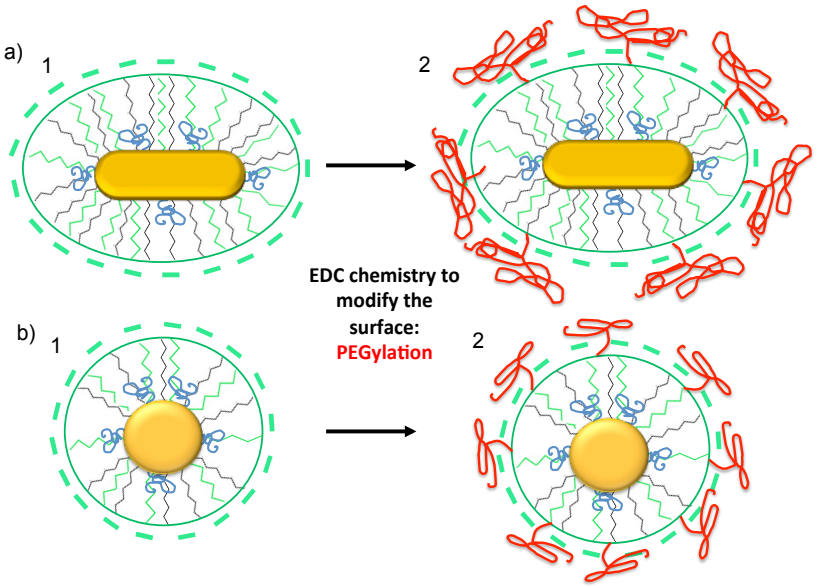


**Figure 20.** PEGylation of a) GNRs, b) SGNPs before (1) and after (2) PEGylation, using mPEG-$NH_2$ by EDC chemistry.

**Table 3.** Experimental conditions for all NPs. $C_{NP}$, $C_{DDA}$, $C_{EDC}$ and $C_{PEG}$ refers to concentration of NPs, DDA, EDC and PEG respectively. $R_{p/Area}$ refers to the number of PMA monomer added $nm^2$, $r_{C/P}$ refers to the ratio of crosslinker per polymer monomers, v refers to centrifugation speed and t refers to the centrifugation time.

| Sample | Phase transfer | | Polymer coating | | | | PEGylation | | |
|---|---|---|---|---|---|---|---|---|---|
| | $C_{PEG}/C_{NP}$ | $C_{DDA}$ [M] | $R_p/_{Area}$ | $r_{C/P}$ PEI | Centrifugation | | $C_{EDC}/C_{NP}$ | PEG [kDa] | $C_{PEG}/C_{NP}$ |
| | | | | | v [rpm] | t [min] | | | |
| 25-GNPs | $5 \cdot 10^5$ | 0.75 | 3000 | 0.75 | 9000 | 30 | $5 \cdot 10^6$ | 0.75 | $6 \cdot 10^6$ |
| 50-GNPs | | | | | 4000 | 35 | $30 \cdot 10^6$ | 5 | $3 \cdot 10^6$ |
| 60-GNPs | | | | | 3000 | 35 | $30 \cdot 10^6$ | 10 | $3 \cdot 10^6$ |
| 850-GNRs | | | | | 4000 | 35 | $8 \cdot 10^6$ | 5 | $1 \cdot 10^6$ |
| 1100-GNRs | | | | | 9000 | 30 | $8 \cdot 10^6$ | 10 | $1 \cdot 10^6$ |

## 2.5. Characterization of NPs

The NPs were characterized after each step of surface modification by using the following techniques:

### 2.5.1. Ultraviolet-visible spectroscopy

UV-Vis spectroscopy was used to measure the absorbance and to check the stability of the particles. To measure the particles absorbance, the solvent was placed inside a 1 cm pathway polystyrene cuvette and used as blank. After that, the sample was immersed and diluted in the same cuvette. The UV spectra and SPR absorbance were recorded for all NPs as shown in Figure 21 and Table 4 respectively.

As shown in Figure 21, the SPR position was shifted to higher wavelength for all NPs which were DDA-capped and dispersed in chloroform. The red-shifting is due the effect of the surrounding medium on the SPR wavelength, which the refractive index for chloroform (1.44) is higher than that to the water (1.33) and then, will led to shifting the SPR position to higher wavelength with considering the effect of surfactant on the SPR[17] as I mentioned in section 1.1. In case of GNRs (especially 1100-GNRs), the SPR position was shifted to lower wavelength after PMA and this might be due to some looses of the longer rods (higher aspect ratio) during the surface modification steps and cleaning stages of rods by centrifugation (see Table 4).

**Table 4.** Summarizes the maximum of LSPR absorbance of all the GNPs in all the modification steps.

| Sample | $\lambda_{SPR}$ [nm] | | | | |
|---|---|---|---|---|---|
| | Citrate/CTAB-capped | mPEG-SH | DDA-capped | PMA-coated | mPEG-$NH_2$ |
| 25-GNPs | 523 | 524 | 530 | 524 | 524 |
| 50-GNPs | 535 | 538 | 546 | 536 | 536 |
| 60-GNPs | 541 | 542 | 555 | 542 | 542 |
| 850-GNRs | 836 | 832 | 877 | 824 | 816 |
| 1100-GNRs | 1095 | 1055 | ≥ 1100* | 1075 | 1056 |

(*) Highest wavelength that we can measure with our UV-Vis spectrophotometer

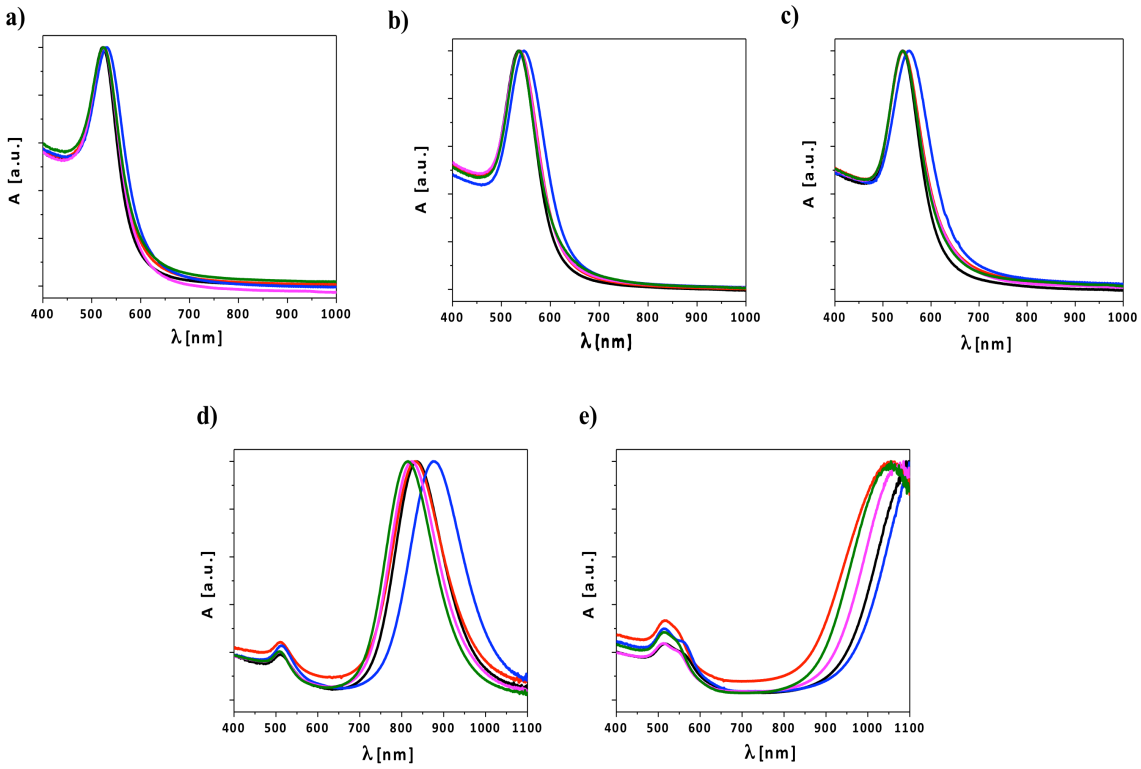


**Figure 21.** Normalized UV spectra for a) 25-GNPs, b) 50-GNPs, c) 60-GNPs, d) 850-GNRs, e) 1100-GNRs. Color codes stand for citrate/CTAB-capping (black), stabilization with mPEG-SH (red), after their phase transfer (DDA-capped) (blue), PMA coating (pink) and after PEGylation (green).

Also, the yield (%Y) of the process was followed by UV-Vis spectroscopy. For each NP type, the concentration and the sample volume was controlled in each step. The concentration was measured using the extinction coefficients described in Table 5, and the NPs amount collected after each step was compared with the NPs obtained directly after the NPs synthesis (100%) as shown in Table 6. There are some problems with the adequation of the extinction coefficient especially for the 1100-GNRs in chloroform, but it is safe to say that the phase transfer is quantitative. Remarkably, the total yield after all the polymer coating procedure, including the cleaning steps is above the 73 % in all the cases (in some is as high as an 80 %).

**Table 5.** Shows the molar extinction coefficients values which were used for each NP for calculation their concentrations. $\lambda_{\varepsilon}$ refers to the wavelength number in which the ε was picked. $\lambda_{LSPR}$ refers to the maximum of absorbance in the longitudinal LSPR of GNRs.

| NPs | ε [$M^{-1}$ $cm^{-1}$] | $\lambda_{\varepsilon}$[nm] |
|---|---|---|
| 25-GNPs | $9.64 \cdot 10^{8}$ | 450[134] |
| 50-GNPs | $9.92 \cdot 10^{9}$ | |
| 60-GNPs | $1.73 \cdot 10^{10}$ | |
| 1100-GNRs | $8.5 \cdot 10^{9}$ | $\lambda_{LSPR}$[133] |
| 850-GNRs | $4.9 \cdot 10^{9}$ | |

**Table 6.** Yield of collected NPs after each step of surface modifications. C [nM] refers to concentration, V [mL] refers to the total volume and Y% refers to the yield.

| Ligand | 25-GNPs | | %Y | 50-GNPs | | %Y | 60-GNPs | | %Y |
|---|---|---|---|---|---|---|---|---|---|
| | V [mL] | C [nM] | | V [mL] | C [nM] | | V [mL] | C [nM] | |
| Citrate/CTAB | 150 | 1.4 | 100 | 150 | 0.43 | 100 | 150 | 0.14 | 100 |
| mPEG-SH | 152.5 | 1.37 | 99.5 | 153 | 0.41 | 97.3 | 152.1 | 0.13 | 94.1 |
| DDA | 20.3 | 10.1 | 97.6 | 20 | 2.7 | 83.7 | 10 | 2 | 95.2 |
| PMA | 2.15 | 82.4 | 84.6 | 8.55 | 5.8 | 76.9 | 4.2 | 3.8 | 76 |
| **Ligand** | **850-GNPs** | | %Y | **1100-GNRs** | | %Y | | | |
| | V [mL] | C [nM] | | V [mL] | C [nM] | | | | |
| Citrate/CTAB | 52 | 6 | 100 | 103 | 0.8 | 100 | | | |
| mPEG-SH | 60 | 5.1 | 98.1 | 108 | 0.74 | 97.0 | | | |
| DDA | 19 | 15.2 | 92.6 | 90 | 0.5 | 54.6 | | | |
| PMA | 4.3 | 57.9 | 79.8 | 19 | 3.2 | 73.8 | | | |

UV-Vis spectroscopy can be used to determine the concentration of the particles using the Beer-Lambert law[135] by Formula 6. The concentration of NPs depends on extinction coefficient of the particles and the absorbance values measured at the wavelengths indicated in the Table 5.

$$A = C \times \varepsilon \times L \qquad (6)$$

Where A is the absorbance of the NPs at wavelength of 450 nm, C is the concentration of NPs; L is the light path length in the cuvette (1 cm) and ε is the extinction coefficient of the particles.

### 1.1.1. Dynamic light scattering (DLS) and laser Doppler anemometry (LDA)

DLS was used to measure the hydrodynamic diameter ($d_h$) of the NP that is used as a good indicator for the colloidal stability of the particles. Increasing $d_h$ with the time may be an indication for NP agglomeration. For measuring the $d_h$, the sample was calibrated for 10 min at room temperature to be the measured movements only belong to Brownian motion. Then, 1 mL of sample in a polystyrene cuvette is placed in the cuvette holder and the SOP (Standard Operating Procedure) setting is selected depend on the material, solvent and cuvette. The hydrodynamic diameter in number (N ($d_h$)) and in intensity (I ($d_h$)) was recorded 3 times for all NPs as shown in Figures 24-29. As indicated by the DLS results, the particles are very stable during the steps of surface modifications and the $d_h$ for all nanospheres was in the same range (from synthesis to PMA). After PEGylation of NPs as shown in Figure 22 and Table 7, the $d_h$ is increased about 10 nm in case of 50-GNPs and about 18 nm in case of 60-GNPs depending the length of the PEG molecule

LDA can be used to measure the zeta ( $\zeta$ ) potentials. For this purpose, the Malvern Dip Cell Kit was used and the measurement conditions were the same as DLS with changing the SOP setting to be compatible with this measurement. The $\zeta$ -potential was recorded 3 times for all NPs as shown in Figures 30-34.

As shown in Figure 23, the surface net charge of the spherical particles changed from highly negative (citrate and PMA-coating), which is rich with negatively -COOH to less negative after PEG stabilization. After PEGylation, the surface net charge changed to be close to zero (neutral state) due to saturation of particles with PEG especially, in case of 50-GNPs and 60-GNPs, which the number of -COOH are decreased and the particles surface is rich with non-charged methoxy groups ($-CH_3$) as confirmed also with gel electrophoresis (section 1.1.2). In case of GNRs, the surface net charge changed from positive (CTAB-capped), which is rich with positively ammonium groups ($-NH_3^+$) to less positivity (stabilized with PEG), to highly negative (PMA-coated) and finally changed to be close to Zero after PEGylation.

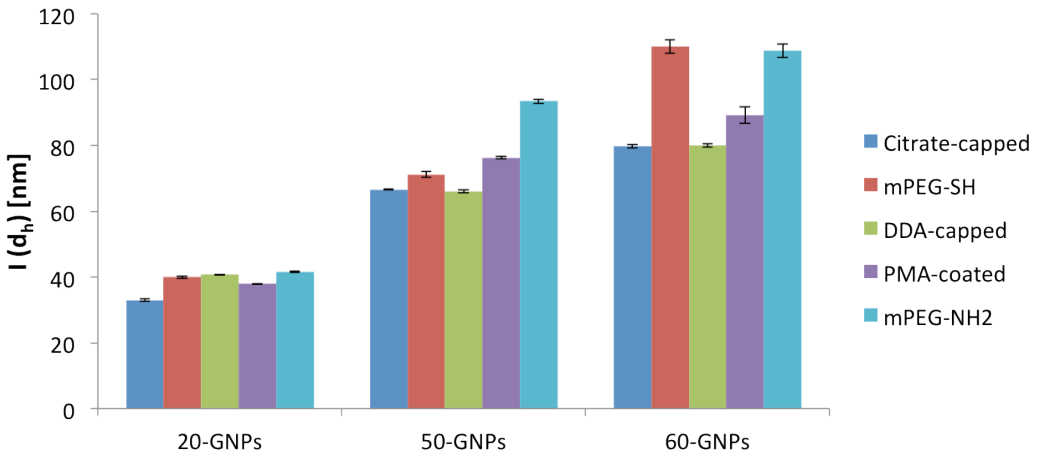


**Figure 22.** Shows the hydrodynamic diameter in intensity ($I(d_h)$) for the SGNPs after each step of surface modifications

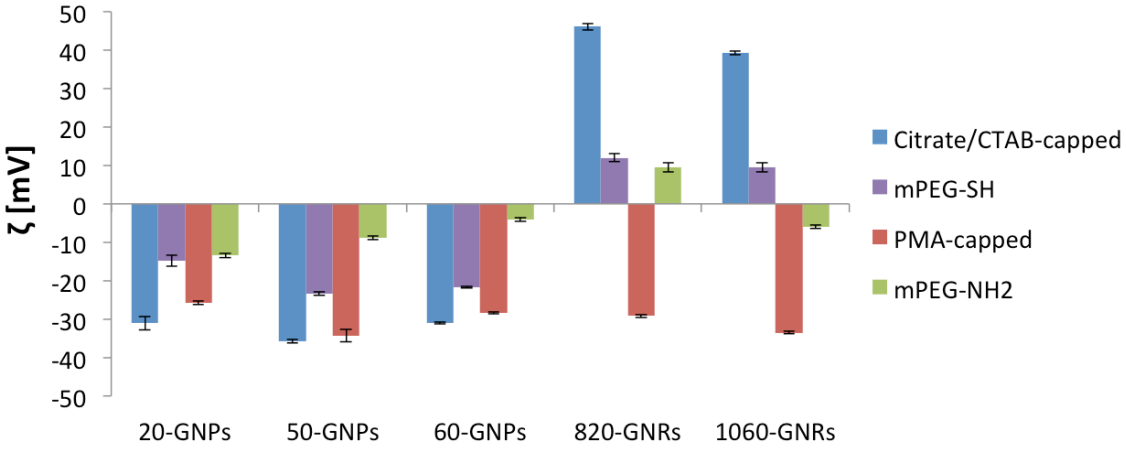


**Figure 23.** ζ -potential values [mV] for all NPs in all the steps of the round phase transfer.

**Table 7.** $d_h$ [nm] in number (N ($d_h$)) and intensity (I ($d_h$)), Z-average ($Z_{ave}$), polydispersity index (PDI) and ζ -potential values (N (ζ)) for all NPs in all the steps. The size values for GNRs were used only as indicator to the colloidal stability in all the steps of the round phase transfer and have no physical meaning.

| Sample | Modification | N ($d_h$)[nm] | $Z_{ave}$[nm] | PDI | I ($d_h$)[nm] | N (ζ) [mV] |
|---|---|---|---|---|---|---|
| **25-GNPs** | Citrate-capped | 21.0 ± 0.5 | 29.3 ± 0.1 | 0.11 ±0.01 | 33.0 ± 0.4 | - 31.1 ± 1.7 |
| | mPEG-SH (750 Da) | 26.4 ± 0.7 | 35.8 ± 0.3 | 0.11 ± 0.01 | 39.9 ± 0.3 | - 14.8 ± 1.5 |
| | DDA-capped | 26.1 ± 0.8 | 36.5 ± 0.1 | 0.10 ± 0.01 | 40.7 ± 0.1 | - |
| | PMA-coated | 27.0 ±0.2 | 34.8 ± 0.1 | 0.08 ± 0.01 | 37.9 ± 0.1 | - 25.7 ± 0.5 |
| | mPEG-$NH_2$ (750 Da) | 28.6 ± 0.7 | 37.7 ± 0.2 | 0.09 ± 0.01 | 41.6 ± 0.2 | - 13.4 ± 0.6 |
| **50-GNPs** | Citrate-capped | 35.4 ± 1.1 | 53.2 ± 0.2 | 0.21 ± 0.01 | 66.6 ± 0.2 | - 35.8 ± 0.4 |
| | mPEG-SH (750 Da) | 38.6 ± 0.8 | 57.8 ± 0.1 | 0.19 ± 0.01 | 71.2 ± 1.0 | - 23.3 ± 0.5 |
| | DDA-capped | 38.2 ±0.2 | 54.2 ± 0.4 | 0.18 ± 0.01 | 66.1 ± 0.5 | - |
| | PMA-coated | 43.4 ± 1.6 | 61.9 ± 0.1 | 0.19 ± 0.01 | 76.3 ± 0.4 | - 34.3 ± 1.6 |
| | mPEG-$NH_2$ (5 kDa) | 53.5 ±1.9 | 79.6 ± 0.3 | 0.15 ± 0.01 | 93.4 ± 0.7 | - 8.8 ± 0.5 |
| **60-GNPs** | Citrate-capped | 49.5 ± 1.1 | 68.3 ± 0.8 | 0.15 ± 0.01 | 79.7 ± 0.5 | - 31.0 ± 0.3 |
| | mPEG-SH (750 Da) | 43.2 ± 2.7 | 85.3 ± 1.0 | 0.23 ± 0.01 | 110.0 ± 2.1 | - 21.7 ± 0.2 |
| | DDA-capped | 47.7 ± 1.1 | 60.0 ± 0.3 | 0.13 ± 0.01 | 80.0 ± 0.5 | - |
| | PMA-coated | 47.4 ± 1.1 | 74.3 ± 0.5 | 0.18 ± 0.01 | 89.2 ± 2.5 | - 28.4 ± 0.3 |
| | mPEG-$NH_2$ (10kDa) | 65.1 ± 2.0 | 95.4 ± 0.8 | 0.11 ± 0.01 | 108.7 ± 2.05 | - 4.1 ± 0.5 |
| **850-GNRs** | CTAB-capped | - | 10.4 ± 0.05 | 0.40 ± 0.01 | 8.24 ± 0.03 | 46.1 ± 0.9 |
| | mPEG-SH (750 Da) | - | 8.23 ± 0.67 | 0.37 ± 0.02 | 7.17 ± 0.30 | 12 .0± 1.0 |
| | DDA-capped | - | 27.27 ± 3.6 | 0.49 ± 0.11 | 11.23 ± 1.3 | - |
| | PMA-coated | - | 14.38 ± 0.48 | 0.55 ± 0.07 | 8.99 ± 0.25 | - 29.2 ± 0.4 |
| | mPEG-$NH_2$ (5 kDa) | - | 10.86 ± 0.1 | 0.27 ± 0.01 | 11.79 ± 0.33 | 9.5 ± 1.2 |
| **1100-GNRs** | CTAB-capped | - | 27.84 ± 0.65 | 0.61 ± 0.04 | 58.91 ± 2.79 | 39.3 ± 0.5 |
| | mPEG-SH (750 Da) | - | 33.32 ± 0.4 | 0.27 ± 0.01 | 48.24 ± 0.61 | 9.4 ± 1.2 |
| | DDA-capped | - | 23.1 ± 0.8 | 0.52± 0.08 | 41.43 ± 1.92 | - |
| | PMA-coated | - | 12.85 ± 0.11 | 0.57 ± 0.01 | 29.61 ± 0.48 | - 33.5 ± 0.3 |
| | mPEG-$NH_2$ (10 kDa) | - | 22.38 ± 0.2 | 0.55± 0.03 | 49.68 ± 3.22 | - 6.0 ± 0.4 |

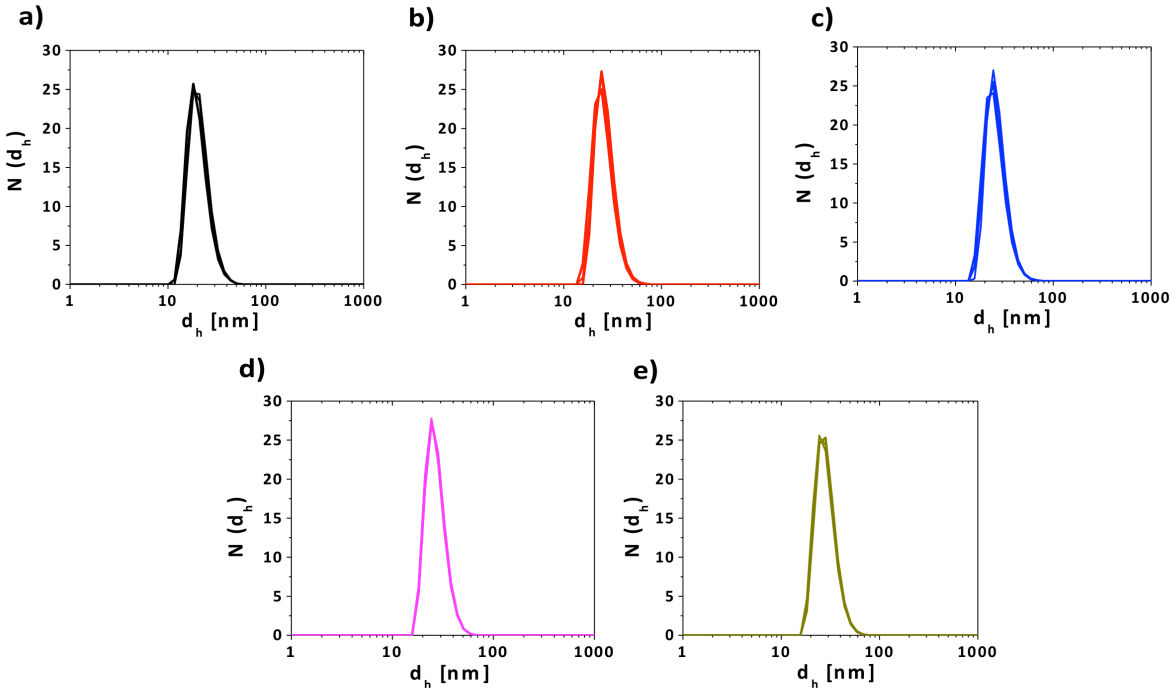


**Figure 24.** Hydrodynamic diameter in number ($N(d_h)$) for 25-GNPs after each step of surface modifications: a) citrate-capped b) after their stabilization with mPEG-SH; c) DDA-capped d) PMA-coated and e) after modification with mPEG-$NH_2$ ($M_w$= 750 Da).

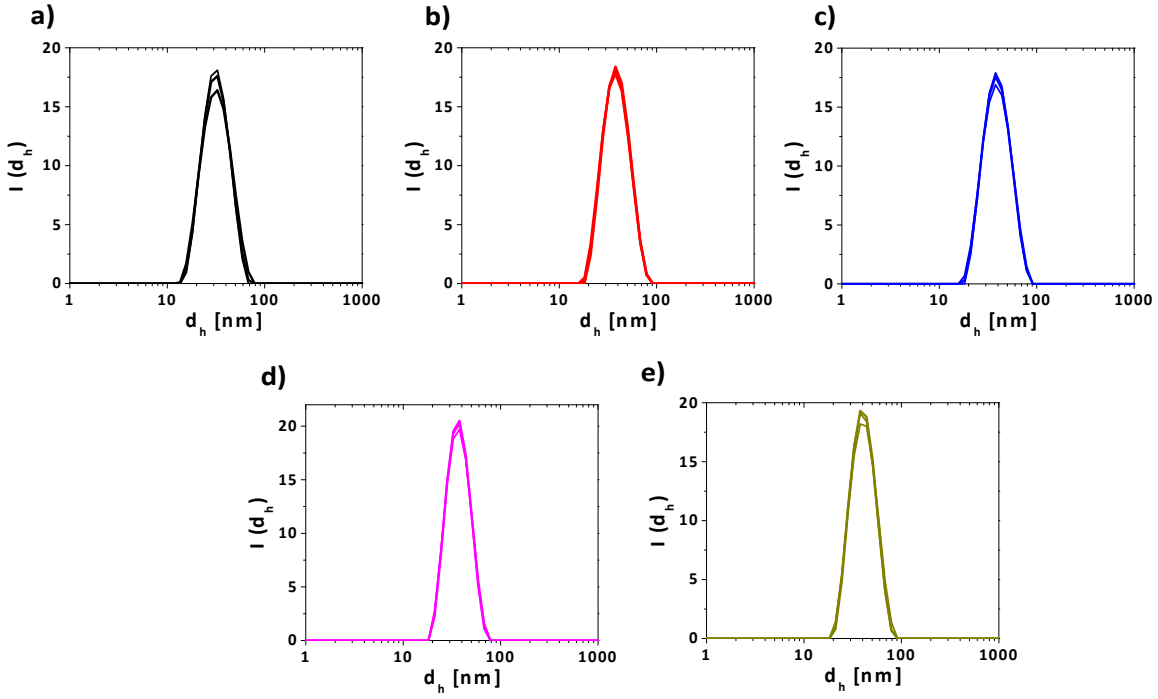


**Figure 25.** Hydrodynamic diameter distribution in intensity ($I(d_h)$) for 25-GNPs after each step of surface modifications:a) citrate-capped b) after their stabilization with mPEG-SH; c) DDA-capped d) PMA-coated and e) after modification with mPEG-$NH_2$ ($M_w$= 750 Da).

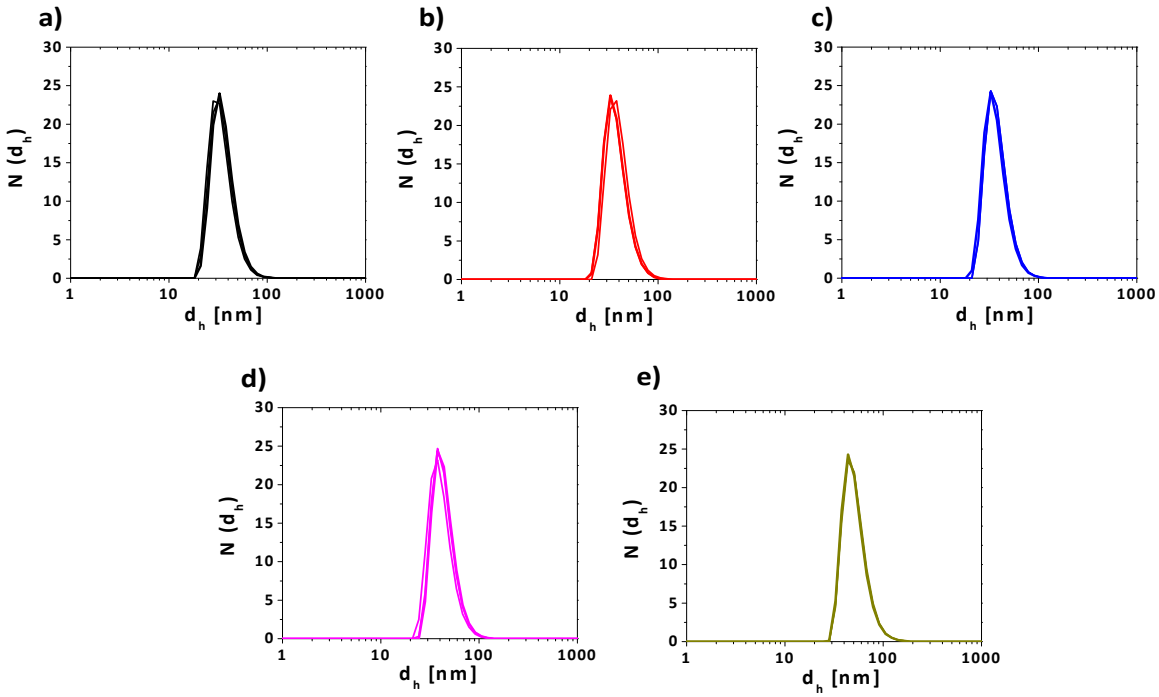


**Figure 26.** Hydrodynamic diameter distribution in number ($N(d_h)$) for 50-GNPs after each step of surface modifications: a) citrate-capped b) after their stabilization with mPEG-SH; c) DDA-capped d) PMA-coated and e) after modification with mPEG-$NH_2$ ($M_w$= 5kDa).

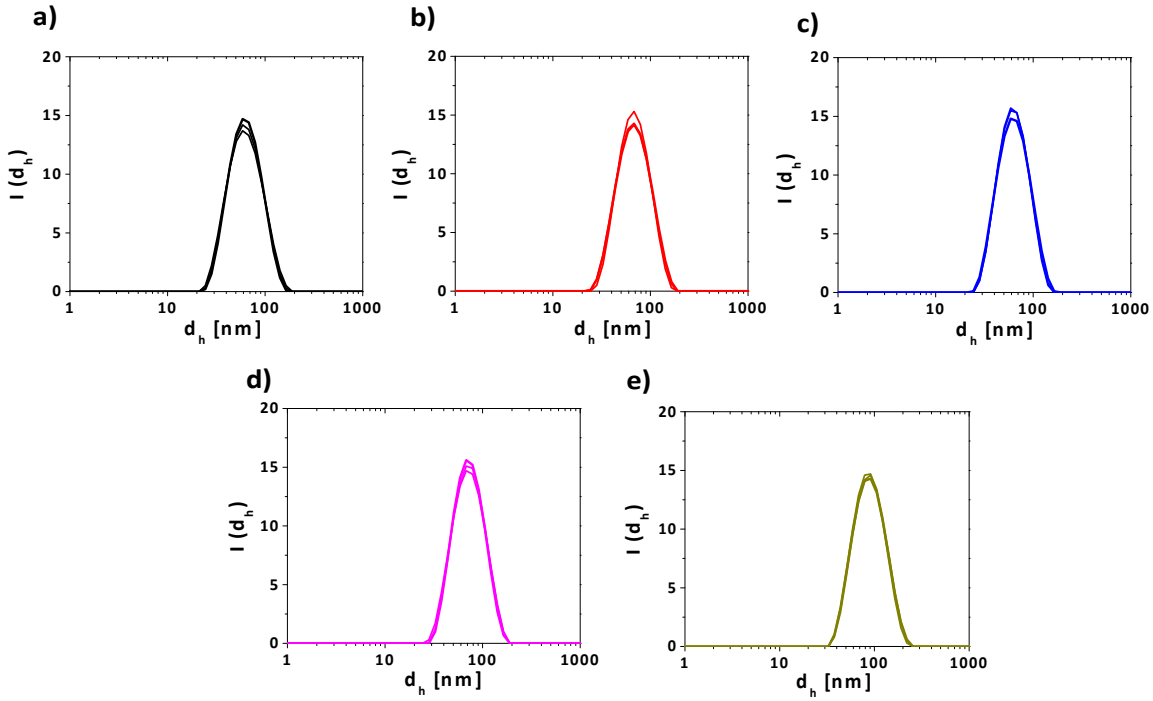


**Figure 27.** Hydrodynamic diameter distribution in intensity ($I(d_h)$) for 50-GNPs after each step of surface modifications: a) citrate-capped b) after their stabilization with mPEG-SH; c) DDA-capped d) PMA-coated and e) after modification with mPEG-$NH_2$ ($M_w$= 5kDa).

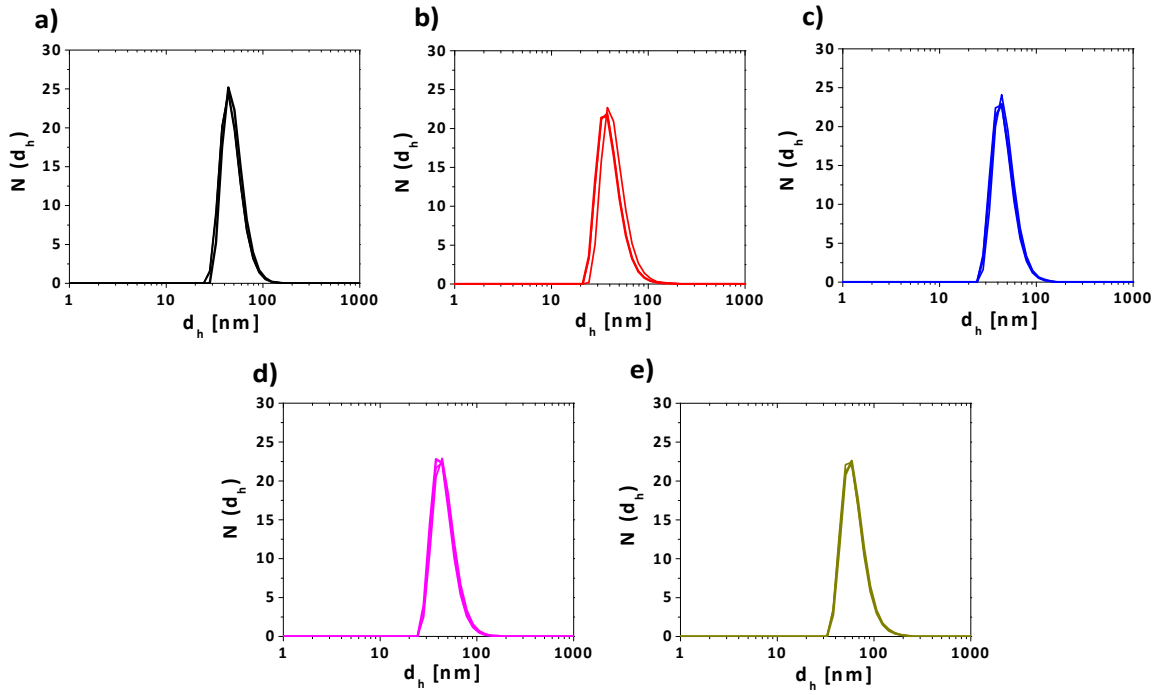


**Figure 28.** Hydrodynamic diameter distribution in number ($N(d_h)$) for 60-GNPs after each step of surface modifications: a) citrate-capped b) after their stabilization with mPEG-SH; c) DDA-capped d) PMA-coated and e) after modification with mPEG-$NH_2$ ($M_w$= 10kDa).

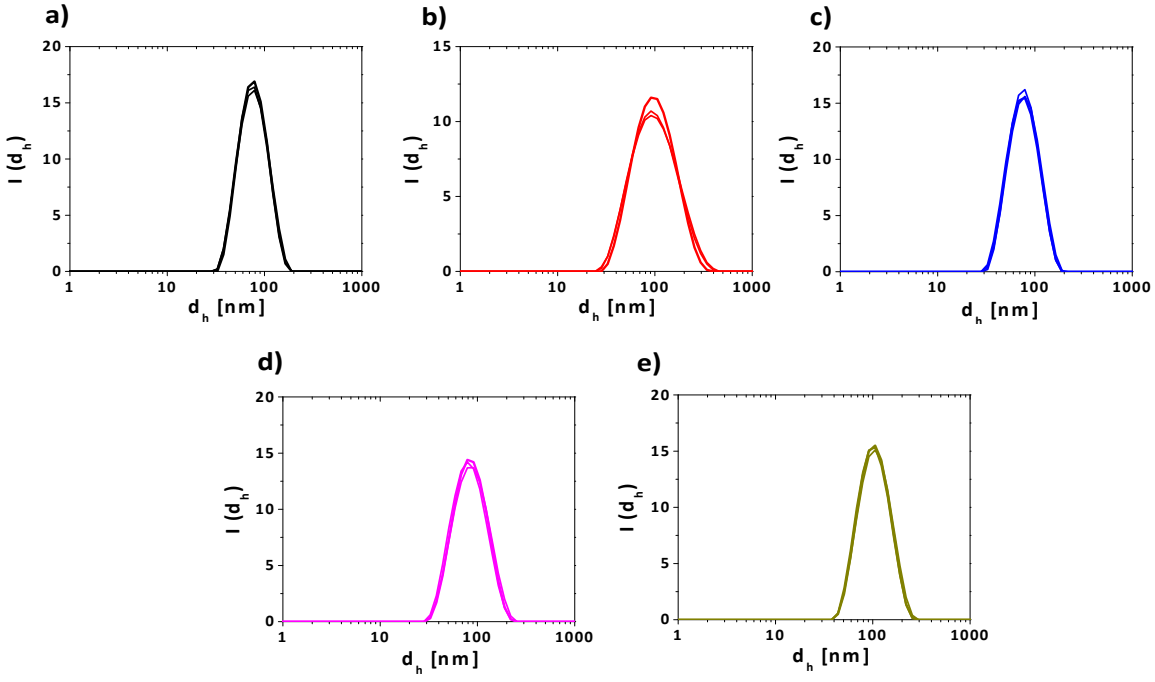


**Figure 29.** Hydrodynamic diameter distribution in intensity ($I(d_h)$) for 50-GNPs after each step of surface modifications: a) citrate-capped b) after their stabilization with mPEG-SH; c) DDA-capped d) PMA-coated and e) after modification with mPEG-$NH_2$ ($M_w$= 10 kDa).

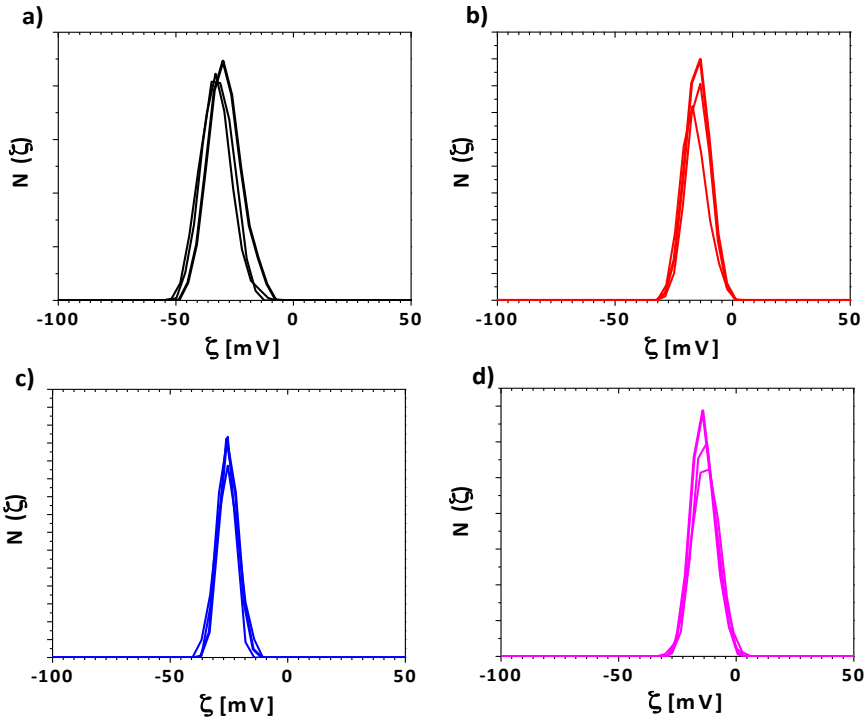


**Figure 30.** ζ-potential distribution (N(ζ)) for 25-GNPs along their surface modifications: a) citrate-capped; b) after their stabilization with mPEG-SH; c) DDA-capped; d) PMA-coated; e) after modification with mPEG-$NH_2$ ($M_w$= 750 Da).

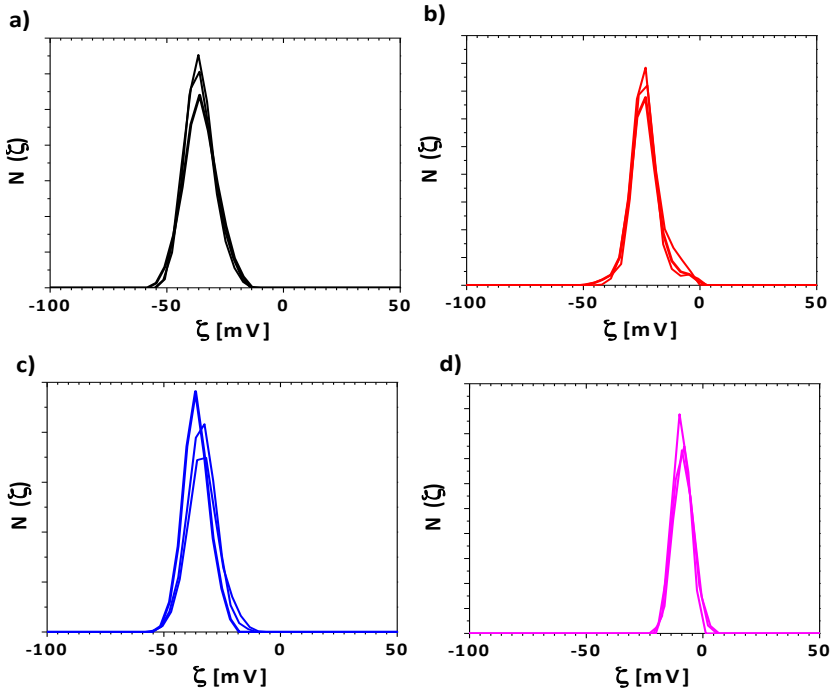


**Figure 31.** ζ-potential distribution (N(ζ)) for 50-GNPs along their surface modifications: a) citrate-capped; b) after their stabilization with mPEG-SH; c) DDA-capped; d) PMA-coated; e) after modification with mPEG-$NH_2$ ($M_w$= 5kDa).

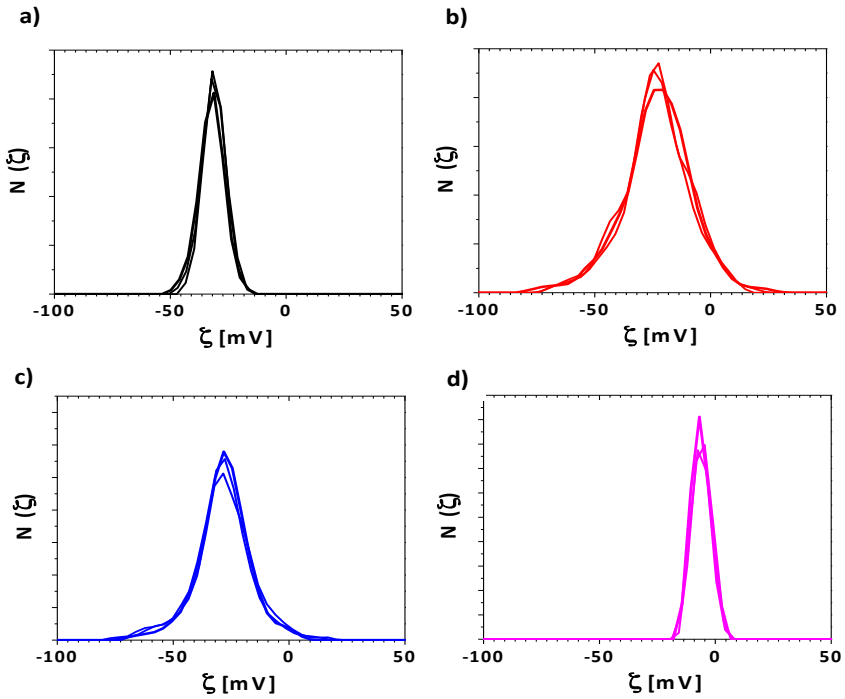


**Figure 32.** ζ-potential distribution (N(ζ)) for 60-GNPs along their surface modifications: a) citrate-capped; b) after their stabilization with mPEG-SH; c) DDA-capped; d) PMA-coated; e) after modification with mPEG-$NH_2$ ($M_w$= 10 kDa).

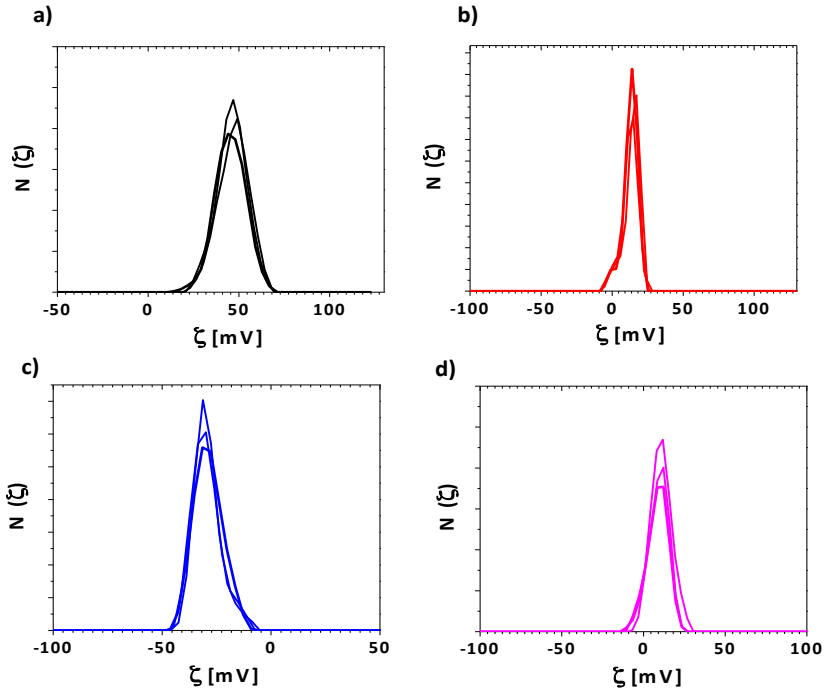


**Figure 33.** ζ-potential distribution (N(ζ)) for 850-GNRs along their surface modifications: a) CTAB-capped; b) after their stabilization with mPEG-SH; c) DDA-capped; d) PMA-coated; e) after modification with mPEG-$NH_2$ ($M_w$= 5 kDa).

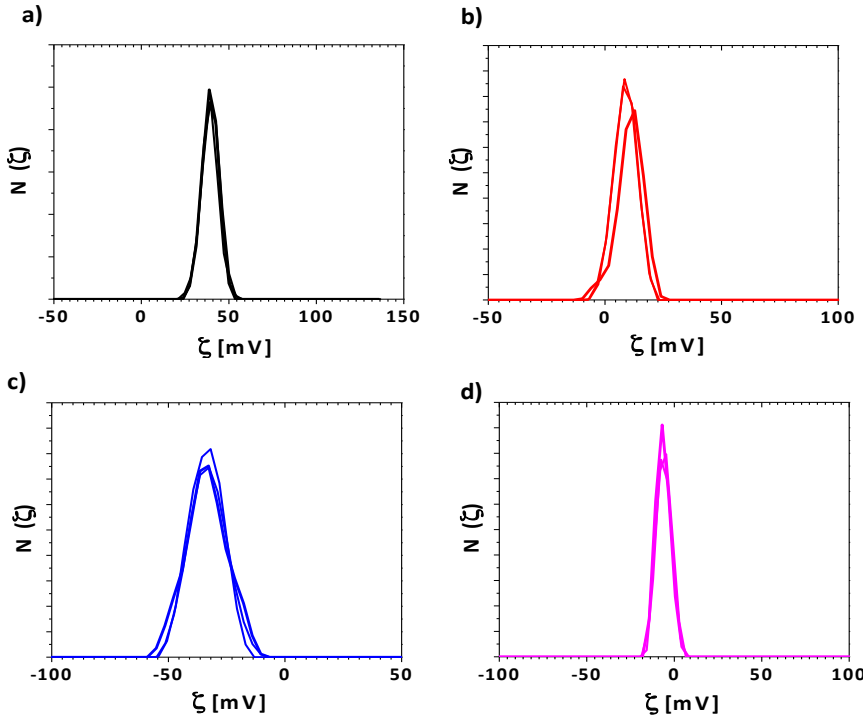


**Figure 34.** ζ-potential distribution (N(ζ)) for 1100-GNRs along their surface modifications: a) CTAB-capped; b) after their stabilization with mPEG-SH; c) DDA-capped; d) PMA-coated; e) after modification with mPEG-$NH_2$ ($M_w$= 10 kDa).

### 1.1.2. Gel electrophoresis

Normally, gel electrophoresis is used for purification of the particles by the separation from other molecules depending on their size, shape and charge. Also, it can be used to check the colloidal stability of the NPs. The particles which have a stable surface coating, can run through the gel without precipitation or aggregation. For using gel electrophoresis, 1 % of gel was prepared by dissolving 1.75 g of Agarose in 175 mL of Trisborate-EDTA buffer (TBE 0.5x) and placing the solution into the gel tray. After 1 h, the gel was placed into the electrophoresis chamber, which is filled with TBE buffer. The sample was mixed with a specific volume of a gel-loading buffer to increase the density of the sample and loaded to the gel. 20 µL of 10 nm commercial gold particles stabilized with triphenyl phosphine (bis(p-sulfonatophenyl) phenylphosphine dehydratwere loaded to the gel and used as reference[136]. After that, an electric field of 10 $V \cdot cm^{-1}$ was applied for 1 h and the particles started to move through the gel because of their surface charge. After that, the piece of gel was removed from the gel chamber and filmed using digital camera.

The migration of the particles after PMA through the gel is an indication for the colloidal stability of the particles, which is due to electrostatic repulsion of -COOH. As shown in Figure 35, the motion speed of the particles depends on the size and the charge of NPs. Also, all the particles have single and narrow band through the gel and this is an indication of that all NPs are uniformly wrapped by the polymer due to the good coating process.

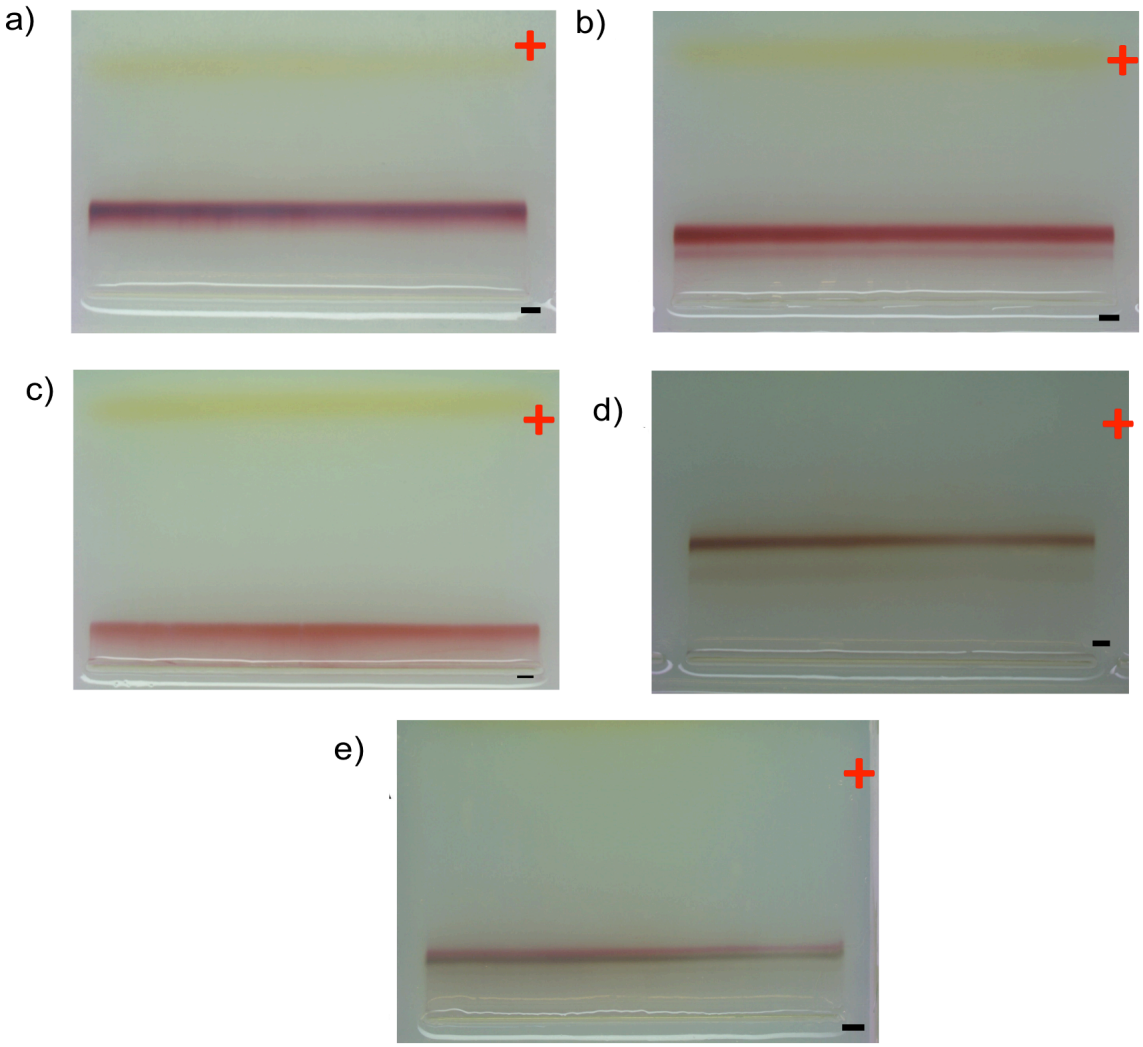


**Figure 35**. Mothion path of PMA coated a) 25-GNPs; b) 50-GNPs; c) 60-GNPs; d) 850-GNRs and e) 1100-GNRs through a 1% agarose gel and the electric field was 10 $V \cdot cm^{-1}$ for 1 h.

In the following Figure 36, the motion path of the particles through the gel is broaden due to the attachment of the PEI (used as cross-linker) to the surface of the NPs during the polymer coating process as I mentioned in section 2.3.

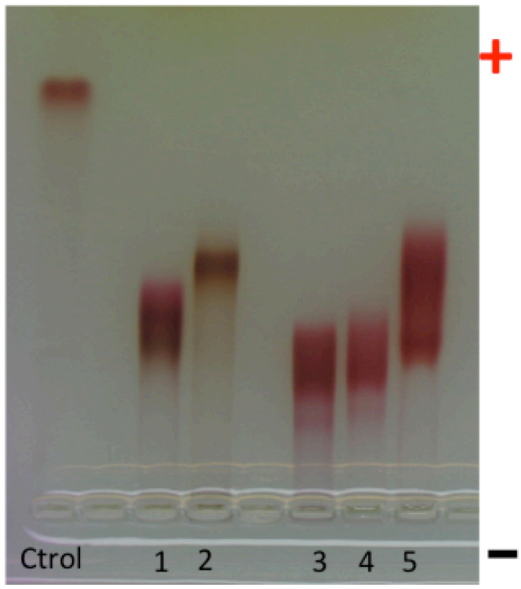


**Figure 36**. Motion path of PMA+PEI coated a) 25-GNPs; b) 50-GNPs; c) 60-GNPs; d) 850-GNRs and e) 1100-GNRs through a 1% agarose gel and the electric field was 10 $V \cdot cm^{-1}$ for 1 h. 10 nm GNPs phosphine-capped was used as control.

As I mentioned before, the PMA coating make the NPs surface rich in negative –COOH groups. These groups are used during the linkage of mPEG-$NH_2$ to the surface of NPs *via* EDC chemistry. Then, the surface of the NPs will be rich with non-charged methoxy groups, which decrease the negativity of the NPs surface. As shown in Figure 37, the motion speed of the particles after PMA is much faster than the speed of the particles after PEGylation and in some cases, especially in case of 60-GNPs and 850-GNRs, the particles didn't move (or just a little bit) through the gel when the surface is saturated with PEG.

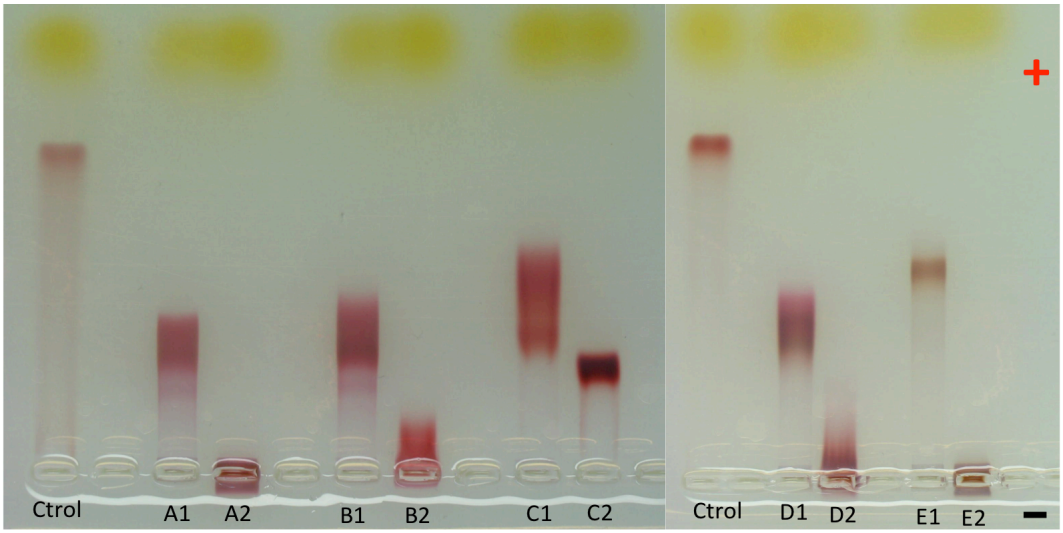


**Figure 37**. Mothion path of the particles coated with PMA+PEI and PMA+PEI+PEG through a 1% agarose gel run at 100 V for 1 h. From left to right: (A1, A2) correspond to 60-GNPs coated with PMA+PEI and with PMA+PEI+PEG ($M_w$ of PEG = 10 kDa) respectively; (B1, B2) correspond to 50-GNPs coated with PMA+PEI and with PMA+PEI+PEG ($M_w$ of PEG = 5 kDa) respectively; (C1, C2) corresponds to 25-GNPs coated with PMA+PEI and with PMA+PEI+PEG ($M_w$ of PEG = 750 Da) respectively; (D1, D2) correspond to 850-GNRs PMA-coated with PMA+PEI and with PMA+PEI+PEG ($M_w$ of PEG = 5 kDa) respectively; and (E1, E2) correspond to 1100-GNRs PMA-coated with PMA+PEI and with PMA+PEI+PEG ($M_w$ of PEG = 10 kDa) respectively. 10 nm GNPs phosphine-capped was used as control.

### 1.1.3. Transmission electron microscopy (TEM)

TEM was used to get information about the particles core dimensions, shape, monodispersity and agglomeration. For TEM measurement, the sample was prepared depend on the type of solvent. For the sample dispersed in organic solvent, the sample was placed at the copper grid and dried for short time at room temperature. For the sample dispersed in aqueous solvent, the copper grid was converted to be hydrophilic by dipping it in a little bit of ethanol in closed tube for about 4 hours. Then, 20 µL of the sample was placed at the copper grid and the tube was opened overnight to allow the sample to dry.

As shown in the following Figures 38-42, the Au cores appear as black spots (in case of SGNPs) and gray spots (in case of GNRs) with high contrast. The intermediate space between NPs is indication for the presence of surfactants, which prevent the Au cores from agglomeration.

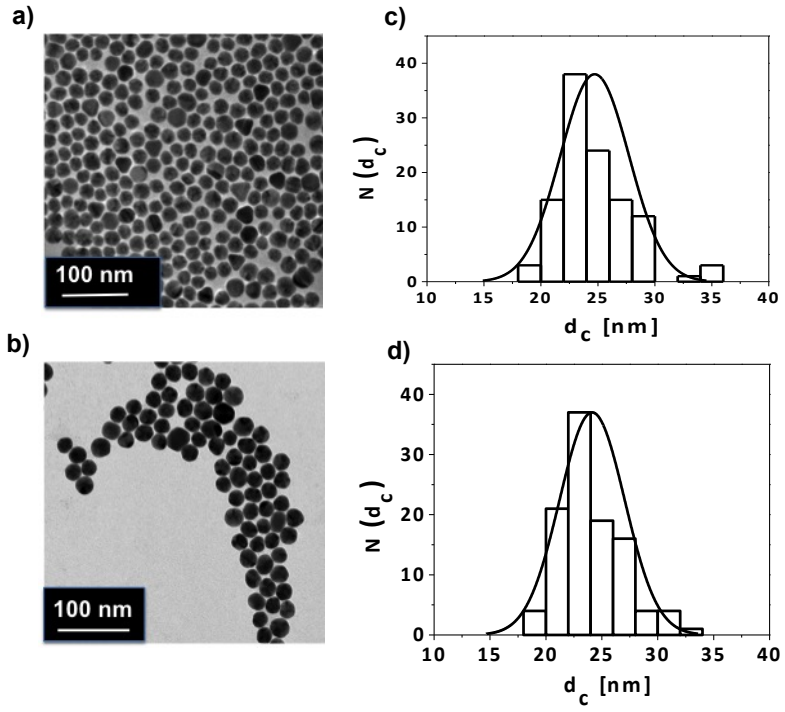


**Figure 38**. TEM picture of 25-GNPs: a) DDA-capped; b) PMA-coated NPs; and core diameter ($d_c$) size distribution ($N(d_c)$) graph of c) DDA-capped with $d_c$ =24.7 ± 3.0 nm and d) PMA-coated NPs with $d_c$ =24.1 ± 3.0 nm. The scale bars correspond to 100 nm.

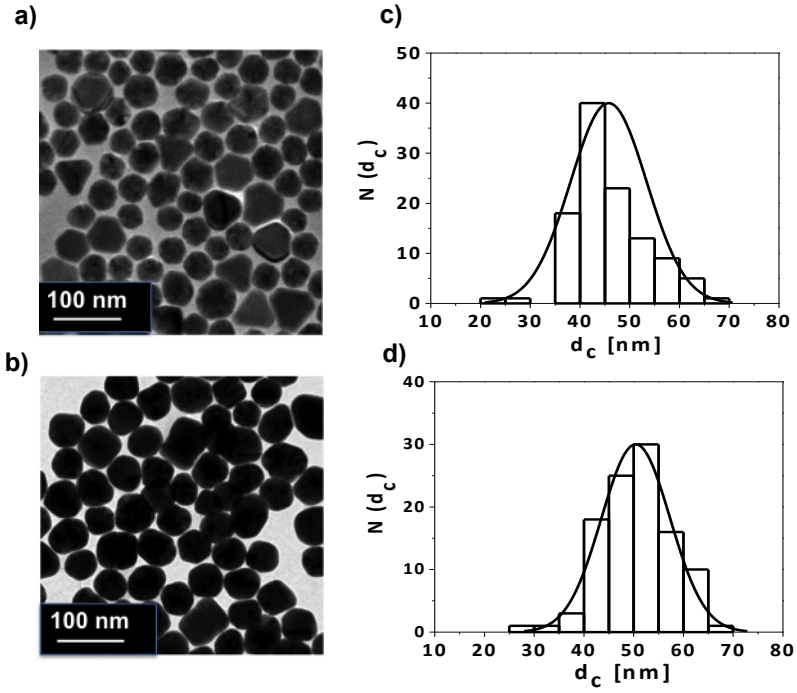


**Figure 39**. TEM picture of 50-GNPs: a) DDA-capped and b) PMA-coated NPs; and core diameter ($d_c$) size distribution ($N(d_c)$) graph of c) DDA-capped with $d_c$ =45.7 ± 7.7 nm and d) PMA-coated NPs with $d_c$ =50.4 ± 6.9 nm. The scale bars correspond to 100 nm.

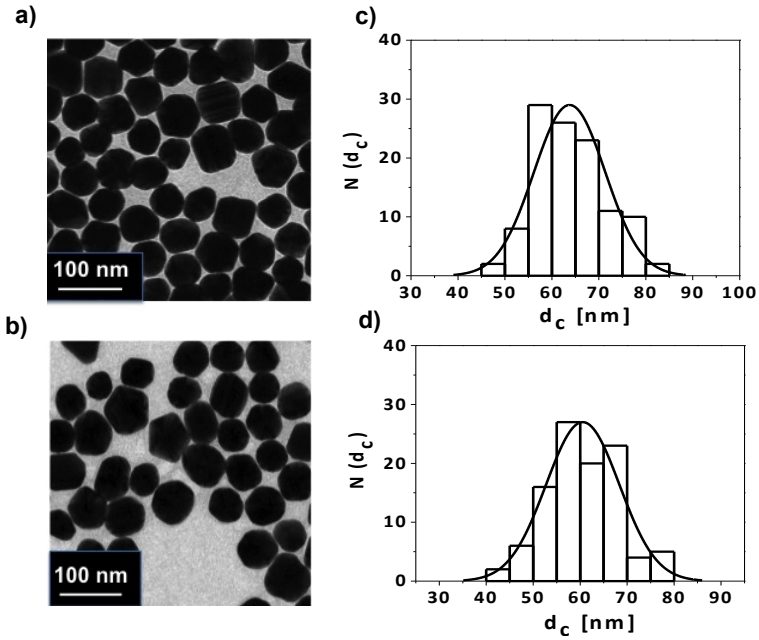


**Figure 40**. TEM picture of 60-GNPs a) conjugated with mPEG-SH (750 Da) b) PMA-coated NPs; and core diameter ($d_c$) size distribution ($N(d_c)$) graph of c) conjugated with mPEG-SH with $d_c$ =63.8 ±7.6 nm and d) PMA-coated NPs with $d_c$ =60.5 ± 7.8 nm. The scale bars correspond to 100 nm.

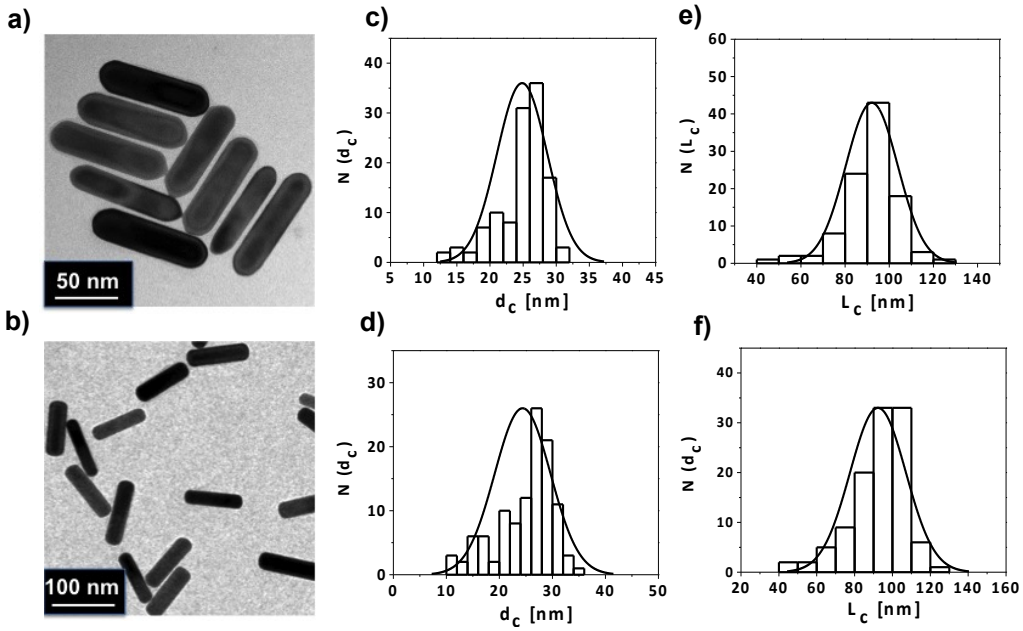


**Figure 41**. TEM picture of 850-GNRs: a) CTAB-capped and b) PMA-coated NPs; core diameter ($d_c$) size distribution ($N(d_c)$) graph of the GNRs thickness of c) CTAB-capped with $d_c$ =24.5 ± 4.8 nm and d) PMA-coated NPs with $d_c$ =24.4 ± 5.3 nm. The core length ($L_c$) size distribution ($N(L_c)$) graph of the GNRs length of e) CTAB-capped with $L_c$=92.1 ±11.8 nm and f) PMA-coated with $L_c$=92.3 ± 14.8 nm. The scale bars correspond to a) 50 nm and b) 100 nm.

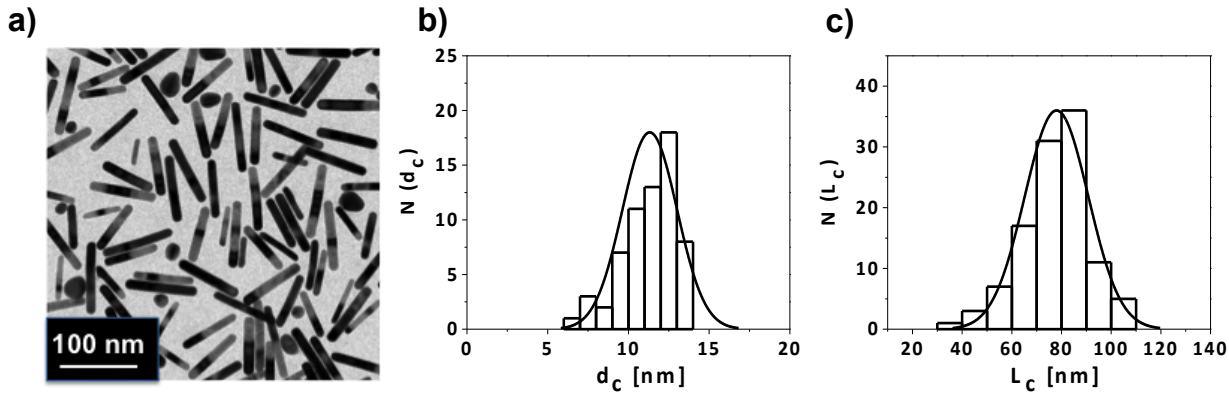


**Figure 42**. TEM picture of 1100-GNRs: a) PMA-coated NPs; b) core diameter ($d_c$) size distribution ($N(d_c)$) graph of the GNRs thickness with $d_c$= 11.3 ±1.7 nm and c) core length ($L_c$) size distribution ($N(L_c)$) of the GNRs length with $L_c$= 77.3 ± 12.8 nm. The scale bar corresponds to 100 nm.

## 3. Stability assays

Aiming to understand and assess the colloidal stability of the NPs. The NPs stability at different media, see Table 8, was tested using different techniques (*e.g.* UV/Vis spectroscopy and DLS). Those media were selected to prove the effect of the presence of high ionic strength, protein concentration, and a combination of both. All of them are media used in the most tradition *in vitro* experiments.

**Table 8**. Composition of all media used for studying the stability of NPs[137]. [a]Fresh Mili-Q water.[b]Phosphate buffered saline.[c]Dulbecco's modified Eagle's medium. [d]Penicillin/streptomycin. [e]L-glutamin.[f]Bovine serum albumin.[g]Fetal bovine serum.

| Medium / Compound | # 1 | # 2 | # 3 | # 4 | # 5 | # 6 | # 7 | # 8 |
|---|---|---|---|---|---|---|---|---|
| Solvent | Water[a] | PBS[b] | DMEM[c] | PBS | DMEM | PBS | DMEM | DMEM |
| 1% P/S[d] | - | - | - | yes | yes | - | yes | yes |
| 1% L-Glu[e] | - | - | - | yes | yes | - | yes | yes |
| 800 µM BSA[f] | - | - | - | - | - | yes | yes | 10% FBS[g] |

## 3.1. Stability of three surface coating (NPs@PMA, NPs@PMA+PEI and NPs@PMA+PEI+PEG) in complete cell media.

In this case, the stability of all NPs with three surface coating (NPs@PMA, NPs@PMA+PEI and NPs@PMA+PEI+PEG (PEGylated NPs)) in complete cell media[137] (media 8, Table 7) was tested using UV-Vis spectroscopy. The particles were incubated in complete cell media for 3 days (d) and at different points of time, the UV spectra were recorded as shown in the following Figures 43-45.

As indicated by the UV spectra, at the initial stages of NPs immersion in cell media, a SPR broadening was observed for PMA-coated 50 and 60-GNPs indication for the NPs stability defect. This broadening was disappearing gradually with time due to adsorption and the arrangement of the proteins on the NPs surface. The attachment of the PEI to the NPs surface help to avoid this SPR broadening, which is prevented completely after PEGylation of the same NPs. Notice that, all the particles after PEGylation are highly stable in the cell media for at least 3 d.

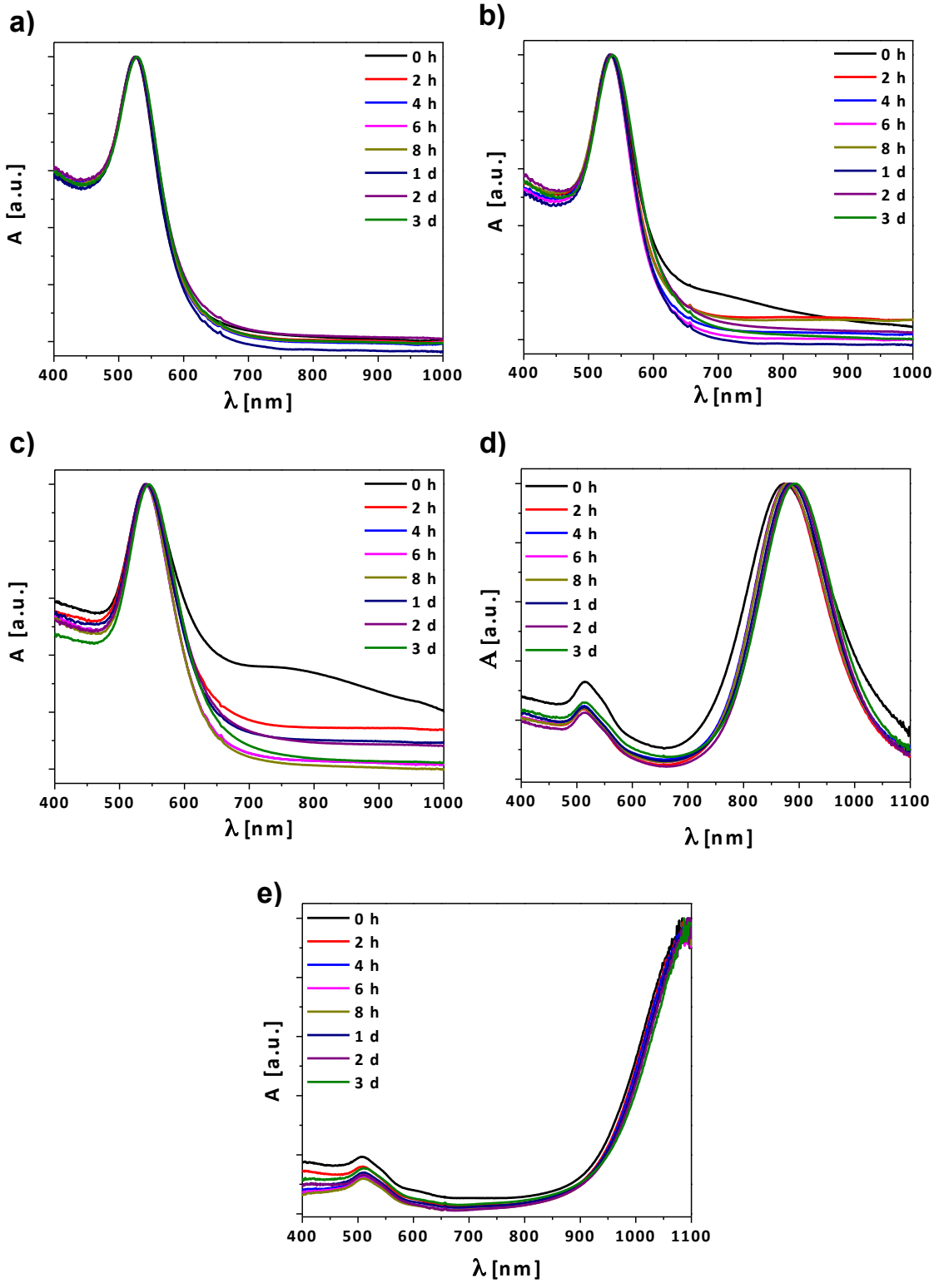


**Figure 43.** Normalized absorption spectra of the PMA-coated NPs in complete cell media for 3 d: a) 25-GNPs; b) 50-GNPs; c) 60-GNPs; d) 850-GNRs and e) 1100-GNRs.

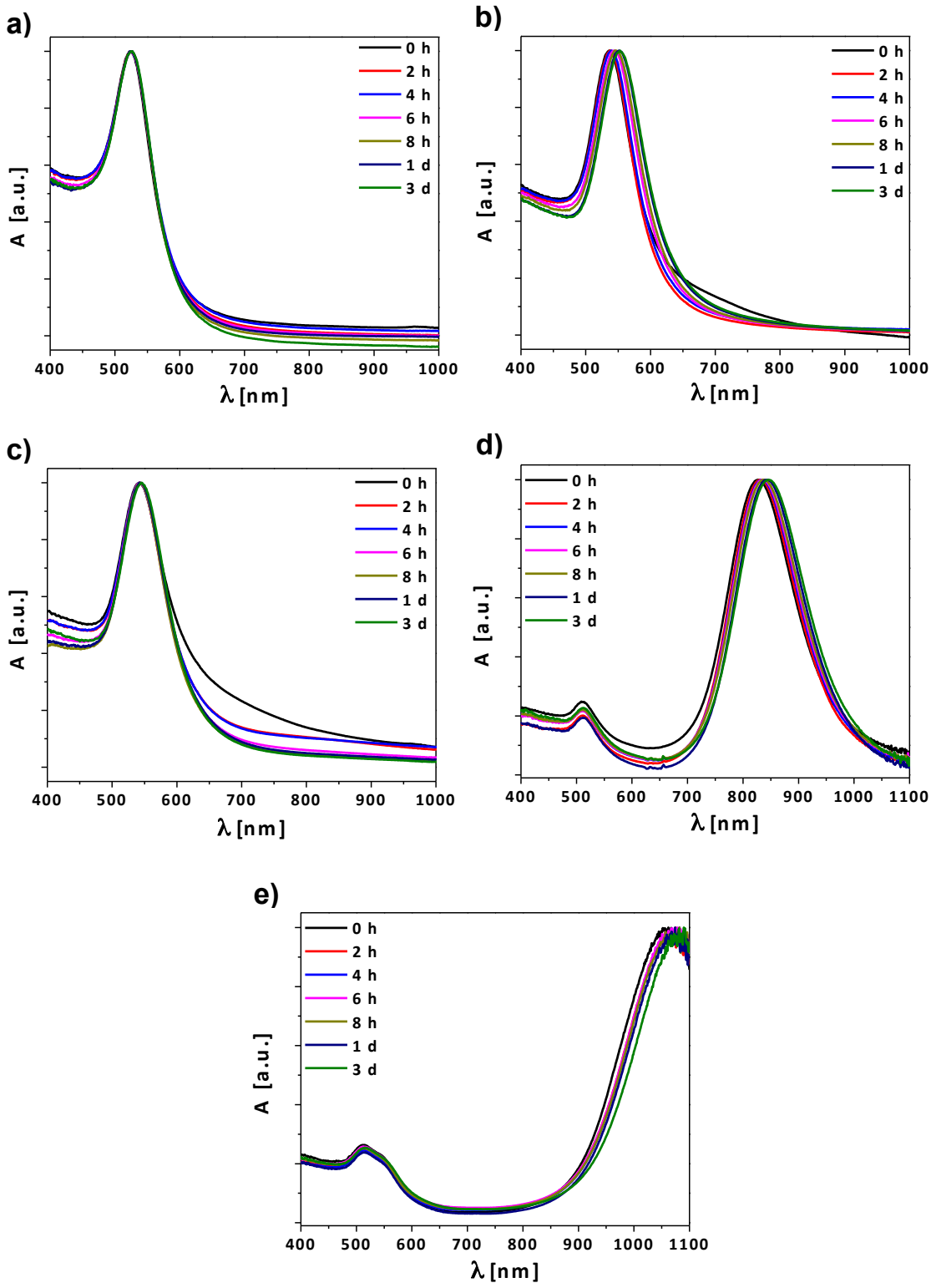


**Figure 44.** Normalized absorption spectra of the PMA+PEI-coated NPs in complete cell media for 3 d; a) 25-GNPs; b) 50-GNPs; c) 60-GNPs; d) 850-GNRs and e) 1100-GNRs.

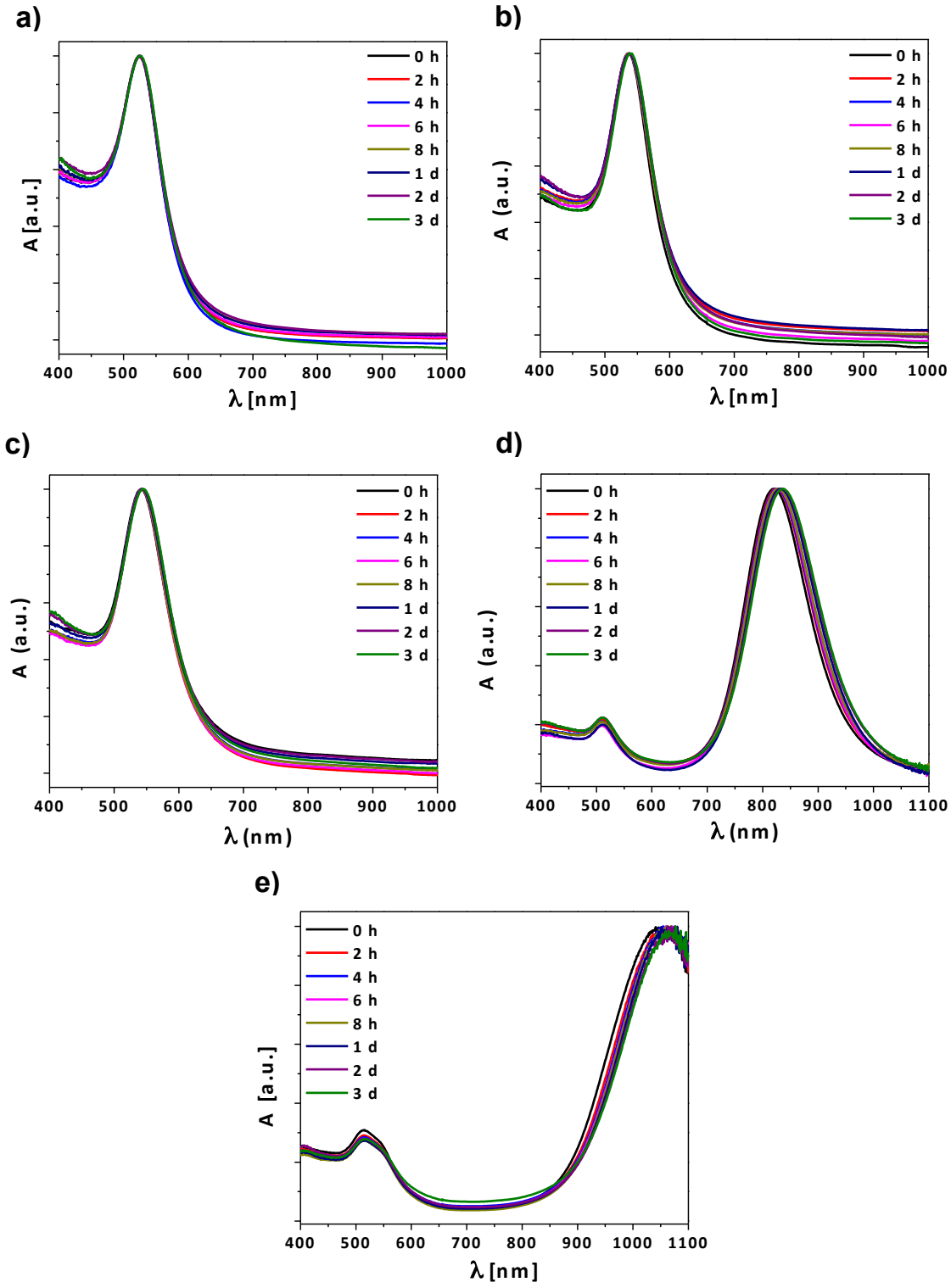


**Figure 45.** Normalized absorption spectra of the PEGylated NPs in the media 8, up to 3 days, for: a) 25-GNPs; b) 50-GNPs; c) 60-GNPs; d) 850-GNRs and e) 1100-GNRs.

## 3.2. Stability of PEGylated NPs in different media.

The colloidal stability of all PEGylated NPs was studied in different media as shown in Table 7 by using UV-Vis spectroscopy and DLS. The NPs were incubated in the different media for 3 days and at different time-points, the UV spectra and the hydrodynamic diameter were recorded. Results are shown in the following Figures 46-57. The concentration of 1100-GNRs, 850-GNRs, 60-GNPs, 50-GNPs and 25-GNPs were 0.094 nM, 0.16 nM, 0.016 nM, 0.04 nM and 0.42 nM respectively. The original media were taken as blank in the UV-Vis measurements and then the changes in absorption could be identified as interaction between medium and the NPs.

*Study of the stability of NPs in different media by UV-Vis spectroscopy:*

The aggregation of all NPs was observed when the NPs were incubated in media (2, 3, 4 and 5) due to the high ionic strength of the media. In some of the free-protein media, most of NPs were completely aggregated after 8 h. This indicates that the presence of salt in the media will compromise the NPs stability due to the screening of the NPs surface charge. In the media containing proteins (6, 7 and 8), the stability of all the NPs was improved compared to the stability in free-protein media and this due to adsorption of proteins (protein corona) on the NPs surface, which improve their stability. Shifting the SPR a few nanometers to higher wavelength in UV spectra is indication to the formation of protein corona around the NPs. These results were also confirmed by DLS.

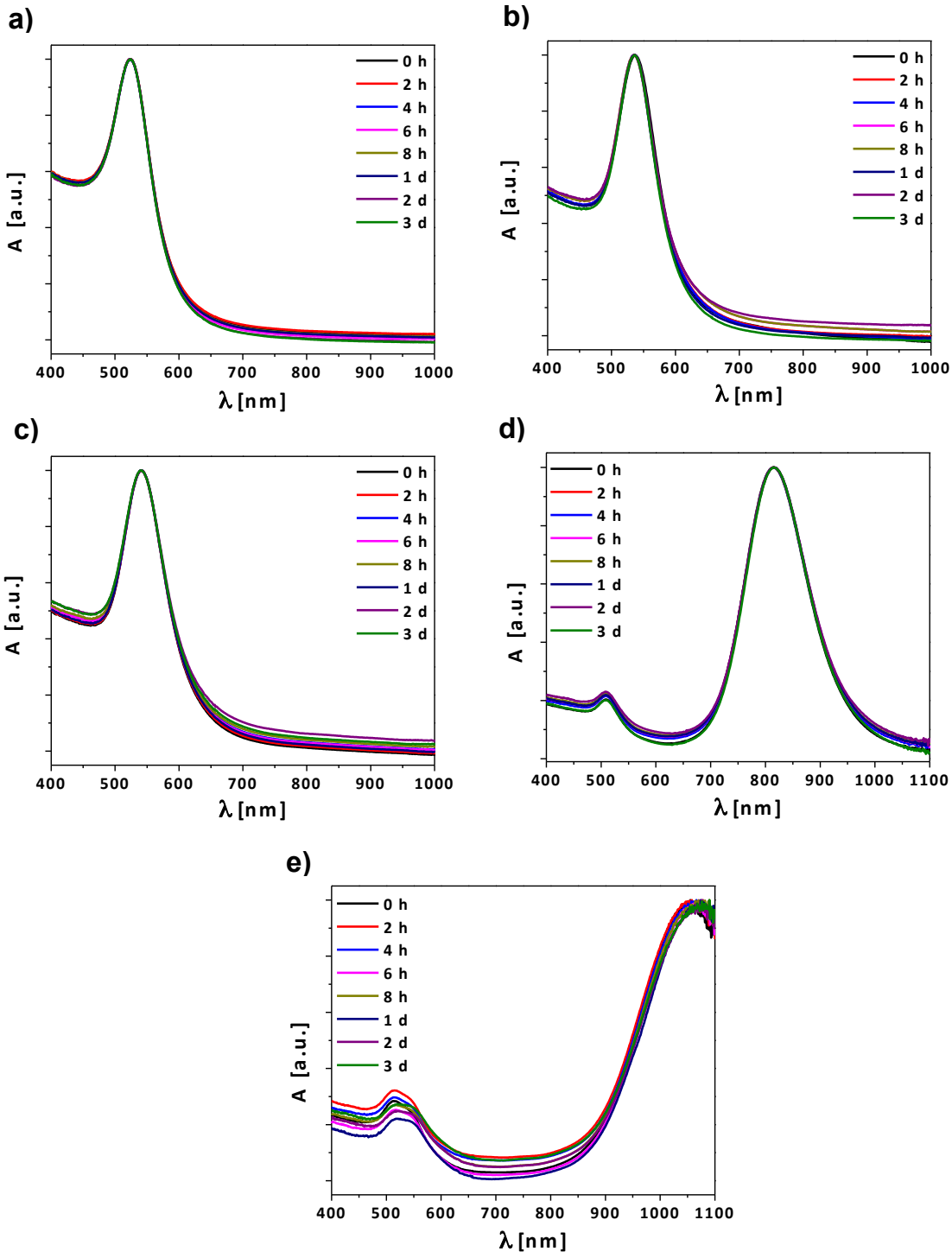


**Figure 46.** Normalized absorption spectra of the PEGylated NPs in the media 1, at different time points, for: a) 25-GNPs; b) 50-GNPs; c) 60-GNPs; d) 850-GNRs and e) 1100-GNRs.

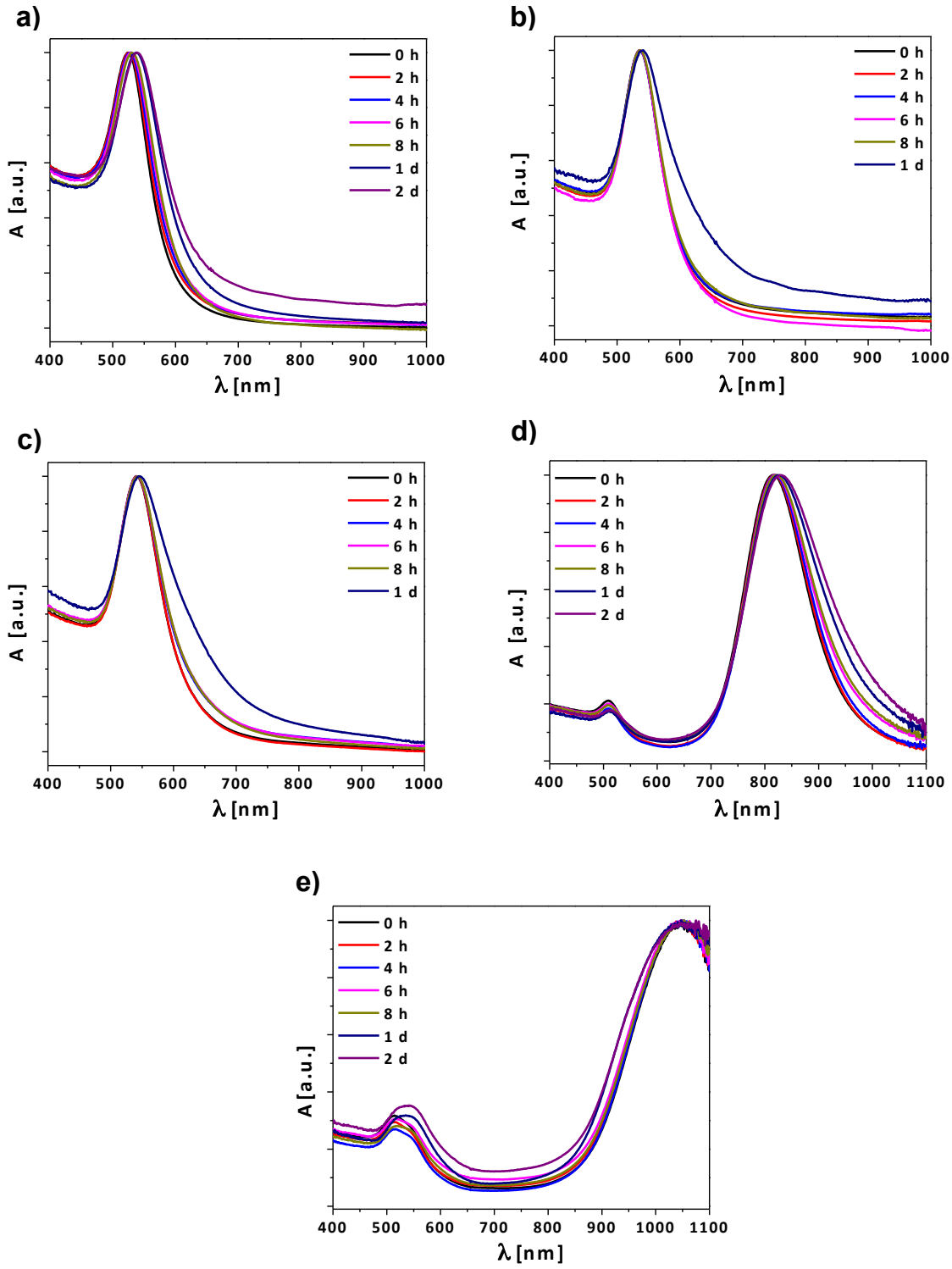


**Figure 47.** Normalized absorption spectra of the PEGylated NPs in the media 2, at different time points, for: a) 25-GNPs; b) 50-GNPs; c) 60-GNPs; d) 850-GNRs and e) 1100-GNRs.

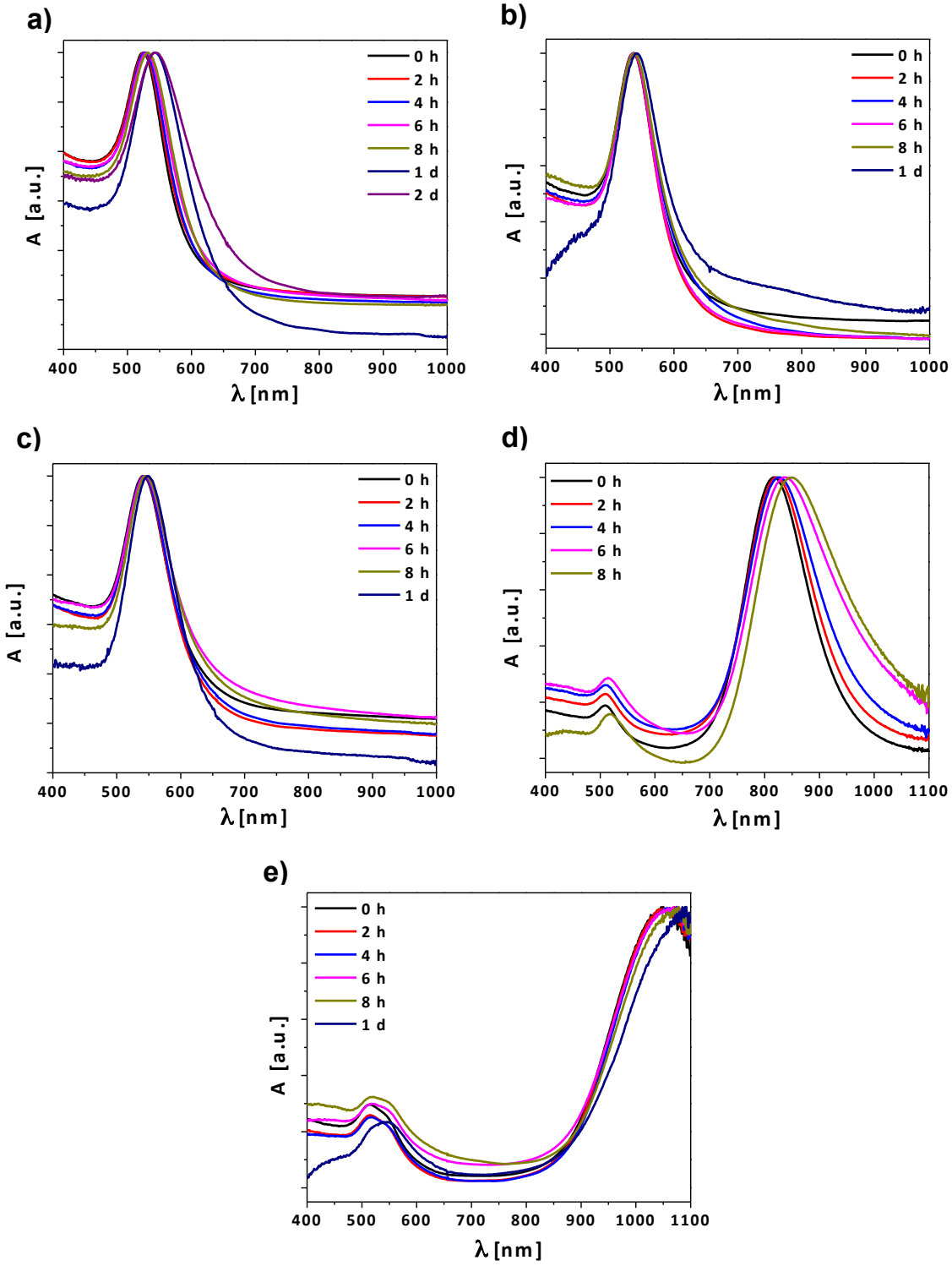


**Figure 48.** Normalized absorption spectra of the PEGylated NPs in the media 3, at different time points, for: a) 25-GNPs; b) 50-GNPs; c) 60-GNPs; d) 850-GNRs and e) 1100-GNRs.

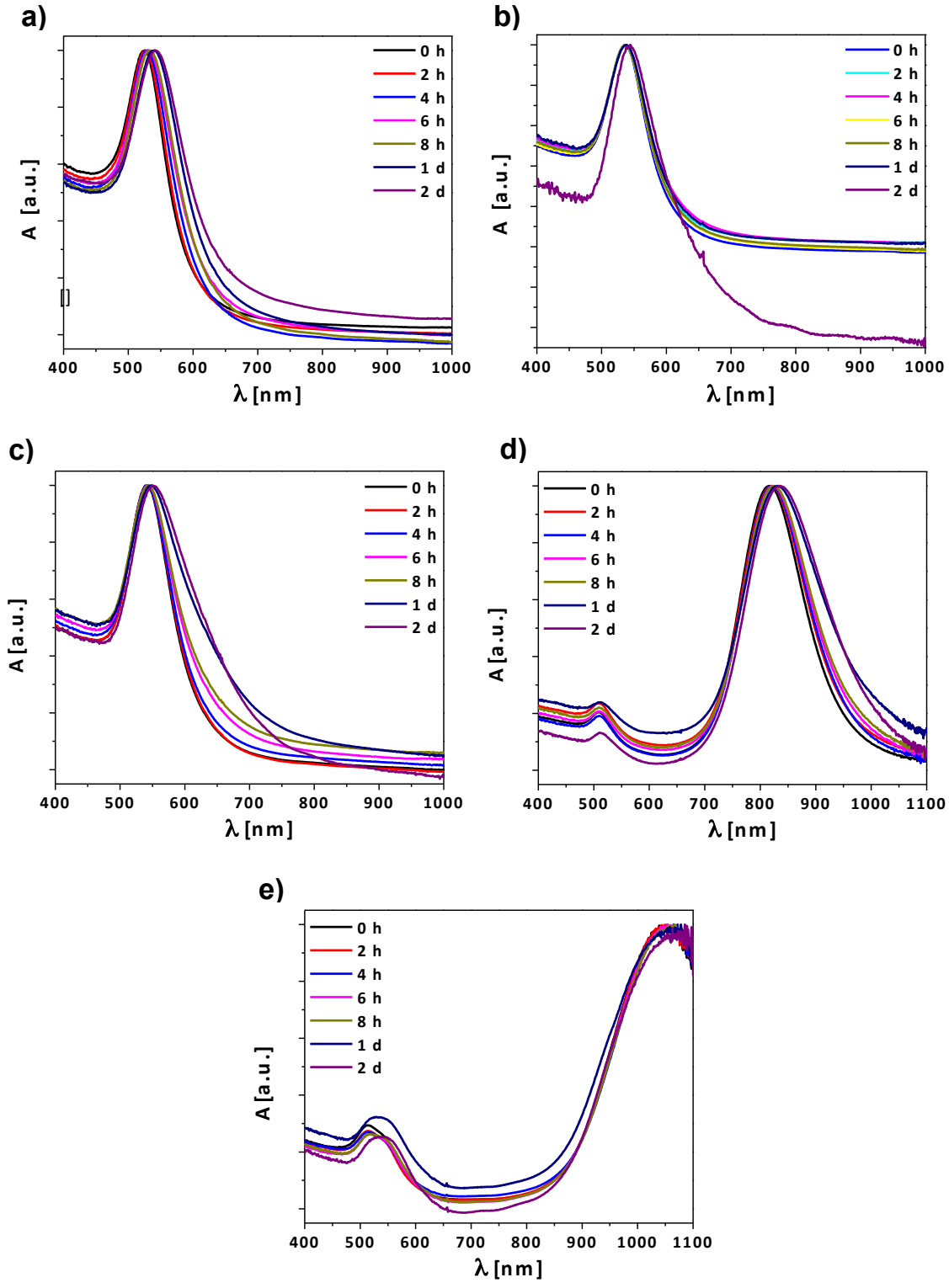


**Figure 49.** Normalized absorption spectra of the PEGylated NPs in the media 4, at different time points, for: a) 25-GNPs; b) 50-GNPs; c) 60-GNPs; d) 850-GNRs and e) 1100-GNRs.

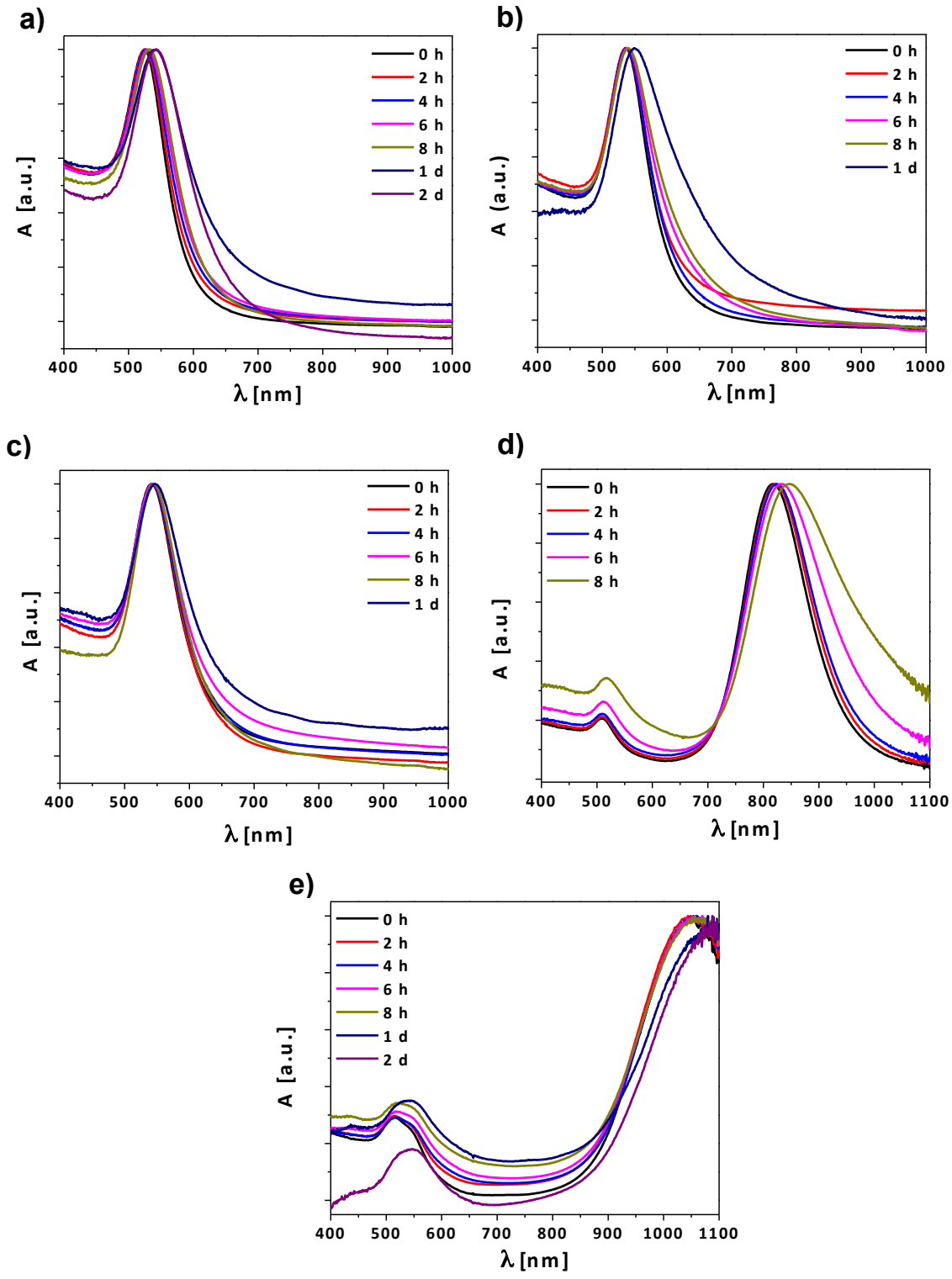


**Figure 50.** Normalized absorption spectra of the PEGylated NPs in the media 5, at different time points, for: a) 25-GNPs; b) 50-GNPs; c) 60-GNPs; d) 850-GNRs and e) 1100-GNRs.

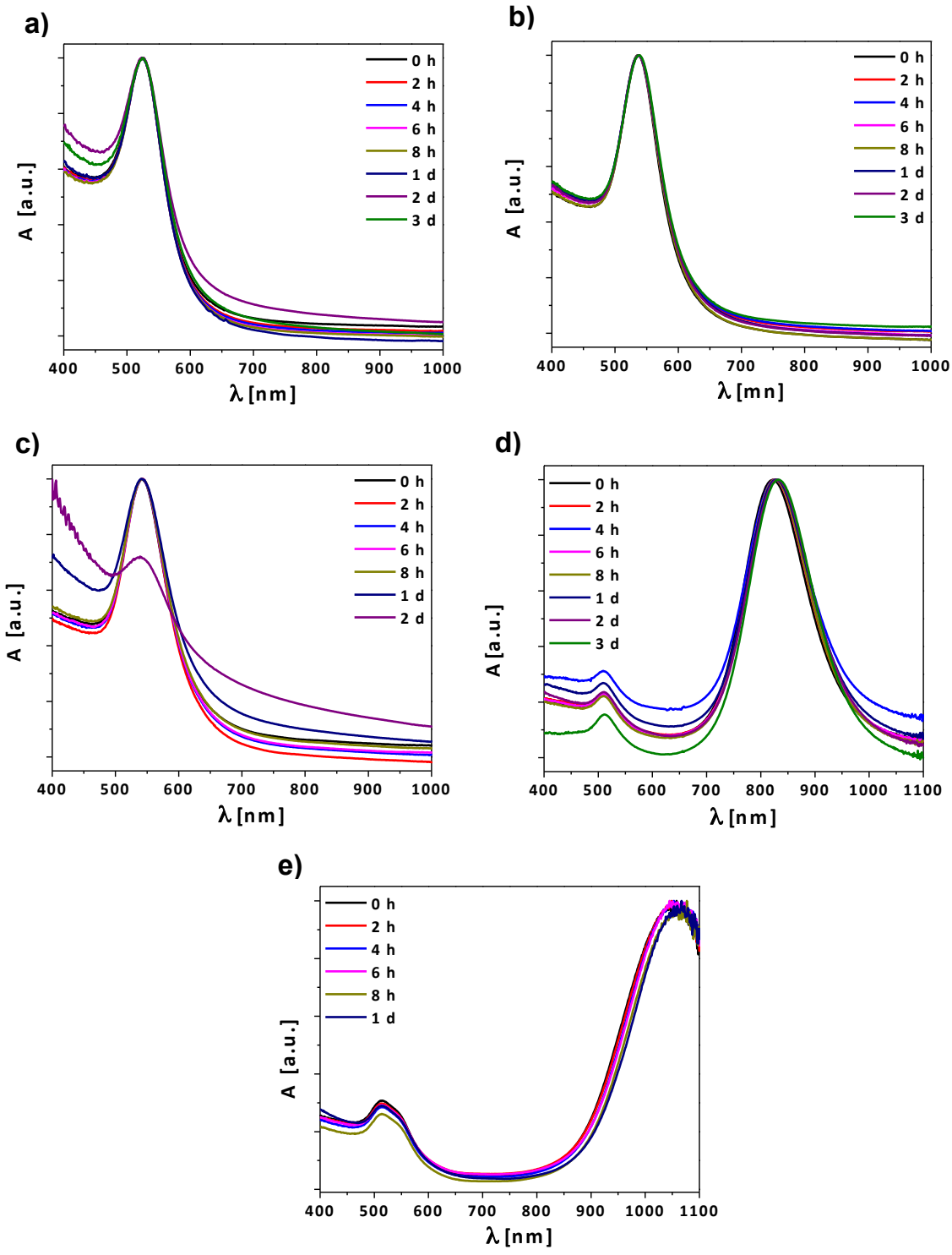


**Figure 51.** Normalized absorption spectra of the PEGylated NPs in the media 6, up to 3 days, for: a) 25-GNPs; b) 50-GNPs; c) 60-GNPs; d) 850-GNRs and e) 1100-GNRs.

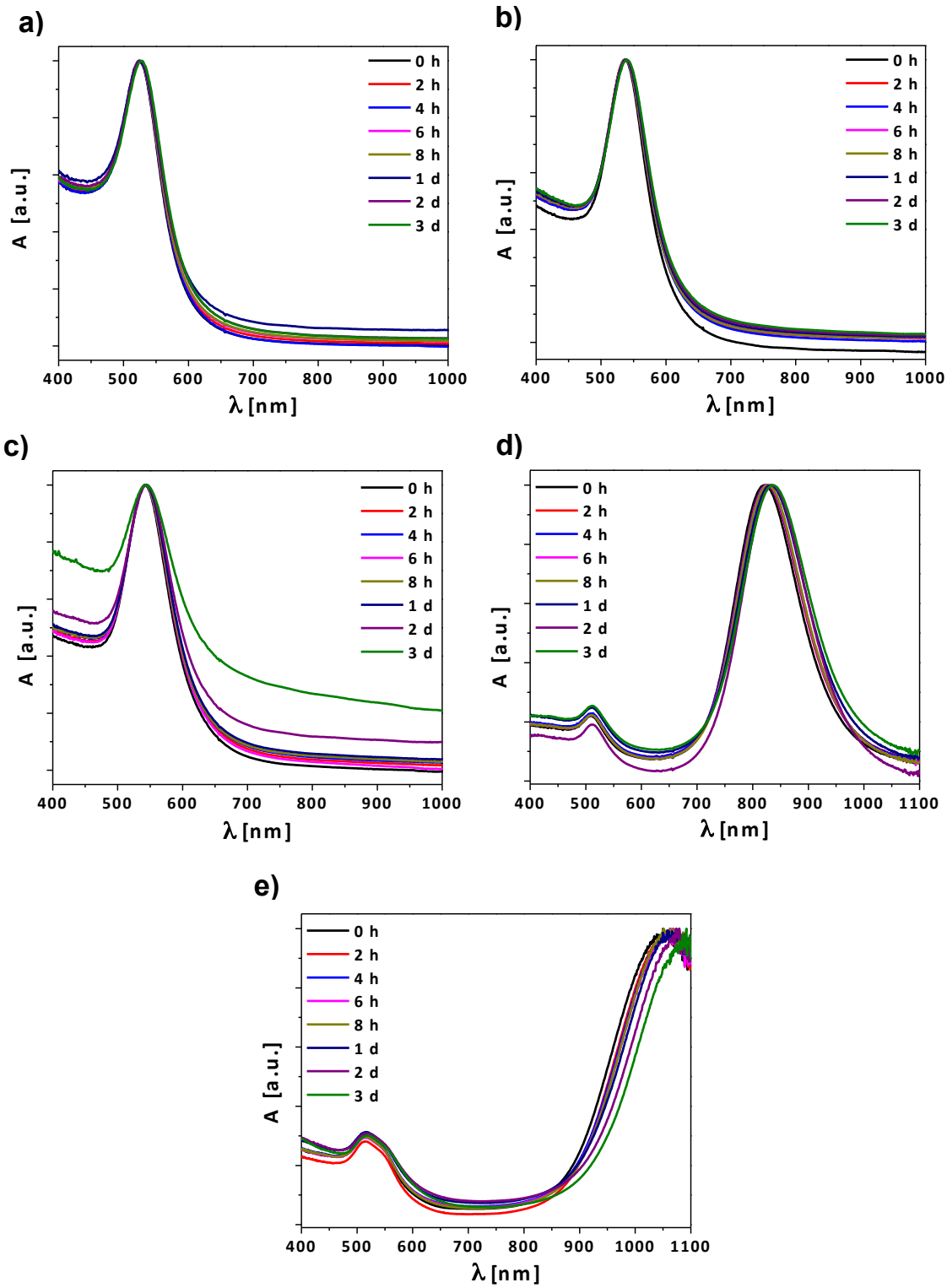


**Figure 52.** Normalized absorption spectra of the PEGylated NPs in the media 7, up to 3 days, for: a) 25-GNPs; b) 50-GNPs; c) 60-GNPs; d) 850-GNRs and e) 1100-GNRs.

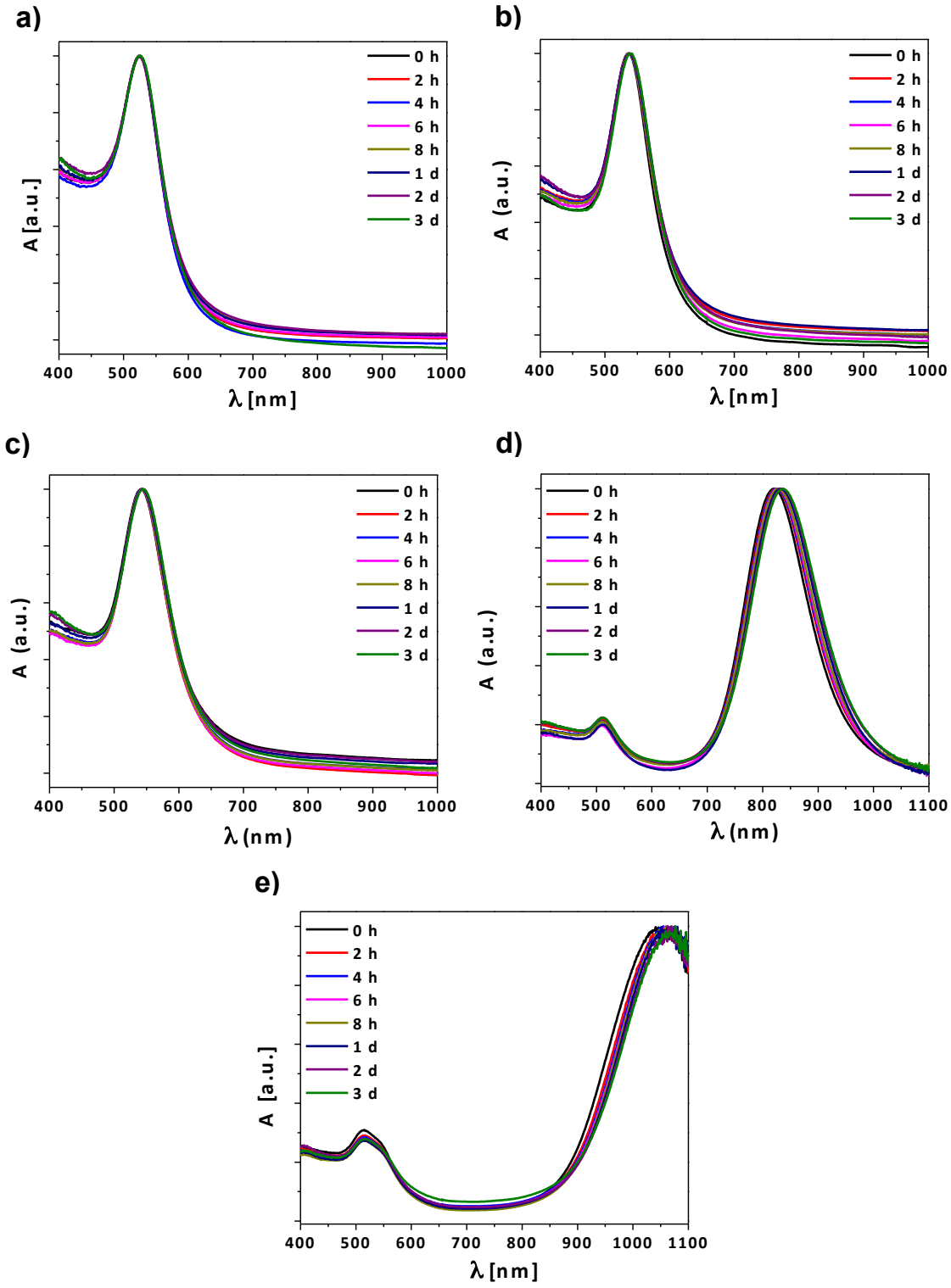


**Figure 53.** Normalized absorption spectra of the PEGylated NPs in the media 8, up to 3 days, for: a) 25-GNPs; b) 50-GNPs; c) 60-GNPs; d) 850-GNRs and e) 1100-GNRs.

*Study of the stability of NPs in different media by DLS:*

DLS results are in agreement with the UV-Vis results where the aggregation of the NPs was detected after 8 h in protein-free media (2, 3, 4 and 5). On the other hand, the particles are more stable in proteins containing media (6, 7 and 8) and the hydrodynamic diameter was shifted to higher values due to the formation of protein corona around the NPs. The DLS was used for GNRs as quantitative method for checking the colloidal stability and has no physical meaning. In the following figures (Figure 54-57) the results for all the NPs in all the media are summarized.

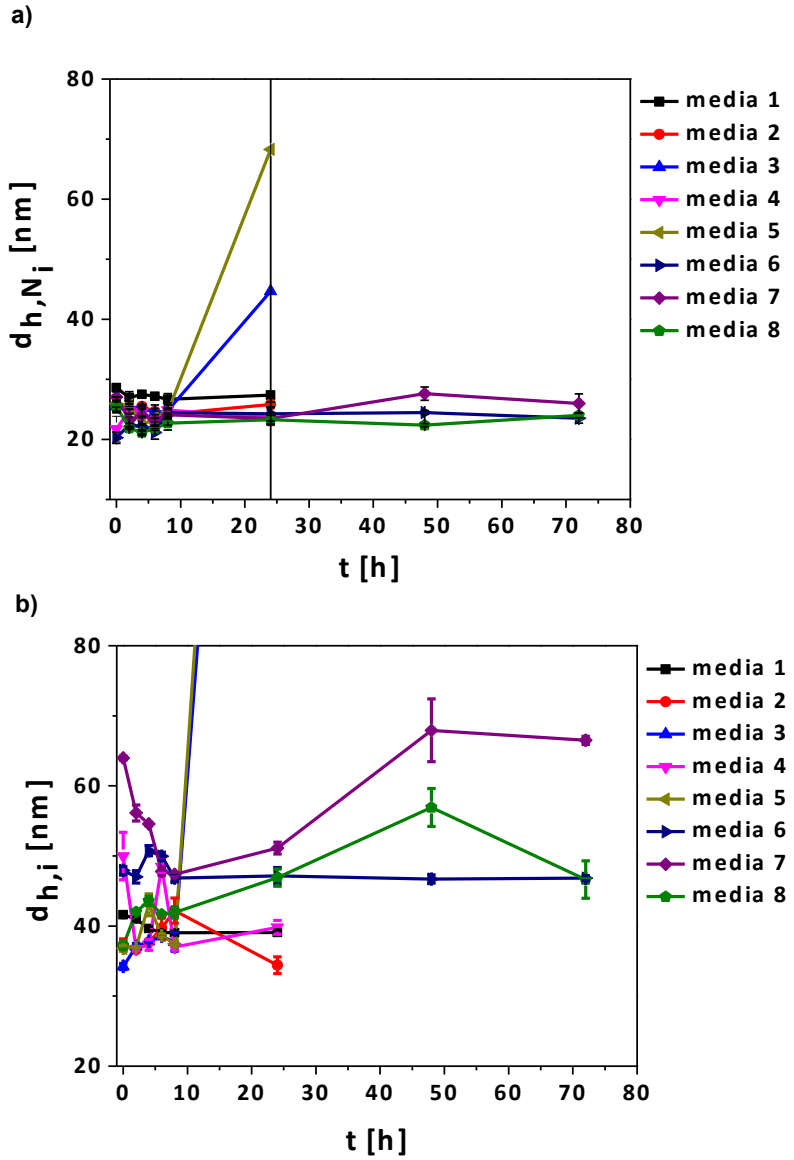


**Figure 54.** Summary of the a) number, $d_{h,Ni}$, and b) intensity, $d_{h,i}$, hydrodynamic diameter distributions for the 8 media *versus* time for 25-GNPs.

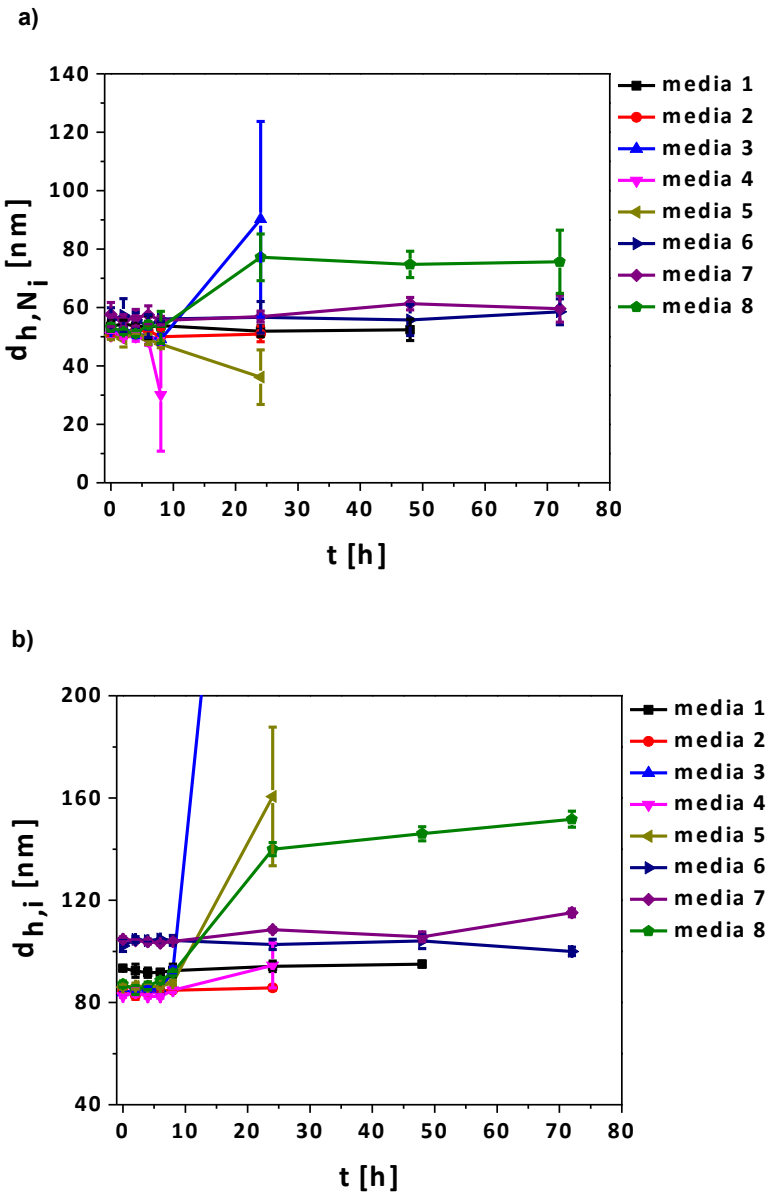


**Figure 55.** Summary of the a) number, $d_{h,Ni}$, and b) intensity, $d_{h,i}$, hydrodynamic diameter distributions for the 8 media *versus* time for 50-GNPs.

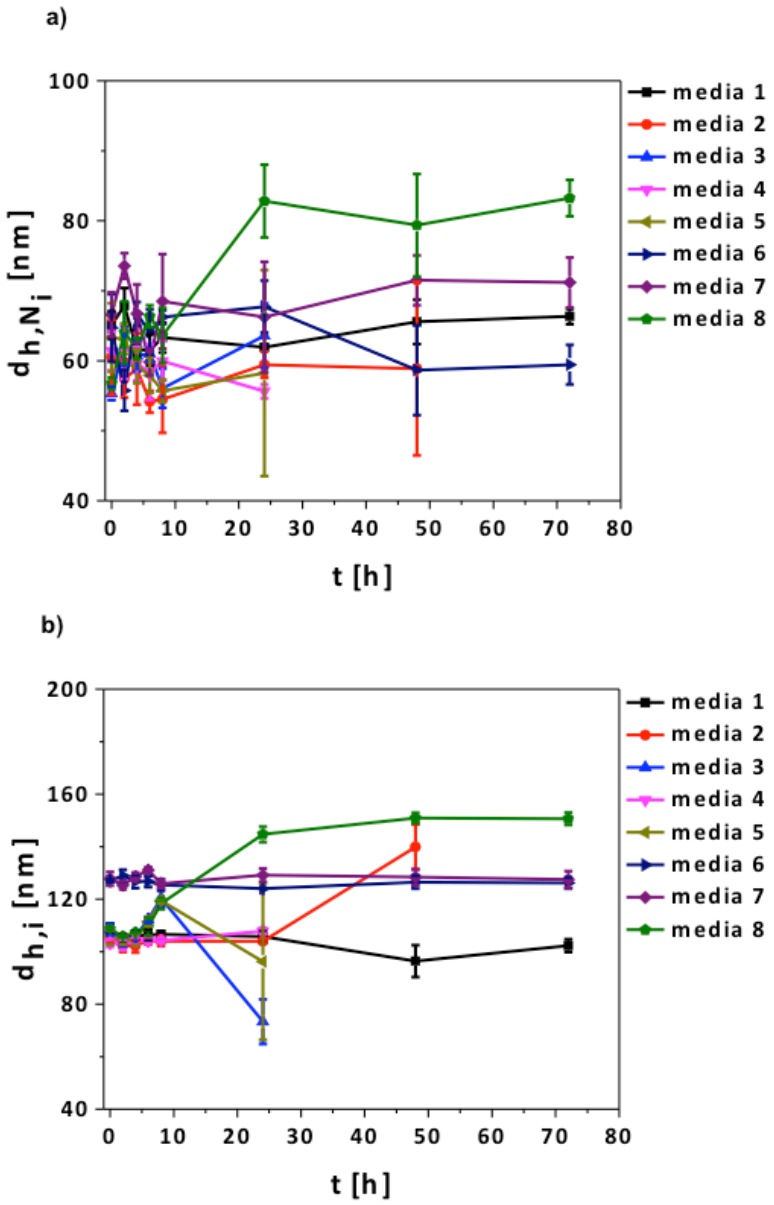


**Figure 56.** Summary of the a) number, $d_{h,Ni}$, and b) intensity, $d_{h,i}$, hydrodynamic diameter distributions for the 8 media *versus* time for 60-GNPs.

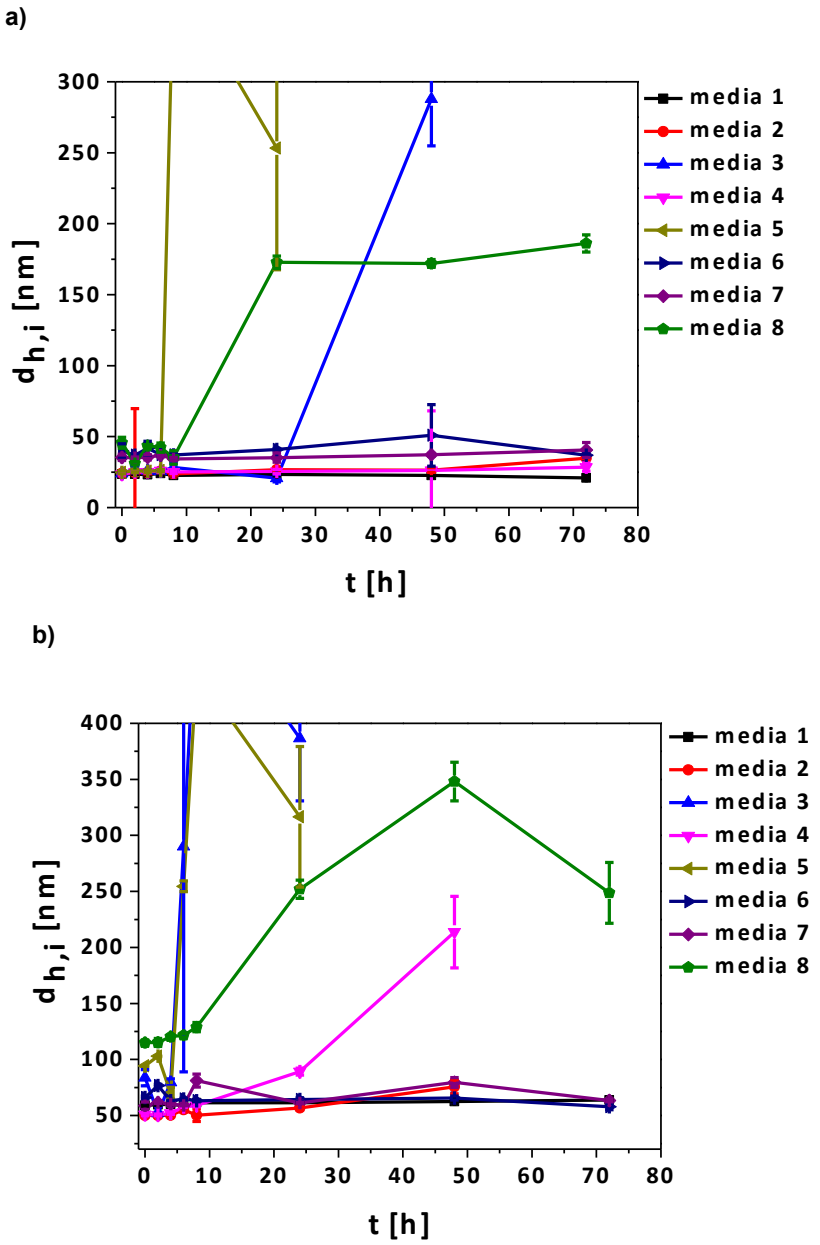


**Figure 57.** Summary of the intensity hydrodynamic diameter distributions, $d_{h,I}$, for the 8 media *versus* time for a) 850-GNRs and b) 1100-GNRs.

### 3.3. Stability of different surface coating of NPs *vs* different pH values

As described above, the properties of NPs, including their stability, aggregation behavior, sensing abilities, etc. are controlled by their size, shape, surface coating, surface charge, etc. The predictions of the interaction between the two NPs as a function of the surface coating, pH, size and shape of the NPs enable us to gain insight into the stability of the NPs under different conditions. So, the successful application of the NPs requires that they be highly stable at a wide range of pH values. For this study, the stability of two different samples of GNPs with different shapes (spheres and rods) and different surface coating (PMA and PEG) was tested against different pH values with titration system by using Malvern Zetasizer Nano ZS. For this purpose, 60-GNPs and 850-GNRs were coated firstly with PMA (as described in section 2.3) and then, PEGylated with α-Methoxy-ω-amino PEGs ($M_w$= 10 kDa) following the same protocol described in section 2.4 (see Table 9).

**Table 9.** PEgylation conditions for 60-GNPs and 850-GNRs. $C_{NP}$, $C_{EDC}$ and $C_{PEG}$ refers to concentration of NPs, EDC and PEG respectively.

| Sample | PEGylation | | |
|---|---|---|---|
| | $C_{EDC}/ C_{NP}$ | $M_w$ | $C_{PEG}/ C_{NP}$ |
| 60-GNPs | $30 \cdot 10^6$ | 10 [kDa] | $2 \cdot 10^6$ |
| 850-GNRs | $5 \cdot 10^6$ | | $2 \cdot 10^6$ |

Starting from a colloidally stable of NPs at high pH; the solution was acidified upon addition of a titrant. After each addition, the zeta potential and hydrodynamic diameter of the NPs were measured as shown in Figures 58-59. At higher pH values, the NPs surface is highly gained negative charge due to the deprotonation of carboxylic acids. Upon addition of acidic solution, the negatively charged surface gradually decreases (protonated) to be close to zero. However, the particles are stable at all pH values (under high, moderate, and low pH conditions) indicating that $pK_a$ value of PMA and PEG-coated NPs is less than 5.5, which is the lowest pH value tested.

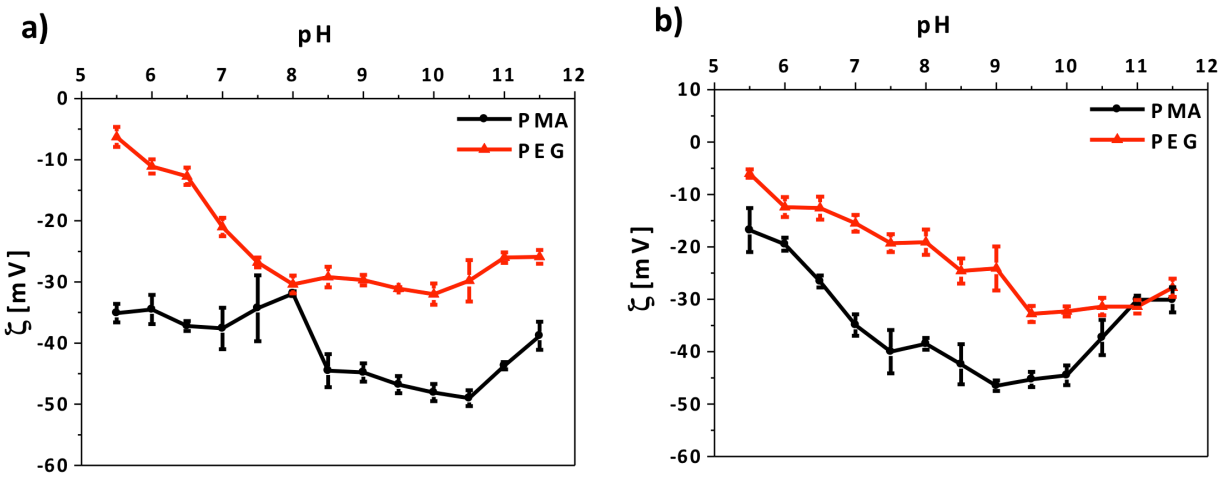


**Figure 58**. ζ-potential distribution (N(ζ)) *vs* different pH values using titration system of a) 60-GNPs and b) 850-GNRs coated with PMA (black line) and PMA+PEG (red line).

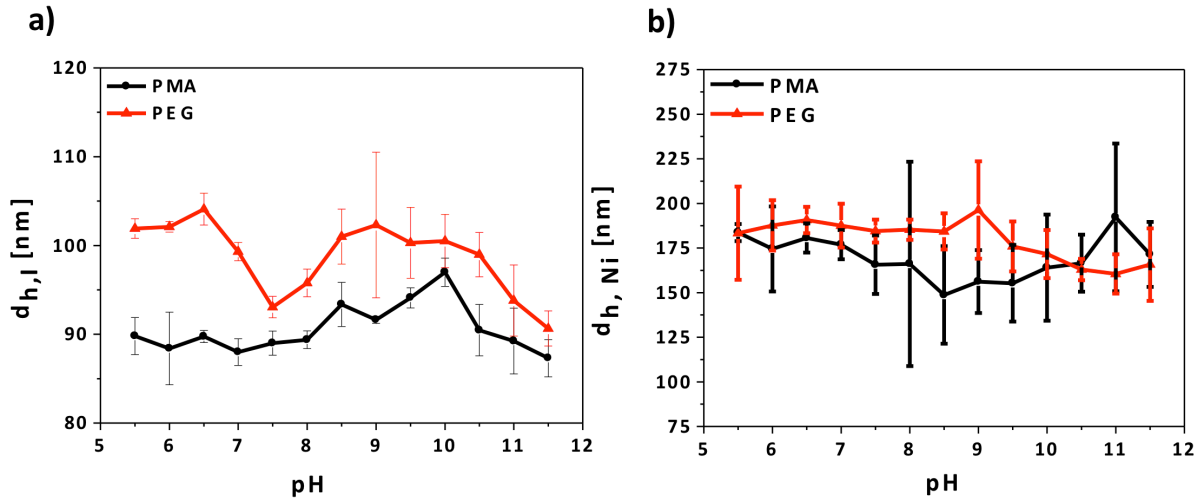


**Figure 59**. Hydrodynamic diameter distributions in intensity ($d_{h,i}$) *vs* different pH values of a) 60-GNPs and b) 850-GNRs coated with PMA (black line) and PMA+PEG (red line).

## 4. Toxicity tests

The toxicity of the PMA coated NPs was tested against two kinds of cells; HeLa and 3T3 cells. These cells were seeded at a cell density of $5 \cdot 10^3$ cells/well of HeLa and $10 \cdot 10^3$ cells/well of 3T3 in a 96 well plate in 100 µL of DMEM media (10% FBS, 1%P/S and 1% L-Glu) and incubated overnight. Next day, the cells were incubated for 24 h with different concentration of NPs as indicated in Figure 58. After that, the cells were washed one time with PBS and 100 µL of 10 % Resazurin solution (blue, non-fluorescent sodium salt) were added to each well in growth solution and incubated for 4 h at 37 $^0$C. The viability date were presented as percentage to the untreated cells with particles (control) depending on the emission (fluorescence) intensity of Resorufin which is resulted due to reduction process of the Resazurin by metabolically active cells. This reduction process needs continually mitochondrial activity by the cells, which is inactivated immediately after their death. The fluorescence spectrum was recorded using Fluorometer at excitation wavelength of 560 nm.

NPs molar concentration was determined based on the UV-Vis absorbance values, as described in Section 2.5. To convert those molar values into µg/mL, the molecular weight ($M_w$) for each NP was calculated by Formulas 7-9. The volume of one NP ($V_{NP}$) was calculated by Formula 7 and 8 for spheres and rods respectively. The rods volume was assumed as a cylinder and the core length ($d_L$) and diameter ($d_c$) was determined by TEM.

$$V_{NP} = \frac{4}{3} \times \pi \times \left(\frac{d_c}{2}\right)^3 \quad (7)$$

$$V_{NP} = \pi \times \left(\frac{d_c}{2}\right)^2 \times d_L \quad (8)$$

The molecular weight of one NP ($M_w$) was calculated by following Formula 9:

$$M_w = V_{NP} \times \rho_{gold} \times N_A \quad (9)$$

Where p is the gold density and $N_A$is the A vogadro number.

With neglecting the contribution of the polymer coating to the mass of the NPs[138], The conversion of mol to mass can be caculated by using the following Formula 10:

$$\left(\frac{m_{NP}}{V}\right) = (C \times M_W) \quad (10)$$

Where C is the concentration [M], m is the mass [mg], $M_w$ is the molecular weight [g/mol] and V, the volume of the NPs solution [mL]. Table 10 shows the molecular weights and the volumes for all NPs.

**Table 10.** Summary of the $V_{NP}$ and $M_w$ of each NP type.

| Sample | $V_{NP}$ [$cm^{-3}$] | $M_w$ [g/mol] |
|---|---|---|
| 25-GNPs | $4.2 \cdot 10^{-18}$ | $4.9 \cdot 10^{7}$ |
| 50-GNPs | $6.5 \cdot 10^{-17}$ | $7.6 \cdot 10^{8}$ |
| 60-GNPs | $1.3 \cdot 10^{-16}$ | $1.3 \cdot 10^{9}$ |
| 850-GNRs | $4.3 \cdot 10^{-17}$ | $5.0 \cdot 10^{8}$ |
| 1100-GNRs | $7.6 \cdot 10^{-18}$ | $8.8 \cdot 10^{7}$ |

As indicated by the following Figure 60, the toxicity of particles was decreased especially, in case of GNRs. This means that the concentration of CTAB was decreased during the round trip process of the phase transfer and polymer coating as confirmed by Figure 18-19. Therefore, the cells are still alive with GNRs concentration up to 2.5 nM. In case of SGNPs, we found that the viability trend is size-dependent where the cells are still alive with NPs concentration up to 4.5, 0.3 and 0.2 nM in case of 25-GNPs, 50-GNPs and 60-GNPs respectively.

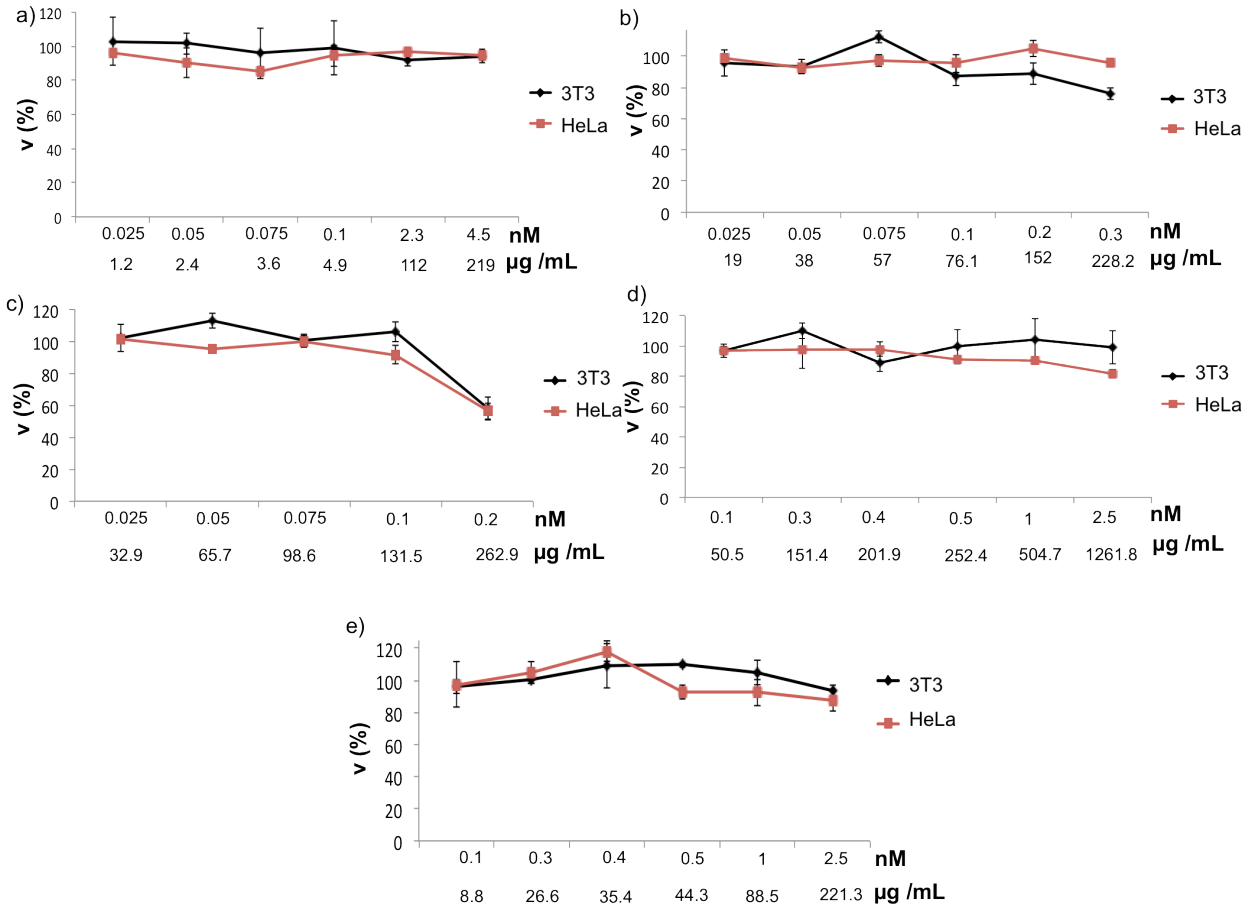


**Figure 60.** Resazurin results after 3T3 and HeLa cells exposure to a) 25-GNPs, b) 50-GNPs; c) 60-GNP, d) 850-GNRs and e) 1100-GNRs for 24 h at the concentrations indicated.

## 5. Biocompatibility Study

For this purpose, I have prepared library of GNPs with different sizes (up to 100 nm), shapes (spheres and rods), and surface coating ((PVP, PMA, and PMA+PEG), Figures 61)) to study their behavior and interaction with plasma proteins and blood cells. This study was done in collaboration with the group of Prof. Sijin Liu at Research Center for Eco-Environmental Sciences Chinese Academy of Sciences/China.

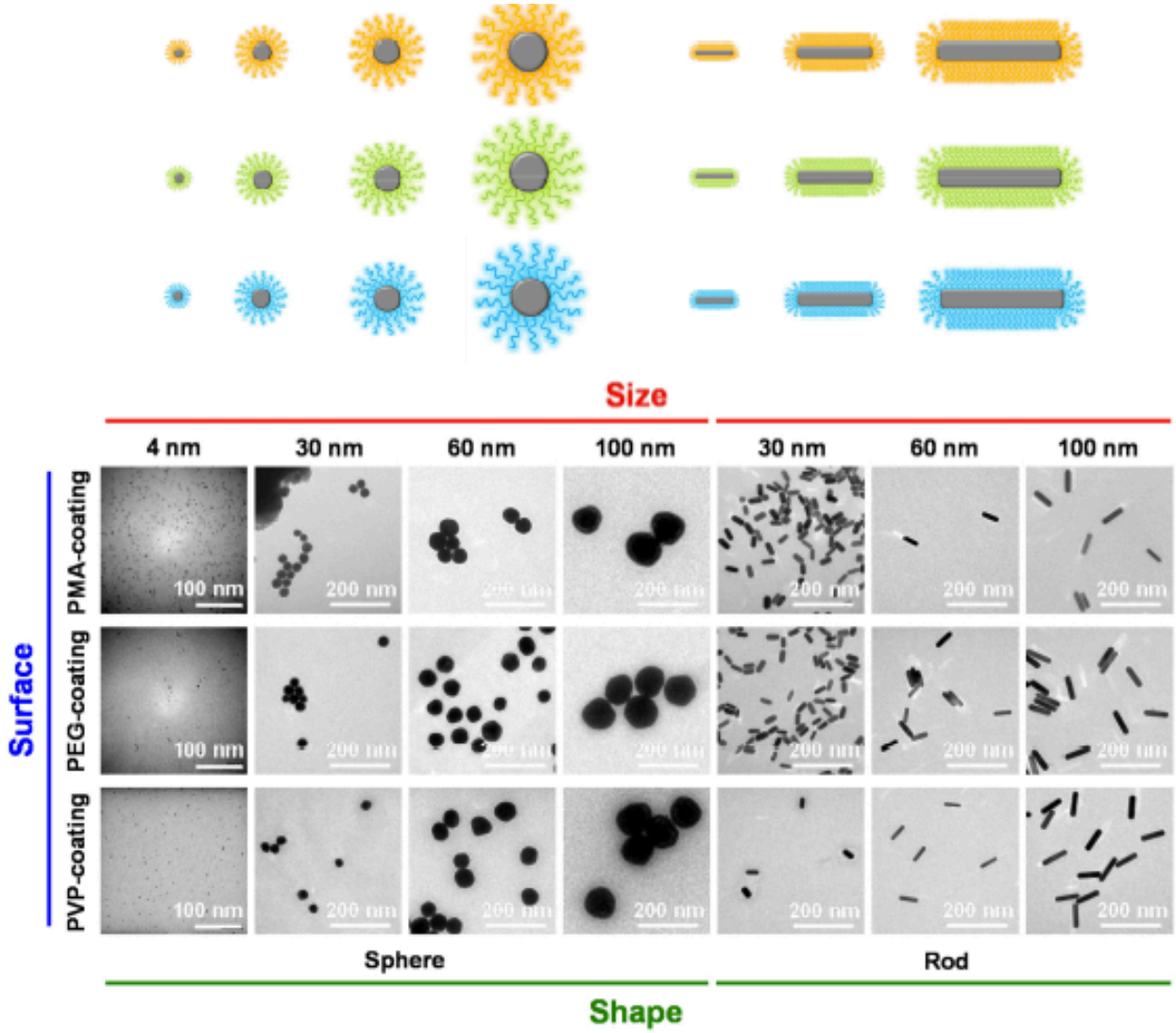


**Figure 61.** Schematic diagram (upper) and TEM images (lower) of all synthesized GNPs with different sizes, shapes and surface modifications.

## A. Synthesis of GNPs

### *A.1. Synthesis of SGNPs*

SGNPs with core diameter of 30 nm, 60 nm, and 100 nm (presented as 30-GNPs, 60-GNPs and 100-GNPs) were prepared by following the same protocol described in section 2.1.1. SGNPs with core diameter of 4 nm (presented as 4-GNPs) were prepared by following Martin method[53] (afterward coated with PVP) and Brust Method[52] (afterward coated with PMA and PEGylated with PEG) as described below: -

- **Protocol I**

Aqueous solution of 4-GNPs was prepared by mixing 1 mL of 50 mM of hydrogen tetrachloroaurate (dissolved in 50 mM of HCl) with 3 mL of 50 mM of $NaBH_4$ (dissolved in 50 mM of NaOH) in glass vial under gentle stirring. The solution changed color from light yellow to orange immediately, and then to red while the vial was stirred for 1 min and heated for 100 s to release hydrogen gas molecules. In order to calculate the concentration of NPs, the absorbance at 450 nm (as measured in UV-Vis; extinction coefficient $\varepsilon(450) = 3.62 \cdot 10^6$ $M^{-1} \cdot cm^{-1}$) was used, as previously reported.

- **Protocol II**

At room temperature, aqueous solution of hydrogen tetrachloroaurate (25 mL, 0.9 mmol) was mixed with 80 mL of toluene contains tetraoctylammonium bromide (TOAB, 3.9 mmol)) in a 500 mL separation funnel, and were shaken vigorously for about 5 min. The $AuCl_4$ ions were gradually transferred into the organic phase through the formation of tetraoctylammonium-gold tetrachloroaurate ion pairs. The toluene solution was transferred to a 250 mL round bottom flask. Then, a freshly prepared aqueous solution of $NaBH_4$ (25 mL, 8.8 mmol) was added under strong stirring of gold precursors in toluene. After 1 h stirring, the solution was transferred to a 500 mL clean separation funnel and 25 mL of 0.01 M HCl were added to remove the excess of sodium borohydride. The mixture was vigorously shaken and the aqueous phase was discarded. Then, 25 mL of 0.01 M NaOH were added in order to remove the excess of acid and finally, 4 x 25 mL of Milli-Q water were added to reduce the ion excess. The aqueous phase was discarded and the remaining solution was transferred to a 250 mL round bottomed flask. Then, the solution was stirred overnight to allow the NPs reaching

a thermodynamically stable size distribution, in a process called Ostwald ripening. In order to increase the colloidal stability of the NPs, 10 mL (41.7 mmol) of 1- dodecanethiol (DDT) was added to NPs and the solution was stirred at 65 °C for 3 h. After that, the solution of DDT-coated Au NP was cooled down to RT and cleaned by cycles of centrifugation. The larger agglomerates were first removed by centrifugation at 2000 rpm and the supernatant was collected. Then, methanol was added until the solution turned cloudy by precipitation of Au NPs and then, the solution was centrifuged (2000 rpm). After discarding the supernatant, the precipitate containing the GNPs was dissolved in toluene upon vigorous shaking. Again, methanol was added to the NPs solution until it turned cloudy, followed by centrifugation. The supernatant was removed and the precipitate containing the purified Au NPs. In order to calculate the concentration of NPs, the absorbance at 520 nm (as measured in UV-Vis; extinction coefficient $\varepsilon(520) = 8.7 \cdot 10^6\ M^{-1} \cdot cm^{-1}$) was used, as previously reported[139].

*A.2. Synthesis of GNRs*

GNRs with Length diameter of 100 nm (presented as 100-GNRs) were prepared by following the same protocol described in section 2.1.2. GNRs with Length diameter of 30 nm and 60 nm (presented as 30-GNRs and 60-GNRs) were prepared by following the report reported by Murray et al. [63] as described below: -

Seed solution: seed solution was prepared by the same protocol described in section 2.1.2.

Growth solution: growth solution was prepared by following the protocol reported by Murray et al. [63] Briefly, 9.0 g of CTAB and 0.8 g of sodium salicylate in case of 30-GNRs (or 1.1 g of 5-bromosalicylic acid in case of 60-GNRs) were dissolved in 250 mL of warm water (60 $^oC$) in a 500 mL Erlenmeyer flask. The solution was allowed to cool to 30 $^oC$ and a specific amount of $AgNO_3$ (4 mM) was added. The mixture was kept undisturbed at 30 $^oC$ for 15 min, after which 250 mL of 1 mM $HAuCl_4$ solution was added. After 15 min of slow stirring (400 rpm), a specific amount of 0.064 M of AA (Table 11) was added, and the solution was vigorously stirred for 30 s until it became colorless. Finally, a small amount of seed solution (freshly prepared as described above) was injected into the growth solution (Table 11), stirred for 30 s and kept at 30 °C without stirring overnight for GNRs growth. The final products were isolated by centrifugation and its concentration was calculated by UV-Spectroscopy.

**Table 11.** Growth conditions for GNRs. $V_{HCl}$ refers to the volume of HCl which used to optimize the pH of growth solution, $V_{AgNO3}$ refers to the volume of $AgNO_3$, $V_{AA}$ refers to the volume of ascorbic acid and $V_{seed}$ refers to the volume of seed solution

| Sample | pH | $V_{AgNO3}$ [mL] | $V_{AA}$ [mL] | $V_{seed}$ [mL] | $\lambda_{LSPR}$ [nm] |
|---|---|---|---|---|---|
| 30-GNRs | 3.05 | 6 | 1 | 0.8 | 650 |
| 60-GNRs | 2 | 18 | 2 | 0.4 | 825 |

## B. GNPs surface functionalization

GNPs were coated with three different surface coating: PVP, PMA and PEGylation of PMA coating as described below: -

### *B.1. PVP coating*

At room temperature, SGNPs and GNRs were coated with PVP ($M_w$=10 kDa) by using the equations (1-5) as described in section 2.3. Briefly, a specific amount of 0.5 M of PVP in water ($R_p/_{Area}$= 3000) was added dropwise to the SGNPs solution, and the mixture was further stirred at room temperature for 24 hours. The PVP-stabilizd SGNPs were collected by centrifugation (Table 12), washed by water for two times, and final dispersed in water. In case of GNRs, the particles were coated firstly with PSS ($M_w$= 70 kDa) and then coated with PVP ($M_w$=10 kDa). Briefly, The GNRs suspensions were subjected to centrifugation (Table 10) for one time. The supernatant was discarded, and the pellet was redispersed again in water. A specific amount of 0.25 M of PSS in water ($R_p/_{Area}$= 500) was added dropwise to the GNRs solution, and the mixture was further stirred at room temperature for 5 h in order to exchange the CTAB. The PSS-stabilized GNRs were collected by centrifugation, washed by water twice and final dispersed in water. For this solution, a specific amount of 0.5 M of PVP in water ($R_p/_{Area}$= 3000) was added dropwise, and the mixture was further stirred at room temperature for 24 h. The PVP-stabilized GNRs were collected by centrifugation (Table 12), washed by water for two times, and final dispersed in water. The PVP-GNPs dispersions were stable at room temperature for at least several months.

*B.2. PMA coating*

For this purpose, the particles were transferred from water to chloroform and then coated with DDA-grafted PMA by using the same protocol reported in section 2.3. 4-GNPs (synthesized by Brust Method (protocol II)) were coated directly by DDA-grafted PMA. For phase transfer and polymer coating conditions see Table 12.

**Table 12.** Experimental conditions for all NPs. $C_{NP}$, $C_{DDA}$, $C_{EDC}$ and $C_{PEG}$ refers to concentration of NPs, DDA, EDC and PEG respectively. $R_{p/Area}$ refers to the number of PMA monomer added $nm^2$ v refers to centrifugation speed and t refers to the centrifugation time.

| Sample | **Phase transfer** | | **Polymer coating** | | | **PEGylation** | | |
|---|---|---|---|---|---|---|---|---|
| | $C_{PEG}$/ $C_{NP}$ | $C_{DDA}$ [M] | $R_p/_{Area}$ | Centrifugation | | $C_{EDC}$/ $C_{NP}$ | PEG [kDa] | $C_{PEG}$/ $C_{NP}$ |
| | | | | v [rpm] | t [min] | | | |
| 4-GNPs | - | - | 350 | Cleaned by gel electrophoresis | | $128 \cdot 10^3$ | 10 | $1 \cdot 10^5$ |
| 30-GNPs | $3 \cdot 10^4$ | 75 | 3000 | 9000 | $30 \cdot 10^6$ | $5 \cdot 10^6$ | | $2 \cdot 10^6$ |
| 60-GNPs | $5 \cdot 10^5$ | 75 | 3000 | 6000 | $30 \cdot 10^6$ | $30 \cdot 10^6$ | | $2 \cdot 10^6$ |
| 100-GNPs | $6 \cdot 10^5$ | 75 | 4000 | 3000 | $10 \cdot 10^6$ | $10 \cdot 10^6$ | | $2 \cdot 10^6$ |
| 30-GNRs | $3 \cdot 10^4$ | 75 | 3000 | 9000 | $8 \cdot 10^6$ | $8 \cdot 10^6$ | | $2 \cdot 10^6$ |
| 60-GNRs | $3 \cdot 10^4$ | 75 | 3000 | 9000 | $8 \cdot 10^6$ | $8 \cdot 10^6$ | | $2 \cdot 10^6$ |
| 100-GNRs | $8 \cdot 10^4$ | 75 | 3000 | 6000 | $8 \cdot 10^6$ | $5 \cdot 10^6$ | | $2 \cdot 10^6$ |

*B.3. PEGylation of PMA coating*

After polymer coating, the NPs surface is rich in –COOH groups. Therefore, by using EDC chemistry as reported in section 2.4, they can be activated and functionalized with α-Methoxy-ω-amino PEGs ($M_w$= 10 kDa). The reaction was left overnight and after that, the NPs were cleaned using dialysis for 1 h and concentrated by centrifugation (see Table 12).

Due to the huge number of date, I am going to present only some date of the biocompatibility studies of PMA and PEGylation of 4-GNPs and 100-GNRs.

## 5.1. Biocompatibility in Blood Stream

Blood circulation is the most important way for the nanoparticles translocation and immune response[140]. Therefore, the behavior of GNPs in blood stream is critical for understanding its final *in vivo* metabolism and distribution. First, hemolysis assay was carried out to evaluate the interaction between four GNPs and red blood cells (RBC). Fresh mouse RBCs were isolated by centrifugation and washed with PBS for at least five times, then aliquots of 100 μL RBCs were diluted to 1 mL with PBS and deionized water as the negative and positive control. Samples were prepared in the same manner as the above negative control except adding 40 μg GNPs. After 30 min incubation at 37 °C, the samples were centrifuged and the released hemoglobin from damaged RBCs in supernatant was measured (Figure 62a). Unexpectedly, only the PMA@4-GNPs induced a serious hemolysis (59±1%), while the left three have a good hemocompatibility (<5%). It is supposed that the strong negative charge and ultra-small size of PMA@4-GNPs may cause the disruption of RBC membrane to release the hemoglobin. However, the PMA@100-GNRs with the same negative charged coating nearly has no effect (<1%) on the RBCs, while the PEG@4-GNPs exhibited a slight hemolysis (*ca.* 4.3%). Therefore, the hemolysis of PMA@4-GNPs on RBCs is resulted by a combination of two factors (*i.e.* its negative surface charge and ultra-small size), which is usually ignored in previous nanoparticle studies[139-143]. Following, in order to find a safe condition for the later animal experiments, the does-response of PMA@4-GNPs on RBCs is tested with three concentrations of 2, 20 and 40 μg/mL without or with 10% FBS. As expected, the hemolysis phenomenon can be effectively reduced with decreasing PMA@4-GNPs concentration, and nearly be undetectable for 2 μg/mL (Figure 62b and 62c). Besides, the addition of FBS could also reduce the hemolysis extent because of the formation of protein corona on its surface as described above. Finally, the does of 2 μg/mL was chosen for the *in vivo* animal experiments in this work.

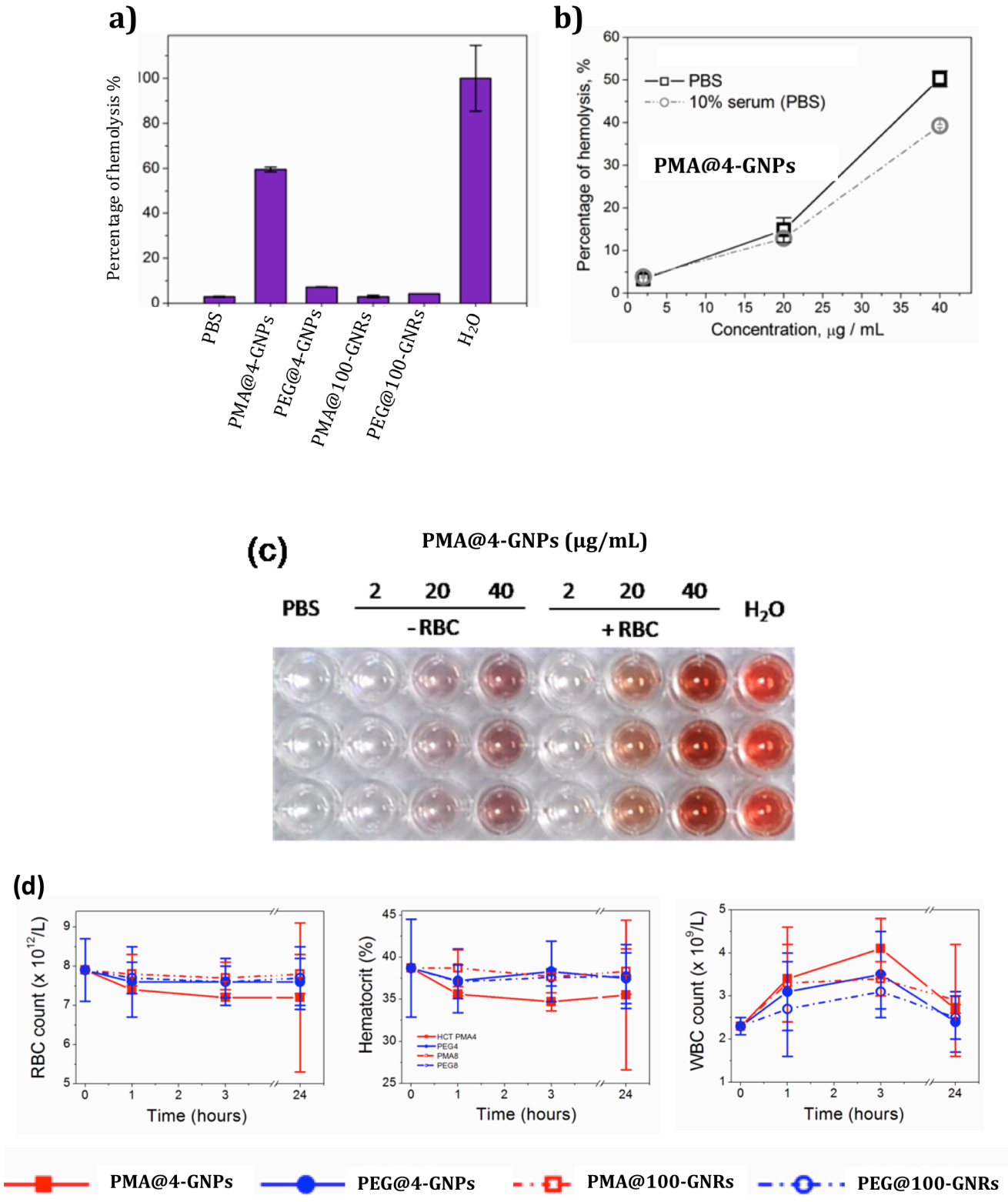


**Figure 62.** (a) Hemolysis assay of four GNPs (n=4). The negative and positive control is PBS and deionized water; (b) and (c) are the hemolysis assay of PMA@4-GNPs at 2, 20 and 40 μg/mL; (d) the red blood cell (RBC) count, hematocrit (volume percentage of RBCs in blood) and white blood cell (WBC) count of BALB/c mouse (n=5) at 0, 1, 3 and 24 h after GNPs administration.

Based on the reported work, the blood volume of mouse accounts its 6.7% of total body weight[144]. For the BALB/c mouse used in this study, their blood volume is estimated to be 1.7 mL according to their average body weight (25 g). So a does of 4 μg SGNPs in 100 μL PBS was intravenous injected. After 1, 3 and 24 h administration, mouse were anesthetized and euthanized. The blood was withdrawn and the organs and tissues (liver, spleen, kidney, lung, heart, brain, muscle, bone marrow, *etc.*) were collected for latter analysis. After blood collection, the relevant clinical parameters used for evaluating hematic condition, including RBC count, hematocrit (volume percentage of RBCs in blood) and WBC counts were immediately assessed for each group (n=5). Comparison of these parameters between control and GNPs-injected groups, distinct changes could be observed in the PMA@4-GNPs group with decreasing RBC count and hematocrit (Figure 62d), indicating that even a relative safe does (4 μg) was applied based on the *in vitro* hemolysis assay, its adverse effects on blood system may still exist. Meanwhile, the WBC count increased within 1 h after GNPs administration, meaning the immune system quickly response to these foreign particles.

Besides direct hemolysis effect on RBCs, if the GNPs could induce the apoptosis of blood cell has rarely been studied based on our knowledge, which is able to affect the differentiation and maturity of RBCs and lead to the decreasing RBCs in blood vessel as observed. To inspect this hypothesis, a MEL (murine erythroleukemia) cell line that is erythroid precursors useful in examining factors regulating terminal differentiation, was employed as an *in vitro* model. After exposed to the GNPs for 24 h, the MEL cell viability of PMA@4-GNPs, PMA@100-GNRs and PEG@100-GNRs show no difference to control group even at 4 μg/mL (data not shown here). Similarly with above observation of PMA@4-GNPs, the MEL cell viability markedly decreased even at 0.4 μg/mL, and the percentage of apoptosis cell reached 99% at 2 μg/mL (Figure 63). Thus, we can make a conclusion that PMA@4-GNPs shows toxicity to blood cells even at a low concentration and could impair the RBCs.

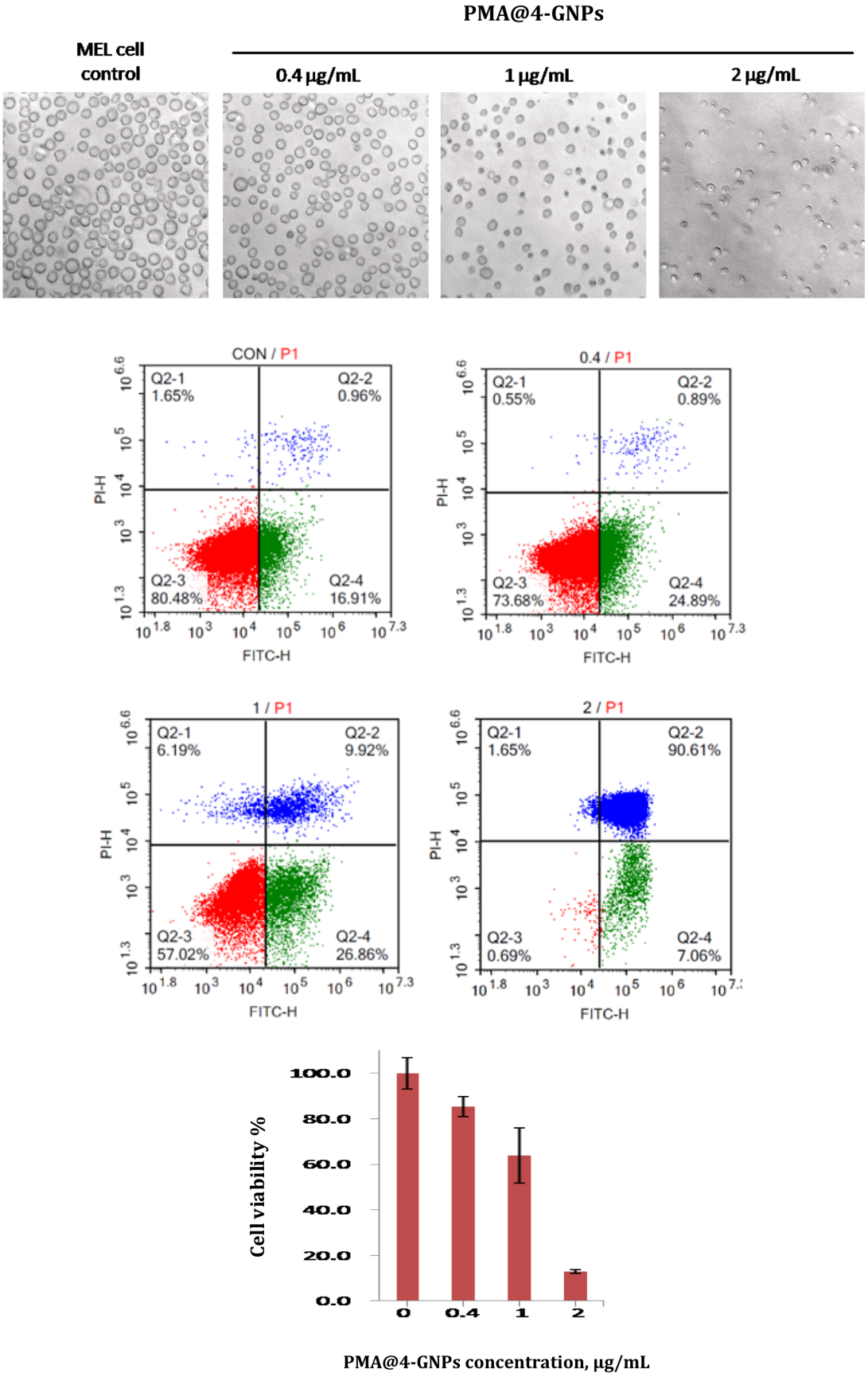


**Figure 63.** The viability, morphology and flow cytometry images of MEL cells exposed to 0, 0.4, 1 and 2 µg/mL PMA@4-GNPs after 24 h.

## 5.1. *In vivo* Translocation and Distribution

As shown in Figure 64, major organs and tissues of GNPs-injected mouse were collected, digested and analyzed by ICP MS to study the *in vivo* distribution and biokinetics. In agreement to previous reported work, at the time point of 24 h, the GNPs major accumulated in liver and spleen as shown in Figures 65-66. Compared to 100 nm-GNRs in liver at 24 h (>80%), only 41 ± 10% and 32 ± 9% PMA@4-GNPs and PEG@4-GNPs accumulated, indicating their ultra-small size is helpful for retaining in the blood circulation. Except liver, the 4-GNPs nanosphere seemed to preferentially accumulate in the spleen, kidney, lung, heart, muscle and bone marrow, probably because of their easier passing through the blood vessel to reach these organs/tissues during the blood circulation. Surprisingly, although only the bone marrow from two mouse hind legs was sampled (containing *ca.* 0.1% 4-GNPs), under consideration of the whole body bone marrow, non-negligible amount of PMA@4-GNPs could reach this place. It is probably because the bone marrow contains high numbers of macrophages as liver and spleen. In consideration of PMA@4-GNPs and PEG@4-GNPs nm, the former more easily accumulated in the organs/tissues such as spleen, lung and bone marrow, respectively about 2, 3 and 1.3 times higher than the latter.

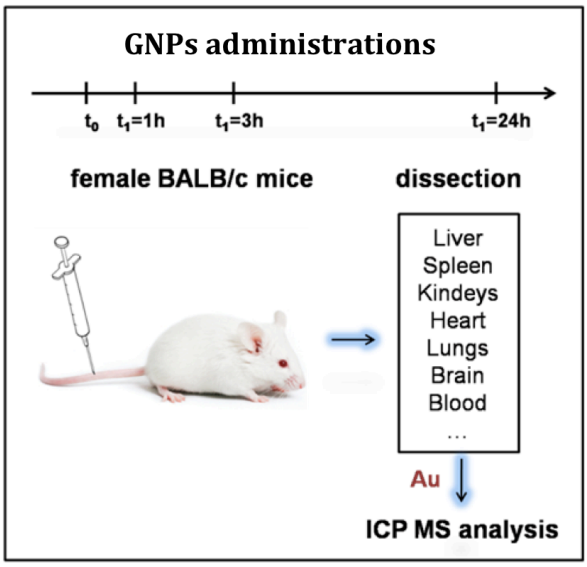


**Figure 64.** Schematic illustrations of the animals experiments for *in vivo* distribution and biokinetics analysis

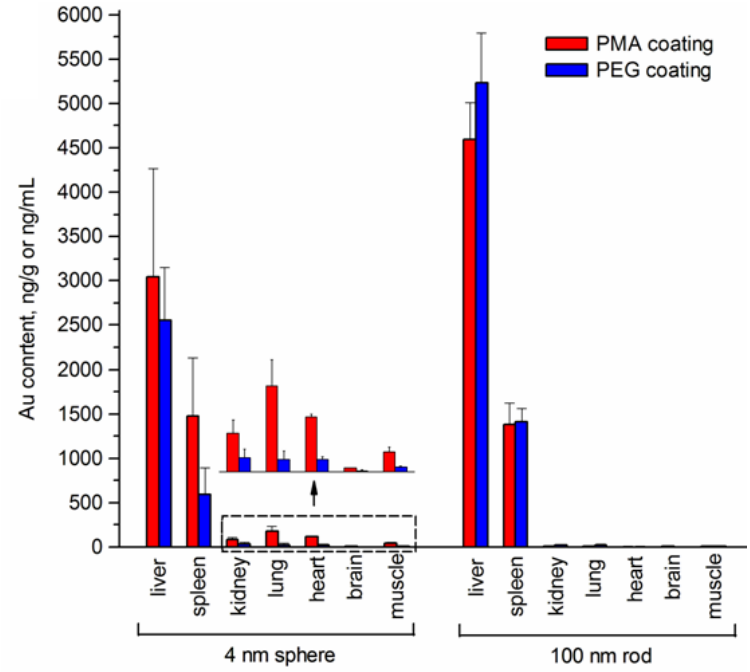


**Figure 65**. GNPs distribution among different organs/tissues (liver, spleen, kidney, lung, heart, brain and muscle). (c) *in vivo* biokinetics analysis of GNPs in organs/tissues at 1, 3 and 24 h after GNPs administration.

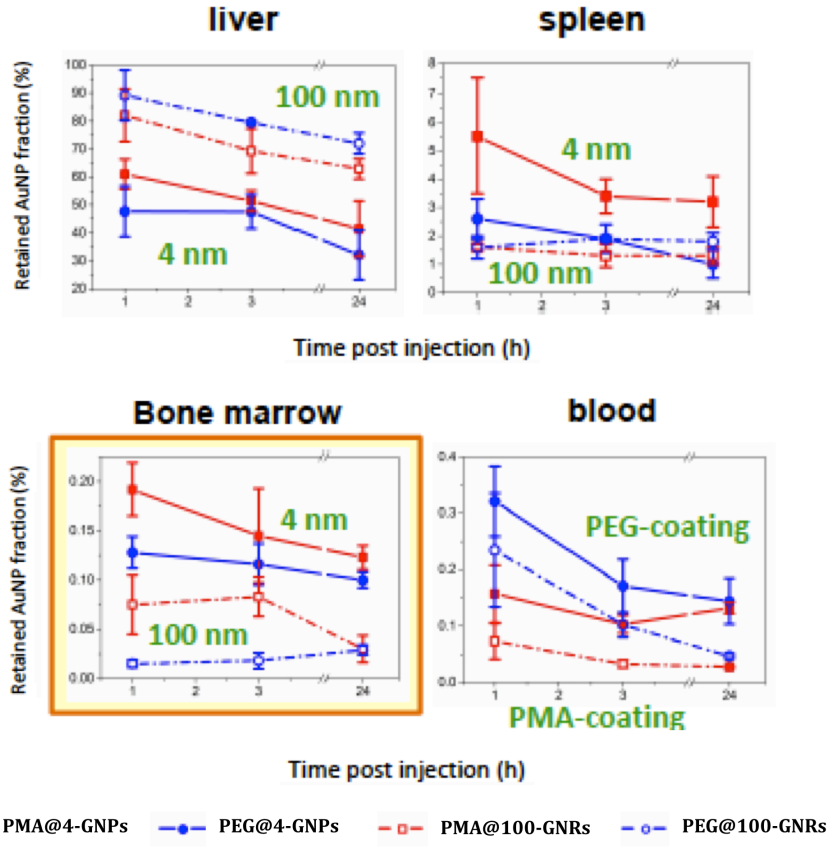


**Figure 66.** *In vivo* biokinetics analysis of GNPs in organs/tissues at 1, 3 and 24 h after GNPs administration.

# 6. Conclusion and Outlook

In the present work, GNPs with different sizes and shapes were synthesized in aqueous media and their surface was subjected to some modifications with three steps. First, the NPs were capped with short PEG chains ($M_w$= 750 Da), which used as stabilizers at the point of transferring to organic solvent. Second, the NPs were transferred from aqueous media (water) to organic solvent (chloroform) by using DDA. This protocol is very versatile, as it allows the transference of aqueous NPs within a long range of sizes to the organic phase and does not affect on the optical properties of the NPs. Third, the NPs were transferred again to aqueous media using modified polymer (PMA) that allows to form a universal surface for all the NPs. Also, PEI as cross-liker was attached to PMA-coated NPs during the coating process to improve their stability. This polymer can be used as platform for attachment additional biomolecules for different applications and then different molecular weights of PEG (mPEG-$NH_2$) were attached to surface of the NPs by EDC chemistry. The NPs were characterized with different techniques as reported in the thesis that exhibit a good colloidal stability for all the NPs after each step of surface modifications.

Afterwards, the stability of NPs@PMA, NPs@PMA+PEI and PEGylated NPs was tested in complete cell medium using UV-Vis spectroscopy that reported that the particles stability improved in case of using of PEI and more better in case of attachment of PEI and PEG to PMA-coated particles. Also, the stability of PEGylated NPs was tested in free-proteins media and contain-proteins media using UV-Vis spectroscopy and DLS, which reported that the particles aggregation was detected after 8 h in free-proteins media due the presence of salt which screen the surface charge of the NPs. But the NPs were stable in contain-proteins media due to the adsorption of NPs on the surface of the NPs, which improve their stability.

Furthermore, the toxicity of the NPs@PMA and PEGylated NPs was tested for two kinds of cells; HeLa and 3T3 cells. The test reported that the nanorods are not toxic for both cell lines up to 1 mg/mL but in case of spherical NPs, the viability trend is size-dependent as 60-GNPs are more toxic and can be used for both cell lines up to 200 µg/mL.

Additionally, it can be concluded that physicochemical properties of the nanoparticles (e.g. size, shape, surface functionalization, surface charge, *etc.*), along with the administration routes/doses, can play critical roles in determining the biodistribution pattern of nanoparticles.

A major task for the future is encapsulation of GNRs inside zeolitic-imidazolate-framework (ZIF-8) as core–shell nanostructures, which can be used as drug carrier in biological system. Taking the advantage of the porous provided by the outer ZIF-8 shell and loading these porous with anticancer. Then, the therapeutic efficacy can be improved with the combination of external near-infrared (NIR) photothermal therapy of GNRs and the local specific chemotherapy of anticancer.

.

# 7. Publications:

This thesis is written in a cumulative way and displays parts of the results of the scientific researches that are published and the contribution of the author is described.

## 7.1. *Metal NPs, Synthesis, Surface Modification, Characterization and Bio-Interaction.*

- [82] **Soliman, G. M**.; Pelaz, B.; Parak, W. J.; Del Pino, P., Phase Transfer and Polymer Coating Methods toward Improving the Stability of Metallic Nanoparticles for Biological Applications. Chem. Mater. 2015, 27, 990−997.

Indispensable requirements are colloidal stability, water solubility and non-toxicity for using the NPs for biological applications. Ligand molecules capped aqueous NPs from the synthesis process are often weak ligands and they cannot stabilize the particles in biological environment. Therefor, these ligands were exchanged with other ligands by transferring the particles from aqueous media to organic solvent by using DDA, which stabilize the particles in this new medium by hydrophobic chains. To get water solubility, Another hydrophobic chains at one side of modified-amphiphilic polymer interact with those chains on the NPs surface and the -COOH on the other side of the polymer will generate a net negative charge and represent anchor points for the further functionalization. After each step of surface modifications, the particles were characterized by different techniques including UV-Vis spectroscopy, TEM, gel electrophoresis, DLS, and LDA. Also, the stability of the particles was studied in different media containing and non-containing-proteins. The NPs were not stable for long time in protein-free media compared with the same particles in protein-contain media, which their stability was improved due to the formation of protein corona around the NPs. In addition to, the toxicity of particles was tested in cancer and non-cancer cells showing non-toxic in the cells lines.

The author did all samples synthesis, surface modification, characterization and most of biological interaction. Also, he did all data evaluation and wrote part of the manuscript and supporting information and did the editing before the submission. He as well did part of the revision before final acceptance.

- [136] Tan, G.; Kantner, K.; Zhang, Q.; **Soliman, M. G**.; Del Pino, P.; Parak, W. J.; Onur, M. A.; Valdeperez, D.; Rejman, J.; Pelaz, B., Conjugation of polymer-coated gold nanoparticles with antibodies - synthesis and characterization. Nanomaterials, 2015, 1297-1316.

In this article, the preparation and characterization of GNPs were highlighted. GNPs were conjugated with fluorescent labeled-protein and the number of antibodies bound per NP was determined. The toxicity of antibody-conjugated NPs and their interaction with cells were studied.

The author contributes in the GNPs synthesis, characterization and functionalization with antibody.

- Nold, P.; Hartmann, R.; Kantner, K.; Feliu, N.; **Soliman, M. G.;** Pelaz, B.; Lim, M.; Sjöqvist, S.; Jungebluth, P.; del Pino, P.; Hackstein, H.; Macchiarini, P.; Parak, W. J.; Brendel1, C., Labelling of mesenchymal stromal cells (MSCs) with gold nanoparticles - an initial *in vitro* study towards optimized detection conditions for future *in vivo* tracking of MSCs. In preparation.

To further assess the biocompatibility and suitability of GNPs for mesenchymal stem cells (MSC) tracking, we investigated cellular responses to GNP labelling in mesenchymal stem cells derived from rats (rMSCs) and humans (hMSCs), such as uptake, cytotoxicity, proliferation, migration, morphology and immunophenotype. For MSC detection *via* mass spectrometry we elucidated the detection sensitivity by quantifying the required number of labeled cells to be able to prove MSC presence in a population of cancer cells.

The author contributes preparing of GNPs with different sizes and shapes, stabilizing them through the polymer coating technique and fully characterize them. Currently, the author is involved in the manuscript preparation.

- Pelaz, B.; Hühn, J.; Carrillo-Carrion, C.; Kantner, K.; Sabir, N.; del Pino, P.; Feliu, N.; Valdeperez, V.; **Soliman, M. G.;** Nelissen, I.; Jackons, A.; Gounko, I.; Parak, W.J., Can doping reduce the cytotoxicity of cadmium containing quantum dots? In preparation.

In the present work we wanted to investigate if QDs toxicity can be reduced by appropriate doping. Doping of QDs is widely reported in literature for several different QD materials. However, effects on toxicity are not investigated in detail so far.

The author contributes GNPs as reference material for the experiments with QDs. Currently, the author is involved in the manuscript preparation.

### *7.2. Reviews*

- [120] Nazarenus, M.; Zhang, Q.; **Soliman, M. G**.; Del Pino, P.; Pelaz, B.; Romero, S. C.; Rejman, J.; Rutishauser, B. R.; Clift, M. J. D.; Zellner, R.; Nienhaus, G. U.; Delehanty, J. B.; Medintz, I. L.; Parak, W. J., *In vitro* interaction of colloidal nanoparticles with mammalian cells: What have we learned thus far? Beilstein J. Nanotechnol. 2014, 5, 1477–1490.

This review article is focus in the interaction of colloidal NPs with mammalian cells *in vitro*. The fate of NPs in biological media depends on several parameters like core material, the surface coating which is used to stabilize the particle, bio-conjugated molecules (*e.g.* affinity, number or ratio per NPs, *etc.*), the functionalization for specific and non-specific targeting, *etc*. All these parameters affect the absorption of proteins on the surface of the NPs forming protein corona, which influence the interaction of the NPs with cell plasma membrane and the mechanism of their internalization to the cells.

The author contributes in the literature research and in the manuscript writing and edition.

- [121] Ashraf, S.; Pelaz, B.; Del Pino, P.; Carril, M.; Escudero1, A.; Parak, W. J.; **Soliman, M. G.;** Zhang, Q.; Carrionl, C. C., Gold-based nanomaterials for applications in nanomedicine. Top Curr Chem. 2016, 370, 169-202.

In this review, the synthesis methods for GNPs with different sizes and shapes were indicated. The easy preparation, high colloidal stability, biocompatibility, low cytotoxicity and unique physico-chemical properties make the GNPs widely used in nano-medicine including detection, sensing, drug delivery, photothermal therapy, clinical trials, *etc.* The stabilization

and functionalization of GNPs by using different ligands and biomolecules, respectively, were presented.

The author contributes in the literature research and in the manuscript writing and edition.

- [146] Ashraf, S.; Carrion, C. C.; Zhang, Q.; **Soliman**, **M. G.;** Hartmann, R.; Pelaz, B.; Del Pino, P.; Parak, W. J., Fluorescence-based ion sensing with colloidal particles. Current Opinion in Pharmacology 2014, 18, 98–103.

This review article is regarding the function of colloidal NPs based on ion sensing. Particles based fluorescence sensing can be made by linking a sensitive organic fluorophores to the surface of carrier particles or by using fluorescent particles (quantum dots, carbon dots, *etc.*). Using this methodology in the field of sensing in life science applications is very convenient due to its high sensitivity, simplicity, and diversity of fluorescent materials available. Problems (and their solution) involved with using particles based fluorescence sensing for detection of ion concentrations in cells were highlighted.

The author contributes in the literature research and in the manuscript writing and edition.

- **Soliman, G. M**.; Pelaz, B.; Del Pino, P.; Parak, W. J., Functionalized GNPs for biomedical applications. In preparation.

In this review, the different methods of stabilization of gold nanoparticles were reported. Also, the functionalization of gold nanopartilces by using different strategies and biomolecules in order to be used for different biomedical applications was described.

The author contributes in the literature research and in the manuscript writing and edition.

# Chemicals and Techniques

The following chemicals were used for synthesis and modification of the NPs. All these chemicals were used without additional purification.

**Strem Chemicals:**

Hydrogen tetrachloroaurate (III) hydrate (#16903-35-8).

**Sigma-Aldrich:**

Hexadecyltrimethylammonium bromide (#H9151), sodium citrate (#W302600), silver nitrate (#209139), ascorbic acid (#A7506), sodium borohydride (#71321), dodecylamine (DDA, # 325163), tetraoctylammonium bromide (#29413-6), PMA (#531278), polyethylenimine (#408727), Polyvinylpyrrolidone (#PVP10), Poly(sodium 4-styrenesulfonate) (#243051) sodium oleate (#O7501), 1-ethyl-3-(3- (dimethylamino)propyl) carbodiimid (#E6383), TBE (#T3913), hydrochloric acid (#320331), streptomycin/penicillin (# P4333), L-glutamine (# G8540), Dulbecco's modified Eagle's medium (DMEM, # D5796), Bovine serum albumin (# A9647) and Resazurin (#199303).

**Rapp-Polymer:**

$CH_3$-PEG-SH ($M_w$= 750 Da) and $CH_3$-PEG-$NH_2$ ($M_w$= 750, 5000 and 10000 Da).

**Biochrom:**

Phosphine buffered saline (PBS, # L1825) and Fetal bovine serum (FBS, # S0615).

**Carl Roth:**

- Chloroform (#Y015.2), Ethanol (#9065.2), Methanol (#8388.6), Sodium chloride (#HN00.2), Tetrahydrofuran (#AE07.1), Sodium hydroxide (#6771.3), Dialysis membrane ($M_W$ = 50 kDa, # 1893.1), syringe filter (0.22 $\mu$ m, # P818.1)

**Fluka**

- Toluene (#89682).

**Invitrogen:**

- Ultra Pure™Agarose (#16500500),

**British Biocell International:**

- Au NPs (10 nm colloidal gold, #EM.GC10).

The following Techniques were used for preparation, purification and characterization of the NPs.

- UV-Vis spectroscopy and Fluorometer: Agilent Technologies 8453 UV-Vis and Horiba FluoroLog.
- Gel electrophoresis: Bio Rad PowerPac Basic.
- Centrifuge: Hettich Universal 320 R.
- Dynamic light scattering (DLS) and laser Doppler anemometry (LDA): Malvern Zetasizer Nano ZS.
- Transmission electron microscopy (TEM): JEOL JEM-1400PLUS.
- Rotavap (Laborota 4000, Heidolph).
- Flow cytometry.
- Inductively coupled plasma mass spectrometry. Agilent 7900 ICP-MS.

# Abbreviations

| | |
|---|---|
| AA | Ascorbic acid |
| AuNPs | Au seeds |
| WBC | white blood cell |
| CTAB | Hexadecyltrimethylammonium bromide |
| CuAAC | Cu(I)-catalyzed azide alkyne cycloaddition |
| DCC | Dicyclohexylcarbodiimide |
| DCHA | Dicyclohexylamine |
| DDA | Dodecylamine |
| DDT | Dodecanthiol |
| DLS | Dynamic light scattering |
| DMAP | Dimethylamino pyridine |
| DMEM | Dulbecco's modified Eagle's medium |
| DNA | Deoxyribonucleic acid |
| EDC | N-(3-dimethylaminopropyl)-N'-ethylcarbodiimide |
| FBS | Fetal bovine serum |
| GNPs | Gold nanoparticles |
| GNRs | Gold nanorods |
| h | Hour |
| LDA | Laser Doppler anemometry |
| LBL | Layer-by-layer |
| L-Glu | L-glutamine |
| MAA | Mercaptoacetic acid |
| MEL | Murine erythroleukemia |
| MHA | Mercaptohexanoic acid |
| MUA | Mercaptoundecanoic acid |
| NNI | National nanotechnology initiative |
| NP(s) | Nanoparticle(s) |
| OA | Oleylamine |
| PAA | Poly(acrylic acid) |
| PAH | Poly(allylamine hydrochloride) |
| PBS | Phosphate buffered saline |
| PEG(s) | Polyethylene glycol(s) |
| PEI | Polyethylenimine |
| PDI | Polydispersity index |
| PMA | Poly(isobutylene-alt-maleic anhydride) |
| P/S | Penicillin/streptomycin |
| PTT | Photothermal therapy |
| PSS | Poly(sodium 4-styrenesulfonate) |
| PVP | Poly(vinylpyrrolidone) |
| RBC | Red blood cell |

| | |
|---|---|
| s | Second |
| SGNPs | Sperical gold nanoparticles |
| SOP | Standard operating procedure |
| SPR | Surface plasmon resonance |
| TBE | Tris-borate-EDTA |
| TEM | Transmission electron microscopy |
| THF | Tetrahydrofuran |
| t | Time |
| TOAB | Tetraoctylammonium bromide |
| Tris | Tris(hydroxymethyl)aminomethane |
| UV | Tltra violet |
| v | Speed |
| vis | Visible |

# Bibliography


1. Silva, G. A., Introduction to Nanotechnology and Its Applications to Medicine. Surg. Neurol. **2004**, *61*, 216–220.
2. Nanoscience and Nanotechnologies: Opportunities and Uncertainties, The Royal Society and the Royal Academy of Engineering **2004**.
3. Whitesides, G. M., Nanoscience, Nanotechnology, and Chemistry. Small **2005**, *1*,172 –179.
4. Caruthers, S. D.; Wickline, S. A.; Lanza, G. M., Nanotechnological applications in medicine. Curr. Opin. Biotechnol. **2007**, *18*, 26–30.
5. Walmsley, G. G.; McArdle, A.; Tevlin, R.; Momeni, A.; Atashroo, D.; Hu, M. S.; Feroze, A. H.; Wong, V. W.; Lorenz, P. H.; Longaker, M. T.; Wan, D. C., Nanotechnology in bone tissue engineering. Nanomedicine **2015**, *11*, 1253–1263.
6. Bawa, R.; Bawa, S. R.; Maebius, S. B.; Flynn, T.; Wei, C., Protecting new ideas and inventions in nanomedicine with patents. Nanomedicine **2005**, *1*, 150–158.
7. Warren, H. H., Nanomaterials: Nomenclature, Novelty, and Necessity. JOM, **2004**. (See also, www.nano.gov).
8. Chen, C.; Wang, L.; Jiang, G.; Zhou, J.; Chen, X.; Yu, H.; Yang, Q., Study on the synthesis of silver nanowires with adjustable diameters through the polyol process. Nanotechnology, **2006**, *17*, 3933–3938.
9. El-Sayed, M. A., Small is different: Shape-, size- and composition-dependent properties of some colloidal semiconductor nanocrystals. Acc. Chem. Res. **2004**, *37*, 326–333.
10. El-Sayed, M. A., Some interesting properties of metals confined in time and nanometer space of different shapes. Acc. Chem. Res. **2001**, *34*, 257–264.
11. Losasso, C.; Belluco, S.; Cibin, V.; Zavagnin, P.; Mičetić I.; Gallocchio, F.; Zanella, M.; Bregoli. L.; Biancotto, G.; Ricci A., Antibacterial activity of silver nanoparticles: sensitivity of different Salmonella serovars. Front. Microbiol. **2014**, *5*. Article ID 227.
12. Prabhu, S.; Poulose, E. K., Silver nanoparticles: mechanism of antimicrobial action, synthesis, medical applications, and toxicity effects. Int. Nano Lett. **2012**, *2*. Article ID 32.
13. Feynman, R. P., There's plenty of room at the bottom. Caltech. Engineering and Science, **1960**, *23*, 22–36.
14. Shimomura, M.; Sawadaishi, T., Bottom-up strategy of materials fabrication: a new trend in nanotechnology of soft materials. Curr. Opin. Colloid Interface Sci. **2001**, *6*, 11–16.
15. Dykman, L. A.; Khlebtsov, N. G., Gold Nanoparticles in Biology and Medicine: Recent Advances and Prospects. Acta Naturae **2011**, *3*, 34–55. (See also, http://en.wikipedia.org/wiki/Photothermal_therapy, Visited May **2016**).
16. Huang, X.; Jain, P. K.; El-Sayed, I. H.; El-Sayed, M. A., Gold nanoparticles: interesting optical properties and recent applications in cancer diagnostics and therapy. Nanomedicine (Lond) **2007**, *2*, 681-693.
17. Daniel, M. C.; Astruc, D., Gold Nanoparticles: Assembly, Supramolecular Chemistry,

Quantum-Size-Related Properties, and Applications toward Biology, Catalysis, and Nanotechnology. Chem. Rev. **2004**, *104*, 293–346.
18. Wagner, F. E.; Haslbeck, S.; Stievano, L.; Calogero, S.; Pankhurst, Q. A.; Martinek, K. P., Before striking gold in gold-ruby glass. Nature **2000**, *407*, 691-692. (See also http://www.nature.com/nphoton/journal/v1/n4/fig_tab/nphoton.2007.38_F1.html. Visited May 2016).
19. http://nano--tech.blogspot.de/p/history.html. Visited May **2016**.
20. Andreas, O., Excitation of nonradiative surface plasma waves in silver by the method of frustrated total reflection. Zeitschrift für Physik **1968**, *216*, 398-410.
21. Jonsson, U.; Fagerstam, L.; Ivarsson, B.; Johnsson, B.; Karlsson, R.; Lundh, K.; Lofas, S.; Persson, B.; Roos, H.; Ronnberg, I.; Sjolander, E.; Stenberg, S.; Stahlberg, R.; Urbaniczky, C.; Ostlin, H; Malmqvist, M., Real-time Bio-specific Interaction Analysis Using Surface-Plasmon Resonance and a Sensor Chip Technology. Biotechniques **1991**, *11*, 620-622 and 624-627.
22. Khlebtsov, N. G.; Dykman, L. A., Optical properties and biomedical applications of plasmonic nanoparticles. J. Quant. Spectrosc. Radiat. Transfer **2010**, *111*, 1–35.
23. Huang, X.; El-Sayed, M. A., Gold nanoparticles: Optical properties and implementations in cancer diagnosis and photothermal therapy. Journal of Advanced Research **2010**, *1*, 13–28.
24. Eustis, S.; El-Sayed, M. A., Why gold nanoparticles are more precious than pretty gold: Noble metal surface plasmon resonance and its enhancement of the radiative and nonradiative properties of nanocrystals of different shapes. Chem. Soc. Rev. **2006**, *35*, 209–217.
25. Garcia, M. A., Surface plasmons in metallic nanoparticles: fundamentals and applications. J. Phys. D: Appl. Phys. **2011**, *44*. Article ID 389501.
26. Huang, B. X.; Neretina, S.; El-Sayed, M. A., Gold Nanorods: From Synthesis and Properties to Biological and Biomedical Applications. Adv. Mater. **2009**, *21*, 1–31.
27. Noguez, C., Surface Plasmons on Metal Nanoparticles: The Influence of Shape and Physical Environment. J. Phys. Chem. C **2007**, *111*, 3806-3819.
28. Lee, K. S.; El-Sayed, M. A., Gold and Silver Nanoparticles in Sensing and Imaging: Sensitivity of Plasmon Response to Size, Shape, and Metal Composition. J. Phys. Chem. B **2006**, *110*, 19220-19225.
29. Hu, M.; Chen, J.; Li, Z. Y.; Au, L.; Hartland, G. V.; Li, X.; Marquez, M.; Xia Y., Gold nanostructures: engineering their plasmonic properties for biomedical. Chem. Soc. Rev. **2006**, *35*, 1084–1094.
30. El-Sayed, M. A., Some Interesting Properties of Metals Confined in Time and Nanometer Space of Different Shapes. Acc. Chem. Res. **2001**, *34*, 257–264.
31. Oza, G.; Pandey, S.; Shah, R.; Vishwanathan, M.; Kesarkar, R.; Sharon, M.; Sharon M., Tailoring Aspect Ratio of Gold Nano Rods: Impact of temperature, pH, silver ions, CTAB concentration and centrifugation. Adv. Appl. Sci. Res. **2012**, *3*, 1027-1038.
32. Nikoobakht, B.; El-Sayed, M. A., Preparation and Growth Mechanism of Gold Nanorods (NRs) Using Seed-Mediated Growth Method. Chem. Mater. **2003**, *15*, 1957-1962

33. Park, J.; Joo, J.; Kwon, S. G.; Jang, Y.; Hyeon, T., Synthesis of Monodisperse Spherical Nanocrystals. Angew. Chem. Int. Ed. **2007**, *46*, 4630–4660.
34. Bréchignac, C.; Houdy, P.; Lahmani, M., Nanomaterials and Nanochemistry. Springer, Berlin, New York, **2007**.
35. Xia Y.; Xiong Y.; Lim B.; Skrabalak S. E., Shape-controlled synthesis of metal nanocrystals: simple chemistry meets complex physics? Angew. Chem. Int. Ed. Engl. **2009**, *48*, 60-103.
36. Pastoriza-Santos, I.; Liz-Marzán L. M., N,N-Dimethylformamide as a Reaction Medium for Metal Nanoparticle Synthesis. Adv. Funct. Mater. **2009**, *19*, 679-688.
37. Murphy, C. J.; Sau, T. K.; Gole, A. M.; Orendorff, C. J.; Gao, J.; Gou, L.; Hunyadi, S. E.; Li, T., Anisotropic Metal Nanoparticles: Synthesis, Assembly, and Optical Applications. J. Phys. Chem. B **2005**, *109*, 13857-13870.
38. Johnson, C. J.; Dujardin, E.; Davis, S. A.; Murphy, C. J.; Mann, S., Growth and form of gold nanorods prepared by seed-mediated, surfactant-directed synthesis. J. Mater. Chem. **2002**, *12*, 1765–1770.
39. Faraday, M., The Bakerian Lecture: Experimental Relations of Gold (and Other Metals) to Light. Philos. Trans. R. Soc. London **1857**, *147*, 145-181.
40. Sharma, V.; Park, K.; Srinivasarao, M., Colloidal dispersion of gold nanorods: Historical background, optical properties, seed-mediated synthesis, shape separation and self-assembly. Mater. Sci. Eng. R-Rep. **2009**, *65*, 1–38.
41. Turkevich, J.; Stevenson, P. C.; Hillier, J., A study of the nucleation and growth processes in the synthesis of colloidal gold. Discuss. Faraday Soc. **1951**,*11*, 55-75.
42. Frens, G., Controlled Nucleation for the Regulation of the Particle Size in Monodisperse Gold Suspensions. Nature physical science **1973**, *241*,19–22.
43. http://www.nano.gov/timeline. Visited May **2016**.
44. Tabrizi, A.; Ayhan, F.; Ayhan, H., Gold Nanoparticle Synthesis and Characterisation. Hacettepe J. Biol. & Chem. **2009**, *37*, 217-226.
45. Ji, X.; Song, X.; Li, J.; Bai, Y.; Yang, W.; Peng, X., Size control of gold nanocrystals in citrate reduction: the third role of citrate. J. Am. Chem. Soc. **2007**,*129*,13939-13948.
46. Zabetakis, K.; Ghann, W. E.; Kumar, S., Effect of high gold salt concentrations on the size and polydispersity of gold nanoparticles prepared by an extended Turkevich–Frens method. Gold Bull **2012**, *45*, 203–211.
47. Ojea-Jimenez, I.; Bastus, N. G.; Puntes, V., Influence of the Sequence of the Reagents Addition in the citrate-mediated Synthesis of Gold Nanoparticles. J. Phys. Chem. C **2011**, *115*, 15752–15757.
48. Lee, J.; Choi, S. U. S.; Jang, S. P.; Lee, S. Y., Production of aqueous spherical gold nanoparticles using conventional ultrasonic bath. Nanoscale Res. Lett. **2012**, *7*. Article ID 420.
49. Link, S.; El-Sayed, M. A., Size and Temperature Dependence of the Plasmon Absorption of Colloidal Gold Nanoparticles. J. Phys. Chem. B **1999**, *103*, 4212–4217.
50. Templeton, A. C.; Wuelfing, W. P.; Murray, R. W., Monolayer-Protected Cluster Molecules. Acc. Chem. Res. **2000**, *33*, 27–36.
51. Bastus, N. G.; Comenge, J.; Puntes, V., Kinetically Controlled Seeded Growth

Synthesis of Citrate-Stabilized Gold Nanoparticles of up to 200 nm: Size Focusing versus Ostwald Ripening. Langmuir **2011**, *27*, 11098–11105.
52. Brust, M.; Walker, M.; Bethell, D.; Schiffrin, D. J.; Whyman, R., Synthesis of thiol-derivatised gold nanoparticles in a two-phase Liquid–Liquid system. J. Chem. Soc., Chem. Commun.**1994**, 801-802.
53. Martin, M. N.; Basham, J. I.; Chando, P.; Eah, S., Charged Gold Nanoparticles in Non-Polar Solvents: 10-min Synthesis and 2D Self-Assembly. Langmuir **2010**, *26*, 7410–7417.
54. Lohse, S. E.; Murphy, C. J., The Quest for Shape Control: A History of Gold Nanorod Synthesis. Chem. Mater. **2013**, *25*, 1250–1261.
55. Jana, N. R.; Gearheart, L.; Murphy, C. J., Wet Chemical Synthesis of High Aspect Ratio Cylindrical Gold Nanorods. J. Phys. Chem. B **2001**, *105*, 4065-4067.
56. Jana, N. R.; Gearheart, L.; Murphy, C. J., Seed-Mediated Growth Approach for Shape-Controlled Synthesis of Spheroidal and Rod-like Gold Nanoparticles Using a Surfactant Template. Adv. Mater. **2001**, *13*, 1389-1393.
57. Busbee, B. D.; Obare, S. O.; Murphy, C. J., An Improved Synthesis of High-Aspect-Ratio Gold Nanorods. Adv. Mater. **2003**, *15*, 414-416.
58. Murphy, C. J.; Thompson, L. B.; Alkilany, A. M.; Sisco, P. N.; Boulos, S. P.; Sivapalan, S. T.; Yang, J. A.; Chernak, D. J.; Huang, J., The Many Faces of Gold Nanorods. J. Phys. Chem. Lett. **2010**, *1*, 2867–2875.
59. Murphy, C. J.; Thompson, L. B.; Chernak, D. J.; Yang, J. A.; Sivapalan, S. T.; Boulos, S. P.; Huang, J.; Alkilany, A. M.; Sisco, P. N., Gold nanorod crystal growth: From seed-mediated synthesis to nanoscale sculpting. Curr. Opin. Colloid Interface Sci. **2011**, *16*, 128-134.
60. Ward, C. J.; Tronndorf, R. Eustes, A. S.; Auad, M. L.; Davis, E. W., Seed-Mediated Growth of Gold Nanorods: Limits of Length to Diameter Ratio Control. Journal of Nanomaterials **2014**, 1-7. Article ID 765618.
61. Wei, Q.; Ji, J.; Shen, J., pH Controlled Synthesis of High Aspect-Ratio Gold Nanorods. J. Nanosci. Nanotechnol. **2008**, *8*, 5708–5714.
62. Gole, A.; Murphy, C. J.; Seed-Mediated Synthesis of Gold Nanorods: Role of the Size and Nature of the Seed. Chem. Mater. **2004**, *16*, 3633–3640.
63. Ye, X.; Jin, L.; Caglayan, H.; Chen, J.; Xing, G.; Zheng, C.; Doan-Nguyen, V.; Kang, Y.; Engheta, N.; Kagan, C. R.; Murray, C. B., Improved Size-Tunable Synthesis of Monodisperse Gold Nanorods through the Use of Aromatic Additives. ACS Nano 2012, 6, 2804–2817.
64. Ye, X.; Zheng, C.; Chen, J.; Gao, Y.; Murray, C. B., Using binary surfactant mixtures to simultaneously improve the dimensional tunability and monodispersity in the seeded growth of gold nanorods. Nano Lett. **2013**, *13*, 765–771.
65. Weisbecker, C. S.; Merritt, M. V.; Whitesides, G. M., Molecular Self-Assembly of Aliphatic Thiols on Gold Colloids. Langmuir **1996**, *12*, 3763-3772.
66. Love, J. C.; Estroff, L. A.; Kriebel, J. K.; Nuzzo, R. G.; Whitesides, G. M., Self-assembled monolayers of thiolates on metals as a form of nanotechnology. Chem. Rev. **2005**, *105*, 1103-1169.
67. Sakura, T.; Takahashi; T.; Kataoka, K.; Nagasaki, Y., One-pot preparation of mono-

dispersed and physiologicallystabilized gold colloid. Colloid. Polym. Sci. **2005**, *284*, 97-101.
68. Sperling, R. A.; Parak, W. J., Surface modification, functionalization and bioconjugation of colloidal inorganic nanoparticles. Phil. Trans. R. Soc. A **2010**, *368*, 1333–1383.
69. Alkilany, A. M.; Nagaria, P. K; Hexel, C. R; Shaw, T. J; Murphy, C. J.; Wyatt, M. D., Cellular uptake and cytotoxicity of gold nanorods: molecular origin of cytotoxicity and surface effects. Small **2009**, *5*, 701-718.
70. Labouta, H. I.; Schneider, M., Tailor-made biofunctionalized nanoparticles using layer-by-layer technology. Int. J. Pharm. **2010** *395*, 236-242.
71. Masereel, B.; Dinguizli, M.; Bouzin, C.; Moniotte, N.; Feron, O.; Gallez, B.; Borght, T. V.; Michiels, C.; Lucas, S., Antibody immobilization on gold nanoparticles coated layer-by-layer with polyelectrolytes. J. Nanopart. Res. **2011**, *13*, 1573-1580.
72. Zhou, M.; Wang, B.; Rozynek, Z.; Xie, Z.; Fossum, J. O.; Yu, X.; Raaen, S., Minute synthesis of extremely stable gold nanoparticles. Nanotechnology **2009**, *20*. Article ID 505606.
73. Seola, S.; K.; Kima, D.; Junga, S.; Changa, W. S.; Baea, Y. M.; Leea, K. H.; Hwu, Y., Effect of citrate on poly(vinyl pyrrolidone)-stabilized gold nanoparticles formed by PVP reduction in microwave (MW) synthesis. Mater. Chem. Phys. **2012**,*137*, 135–139.
74. Pimpang, P.; Choopun, S., Monodispersity and Stability of Gold Nanoparticles Stabilized by Using Polyvinyl Alcohol. Chiang Mai J. Sci. **2011**, *38*, 31-38.
75. Pastoriza-Santos, I.; Perez-Juste, J.; Liz-Marzan, L. M., Silica-Coating and Hydrophobation of CTAB-Stabilized Gold Nanorods. Chem. Mater. **2006**, *18*, 2465-2467.
76. Mehtala, J. G.; Zemlyanov, D. Y.; Max, J. P.; Kadasala, N.; Zhao, S.; and Wei, A., Citrate-Stabilized Gold Nanorods. Langmuir **2014**, *30*, 13727–13730.
77. Wei, G. T.; Yang, Z.; Lee, C. Y.; Yang, H. Y.; Wang, C. R. C., Aqueous-Organic Phase Transfer of Gold Nanoparticles and Gold Nanorods Using an Ionic Liquid. J. Am. Chem. Soc. **2004**, *126*, 5036-5037.
78. Misra, T. K.; Chen, T. S.; Liu, C. Y., Phase transfer of gold nanoparticles from aqueous to organic solution containing resorcinarene. J. Colloid Interface Sci. **2006,** *297*, 584–588.
79. Huschka, R.; Zuloaga, J.; Knight, M. W.; Brown, L. V.; Nordlander, P.; Halas, N. J., Light-Induced Release of DNA from Gold Nanoparticles: Nanoshells and Nanorods. J. Am. Chem. Soc. **2011**, *133*, 12247–12255.
80. Alkilany, A. M.; Yaseen, A. I. B.; Park, J.; Ellerb, J. R.; Murphy, C. J., Facile phase transfer of gold nanoparticles from aqueous solution to organic solvents with thiolated poly(ethylene glycol). RSC Adv. **2014**, *4*, 52676–52679.
81. McMahon, J. M.; Emory, S. R., Phase Transfer of Large Gold Nanoparticles to Organic Solvents with Increased Stability. Langmuir **2007**, *23*, 1414-1418.
82. Soliman, M. G.; Pelaz, B.; Parak, W. J.; Del Pino, P., Phase Transfer and Polymer Coating Methods toward Improving the Stability of Metallic Nanoparticles for Biological Applications. Chem. Mater. **2015**, *27*, 990–997.

83. Lin, C. A., Sperling, R. A.; Li, J. K.; Yang, T. Y.; Li, P. Y.; Zanella, M.; Chang, W. H.; Parak, W. J., Design of an amphiphilic polymer for nanoparticle coating and functionalization. Small **2008**, *4*, 334-341.
84. Pellegrino, T.; Manna, L.; Kudera, S.; Lied, T.; Koktysh, D.; Rogach, A. L.; Keller, S.; Radler, J.; Natile, G.; Parak, W. J., Hydrophobic Nanocrystals Coated with an Amphiphilic Polymer Shell: A General Route to Water Soluble Nanocrystals. Nano Lett. **2004**, *4*, 703-707.
85. Malvindi, M. A.; Carbone, L.; Quarta, A.; Tino, A.; Manna, L.; Pellegrino, T.; Tortiglione, C., Rod-shaped nanocrystals elicit neuronal activity in vivo. Small **2008**, *4*,1747–1755.
86. Griffin, F.; Fitzmaurice D., Preparation and Thermally Promoted Ripening of Water-Soluble Gold Nanoparticles Stabilized by Weakly Physisorbed Ligands. Langmuir **2007**, *23*, 10262–10271.
87. Slocik, J. M.; Stone, M. O.; Naik, R. R., Synthesis of Gold Nanoparticles Using Multifunctional Peptides. Small **2005**, *1*, 1048-1052.
88. Yan Zhao, Waleska Pérez-Segarra, Qicun Shi, and Alexander Wei. Dithiocarbamate Assembly on Gold. J. Am. Chem. Soc. **2005**, *127*, 7328–7329.
89. Paeza, J. I.; Coronadob, E. A.; Strumia, M. C., Preparation of controlled gold nanoparticle aggregates using a dendronization strategy. J. Colloid Interface Sci. **2012**, *384*, 10–21.
90. Zheng, J.; Stevenson, M. S.; Hikida, R. S.; Patten, P. G. V., Influence of pH on Dendrimer-Protected Nanoparticles. J. Phys. Chem. B **2002**, *106*, 1252–1255.
91. Song W. J.; Du, J. Z.; Sun, T. M.; Zhang, P. Z.; Wang, J., Gold nanoparticles capped with polyethyleneimine for enhanced siRNA delivery. Small **2010**, *6*, 239-246.
92. Jans, H.; Jans, K.; Lagae, L.; Borghs, G.; Maes, G.; Huo, Q., Poly(acrylic acid)-stabilized colloidal gold nanoparticles: synthesis and properties. Nanotechnology **2010**, *21*. Article ID 455702.
93. Minea, E.; Yamadaa, A.; Kobayashia, Y.; Konnoa, M.; Liz-Marzánb, L. M., Direct coating of gold nanoparticles with silica by a seeded polymerization technique. J. Colloid Interface Sci. **2013**, *264*, 385–390.
94. Tiwari, P. M.; Vig, K.; Dennis, V. A.; Singh, S. R., Functionalized Gold Nanoparticles and Their Biomedical Applications. Nanomaterials **2011**, *1*, 31-63.
95. Nakajima, N.; Ikada, Y., Mechanism of Amide Formation by Carbodiimide for Bioconjugation in Aqueous Media. Bioconjugate Chem. **1995**, *6*, 123–130.
96. Zhang, F.; Lees, E.; Amin, F.; Gil, P. R.; Yang, F.; Mulvaney, P.; Parak, W. J., Polymer-Coated Nanoparticles: A Universal Tool for Biolabelling Experiments. Small **2011**, *7*, No. 22, 3113–3127.
97. Kolb, H. C.; Finn, M. G.; Sharpless, K. B., Click Chemistry: Diverse Chemical Function from a Few Good Reactions. Angew. Chem. Int. Ed. **2001**, *40*, 2004–2021.
98. Binder, W. H.; Sachsenhofer, R., 'Click' Chemistry in Polymer and Material Science: An Update. Macromol. Rapid Commun. **2008**, *29*, 952–981.
99. Rostovtsev, V. V.; Green, L. G.; Fokin, V. V.; Sharpless, K. B., A Stepwise Huisgen Cycloaddition Process: Copper(I)-Catalyzed Regioselective "Ligation" of Azides and Terminal Alkynes. Angew. Chem. Int. Ed. **2002**, *41*, 2596–2599.

100. Meldal, M.; Tornøe, C. W., Cu-Catalyzed Azide-Alkyne Cycloaddition. Chem. Rev. **2008**, *108*, 2952–3015.
101. Brennan, J. L., Hatzakis, N. S.; Tshikhudo, T. R.; Dirvianskyte, N.; Razumas, V.; Patkar, S.; Vind, J.; Svendsen, A.; Nolte, R. J. M.; Rowan, A. E.; Brust. M., Bionanoconjugation via Click Chemistry: The Creation of Functional Hybrids of Lipases and Gold Nanoparticles. Bioconjugate Chem. **2006**, *17*, 1373–1375.
102. Oyelere, A. K.; Chen, P. C.; Huang, X.; El-Sayed, I. H.; El-Sayed, M. A., Peptide-conjugated gold nanorods for nuclear targeting. Bioconjugate Chem. **2007**, *18*,1490–1497.
103. Amici, J.; Allia, P.; Tiberto, P.; Sangermano, M., Poly(ethylene glycol)-Coated $Fe_3O_4$ Nanoparticles by UV-Thiol-Ene Addition of PEG Dithiol on Vinyl-Functionalized Magnetite Surface. Macromol. Chem. Phys. **2011**, *212*, 1629–1635.
104. Roberts, M. J.; Bentley, M. D.; Harris, J. M., Chemistry for peptide and protein PEGylation. Adv Drug Deliv Rev **2002**, *54*, 459–476.
105. Wattendorf, U.; Merkle, H. P., PEGylation as a Tool for the Biomedical Engineering of Surface Modified Microparti- cles. J. Pharm. Sci. **2008**, *97*, 4655–4669.
106. Logie, J.; Owen, S. C.; McLaughlin, C. K.; Shoichet, M. S., PEG-Graft Density Controls Polymeric Nanoparticle Micelle Stability. Chem. Mater. **2014**, *26*, 2847–2855.
107. Niidome, T.; Yamagata, M.; Okamoto, Y.; Akiyama, Y.; Takahashi, H.; Kawano, T.; Katayama, Y.; Niidome, Y., PEG-modified gold nanorods with a stealth character for in vivo applications. J. Controlled Release **2006**, *114*, 343-347.
108. Pierrat, S.; Zins, I.; Breivogel, A.; Sönnichsen, C., Self-Assembly of Small Gold Colloids with Functionalized Gold Nanorods. Nano Lett. **2007**, *7*, 259–263.
109. Pelaz, B.; Del Pino, P.; Maffre, P.; Hartmann, R.; Gallego, M.; Fernandez, S. R.; De la Fuente, J. M.; Nienhaus, G. U.; Parak, W. J., Surface Functionalization of Nanoparticles with Polyethylene Glycol: Effects on Protein Adsorption and Cellular Uptake. ACS Nano **2015**, *9*, 6996–7008.
110. Pozzi, D.; Colapicchioni, V.; Caracciolo, G.; Piovesana, S.; Capriotti, A. L.; Palchetti, S.; De Grossi, S.; Riccioli, A.; Amenitsch H.; Laganà, A., Effect of polyethyleneglycol (PEG) chain length on the bio–nano-interactions between PEGylated lipid nanoparticles and biological fluids: from nanostructure to uptake in cancer cells. Nanoscale **2014**, *6*, 2782-2792.
111. Larson, T. A.; Joshi, P. P.; Sokolov, K., Preventing protein adsorption and macrophage uptake of gold nanoparticles via a hydrophobic shield. ACS Nano **2012**, *6*, 9182-9190.
112. Monopoli, M. P.; Walczyk, D.; Campbell, A.; Elia, G.; Lynch, I.; Bombelli, F. B.; Dawson, K. A., Physical−Chemical Aspects of Protein Corona: Relevance to in Vitro and in Vivo Biological Impacts of Nanoparticles. J. Am. Chem. Soc. **2011**, *133*, 2525–2534.
113. Del Pino, P.; Pelaz, B.; Zhang, Q.; Maffre, P.; Nienhaus, G. U.; Parak, W. J., Protein corona formation around nanoparticles–from the past to the future. Mater. Horiz. **2014**, *1*, 301-313.
114. Cedervall, T.; Lynch, I.; Lindman, S.; Berggård, T.; Thulin, E.; Nilsson, H.; Dawson,

K. A.; Linse, S., Understanding the nanoparticle–protein corona using methods to quantify exchange rates and affinities of proteins for nanoparticles. Proc. Natl. Acad. Sci. U. S. A. **2007**, *104*, 2050-2055.

115. Fadeel, B.; Feliu, N.; Vogt, C.; Abdelmonem, A. M.; Parak, W. J., Bridge over troubled waters: understanding the synthetic and biological identities of engineered nanomaterials. WIREs Nanomed Nanobiotechnol **2013**, *5*,111–129.
116. Gunawan, C.; Lim, M.; Marquis, C. P.; Amal, R., Nanoparticle–protein corona complexes govern the biological fates and functions of nanoparticles. J. Mater. Chem. B **2014**, *2*, 2060-2083.
117. Lundqvist, M.; Stigler, J.; Elia, G.; Lynch, I.; Cedervall, T.; Dawson, K. A., Nanoparticle size and surface properties determine the protein corona with possible implications for biological impacts. Proc. Natl. Acad. Sci. U.S.A. **2008**, *105*, 14265–14270.
118. Lynch, I.; Dawson, K. A., Protein-nanoparticle interactions. Nano Today 2008, 3, 40–47.
119. Lundqvist, M.; Stigler, J.; Cedervall, T.; Berggård, T.; Flanagan, Michelle, B.; Lynch, I.; Elia, G.; Dawson, K., The Evolution of the Protein Corona around Nanoparticles: A Test Study. ACS Nano **2011**, *5*, 7503–7509.
120. Nazarenus, M.; Zhang, Q.; Soliman, M. G.; Del Pino, P.; Pelaz, B.; Romero, S. C.; Rejman, J.; Rutishauser, B. R.; Clift, M. J. D.; Zellner, R.; Nienhaus, G. U.; Delehanty, J. B.; Medintz, I. L.; Parak, W. J., In vitro interaction of colloidal nanoparticles with mammalian cells: What have we learned thus far? Beilstein J. Nanotechnol. **2014**, *5*, 1477–1490.
121. Ashraf, S.; Pelaz, B.; Del Pino, P.; Carril, M.; Escudero1, A.; Parak, W. J.; Soliman, M. G.; Zhang, Q.; Carrion-Carrillo, C. C., Gold-based nanomaterials for applications in nanomedicine. Top Curr Chem. **2016**, *370*, 169-202.
122. Brewer, S. H.; Glomm, W. R.; Johnson, M. J.; Knag, M. K.; Franzen, S., Probing BSA Binding to Citrate-Coated Gold Nanoparticles and Surfaces. Langmuir **2005**, *21*, 9303–9307.
123. Zook, J. M.; MacCuspie, R. I.; Locasicio, L. E.; Halter, M. D.; Elliott, J. T., Stable Nanoparticle Aggregates/Agglomerates of Different Sizes and the Effect of Their Size on Hemolytic Cytotoxicity. Nanotoxicology **2011**, *5*, 517–530.
124. Chanana, M.; Correa-Duarte, M. A.; Liz-Marzán, L. M., Insulin-Coated Gold nanoparticles: A Plasmonic Device for Studying Metal-Protein Interactions. Small **2011**, *7*, 2650–2660.
125. Bharti, B.; Meissner, J.; Findenegg, G. H., Aggregation of Silica Nanoparticles Directed by Adsorption of Lysozyme. Langmuir **2011**, *27*, 9823–9833.
126. Thanh, N. T. K.; Rosenzweig, Z., Development of an Aggregation-Based Immunoassay for Anti-Protein A Using Gold Nanoparticles. Anal. Chem. **2002**, *74*, 1624–1628.
127. Zook, J. M.; Rastogi, V.; MacCuspie, R. I.; Keene, A. M.; Fagan, J., Measuring Agglomerate Size Distribution and Dependence of Localized Surface Plasmon Resonance Absorbance on Gold Nanoparticle Agglomerate Size Using Analytical Ultracentrifugation. ACS Nano **2011**, *5*, 8070–8079.

128. Schulze, C.; Kroll, A.; Lehr, C. M.; Schäfer, U. F.; Becker, K.; Schnekenburger, J.; Isfort, C. S.; Landsiedel, R.; Wohlleben, W., Not Ready to Use - Overcoming Pitfalls when Dispersing Nanoparticles in Physiological Media. Nanotoxicology **2008**, *2*, 51–61.
129. Huang, D.; Liao, F.; Molesa, S.; Redinger, D.; Subramanin, V.; Plastic-Compatible Low Resistance Printable Gold Nanoparticle Conductors for Flexible Electronics. Journal of The Electrochemical Society **2003**, *150*, 412-417.
130. Stuchinskaya, T.; Moreno, M.; Cook, M. J.; Edwards, D. R.; Russell, D. A., Targeted photodynamic therapy of breast cancer cells using antibody–phthalocyanine–gold nanoparticle conjugates. Photochem. Photobiol. Sci. **2011**,*10*, 822-831.
131. Dreaden, E. C.; Austin, L. A.; Mackey, M. A.; El-Sayed, M. A.; Size matters: gold nanoparticles in targeted cancer drug delivery. Ther Deliv **2012**, *3*, 457–478.
132. Boisselier, E.; Astruc, D., Gold nanoparticles in nanomedicine: preparations, imaging, diagnostics, therapies and toxicity. Chem. Soc. Rev. **2009**, *38*, 1759-1782
133. Jain, P. K.; Lee, K. S.; El-Sayed, I. H.; El-Sayed, M. A., Calculated Absorption and Scattering Properties of Gold Nanoparticles of Different Size, Shape, and Composition: Applications in Biological Imaging and Biomedicine. J. Phys. Chem. B **2006**, *110*, 7238-7248.
134. Haiss, W.; Thanh, N. T. K.; Aveyard, J.; Fernig, D. G., Determination of Size and Concentration of Gold Nanoparticles from UV-Vis Spectra. Anal. Chem. **2007**, *79*, 4215- 4221.
135. Tan, G.; Kantner, K.; Zhang, Q.; Soliman, M. G.; Del Pino, P.; Parak, W. J.; Onur, M. A.; Valdeperez, D.; Rejman, J.; Pelaz, B., Conjugation of polymer-coated gold nanoparticles with antibodies - synthesis and characterization. Nanomaterials **2015**, *5*, 1297-1316.
136. Pellegrino, T.; Sperling, R. A.; Alivisatos, A. P.; Parak, W. J., Gel electrophoresis of Gold- DNA Nanoconjugates. J. Biomed. Biotechnol. **2007**, 1-9. Article ID 26796.
137. Hühn, D.; Kantner, K.; Geidel, C.; Brandholt, S.; De Cock, I.; Soenen, S. J. H.; Rivera Gil, P.; Montenegro, J. M.; Braeckmans, K.; Müllen, K.; Nienhaus, G. U.; Klapper, M.; Parak, W. J., Polymer-Coated Nanoparticles Interacting with Proteins and Cells: Focusing on the Sign of the Net Charge. ACS Nano **2013**, *7*, 3253-3263.
138. Rivera Gil, P.; Jimenez de Aberasturi, D.; Wulf, V.; Pelaz, B.; Del Pino, P.; Zhao, Y.; de la Fuente, J.; Ruiz de Larramendi, I.; Rojo, T.; Liang, X. J.; Parak, W. J., The Challenge to Relate the Physicochemical Properties of Colloidal Nanoparticles to Their Cytotoxicity. Acc. Chem. Res. **2013**, *46*, 743-749.
139. Kreyling, W. G.; Abdelmonem, A. M.; Ali, Z.; Alves, F.; Geiser, M.; Haber, N.; Hartmann, R.; Hirn, S.; de Aberasturi, D. J.; Kantner, K.; Khadem-Saba, G.; Montenegro, J.; Rejman, J.; Rojo, T.; de Larramendi, I. R.; Ufartes, R.; Wenk A.; Parka, W. J., In vivo integrity of polymer-coated gold nanoparticles. Nature nanotechnology **2015**, *10*, 619-623.
140. Krajewski, S.; Prucek, R.; Panacek, A.; Avci-Adali, M.; Nolte, A.; Straub, A.; Zboril, R.; Wendel, H. P.; Kvitek, L., Hemocompatibility evaluation of different silver nanoparticle concentrations employing a modified Chandler-loop in vitro assay on human blood. Acta Biomater. **2013**, *9*, 7460-7468.

141. Schleh, C.; Semmler-Behnke, M.; Lipka, J.; Wenk, A.; Hirn, S.; Schäffler, M.; Schmid, G.; Simon, U.; Kreyling, W.G., Size and surface charge of gold nanoparticles determine absorption across intestinal barriers and accumulation in secondary target organs after oral administration. Nanotoxicology **2012**, *6*, 36-46.
142. Kreyling, W. G.; Hirn, S.; Möller, W.; Schleh, C.; Wenk, A.; Celik, G.; Lipka, J.; Schäffler, M.; Haberl, N.; Johnston, B. D.; Sperling, R.; Schmid, G.; Simon, U.; Parak, W. J.; Semmler-Behnke, M., Air–blood barrier translocation of tracheally instilled gold nanoparticles inversely depends on particle size. ACS Nano **2014**, *8*, 222–233.
143. Li, X.; Wang, L.; Fan, Y.; Feng, Q.; Cui, F., Biocompatibility and Toxicity of Nanoparticles and Nanotubes. Journal of Nanomaterials **2012**, *2012*, Article ID 548389.
144. Kreyling, W. G.; Abdelmonem, A. M.; Ali, Z.; Alves, F.; Geiser, M.; Haber, N.; Hartmann, R.; Hirn, S.; de Aberasturi, D. J.; Kantner, K.; Khadem-Saba, G.; Montenegro, J.; Rejman, J.; Rojo, T.; de Larramendi, I. R.; Ufartes, R.; Wenk A.; Parka, W. J., In vivo integrity of polymer-coated gold nanoparticles. Nature nanotechnology **2015**, *10*, 619-623.
145. Schäffler, M.; Sousa, F.; Wenk, A; Sitia, L.; Hirn, S.; Schleh, C.; Haberl, N.; Violatto, M.; Canovi, M.; Andreozzi, P.; Salmona, M.; Bigini, P.; Kreyling, W. G.; Krol, S., Blood protein coating of gold nanoparticles as potential tool for organ targeting. Biomaterials 2014 35, 3455-3466.
146. Ashraf, S.; Carrion, C. C.; Zhang, Q.; **Soliman**, **M. G.;** Hartmann, R.; Pelaz, B.; Del Pino, P.; Parak, W. J., Fluorescence-based ion sensing with colloidal particles. Curr. Opin. Pharmacol. **2014**, *18*, 98–103.

# Appendix

## Wissenschaftlicher Lebenslauf

### 1. Persönliche Angaben


| | |
|---|---|
| Vorname/ Name: | Mahmoud/ Soliman |
| Geburtsdatum: | June 20, 1984 (El Behira, Ägypten). |
| Anschrift: | Dürerstraße 36, 35396 Gießen, Deutschland. |
| E-Mail: | m.siliman@yahoo.com/<br>Solimanm@students.uni-marburg.de |


### 2. Ausbildung

| | |
|---|---|
| 04/ 2012- dato | Promotionan der Philipps-Universität Marburg.<br>Thema der Dissertation: Synthese, Oberflächenmodifizierung und Funktionalisierung von Gold-Nanopartikel für Biomedizinische.<br>Betreue: Prof. Dr. Wolfgang. J. Parak. |
| 10/2008 - 09/2011 | Masterstudiengang: Physik Wissenschaft, Biophysik Abteilung, Al-Azhar-Universität, Kairo, Ägypten. |
| 10/2007 - 06/2008 | Pre-Master: Physik Wissenschaft, Biophysik Abteilung, Al-Azhar-Universität, Kairo, Ägypten. |
| 10/2002 - 06/2006 | Bachelorstudiengang: Physik Wissenschaft, Biophysik Abteilung, Al-Azhar-Universität, Kairo, Ägypten. |
| 10/1999 - 06/2002 | Gymnasium. |

### 3. Abitur

| | |
|---|---|
| 11/2011 - 03/2012 | Vollzeit Vorführer an Physik Institut, Fakultät für Naturwissenschaften, Al-Azhar-Universität, Kairo, Ägypten. |
| 12/2007 - 10/2011 | Vollzeit Lehrassesstant an Physik Institut, Fakultät für Naturwissenschaften, Al-Azhar-Universität, Kairo, Ägypten.<br>Aufgabe: Unterrichten des Labor-Physik (optische, elektrische und Festkörperphysik). |

CHEMISTRY OF MATERIALS

Article

pubs.acs.org/cm

# Phase Transfer and Polymer Coating Methods toward Improving the Stability of Metallic Nanoparticles for Biological Applications

Mahmoud G. Soliman,[†,‡] Beatriz Pelaz,*[,†,‡] Wolfgang J. Parak,[†,§] and Pablo del Pino*[,§]

[†]Fachbereich Physik, Philipps Universität Marburg, 35037 Marburg, Germany

[§]CIC biomaGUNE, 20009 San Sebastian, Spain

Supporting Information

**ABSTRACT:** This paper describes a general method to generate noble metal nanoparticles (NPs) with polymer coatings. One of the widely used approaches to stabilize NPs in aqueous solution involves wrapping NPs with amphiphilic polymers. This methodology has been extensively employed for polymer coating of small hydrophobic NPs (diameter of inorganic core < 20 nm), thereby enabling phase transfer of NPs from an organic solvent to aqueous solution. The polymer coating approach is herein extended to NPs originally synthesized in aqueous solution by a two-step method. First, NPs are subjected to aqueous-to-organic phase transfer. The phase transfer protocol is demonstrated for NPs made of different materials (Au and Ag), sizes (up to 100 nm), and shapes (spheres, rods, and flat-triangular prisms). Second, NPs are coated with an amphiphilic polymer. The colloidal stability of a variety of the newly designed NPs is assayed against different media of biological relevance. In preliminary cellular studies, the biocompatibility of polymer coated Au NPs is investigated in different cell lines.

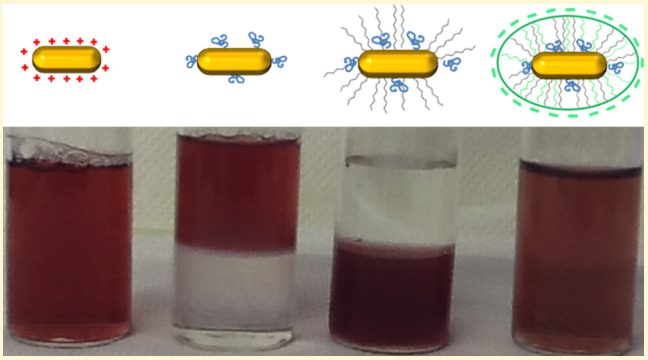

## INTRODUCTION

Current bottom-up chemical methods allow the synthesis of nanoparticles (NPs) with a large range of possible size, shape, and composition. This is possible with a high degree of control in terms of monodispersity and size distribution.[1−4] Synthesis can be carried out either in organic solvents or in aqueous solution. In addition to being able to control the physicochemical properties of the end products by chemical methods, colloidal stability of NPs in physiological media is critical if these are to be used in biological applications.[5] This implies that NPs should be stable in aqueous media with high ionic strength, high protein concentration, and a specific range of pH values. In contrast to NPs synthesized in aqueous media, methods to stabilize hydrophobic NPs require a phase transfer step which can be effectively achieved by different methods, such as the replacement of the hydrophobic chains by hydrophilic ones (ligand exchange)[6] or the use of amphiphilic polymers.[7] Two main advantages of the latter compared to other existing methods are to be highlighted. First, the original surface of the inorganic material (be it metal, semiconductor, or metal oxide) is a priori not affected, and therefore, the physical properties of the core such as quantum yield, absorption, scattering, or magnetism are in general less disturbed as compared to ligand-exchange procedures. Second, the NPs surface is uniformly wrapped with a common polymer, which translates into the generation of a common surface chemistry for different materials. Notably, the latter allows the production of NP models with similar surface chemistry yet with different physicochemical properties due to different inorganic cores. Magnetic, semiconductor, and metallic NPs, with different size, shape, and composition, have been successfully stabilized by the latter.[7−11]

In the literature, the number of works which attempt to evaluate the impact of NPs in cells, or even complex organisms, is overwhelming.[12] Yet correlating physicochemical properties of NPs and their biological fate and impact is still not straightforward.[5] This is partly so because of the enormous variety of NP models employed to date, which will even continue to grow as new methods and materials arise. Besides the variety of NP models, it appears clear that the biological fate of NPs is highly influenced by the NPs' surface chemistry, which has been also demonstrated to be very important in the formation of the so-called protein corona.[13] As proven already with different NP models, varying the coating of NPs greatly influences several important biological parameters such as cellular uptake, NP localization inside cells, toxicity, circulation, biodistribution, protein corona, etc. The design of the surface of NPs represents a key step toward multifunctional NPs, which are typically achieved by anchoring distinct molecules of biological relevance onto the NPs' surface. The biological fate of NPs is also determined by the protein corona. Ultimately, the protein corona formation can be responsible for different

Received: November 24, 2014
Revised: January 19, 2015
Published: January 20, 2015




DOI: 10.1021/cm5043167
Chem. Mater. 2015, 27, 990−997

results observed using similar nanosystems.[14] The use of amphiphilic polymers to coat NPs would eliminate the surface factor from the equation, providing thereby a NP model in which it is possible to determine the role of one parameter at a time, such as size, vectors, stiffness, ions release, etc. Additionally, this methodology provides NPs with a high colloidal stability in cell media, against high salt concentration, and in a broad pH range.[8,15] These reasons make this technique highly interesting to produce NP models for biological applications. However, to date, this methodology has been traditionally limited to small NPs, typically with inorganic cores with diameter < 20 nm, originally synthesized in organic solvent, and therefore, many biorelevant NPs originally synthesized in aqueous media (e.g., anisotropic plasmonic NPs) have not benefited from this technique. In order to apply this methodology to such NPs (e.g., CTAB-coated gold nanorods, where CTAB stands for the cationic surfactant cetyltrimethylammonium bromide), a previous phase transfer to an organic solvent should be performed.

For the aqueous-to-organic media transfer of Au NPs the ligand exchange technique has been applied by using aliphatic chains with a terminal thiol group such as dodecanethiol (DDT)[16] or by using chains with a terminal amine group such as dodecylamine (DDA) or hexadecylamine (HDA).[17] The main limitation of the ligand-exchange method is again the size, as it typically works with NPs of diameters smaller than ca. 20 nm, in the case of free-surfactant capped NPs. To our knowledge, only a few examples with NPs > 20 nm have been described in the literature.[18,19] The need of surfactants to transfer large particles is obvious according to the published works in this direction, in which CTAB or similar surfactants are typically involved, be it as additives for the phase transfer process or in the NPs synthesis.[16,20] For anisotropic Au NPs, the phase transfer of gold nanorods using DDT has been used, with the aim of washing out the excess of the cytotoxic surfactant CTAB. The toxic effects of CTAB have been extensively proved.[21,22] In order to decrease the amount of CTAB, a round trip from aqueous phase to organic media and again to aqueous media has been previously reported.[23−25]

Herein, we report on a straightforward method which allows for aqueous-to-organic phase transfer of relevant Au NPs with different sizes (inorganic cores with diameters of 25, 50, and 60 nm up to nanorods with 90 nm in length) and shapes (spherical and rods). As a proof-of-concept to extend this methodology to an additional shape and another plasmonic material, Ag nanoprisms were also successfully polymer coated using equivalent methods as for Au NPs. The basis of the proposed method relies on a prestabilization step using short (low molecular weight) polyethylene glycol (PEG) chains. A recent work in which long alkyl-PEG chains has been described as ligands to transfer nanorods to the organic phase using centrifugal forces has been recently reported.[26] NPs smaller than 20 nm were transferred using mixed chains containing an aliphatic domain and a hydrophilic PEG chain, which allow the NPs to be colloidally stable in both solvents.[27] In the present work, short PEG chains were used as prestabilizers and active agents for the phase transfer of NPs. The prestabilization step was required to warrant colloidal stability in the phase transfer process. In case the NP size > 15 nm; i.e., inorganic cores with diameters larger than 15 nm, ligands such as DDT or HDA yielded unsatisfactory results. Thus, as an alternative to toxic surfactants such as CTAB or didecyldimethylammonium bromide (DDAB), the use of short PEG chains was investigated. PEGylated NPs can be driven to an organic phase (chloroform) containing DDA under vigorous stirring at room temperature. The time required depended on the original coating of the NPs. For instance, CTAB-coated gold nanorods (GNRs) required longer times than citrate capped Au NPs. The use of ethanol helped to complete the transfer faster.[28] DDA can then intercalate with the amphiphilic polymer dodecyl-grafted-poly(isobutylene-*alt*-maleic-anhydride) (PMA), enabling aqueous transfer for different colloids. In order to enhance the stability of the polymer-coated NPs in cell media, further PEGylation was employed. Finally, stability and toxicity studies are shown as examples to illustrate the potential of this method to provide NP models for biological applications.

## EXPERIMENTAL SECTION

**Materials.** Prior to use, all glassware was washed with *aqua regia* and rinsed thoroughly with Milli-Q water. All the chemicals were used as received. For the synthesis and modification of the NPs, hydrogen tetrachloroaurate (III) hydrate was purchased from Strem Chemicals; sodium citrate, silver nitrate, CTAB, sodium borohydrade, ascorbic acid, hydrogen peroxide, dodecylamine, poly(isobutylene-maleic-*alt*-anhydride), hydrochloridric acid, sodium borate, 1-ethyl-3-(3-(dimethylamino)propyl) carbodiimide, and sodium oleate were purchased from Sigma-Aldrich. All the different polyethylene glycol polymers (PEG) were obtained from Rapp-Polymere. For the stability studies, phosphine buffered saline (PBS) was purchased in Biochrom, and DMEM, penicillin, streptomycin, and L-glutamine were purchased from Sigma-Aldrich. They were used as received. For the viability tests, resazurin was purchased from Sigma-Aldrich and was used as received.

**Synthesis of NPs.** Citrate-capped spherical gold NPs with diameters of ca. 25, 50, and 60 nm, in the following referred to as 25-GNPs, 50-GNPs, and 60-GNPs, respectively, were synthesized using a seed-growth method reported elsewhere, cf. Supporting Information (section 1).[1] CTAB-capped GNRs with plasmon band (i.e., localized surface plasmon resonance, LSPR) centered at ca. 850 and 1100 nm in the following are referred to as 850-GNRs and 1100-GNRs, respectively, and were prepared by using the seed-mediated growth method recently published by Murray and co-workers, which allows the production of GNRs with a large variety of aspect ratios. We choose as NP models[2,29] short 850-GNRs (low aspect ratio) and long 1100-GNRs (high aspect ratio), cf. Supporting Information (section 1). Citrate-capped silver nanoprisms (ca. 60 nm in length) with plasmon band centered at ca. 600 nm (in the following referred to as AgNPRs) were obtained by the reduction of silver nitrate with $H_2O_2$ and sodium borohydride in aqueous solution, as reported elsewhere,[4] cf. Supporting Information (section 1).

**NP Stabilization: Ligand Exchange with PEG.** After synthesis, the GNPs were cleaned from the free citrate by centrifugation using centrifugal filters (20 mL, 100 kDa, Millipore) at 110 g for 5 min (one time). The GNRs were cleaned by centrifugal precipitation at 7080*g* for 25 min (one time). In all cases the NPs were diluted in Milli-Q water (1.37, 0.41, 0.13, 5.1, and 0.74 nM for 25-, 50-, and 60-GNPs and 850- and 1100-GNRs, respectively) and stabilized by mPEG−SH ($CH_3O$-PEG-SH, $M_w$ = 750 Da (Rapp Polymere)) dissolved in Milli-Q water. A total of 30 $\mu$L of NaOH (100 mM) per mL of GNPs and 10 $\mu$L of NaOH (1 M) per mL of GNRs was added to increase the pH to ca. 10, aiming to increase the reactivity of the thiol group.[3] The stoichiometric ratio of PEG molecules to NP ($C_{PEG}/C_{NP}$) was $5 \times 10^5$. The solution was mixed with stirring (400 rpm) overnight. Please note that $5 \times 10^5$ is the maximum amount required to transfer successfully the "bigger" NPs. To transfer small particles using lower PEG:NP molar ratios is also possible, cf. Table S2 and section 2 in the Supporting Information for further details.

**Phase Transfer.** Upon PEG stabilization of the NPs, i.e., PEGylation, they were transferred from aqueous media to organic solvent (chloroform) by using DDA (0.75 M) dissolved in chloroform with strong magnetic stirring (1200 rpm). The transference for "small" NPs was also feasible by using lower concentrations of DDA, cf. Table


DOI: 10.1021/cm5043167
*Chem. Mater.* 2015, 27, 990−997

S2 in the Supporting Information. The phase transfer requires 12 h for GNPs and 4 days for GNRs. Stirring has to be strong enough to mix the two phases perfectly. After this, the water was removed and the samples were washed twice with chloroform by precipitation. To clean 25-GNPs and 1100-GNRs, 8960*g* during 30 min was used. Meanwhile to clean 50 and 60-GNPs and 850-GNRs, 2240*g* for 40 min were selected. Then, the supernatant was removed. GNPs and GNRs were redispersed in chloroform again prior to polymer coating.

**Polymer Coating.** The NPs were water transferred using the polymer coating technique as described in previous reports.[7,30] Briefly, polymer coating for GNPs and GNRs was done by dissolving an appropriate amount of polymer monomers per NP surface unit ($R_{p/area}$ [$nm^2$]). In all the samples we added 3000 monomers of poly(isobutylene-*alt*- maleic anhydride) modified with dodecylamine (hereinafter referred to as PMA) dissolved in chloroform per $nm^2$ of NPs. For details about the synthesis of the amphiphilic polymer used here we refer to the previous work of Lin et al.[7] Briefly, the PMA was synthesized by grafting dodecylamine onto the poly(isobutylene-*alt*-maleic anhydride) backbone through spontaneous amide linkage, which converts one maleic anhydride into one corresponding amide and one free carboxylic acid. In the amphiphilic polymer used in our work, 75% of its maleic anhydride rings have been reacted with dodecylamine, leaving 25% of its anhydride rings intact. To increase the stability the use of a cross-linker has been also previously proposed.[7,31] We tested two different cross-linkers, bis(6-aminohexyl)-amine and polyethylenimine (branched, $M_w$ = 800 Da). More details about the use of the cross-linker can be found in the Supporting Information. After addition of the polymer, the solvent was slowly evaporated using a low-pressure system, until the sample was completely dry. Then, more chloroform was added and the drying process was repeated. The NPs were quickly dissolved in 0.1 M NaOH, which hydrolyzes the remaining maleic anhydride rings, leaving two carboxylic groups per newly opened anhydride ring. Then, the solution was filtered through a 0.22 $\mu$m syringe filter. After this, the NPs were precipitated by centrifugation (same conditions as for the phase transfer) twice, in order to remove the residual empty polymer micelles.[32] Washing out empty micelles and unwanted byproducts is also possible by gel electrophoresis. After purification, the GNPs and GNRs were redispersed and kept in Milli-Q water. Extinction coefficient values and further calculations for the polymer coating method can be found in the Supporting Information.

**Surface Modification of PMA-Coated NPs: PEGylation.** The surface of PMA-coated gold NPs was modified with mPEG−$NH_2$ ($CH_3O$-PEG-$NH_2$, Rapp Polymere). The carboxylic groups of the polymer (note: generated by grafting of dodecylamine and hydrolysis of the anhydride rings) and the amine groups of PEG were cross-linked by using EDC chemistry in Milli-Q water according to Table 1.

**Table 1. Conditions for PEGylation of PMA-Coated NPs**

| NPs | $C_{EDC}/C_{NP}$ | mPEG−$NH_2$ ($M_w$, kDa) | mPEG−$NH_2$ ($C_{PEG}/C_{NP}$) |
|---|---|---|---|
| 25-GNPs | $5 \times 10^6$ | 0.75 | $6 \times 10^6$ |
| 45-GNPs | $30 \times 10^6$ | 5 | $3 \times 10^6$ |
| 60-GNPs | $30 \times 10^6$ | 10 | $3 \times 10^6$ |
| 850-GNRs | $9 \times 10^6$ | 5 | $7.5 \times 10^5$ |
| 1100-GNRs | $9 \times 10^6$ | 10 | $7.5 \times 10^5$ |

After PEGylation, NPs were cleaned from free PEG by applying an electric field of 10 V/cm for 1 h in an electrophoresis tank. The agarose bands with the NPs were transferred to a dialysis membrane (molecular cutoff (MWCO) = 50 kDa), and then, NPs were extracted from the agarose by electrophoresis using the conditions above-described. Lastly, NPs were centrifuged once using the conditions above-described; the supernatant was removed and the NPs were redispersed and kept in Milli-Q water.

**Characterization.** All NPs were characterized by UV/vis spectroscopy (Agilent 8453 spectrometer), dynamic light scattering (DLS), laser Doppler anemometry (LDA) (Nanosizer, Malvern), electron microscopy (Jeol 1400 plus), and inductively coupled plasma mass spectrometry (ICP-MS) (Agilent 7700 series ICP-MS).

**Stability Studies.** In order to evaluate the NP stability against media of biological relevance, solutions with the same concentration of NPs were dispersed in the following eight different media: (1) water (Milli-Q), (2) phosphate buffered saline (PBS, Biochrom), (3) Dulbecco's modified Eagle's media (DMEM, Sigma-Aldrich), (4) PBS 1% penicillin and streptomycin (P/S, Sigma-Aldrich) and 1% glutamine (L-Glu, Sigma-Aldrich), (5) DMEM 1% P/S and 1% L-Glu, (6) 800 $\mu$M bovine serum albumine (BSA, Sigma-Aldrich) in PBS, (7) 800 $\mu$M BSA DMEM 1% P/S, 1% L-Glu, and (8) DMEM 1% P/S, 1% L-Glu, and 10% fetal bovine serum (FBS, Biochrom).[15] Their hydrodynamic radii and UV−vis spectra were monitored at different time points, from 0 h to 3 days.

**Cytotoxicity Evaluation: Resazurin Test.** The $5 \times 10^3$ tumoral human cells (HeLa) and $10 \times 10^3$ mouse fibroblasts (3T3) were incubated for 24 h in a 96-well plate at 37 °C and 5% $CO_2$ with complete DMEM media (10% FBS, 1%P/S, and 1% L-Glu). After this period, different concentration of NPs dispersed in cell media were added. Three measurements were done for each concentration. Then, after another 24 h of incubation at 37 °C and 5% $CO_2$, cells were washed three times with PBS. A total of 100 $\mu$L from a 10% solution of resazurin (7-hydroxy-3*H*-phenoxazin-3-one 10-oxide; Sigma-Aldrich) in cell media was added into the wells. After 3 h of incubation, the fluorescence spectra (ranging from 572 to 650 nm) were recorded in a fluorescence spectrometer (Horiba Jobin), upon excitation at 560 nm. This test is based on the irreversible oxidation of resazurin to the pink and highly fluorescent resorufin. To analyze the data, the average of the background was subtracted from the maximum value. To get the percentage of viable cells, control wells where just cells were incubated equivalently were considered as 100% viable cells.[8]

## RESULTS AND DISCUSSION

The main aim of this work is to establish methods for the phase transfer and polymer coating of noble metal NPs with diameters larger than 20 nm and high anisotropy. The polymer coating procedure can be thus extended to a wide variety of NPs with numerous bioapplications. The realization of this approach requires a water−chloroform−water round trip for the NPs, cf. Figure 1.

First, a prestabilization of the NPs in the aqueous phase was required. Indeed, without this prestabilization step, we were unable to transfer bare NPs with sizes >15 nm. Small NPs and surfactant-capped NPs (e.g., CTAB capped or TOAB capped) did not require this prestabilization step, but the use of the PEG chains improves the yield of the transference in all of the cases. Short chains of PEG (750 Da) were employed as prestabilizing agent. The selected heterofunctional chains bear a thiol group in one end and a methoxy group in the other. Notice that we used thiolated molecules because, in this study, Ag and Au NPs were our targets (Figure 2), which can readily bind thiolated molecules. This chain, in particular, was selected due to its length and the noncharged methoxy end.

Notice that the approach here described focused on metallic NPs synthesized in aqueous solution, and thus, alternative end-terminal groups might be more efficient to prestabilize with PEG other NPs in aqueous solution. For materials other than Au or Ag, such as metal oxides (e.g., $Fe_3O_4$, ZnO, $TiO_2$, NiO, MnO, CeO, etc.) or QDs, end-terminal groups other than thiol might be required. For instance, one might speculatively hypothesize that PEG−silane, PEG−siloxane, PEG−phosphine oxide, or PEG−phosphoric acid might be used for prestabilization of a variety of metal oxides.[33−36] By a more general approach, poly(histidine)−PEG could be used to prestabilize carboxyl-terminated NPs (independently of the inorganic core), as recently shown by Wegner et al. for poly(histidine)-


DOI: 10.1021/cm5043167
*Chem. Mater.* 2015, 27, 990−997

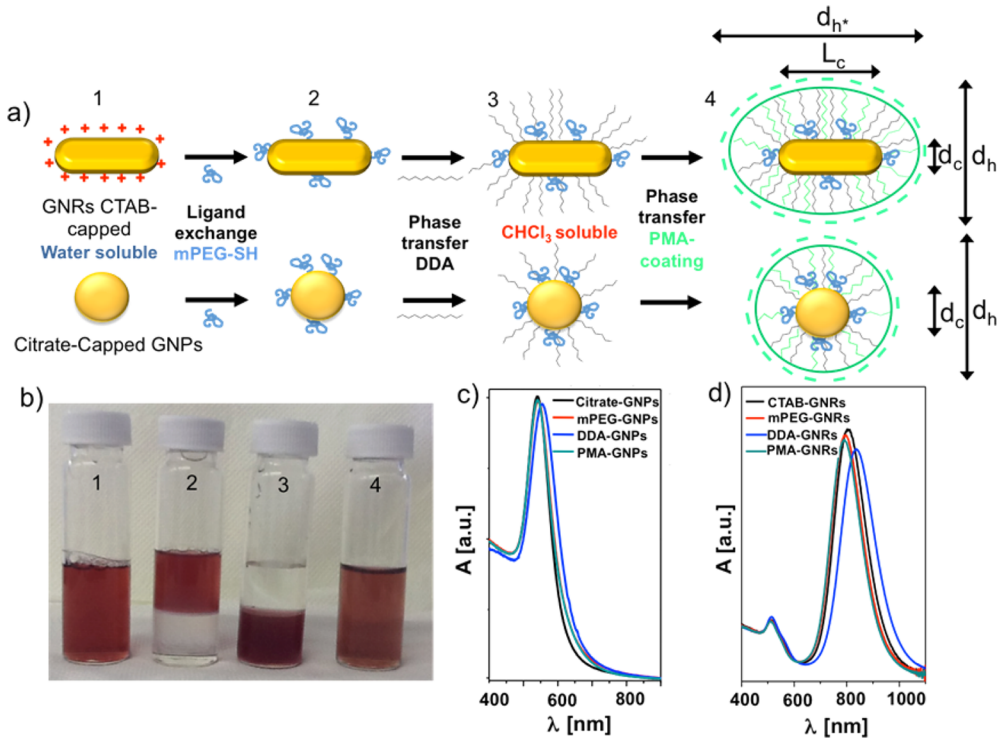


**Figure 1.** (a) Schematic representation of the coating strategy for both spherical GNPs and GNRs. (b) GNRs in water after their synthesis (1), PEGylated GNRs before the phase transfer (2), in chloroform after the phase transfer using DDA (3), and after their polymer coating with PMA (4). Notice that we cannot rule out the presence of short PEGs intercalated within the DDA coating. UV/vis spectra corresponding to all the steps of the process for 60-GNPs (c) and 850-GNRs (d). See Supporting Information for the UV/vis spectra of the other NPs, section 2).

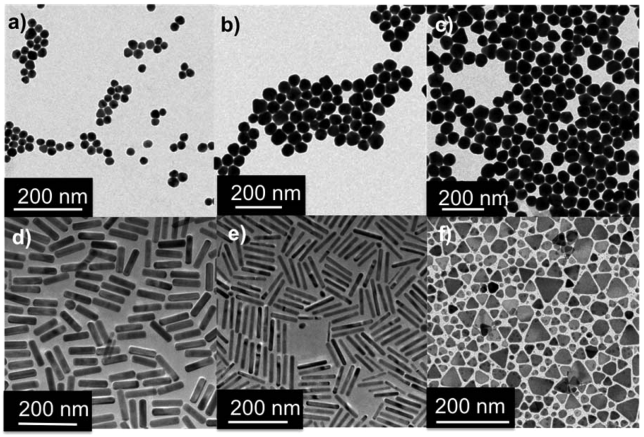


**Figure 2.** Transmission electron microscopy (TEM) micrographs of the NPs: spherical GNPs (a) 25-GNPs, (b) 50-GNPs, and (c) 60-GNPs and anisotropic NPs (d) 850-GNRs, (e) 1100-GNRs, and (f) AgNPRs.

derivatized biomolecules and QDs.[37] Yet, in case of "water-soluble" CdTe QDs[38] thiolated PEGs might efficiently prestabilize them as in the case of Au and Ag. Although as previously stated the use of the prestabilization step is required for "big" metallic NPs, adapting the proposed method to other materials and PEGs (if needed) will need further optimization due to different binding energies.

As previously explained, the main aim is to coat the NPs with PMA as a model polymer, although other polymers and PMA modified with functional molecules (dyes, chelators, SERS tags, etc.)[39] have been successfully employed in previous works. This actually illustrates the versatility of the method proposed in terms of achieving multifunctional NPs. We anticipated that the PEG chains would stabilize the NPs, and due to their short length, they would not prevent the interaction of the aliphatic-PMA domain with the aliphatic chains that will be introduced on the NPs later on in the organic phase. The amphiphilic nature of PEG chains is well-known,[40] and it is supported by the dual solubility either in aqueous solution or organic solvents, such as chloroform. Taking advantage of this double behavior, PEG chains were expected to work as stabilizers and phase transfer helpers. The modification of NPs with PEG is a straightforward procedure extensively used to stabilize NPs.[3,41,42] Once stabilized with PEG, the NPs were ready to be transferred to the organic phase.

In the early stage of the development of the proposed method, different combinations of solvents and aliphatic chains were tested (see Table S2 in the Supporting Information). The combination of chloroform and DDA was found to be the best combination for our purposes. To successfully transfer the NPs, it was only required to let the two phases interact (aqueous and organic) by using vigorous stirring. DDA-capped NPs presented high stability in organic media, and their absorption bands remained very similar to the original ones. Please notice that we cannot rule out the presence of short PEG intercalated within the DDA coating. As expected, only a small red shift was observed due to the change of the NPs environment (see Figure 3, and section 2 from Supporting Information). The DDA-capped NPs were precipitated by centrifugation to remove free, unbound ligands. Although our main aim is toward biological purposes, having plasmonic NPs in organic solvent is very interesting for other applications (e.g., the production of thin films which contain NPs or nanocomposites). The transfer procedure worked similarly for all


DOI: 10.1021/cm5043167
Chem. Mater. 2015, 27, 990−997

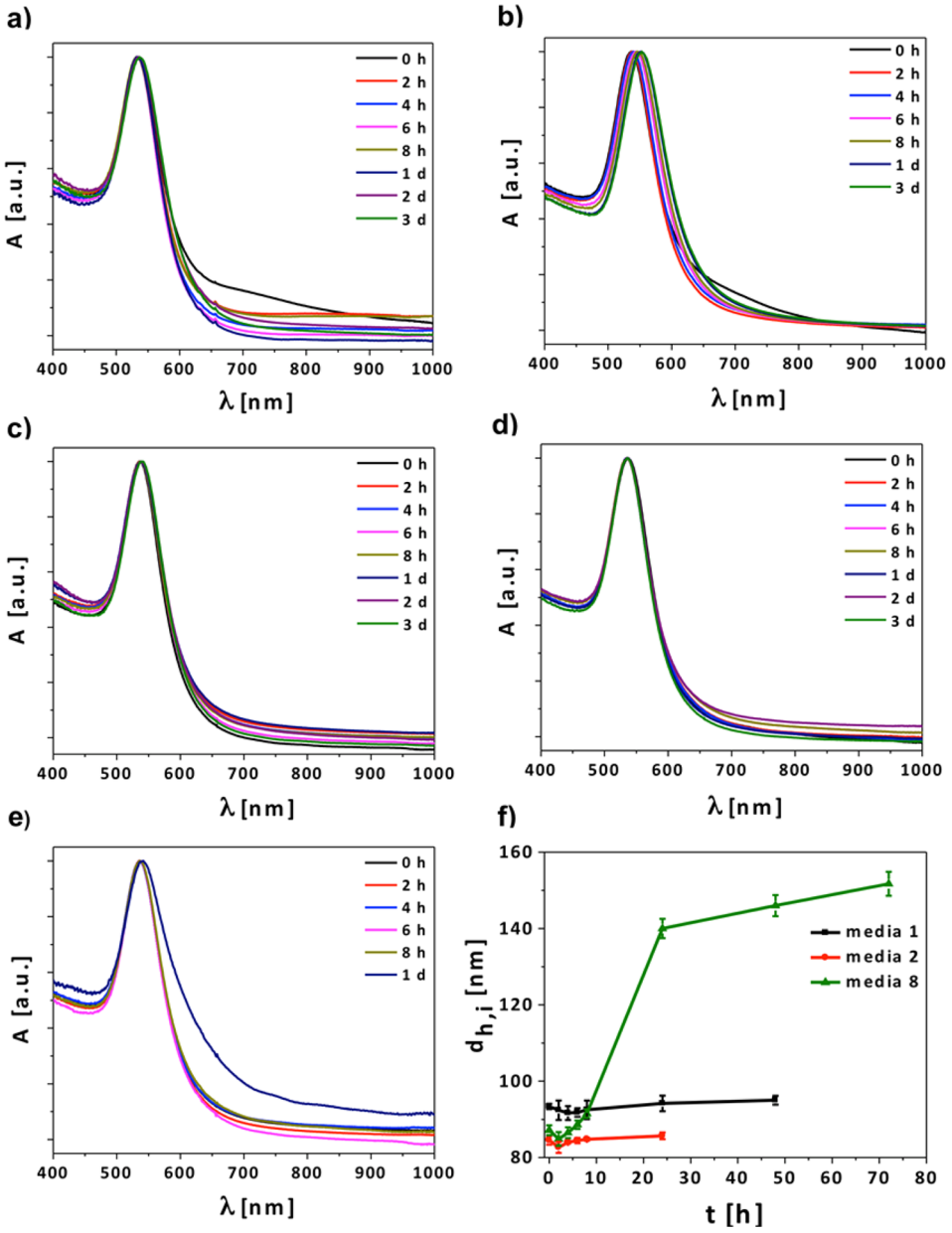


**Figure 3.** Stability tests against complete cell media of 50-GNPs followed by UV−vis spectroscopy versus time of NPs stabilized with (a) just PMA, (b) PMA−PEI, and (c) PMA−PEI PEGylated. Stability of PEGylated PMA−PEI 50-GNPs in water (d) and in PBS (e). Stability followed by DLS for PEGylated PMA−PEI 50-GNPs in water (medium 1), PBS (medium 2), and complete cell media (medium 8).

the NPs reported in this work, the only difference residing in the required time for the transfer. This time depended on the nature of the original ligand on the NPs surface. The transfer time could be shortened by the addition of ethanol to improve the contact between the interfaces.[28] It is interesting to highlight that some NPs could be transferred to the organic phase just by the use of the PEG chains. Nevertheless, the yield of the transferred NPs was much lower compared with the yield obtained using DDA (almost 100%; this yield was determined by ICP-MS, see Table S6 in the Supporting Information). Recently, Alkilany and co-workers have proposed a protocol for aqueous-to-organic phase transfer of gold NPs which combines thiolated PEG chains (with molecular weight > 1 kDa) and methanol.[19]

Once the NPs were dissolved in chloroform, the classic polymer coating technique was applied. To this end an optimization step was done regarding the amount of polymer needed to coat the NPs (see Supporting Information, section 3). In agreement with previous work,[7] the amount of polymer required is expressed in the number of monomers *per* effective NP surface ($R_{P/area}$). The NPs used here required higher $R_{P/area}$ values as compared to typical values previously reported for smaller NPs. Also in comparison with smaller NPs, the polymer coating procedure worked best when the solvent was removed using reduced pressure conditions, i.e., the pressure was kept high and the temperature in the bath was also high (60−70 °C). The high colloidal stability of PMA-coated NPs typically allows for cleaning steps, both by using gel electrophoresis (see Supporting Information, Section 4) and by centrifugation. Aiming to achieve a higher stability (stable in water or biological media for months), the use of cross-linkers was also tested. Cross-linkers were meant to act as stabilizer to


DOI: 10.1021/cm5043167
*Chem. Mater.* 2015, 27, 990−997

"polymerize" the different polymer molecules which wrap the NPs. Initially, the short molecule bis(6-aminohexyl)amine was used as cross-linker as previously reported.[7,31] In this case, probably due to the bigger size of these NPs, this short molecule did not improve the stability of the NPs, and therefore, we tested another cross-linker: poly(ethylenimime) (PEI, 800 Da). After testing the stability of the NPs coated with PMA only, the short cross-linker and PEI, we determined that 0.75% of PEI improved the stability of the NPs (see the data in the Supporting Information, for nanorods) in complete cell media (and for all the NPs, section 6 from Supporting Information).

In order to further improve the colloidal stability of the NPs, stabilization with PEG (mPEG−$NH_2$ chains), i.e., PEGylation, was carried out by 1-ethyl-3-(3-(dimethylamino)propyl)-carbodiimide (EDC) chemistry.[33] The molecular weight of the PEG chains was varied between the different samples (from 0.75 to 10 kDa). In general, the molecular weight of the PEG was increased as the size of the inorganic core increased. The stability of these NPs was tested against 8 different media, which are important in biological applications.[15] The stability was tested for time points up to 3 days by dynamic light scattering (DLS) and UV/vis spectroscopy (Supporting Information section 7). The stability role of the cross-linker (PEI) and PEGylation were also tested using UV/vis spectroscopy (see Figure 3 and section 7 from Supporting Information). To compare the effect on the stability of the individual elements used to wrap the NPs, the same concentrations of NPs coated with PMA only (Figure 3a), coated with PMA and the cross-linker (PEI, Figure 3b), and PEGylated-PMA-PEI coated NPs (Figure 3c) were incubated in complete cell media (media 8), and the changes of their UV/vis spectra were monitored over time, from time 0 to 3 days. The addition of PEI prevents slightly the initial broadening of the plasmon band, which disappears with time, presumably, due to absorption of proteins onto the NPs surface. This broadening is completely prevented by the PEGylation of the NPs. In all the cases the colloidal stability of the NPs is very high, even after 3 days (see Supporting Information for the rest of the stability tests).

The stability of PEGylated NPs against the eight above-described media was tested. Our results indicated that the stability of all the NPs in the media containing proteins (6, 7, and 8) was greatly improved, as compared to their stability in free-protein media (2, 3, 4, and 5) (Figure 3c,e,f). In some of the free-protein media, NPs were not stable for longer than 24 h. This indicates that the presence of salt in the media compromises the NP stability due to the screening of the NPs' charge. Our data seem to indicate that the salt effect is counteracted by the absorption of proteins, i.e., the protein corona.[43] The protein absorption was evidenced by a redshift in the LSPR (Figure 3b) of the NPs in the UV/vis spectra and by an increment in the hydrodynamic radius, as resulted from the DLS analysis. (See section 7 from Supporting Information for all the results.)

Notably, the increment of the hydrodynamic radius observed for media 6 and 7, which contain BSA (0.8 mg/mL), differs from the increment observed for medium 8, which contains FBS (10%). Our results allow us to speculate whether these changes might be due to the different concentrations of BSA in the corresponding medium or due to the presence of different proteins. Indeed, the concentration of BSA in medium 8 was ca. 2.3 mg/mL, considerably higher than in media 6 and 7 (i.e., 0.8 mg/mL). Protein binding, and thus the size and composition of the protein corona, is highly influenced by the concentration of protein species.[43] The major constituent of FBS is BSA. Indeed, it has been previously proposed that the main component of the protein corona is BSA.[44] However, our data do not allow us to rule out that the differences between media 6/7 and 8 are instead due to the absorption of other proteins than BSA and/or due to a PEG conformational change. For media 6 and 7 the trend is very similar, except for 25-GNPs, which has a behavior closer to that in medium 8. Our qualitative studies do not allow this out-of-trend behavior of 25-GNPs to be clarified, which might be due to its different size (also, curvature radius), different PEG length (750 Da), and/or different protein corona. In general protein absorption is a time dependent process.[44,45] For all the other NPs in media 6 and 7, the size increment is observed immediately after the addition of the medium, that is, there is no increase over time. In contrast, in the case of medium 8, the hydrodynamic radius increases significantly after ca. 10 h until reaching a plateau at ca. 20 h, which indicates that longer incubation times are required. These results are supported by the previous work of Maiorano and co-workers.[46] They used citrate-capped Au NPs and evaluated the protein corona evolution along the time. They found that using DMEM supplemented with FBS, the hydrodynamic radius of the NPs needs more than 50 h to reach a plateau. Note that this time is comparable with our results. These qualitative results demonstrate that even though the NPs were saturated with PEG, as indicated by their $\zeta$-potential values and their electrophoretic motilities (see Supporting Information, section 4, and Table S7), the unspecific absorption of proteins was not avoided. These results will lead to further studies regarding the PEG conformation on these kinds of surfaces.

Aiming at proving that this double round trip of the GNRs can be used to remove CTAB[47] or at least to minimize CTAB-release from the NP surface, the toxicity of the GNRs was evaluated. In this case, 3T3 fibroblast cells and HeLa cells were incubated with increasing amounts of PMA-coated GNRs (plasmon band placed at ca. 850 and 1100 nm) for 24 h. For completeness, the impact on cell viability of the rest of the Au NPs was also investigated. In all the cases no acute toxicity features were observed (Figure 4). For the GNRs no acute toxicity was observed in both cell lines when working with concentrations up to 2.5 nM (see Figure 4b). To test viability, the resazurin test was chosen. By this test, the mitochondrial respiration was evaluated, which can be in general related with the cell viability. Interestingly, we found that the viability trend is size-dependent, as 60-GNPs started to exhibit toxicity at 0.2 nM (263 $\mu$g/mL), cf. Supporting Information section 8. However, this trend should be further investigated and confirmed by a multiparametric methodology.[48]

## ■ CONCLUSIONS

This work reports on a phase transfer strategy for NPs with different sizes, shapes, and materials. The use of short PEG chains (750 Da) as prestabilizers of NPs for their transfer to organic solution is reported. This approach is very versatile, as it allows the transference of NPs within a long range of sizes to the organic phase. Nowadays, different functionalized PEG molecules are commercially available, which makes this approach accessible for any kind of laboratory. Additionally, the use of PEG as stabilizer of NPs has been widely reported, and thus, to adapt this strategy to other materials should be


DOI: 10.1021/cm5043167
Chem. Mater. 2015, 27, 990−997

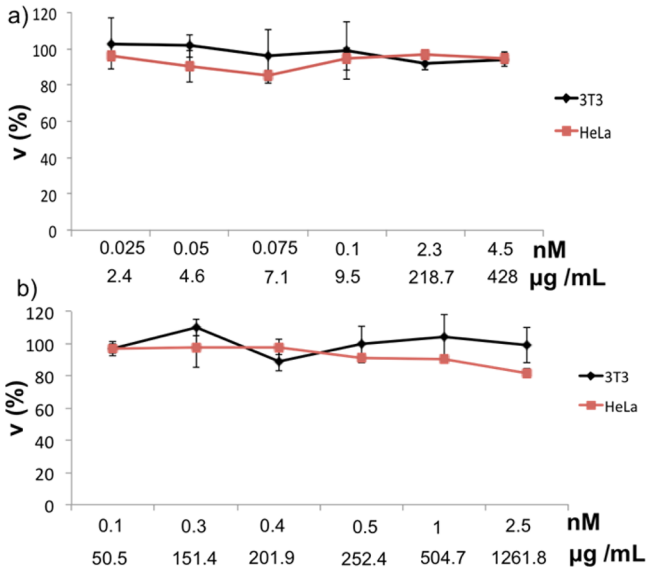


**Figure 4.** Viability V results for (a) 25-GNPs and (b) 850-GNRs after 24 h of incubation for 3T3 and HeLa cells.

very straightforward. The transferred NPs keep their plasmonic properties and a good colloidal stability after their transfer. Notably, the transfer works with big volume samples (more than 500 mL), and the NPs can be dried and redispersed again, keeping their optical properties. The transferred particles were successfully coated with the amphiphilic polymer PMA, which allows equivalent coatings to form for different NPs. This is very interesting for comparing the interaction of different NPs with living cells. This methodology has been typically restricted to aliphatic-coated NPs, typically with inorganic diameters <20 nm, in organic media. Here we have demonstrated that a variety of "big" NPs, after polymer coating, exhibit high colloidal stability in biological media containing high protein concentration. The coated NPs were found to be under realistic concentrations without acute toxicity for either mouse fibroblasts (3T3 fibroblast) or human cells (HeLa).

## ■ ASSOCIATED CONTENT

### Ⓢ Supporting Information

Additional data for synthesis of NPs, phase transfer optimization, polymer coating, PEGylation, NP characterization, enhancing the stability, stability assays, and toxicity tests. This material is available free of charge via the Internet at http://pubs.acs.org.

## ■ AUTHOR INFORMATION

### Corresponding Authors

*Beatriz Pelaz. E-mail: beatriz.pelazgarcia@physik.uni-marburg.de.

*Pablo del Pino. E-mail: pdelpino@cicbiomagune.es.

### Author Contributions

‡These authors contributed equally (Mahmoud G. Soliman and Beatriz Pelaz).

### Funding

Parts of this work were supported by the German Research Foundation (DFG, GRK 1782 to W.J.P.) and the MIMECO (MAT2013-48169-R, NanoFATE, to W.J.P. and P.d.P.). B.P. thanks the Alexander von Humboldt Foundation for a fellowship and M.G.S. thanks to the Youssef Jameel Foundation for a Ph.D. fellowship.

### Notes

The authors declare no competing financial interest.

## ■ ACKNOWLEDGMENTS

The authors are grateful to Marta Gallego for technical assistance with electron microscopy.

## ■ ABBREVIATIONS

NPs, nanoparticles; CTAB, cetyltrimethylammonium bromide; PEG, polyethylenglycol; DDT, dodecanthiol; HDA, hexadecylamine; DDAB, didecylammonium bromide; DDA, dodecylamine; PMA, dodecyl-*graft*-poly(isobutylene-maleic-*alt*-anhydride); GNPs, gold nanoparticles; GNRs, gold nanorods; LSPR, localized surface plasmon band; NPRs, nanoprisms; TOAB, tetraoctylammonium bromide; PEI, polyethylenimine; PBS, phosphate buffer saline; DMEM, Dulbecco's modified Eagle's media; P/S, penicillin/streptomycin; L-Glu, L-glutamine; DLS, dynamic light scattering

## ■ REFERENCES

(1) Bastus, N. G.; Comenge, J.; Puntes, V. *Langmuir* **2011**, *27* (17), 11098−11105.
(2) Ye, X.; Jin, L.; Caglayan, H.; Chen, J.; Xing, G.; Zheng, C.; Doan-Nguyen, V.; Kang, Y.; Engheta, N.; Kagan, C. R.; Murray, C. B. *ACS Nano* **2012**, *6* (3), 2804−2817.
(3) Pelaz, B.; Grazu, V.; Ibarra, A.; Magen, C.; del Pino, P.; de la Fuente, J. M. *Langmuir* **2012**, *28* (24), 8965−8970.
(4) Zhang, Q.; Li, N.; Goebl, J.; Lu, Z.; Yin, Y. *J. Am. Chem. Soc.* **2011**, *133* (46), 18931−18939.
(5) Rivera Gil, P.; Jimenez de Aberasturi, D.; Wulf, V.; Pelaz, B.; del Pino, P.; Zhao, Y.; de la Fuente, J.; Ruiz de Larramendi, I.; Rojo, T.; Liang, X.-J.; Parak, W. J. *Acc. Chem. Res.* **2013**, *46* (3), 743−749.
(6) Salas, G.; Casado, C.; Teran, F. J.; Miranda, R.; Serna, C. J.; Morales, M. P. *J. Mater. Chem.* **2012**, *22* (39), 21065−21075.
(7) Lin, C.-A. J.; Sperling, R. A.; Li, J. K.; Yang, T.-Y.; Li, P.-Y.; Zanella, M.; Chang, W. H.; Parak, W. J. *Small* **2008**, *4* (3), 334−341.
(8) Caballero-Díaz, E.; Pfeiffer, C.; Kastl, L.; Rivera-Gil, P.; Simonet, B.; Valcárcel, M.; Jiménez-Lamana, J.; Laborda, F.; Parak, W. J. *Part. Part. Syst. Charact.* **2013**, *30* (12), 1079−1085.
(9) Anderson, R. E.; Chan, W. C. W. *ACS Nano* **2008**, *2* (7), 1341−1352.
(10) Zhang, F.; Lees, E.; Amin, F.; Rivera_Gil, P.; Yang, F.; Mulvaney, P.; Parak, W. J. *Small* **2011**, *7*, 3113−3127.
(11) Muir, B. W.; Moffat, B. A.; Harbour, P.; Coia, G.; Zhen, G. L.; Waddington, L.; Scoble, J.; Krah, D.; Thang, S. H.; Chong, Y. K.; Mulvaney, P.; Hartley, P. *J. Phys. Chem. C* **2009**, *113* (38), 16615−16624.
(12) Nazarenus, M.; Zhang, Q.; Soliman, M. G.; del Pino, P.; Pelaz, B.; Carregal-Romero, S.; Rejman, J.; Rothen-Ruthishauser, B.; Clift, M. J. D.; Zellner, R.; Nienhaus, G. U.; Delehanty, J. B.; Medintz, I. L.; Parak, W. J. *Beilstein J. Nanotechnol.* **2014**, *5*, 1477−1490.
(13) Pelaz, B.; Charron, G.; Pfeiffer, C.; Zhao, Y. L.; de la Fuente, J. M.; Liang, X. J.; Parak, W. J.; del Pino, P. *Small* **2013**, *9* (9−10), 1573−1584.
(14) Dai, Q.; Walkey, C.; Chan, W. C. *Angew. Chem., Int. Ed.* **2014**, *53* (20), 5093−5096.
(15) Hühn, D.; Kantner, K.; Geidel, C.; Brandholt, S.; De Cock, I.; Soenen, S. J. H.; Rivera Gil, P.; Montenegro, J.-M.; Braeckmans, K.; Müllen, K.; Nienhaus, G. U.; Klapper, M.; Parak, W. J. *ACS Nano* **2013**, *7* (4), 3253−3263.
(16) Lista, M.; Liu, D. Z.; Mulvaney, P. *Langmuir* **2014**, *30* (8), 1932−1938.
(17) Yang, J.; Lee, J. Y.; Ying, J. Y. *Chem. Soc. Rev.* **2011**, *40* (3), 1672−1696.



DOI: 10.1021/cm5043167
*Chem. Mater.* 2015, 27, 990−997

(18) Wang, X.; Xu, S.; Zhou, J.; Xu, W. *J. Colloid Interface Sci.* **2010**, *348* (1), 24−28.
(19) Alkilany, A. M.; Yaseen, A. I. B.; Park, J.; Eller, J. R.; Murphy, C. J. *RSC Adv.* **2014**, *4* (95), 52676−52679.
(20) Goulet, P. J. G.; Bourret, G. R.; Lennox, R. B. *Langmuir* **2012**, *28* (5), 2909−2913.
(21) Alkilany, A. M.; Nagaria, P. K.; Hexel, C. R.; Shaw, T. J.; Murphy, C. J.; Wyatt, M. D. *Small* **2009**, *5* (6), 701−8.
(22) Alkilany, A. M.; Thompson, L. B.; Boulos, S. P.; Sisco, P. N.; Murphy, C. J. *Adv. Drug Delivery Rev.* **2012**, *64* (2), 190−199.
(23) Wijaya, A.; Hamad-Schifferli, K. *Langmuir* **2008**, *24* (18), 9966−9969.
(24) Huschka, R.; Zuloaga, J.; Knight, M. W.; Brown, L. V.; Nordlander, P.; Halas, N. J. *J. Am. Chem. Soc.* **2011**, *133* (31), 12247−12255.
(25) Kinnear, C.; Dietsch, H.; Clift, M. J. D.; Endes, C.; Rothen-Rutishauser, B.; Petri-Fink, A. *Angew. Chem., Int. Ed.* **2013**, *52* (7), 1934−1938.
(26) Liu, M.; Law, W.-C.; Kopwitthaya, A.; Liu, X.; Swihart, M. T.; Prasad, P. N. *Chem. Commun.* **2013**, *49* (81), 9350−9352.
(27) Sekiguchi, S.; Niikura, K.; Matsuo, Y.; Ijiro, K. *Langmuir* **2012**, *28* (13), 5503−5507.
(28) Yang, J.; Lee, J. Y.; Deivaraj, T. C.; Too, H.-P. *J. Colloid Interface Sci.* **2004**, *277* (1), 95−99.
(29) Ye, X.; Zheng, C.; Chen, J.; Gao, Y.; Murray, C. B. *Nano Lett.* **2013**, *13* (2), 765−771.
(30) Li, W. H.; Zamani, R.; Gil, P. R.; Pelaz, B.; Ibanez, M.; Cadavid, D.; Shavel, A.; Alvarez-Puebla, R. A.; Parak, W. J.; Arbiol, J.; Cabot, A. *J. Am. Chem. Soc.* **2013**, *135* (19), 7098−7101.
(31) Pellegrino, T.; Manna, L.; Kudera, S.; Liedl, T.; Koktysh, D.; Rogach, A. L.; Keller, S.; Rädler, J.; Natile, G.; Parak, W. J. *Nano Lett.* **2004**, *4* (4), 703−707.
(32) Fernández-Argüelles, M. T.; Yakovlev, A.; Sperling, R. A.; Luccardini, C.; Gaillard, S.; Medel, A. S.; Mallet, J.-M.; Brochon, J.-C.; Feltz, A.; Oheim, M.; Parak, W. J. *Nano Lett.* **2007**, *7* (9), 2613−2617.
(33) Karakoti, A. S.; Das, S.; Thevuthasan, S.; Seal, S. *Angew. Chem., Int. Ed.* **2011**, *50* (9), 1980−94.
(34) Na, H. B.; Lee, I. S.; Seo, H.; Park, Y. I.; Lee, J. H.; Kim, S.-W.; Hyeon, T. *Chem. Commun.* **2007**, No. 48, 5167−5169.
(35) Luo, M.; Shen, C.; Feltis, B. N.; Martin, L. L.; Hughes, A. E.; Wright, P. F. A.; Turney, T. W. *Nanoscale* **2014**, *6* (11), 5791−5798.
(36) Lu, C.; Bhatt, L. R.; Jun, H. Y.; Park, S. H.; Chai, K. Y. *J. Mater. Chem.* **2012**, *22* (37), 19806−19811.
(37) Wegner, K. D.; Morgner, F.; Oh, E.; Goswami, R.; Susumu, K.; Stewart, M. H.; Medintz, I. L.; Hildebrandt, N. *Chem. Mater.* **2014**, *26* (14), 4299−4312.
(38) Zhou, D.; Lin, M.; Chen, Z.; Sun, H.; Zhang, H.; Sun, H.; Yang, B. *Chem. Mater.* **2011**, *23* (21), 4857−4862.
(39) Ali, Z.; Abbasi, A. Z.; Zhang, F.; Arosio, P.; Lascialfari, A.; Casula, M. F.; Wenk, A.; Kreyling, W.; Plapper, R.; Seidel, M.; Niessner, R.; Knoll, J.; Seubert, A.; Parak, W. J. *Anal. Chem.* **2011**, *83* (8), 2877−2882.
(40) Roberts, M. J.; B, M. D.; Harris, J. M. *Adv. Drug Delivery Rev.* **2002**, *54*, 459−476.
(41) Conde, J.; Ambrosone, A.; Sanz, V.; Hernandez, Y.; Marchesano, V.; Tian, F. R.; Child, H.; Berry, C. C.; Ibarra, M. R.; Baptista, P. V.; Tortiglione, C.; de la Fuente, J. M. *ACS Nano* **2012**, *6* (9), 8316−8324.
(42) Bartczak, D.; Muskens, O. L.; Sanchez-Elsner, T.; Kanaras, A. G.; Millar, T. M. *ACS Nano* **2013**, *7* (6), 5628−5636.
(43) del Pino, P.; Pelaz, B.; Zhang, Q.; Maffre, P.; Nienhaus, G. U.; Parak, W. J. *Mater. Horiz.* **2014**, *1*, 301−313.
(44) Casals, E.; Pfaller, T.; Duschl, A.; Oostingh, G. J.; Puntes, V. F. *ACS Nano* **2010**, *4* (7), 3623−3632.
(45) Tenzer, S.; Docter, D.; Kuharev, J.; Musyanovych, A.; Fetz, V.; Hecht, R.; Schlenk, F.; Fischer, D.; Kiouptsi, K.; Reinhardt, C.; Landfester, K.; Schild, H.; Maskos, M.; Knauer, S. K.; Stauber, R. H. *Nat. Nanotechnol.* **2013**, *8* (10), 772−781.
(46) Maiorano, G.; Sabella, S.; Sorce, B.; Brunetti, V.; Malvindi, M. A.; Cingolani, R.; Pompa, P. P. *ACS Nano* **2010**, *4* (12), 7481−7491.
(47) Lee, S.; Anderson, L. J. E.; Payne, C. M.; Hafner, J. H. *Langmuir* **2011**, *27* (24), 14748−14756.
(48) Soenen, S. J.; Manshian, B.; Montenegro, J. M.; Amin, F.; Meermann, B.; Thiron, T.; Cornelissen, M.; Vanhaecke, F.; Doak, S.; Parak, W. J.; De Smedt, S.; Braeckmans, K. *ACS Nano* **2012**, *6* (7), 5767−5783.


DOI: 10.1021/cm5043167
*Chem. Mater.* 2015, 27, 990−997

*Nanomaterials* **2015**, *5*, 1297-1316; doi:10.3390/nano5031297

OPEN ACCESS

*nanomaterials*

**ISSN 2079-4991**

www.mdpi.com/journal/nanomaterials

*Article*

# Conjugation of Polymer-Coated Gold Nanoparticles with Antibodies—Synthesis and Characterization

**Gamze Tan [1,2], Karsten Kantner [2], Qian Zhang [2], Mahmoud G. Soliman [2], Pablo del Pino [3], Wolfgang J. Parak [2,3], Mehmet A. Onur [4], Daniel Valdeperez [2], Joanna Rejman [2,*] and Beatriz Pelaz [2,*]**

[1] Faculty of Science and Letters, Department of Biology, Aksaray University, Aksaray 68100,Turkey; E-Mail: gamzetan2003@yahoo.com

[2] Philipp University of Marburg, Marburg 35001, Germany; E-Mails: karsten.kantner@physik.uni-marburg.de (K.K.); qian.zhang@physik.uni-marburg.de (Q.Z.); mahmoud.gamalsoliman@physik.uni-marburg.de (M.G.S.); wolfgang.parak@physik.uni-marburg.de (W.J.P.); daniel.valdepereztoledo@physik.uni-marburg.de (D.V.)

[3] Centro de Investigación Cooperativa Biomagune, San Sebastián 20001, Spain; E-Mail: pdelpino@cicbiomagune.es

[4] Faculty of Science, Department of Biology, Hacettepe University, Ankara 06800, Turkey; E-Mail: mali@hacettepe.edu.tr

* Authors to whom correspondence should be addressed; E-Mails: j_rejman@hotmail.com (J.R.); beatriz.pelazgarcia@physik.uni-marburg.de (B.P.); Tel.: +49-6421-2824161 (J.R. & B.P.); Fax: +49-6421-2824131 (J.R. & B.P.).

Academic Editor: Subramanian Tamil Selvan

*Received: 28 June 2015 / Accepted: 30 July 2015 /Published: 7 August 2015*

---

**Abstract:** The synthesis of polymer-coated gold nanoparticles with high colloidal stability is described, together with appropriate characterization techniques concerning the colloidal properties of the nanoparticles. Antibodies against vascular endothelial growth factor (VEGF) are conjugated to the surface of the nanoparticles. Antibody attachment is probed by different techniques, giving a guideline about the characterization of such conjugates. The effect of the nanoparticles on human adenocarcinoma alveolar basal epithelial cells (A549) and human umbilical vein endothelial cells (HUVECs) is probed in terms of internalization and viability assays.

**Keywords:** gold nanoparticles; bioconjugation; nanoparticle characterization; toxicity; nanoparticle-cell interaction; cellular uptake; VEGF

## 1. Introduction

The synthesis in colloidal nanoparticles (NPs) is well advanced [1–6]. Nowadays, a high control concerning material composition, size, shape, *etc.*, is possible [7]. There are also many strategies available to provide water-solubility of these NPs with high colloidal stability [8]. Some correlation of the (nonspecific) interaction of such NPs with cells with their physicochemical properties is possible and some general tendencies are well accepted in literature [9,10]. However, in order to warrant for specific interaction of NPs with cells, their surface has to be modified with ligands targeting cellular receptors. The purpose to bind proteins to the surface of NPs is to provide them a special ligand coat that they interact specifically with cells, *etc.* While there are many reports in literature about the conjugation of NP surfaces with specific ligands, characterization of these NPs is not always sufficient. Bioconjugation in particular may result in unwanted agglomeration, due to crosslinking of NPs. Thus, characterization of the colloidal properties of such conjugates is of high importance. In addition, the ligand density may significantly vary, depending on the used conjugation protocol. In principle, solutions to these hurdles exist, and NPs with a controlled ligand density and controlled ligand orientation can be synthesized [11–13]. However, these synthesis strategies require typically sophisticated protocols, and thus most commonly in literature more simple and less controlled strategies are employed. In the present work, it will be shown that also by simple conjugation strategies, together with appropriate characterization techniques, NP-antibody conjugates can be generated. As, in particular, characterization is crucial in the following, all experimental steps will be presented in the form of a general protocol.

## 2. Materials and Discussions

### *2.1. Synthesis of Gold Nanoparticles*

Au NPs are standard model systems, which are extensively used in literature to study the interaction of NPs with cells. This is in particular due to the fact that Au is an intrinsically nontoxic material. In the following, a protocol for the synthesis of hydrophilic Au NPs is described according to standard protocols from literature [14–17].

For the synthesis of Au NPs of $d_c$ = 20 nm core diameter, hydrogen tetrachloroaurate (III) hydrate (Alfa Aesar #12325, Ward Hill, MA, USA) and sodium citrate dehydrate 99% (Sigma Aldrich #W302600, St. Louis, MS, USA) were used as chemicals. All chemicals were used without further purification. Ultrapure water with a resistance greater than 18.2 $m\Omega \cdot cm^{-1}$ was used for all experiments. All glassware was cleaned in aqua regia and rinsed with ultrapure water. For the synthesis, a solution containing 150 mL (2.2 mM) trisodium citrate dihydrate ($Na_3C_6H_5O_7 \cdot 2H_2O$) was heated in a 250 mL flask to 100 °C with stirring under reflux. Using a syringe, 1 mL of 25 mM $HAuCl_4 \cdot 3H_2O$ was injected into the flask and stirred at 100 °C. Upon formation of Au NPs, the solution turned deep red. The temperature was then reduced to 90 °C, and the solution was stirred continuously for another

30 min. For further NP growth, then 1 mL sodium citrate (60 mM) and 1 mL of $HAuCl_4$ solution (25 mM) were sequentially injected with a time delay of two minutes between the two injections [17]. After 30 min, the reaction was cooled down to room temperature using an ice bath.

While this protocol virtually always will lead to the formation of Au NPs (as visible by the red color of the solution) the quality of the NPs can vary significantly. Concerning colloidal solutions, the two most important quality indicators are dispersion (*i.e.*, the NPs are individually dispersed and do not agglomerate) and size distribution of the NPs (*i.e.*, the diameter of all NPs should be as similar as possible). Even by using the same synthesis protocol over and over, the quality of the resulting NPs may vary for each batch, which warrants a mandatory quality control.

The size distribution of inorganic NPs, *i.e.*, NPs with a core composed out of an inorganic material such as gold, can be determined with transmission electron microscopy (TEM). Note that organic molecules often do not provide sufficient contrast for being visualized with TEM. For TEM analysis, a diluted drop of Au NPs was dried on a copper grid, and NPs were imaged with TEM. From such images (*cf.* Figure 1), a histogram about the distribution of the core diameter, *i.e.*, the diameter $d_c$ of the inorganic NP core can be obtained. In the present case, the core diameter was determined by analysis of more than 300 NPs, using the free software Image J. From the histogram, the mean diameter of the Au cores was determined to be $d_c = 20.9 \pm 4.3$ nm, *cf.* Figure 1.

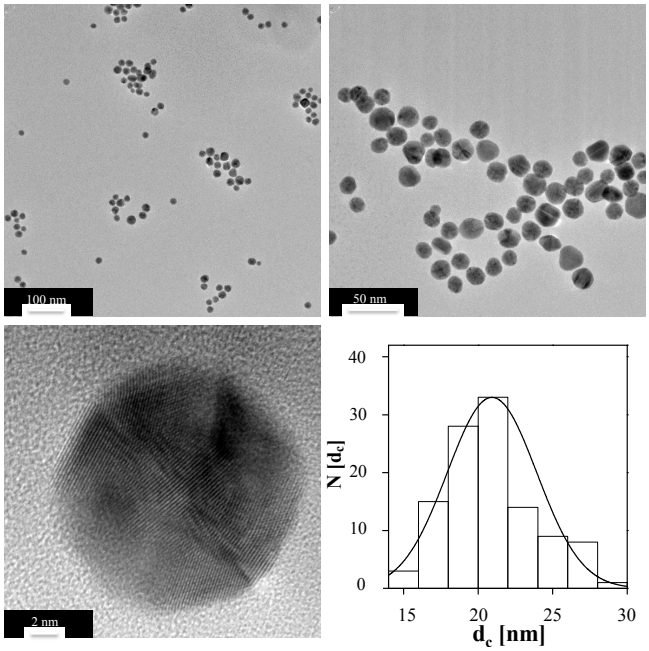


**Figure 1.** TEM images of the Au NPs at different magnifications (scale bars corresponding to 100 nm, 50 nm and 2 nm), and the corresponding histogram N ($d_c$) of the core diameter $d_c$.

The state of dispersion cannot be unequivocally deduced from TEM images, as those are recorded on NPs in dried state. In other words, even well dispersed NPs can form clusters on TEM grids. While the most common method to probe for NP dispersion is measuring the hydrodynamic diameter directly in solution (for example by dynamic light scattering (DLS), as will be described later in more detail), in the case of Au NPs simple analysis can be done by recording UV/Vis absorption spectra. As shown in the absorption spectrum in Figure 2, Au NPs exhibit a peak due to surface plasmon resonance [18].

In case NPs are not well dispersed and start to form agglomerates, this peak is shifted to higher wavelengths and the solution turns from red to blue-black. Agglomeration also leads to scattering at high wavelengths >800 nm. In case of poor size distribution, the plasmon peak broadens.

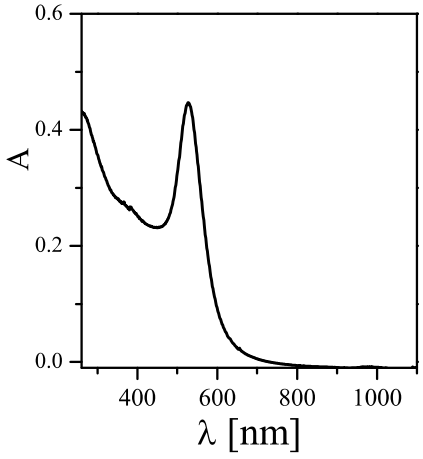


**Figure 2.** UV/Vis absorption spectrum A (λ) of Au NPs dispersed in water, directly recorded after their synthesis as described in this chapter.

Besides giving an indication about the quality of the NP synthesis, UV/Vis absorption spectra are also helpful for the determination of the concentration of the Au NPs. According to the Lambert-Beer Law, the absorption $A$ of a solution of NPs (with a length of the light path $L$) is proportional to the NP concentration $c_{NP}$:

$$A = \varepsilon_{NP} \cdot L \cdot c_{NP} \quad (1)$$

The proportionality factor is the molar extinction coefficient, which is well determined in the case of Au NPs with different sized. In the present case of NPs with a core diameter of $d_c \approx 20$ nm the extinction coefficient at 450 nm is given as $\varepsilon_{NP}$ (450nm) = $5.41 \times 10^8 \cdot M^{-1} \cdot cm^{-1}$ [19]. For the present case, 20 µL of Au NP solution directly taken after their synthesis, after dilution 500 µL with water, lead to an absorbance of $A = 0.23$ at 450 nm ($L = 1$ cm). That means that the Au NP concentration was around $c_{NP} \approx 11.1$ nM.

As citric acid capped Au NPs as prepared above are not highly colloidally stable in cell culture media (due to screening of their surface charge by adsorption of counter ions), the NPs were further stabilized by modification with polyethyleneglycol (PEG) [20]. In this work, the as-prepared Au NPs were modified with a heterofunctional PEG chain with a thiol group at one, and a carboxylic group at the other end (molecular mass $M_w$ = 3 kDa, Rapp polymer #133000-4-32, Tuebingen, Germany). $10^5$ PEG molecules were added *per* each NP, and the pH was risen to 12 with NaOH (1 M). Alkaline conditions facilitate deprotonation of the thiol terminal, which, in this way, attaches faster to the Au surface [21]. Afterwards, the PEGylated NPs were cleaned by centrifugation in order to remove unbound PEG (three times using 14,000 rpm for 30 min, supernatant containing free PEG is discarded and replaced by fresh buffer).

### *2.2. Fluorescence Labelling of Proteins*

Protein concentrations are often determined by absorption measurements, for example by the Bradford assays, as described later. However, as NPs heavily absorb in the same range of wavelengths

absorption measurements are not well suited for determining protein concentrations in NP-protein conjugates. In contrast, in order to quantify protein conjugation to NPs, it is useful to label proteins with a fluorophore. In this way, protein concentration can be determined by measuring fluorescence emission intensities. In the following, a protocol for conjugation of proteins with fluorescein isothiocyanate (FITC) is given. FITC can be directly linked to the proteins as depicted in Figure 3 [22].

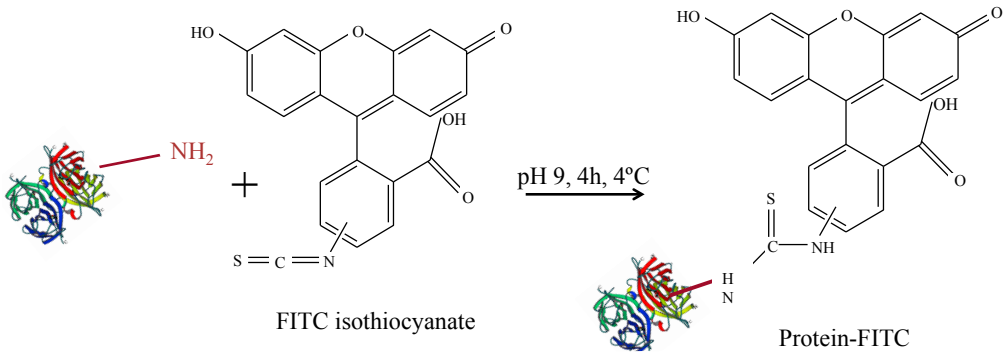


**Figure 3.** Scheme for FITC-labelling of proteins.

First, a calibration curve based on the Bradford assay [23] (Coomassie Blue, Thermo Scientific #23236, Hampton, NH, USA) to determine protein concentrations was obtained. Under the presence of proteins, a shift in the absorption spectrum of Coomassie Blue occurs and protein concentration is proportional (in a certain range) to the (offset-corrected) absorption A at 595 nm. The calibration curve was done following the fabricant specifications [24]. As protein standards, bovine serum albumin (BSA) was used (Thermo Scientific #23029). Two different calibration curves were recorded, one for high protein concentrations (working range of 100–1500 µg/mL protein concentrations $C_P$) and a second one for low protein concentrations (working range 1–25 µg/mL protein concentrations $C_P$). The standard solutions of different protein concentrations $C_P$ were prepared as indicated in the protocol, using 2-(*N*-Morpholino)ethanesulfonicacidhydrate (MES) pH 6.5 as buffer. Following the indication of the guide, in order to get the high concentration curve, 10 µL of NP solution sample were mixed with 300 µL of Coomassie reagent, previously equilibrated at room temperature. To obtain the low concentration curve instead of using 10 µL NP sample and 300 µLCoomassie reagent, 150 µL of sample and 150 µL of reagent were used. After mixing for 30 s and incubating for 10 min for each protein concentration, $C_P$, the absorption of the protein—Coomassie Blue mix at 595 nm—was recorded with an UV/Vis absorption spectrometer (Agilent 8450 spectrometer, Palo Alto, CA, USA). Single-use plastic cuvettes were used to hold the samples. Samples were prepared by triplicate and measured individually. As an offset, the absorption of Coomassie Blue without protein was subtracted. The offset-corrected absorptions A are plotted *versus* the protein concentrations $C_P$ in Figure 4. A polynomial fit was applied to obtain the final calibration curves.

FITC conjugation was performed using the following protocol. First, the concentration of proteins was determined with the Bradford method as described above. Then, a FITC stock solution was prepared in sodium borate buffer (SBB) at pH = 9, equaling 750 FITC molecules *per* protein. FITC was added to the proteins and the mixture was incubated for at least 4 h at 4 °C. For removal of unbound FITC, the sample was run through a PD 10 or a PD 25 column (depending on the solution volume, GE Healthcare #52-1308-00 and #28-9180-07, respectively, Little Chalfont, UK) and only the

protein containing fraction was collected. After the column purification the protein solution becomes diluted, the protein concentration $C_P$ (of the now FITC-conjugated proteins) was determined again with the Bradford assay. A dilution series of the proteins was obtained and, for each protein concentration, the fluorescence intensity $I$ at 519 nm (the emission wavelength of FITC) was determined. By plotting, the fluorescence intensity *versus* the protein concentration as calibration curve was obtained, *cf.* Figure 5.

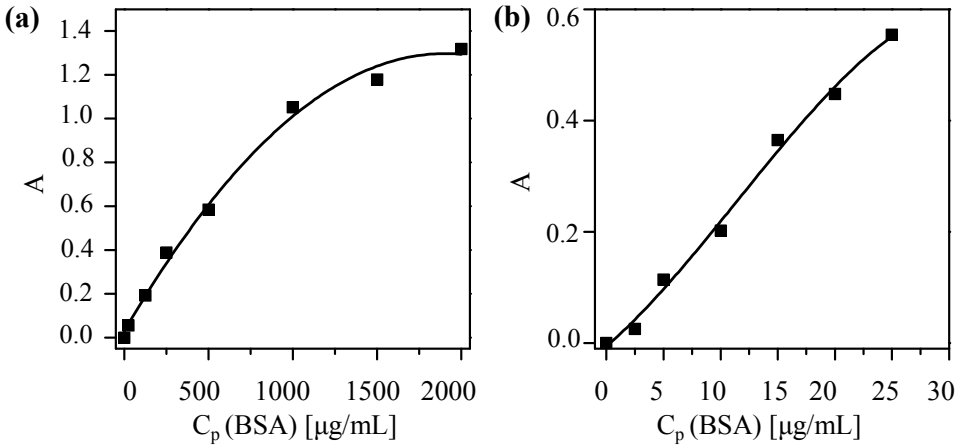


**Figure 4.** Coomassie assay calibration curves to determine the protein concentration $C_P$ of solutions with (**a**) high concentration and (**b**) low concentrations by measuring the offset-corrected absorption $A$ at 595 nm. The fitting curves are (**a**) $A(C_P) = 0.029 + (0.001\ \text{mL/µg})\cdot C_P - (3 \times 10^{-7}\ \text{mL}^2/\text{µg}^2)\cdot C_P^2$, and (**b**) $A(C_P) = -0.005 + (0.017\ \text{mL/µg})\cdot C_P - (6.789 \times 10^{-4}\ \text{mL}^2/\text{µg}^2)\cdot C_P^2 - (1.97 \times 10^{-5}\ \text{mL}^3/\text{µg}^3)\cdot C_P^3$ and the coefficients of determination ($r^2$) are equal to 0.994 and 0.989, respectively.

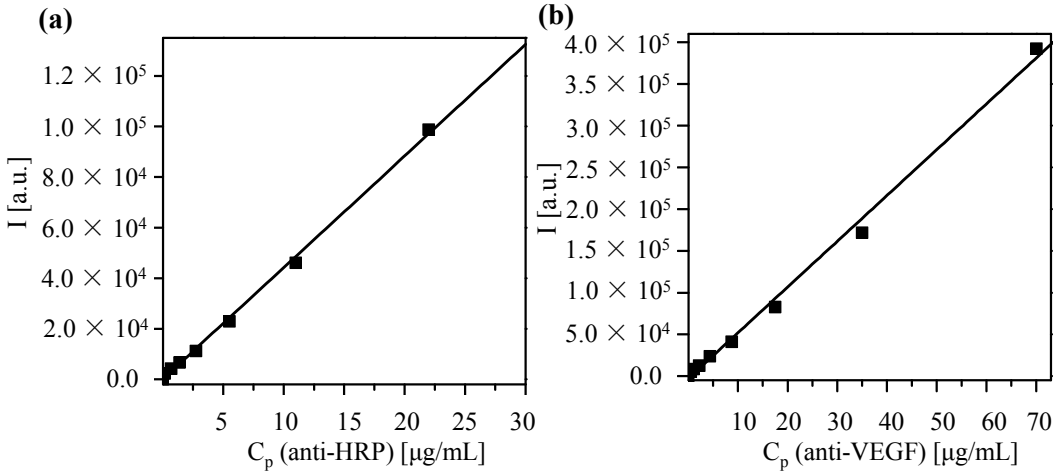


**Figure 5.** Calibration curve in which the fluorescence intensity $I$ at 519 nm is determined for protein solutions of different concentration $C_P$. Data are shown for antibodies against (**a**) horseradish peroxidase (HRP) and (**b**) vascular endothelial growth factor (VEGF). A linear fit leads to the following correlation between fluorescence intensity $I$ and concentration $C_P$: (**a**) $I(\text{C}_\text{P}) = I_0 + (\Delta I/\Delta \text{C}_\text{P})\cdot C_P = -464.28 + (4447.1\ \text{mL/µg})\cdot C_P$; (**b**) $I(C_P) = -3549.4 + (5498.3\ \text{mL/µg})\cdot C_P$. The coefficients of determination ($r^2$) are equal to 0.998 and 0.995 for HRP and VEGF, respectively.

### *2.3. Conjugation of NPs with Proteins*

Here, an often used strategy based on *N*-(3-Dimethylaminopropyl)-*N*′-ethylcarbodiimide hydrochloride (EDC, Sigma Aldrich) was employed [22]. Note that while EDC chemistry is straightforward for the formation of peptide bonds between amine groups (here present on the protein ligands) and carboxyl groups (here present on the NP surface at the PEG terminal pointing towards solution), it may result in the formation of agglomerates, and thus characterization of the resulting conjugates is required. In addition, amine groups which belong to the functional part of the proteins can be deactivated upon linkage (reaction will occur statistically on the present amine groups of the proteins), and some proteins may lose their biological activity—in the present case, antibodies against HRP (anti-peroxidase, Sigma Aldrich) or against VEGF (anti-VEGF, R&D systems, AB-293-NA) where they are linked to the NPs. As described above, the antibodies were optionally tagged with FITC. In addition to the proteins, 5-(6)-carboxytetramethylrhodaminecadaverine ("TAMRA", Anaspec #81507, Fremont, CA, USA) was also attached as additional fluorophore via its amine group to the NP surface. Third ligand short metoxy-PEG-amine (amine-PE; $M_w$ = 750 kDa, Rap Polymer #12750-2, Tuebingen, Germany) was attached via its amine group to the NP surface, in order to preserve the activity of the antibodies [25] and to prevent nonspecific protein absorption [26,27]. In other words, three different ligands (proteins, TAMRA, PEG) were attached to the PEGylated NPs using EDC chemistry. The ratios were chosen that *per* 1 Au NP 7.5 × $10^6$ EDC molecules, 50 antibodies, $10^3$ TAMRA molecules, and 2.5 × $10^4$ amine-PEG molecules were added for reaction. The reaction scheme is presented in Figure 6.

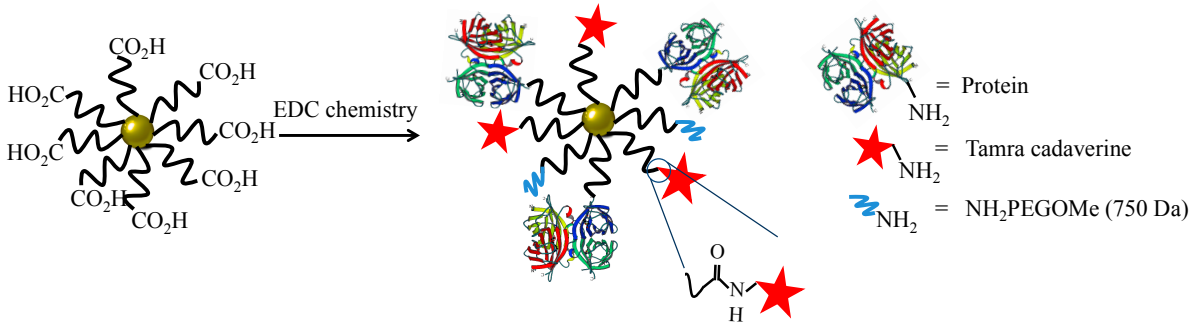


**Figure 6.** Scheme of the NP modification with antibody, dye and PEG (as passivating agent).

For the reaction 19.23 µL of Au, NPs dispersed in water (corresponding to 4pmol) with concentration $c_{NP}$ = 208 nM were taken, and mixed with 923.5 µL of 4-morpholineethanesulfonic acid (MES, Sigma Aldrich #M8250, 50 mM, pH 6.5) and 57.3 µL of EDC stock solution (100 mg/mL). After 20 min, the sample with a total volume $V$ = 1 mL containing the activated NPs was cleaned from unreacted EDC and the salts, using a pre-packed column PD-10 desalting column (GE healthcare #17-0851-01, Bucks, UK) equilibrated with MES (50 mM, pH 6.5). During this step, the NP volume was roughly diluted twice. In addition, using a high pH such as 8 was tried, with the motivation to take advantage of linking antibodies in an oriented manner [28], but the activation process was not working as well as at pH 6.5, and thus, throughout this work, pH 6.5 was used. The volume of the eluted NP solution was adjusted with MES buffer to 2 mL. Immediately after the NP cleaning, 30 µg of antibodies were added. After incubation for 15 min, 2 µg of TAMRA were added. Finally, after another 15 min of incubation,

75 µg of amine-PEG were added to block the remaining reactive carboxylic groups. The reaction mixture was incubated for another 1 h at room temperature and then incubated at 4 °C overnight. Unbound proteins, dye molecules, and PEG were removed by repetitive centrifugation (14,000 rpm 30 min), until no fluorescence was detected in the supernatant. This required at least five cleaning cycles (pelleting of NPs, discarding of supernatant, resuspending the NP pellet in fresh buffer). In the first washing step, 10 µL of sodium dodecylsulfate (SDS, 10%) was added to remove nonspecifically adsorbed dyes or proteins. Following this protocol, NPs conjugated with anti-HRP or anti-VEGF (with optional FITC label) were synthesized. As a control, the reaction was carried out without adding antibodies, but only TAMRA and PEG, leading to control NPs. In the following, the PEGylated Au NPs before bioconjugation will be referred to as Au-PEG NPs. The NPs after bioconjugation with anti-HRP, anti-VEGF, or without having antibody added will be referred to as Au-PEG-anti-HRP NPs, Au-PEG-anti-VEGF NPs, or Au-PEG-control NPs. In case the antibodies had been labelled with FITC, this is indicated as "*": Au-PEG-anti-HRP* NPs, Au-PEG-anti-VEGF* NPs.

In the vicinity of the Au surface, organic fluorophores may be quenched. Distance dependent measurements have been demonstrated that quenching can occur well up to separation distances of the fluorophores from the Au surface of 10 nm [29]. In the present work, no direct contact of fluorophores with the Au surface is possible due to the layer of 3 kDa PEG. This layer will keep the fluorophores at ≈4 nm distance to the Au surface [30]. In the case of TAMRA, conjugation directly to the PEG terminal pointing towards solution quenching does not impose any problem, as no quantitative fluorescence measurements are performed. The TAMRA merely serves as a label for qualitative fluorescence imaging of NPs that have been internalized by cells and thus quenching does not interfere with experiments. In the case of the FITC-labelled proteins, partial quenching of their fluorescence upon binding to the surface of the PEGylated Au NPs cannot be excluded. However, the proteins will randomly orient on the NP surface. Only in the case that the FITC attached to the protein is oriented towards the NP surface, significant quenching is expected, as in the case FITC attached to the protein is oriented towards solution, away from the NP surface, the distance between FITC and the Au surface is further increased by the size of the protein. Together with the PEG spacer, which is always present, one clearly cannot exclude quenching, though it is not estimated to play a huge role. Due to quenching, there is less fluorescence signal from proteins attached to the NP surface as in comparison to the fluorescence of the free proteins, which have been used for obtaining the calibration curve. In this way, in the procedure described here, the number of proteins attached per NP is underestimated.

### *2.4. Determination of the Number of Antibodies Bound per NP*

The number of antibodies per NP ($R_{P/NP}$) can determined from separately measuring the protein concentration $c_P$ and the NP concentration $c_{NP}$ of NP-antibody conjugates:

$$R_{P/NP} = c_P/c_{NP} \quad (2)$$

The NP concentration can be obtained from the absorption spectra of the conjugates at the wavelengths of the surface plasmon peak, at which the antibodies barely absorb. The protein concentration is determined from fluorescence spectra (*cf.* Figure 7) and the calibration curve shown in Figure 4.

Upon excitation of FITC (at 494 nm), there is also some fluorescence of TAMRA, which however can be clearly distinguished from the FITC fluorescence (*cf.* the green curve in Figure 7). From the FITC fluorescence spectra (*cf.* the green curve in Figure 7), the emission $I$ at 519 nm was determined. Based on the calibration curve given in Figure 5, the protein concentration $C_P$ can be determined as:

$$C_P = (I - I_0)/(\Delta I/\Delta C_P) \quad (3)$$

using the fit parameters $I_0$ and $\Delta I/\Delta C_P$ from the calibration curve given in Figure 5. The mass concentration $C_P$ of the proteins can be converted in molar concentrations $c_P$ by using the molecular mass $M_W$ of the proteins: $c_P = C_P/M_W$. The results as obtained for the Au-PEG-anti-HRP* and Au-PEG-anti-VEGF* NPs are given in Table 1, based on the data shown in Figures 5 and 7. For each sample, two different dilutions were measured.

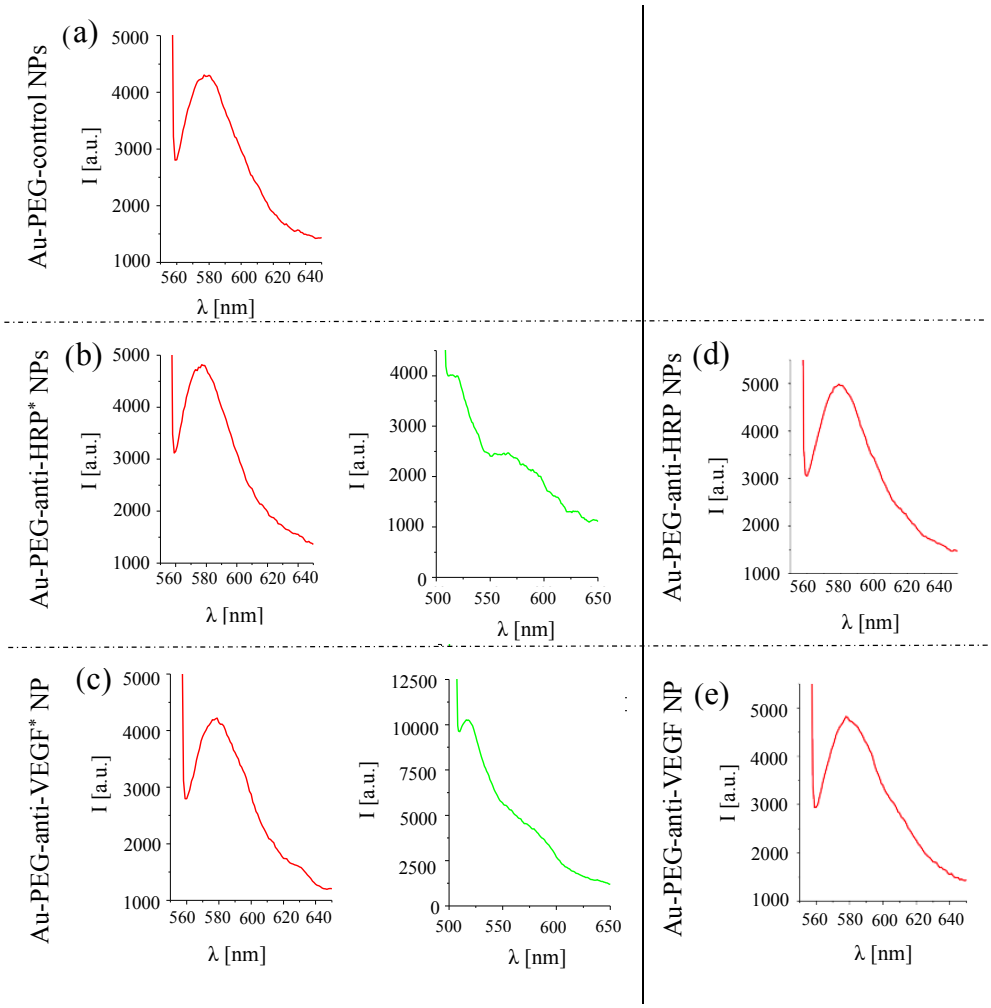


**Figure 7.** Left side: Fluorescence spectra recorded for (**a**) Au-PEG-control NPs, (**b**) Au-PEG-anti-HRP* NPs, and (**c**) Au-PEG-anti-VEGF* NPs at a NP concentration of $c_{NP}$ = 2 nM. Excitation was performed at 545 nm (TAMRA, drawn in red) or at 494 nm (FITC, drawn in green). Fluorescence spectra were recorded under the same conditions as the spectra recorded for the calibration curve Figure 5. Right side: Fluorescence spectra recorded for (**d**) Au-PEG-anti-HRP NPs, and (**e**) Au-PEG-anti-VEGF NPs for TAMRA excitation (545 nm) at a NP concentration of $c_{NP}$ = 2 nM.

**Table 1.** Summary of the calculations for the amount of proteins per nanoparticles (NP).

| Sample | Au-PEG-anti-HRP* NPs | Au-PEG-anti-HRP* NPs | Au-PEG-anti-VEGF* NPs | Au-PEG-anti-VEGF* NPs |
|---|---|---|---|---|
| $c_{NP}$ (nM) | 2.2 | 1.5 | 2.0 | 0.5 |
| $M_W$ (g/mol) | 150,000 | 150,000 | 150,000 | 150,000 |
| $\Delta I/\Delta C_P$ (mL/µg) (*cf.* Figure 5) | 4,447.1 | 4,447.1 | 5,498.3 | 5,498.3 |
| $I_0 = I$ ($C_P$= 0) (a.u.) (*cf.* Figure 5) | −464.28 | −464.28 | −3,549.4 | −3,549.4 |
| $I$ (a.u.) (*cf.* Figure 7) | 3,999 | 2,420 | 10,212 | 2,600 |
| $C_P$ (µg/mL) | 1.0 | 0.65 | 2.5 | 1.12 |
| $c_P$ (nM) | 6.67 | 4.33 | 16.67 | 7.47 |
| $R_P/_{NP}$ | 2.7 | 2.4 | 6.2 | 6.3 |

### *2.5. Physicochemical Characterization of the NP-Antibody Conjugates*

As already mentioned, bioconjugation may change the colloidal properties of NPs. Thus, characterization should be also performed with the resulting samples. The UV/Vis absorption spectra shown in Figure 8 indicate that upon bioconjugation, no significant agglomeration occurred, as scattering for wavelengths >800 nm can be neglected.

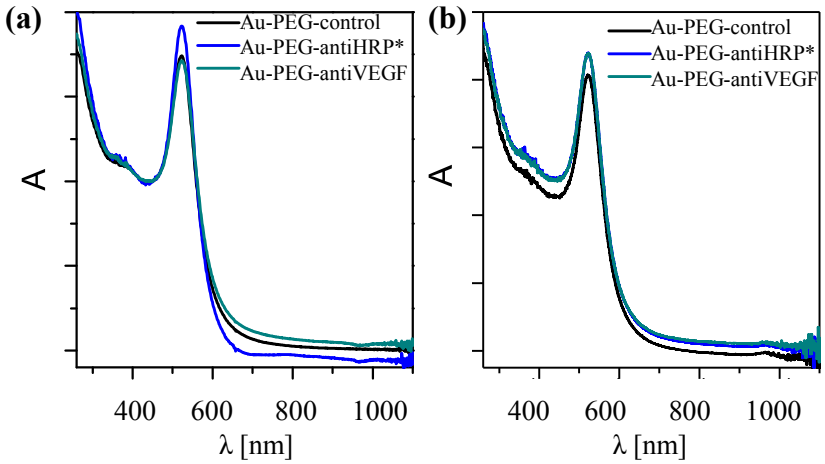


**Figure 8.** Normalized UV/Vis spectra of the NP-antibody conjugates. (**a**) Au-PEG-control, Au-PEG-anti-HRP*, and Au-PEG-anti-VEGF* NPs; (**b**) Au-PEG-control, Au-PEG-anti-HRP, and Au-PEG-anti-VEGF NPs. Spectra were recorded in a spectrometer Agilent 8453.

While UV/Vis absorption spectra can be a first indication about the presence of bigger agglomerates, it is hard to determine the existence of smaller agglomerates from these data. For this purpose, measurements of the hydrodynamic diameter $d_h$ of the NPs are best suited. One common technique in this direction is dynamic light scattering (DLS; Malvern Zetasizer set-up). However, in the case of small NPs, proteins have similar size to the NPs and thus measurements in cell culture media containing serum are complicated [31]. In Figure 9, DLS measurement for the NP-antibody conjugates are displayed. The hydrodynamic diameters $d_h$ as determined from these data (*cf.* Table 2) demonstrate that any larger agglomerates can be excluded. However, in general, no significant increase in size of the NPs upon antibody attachment could be observed, though the FITC fluorescence clearly proves the presence of the antibodies.

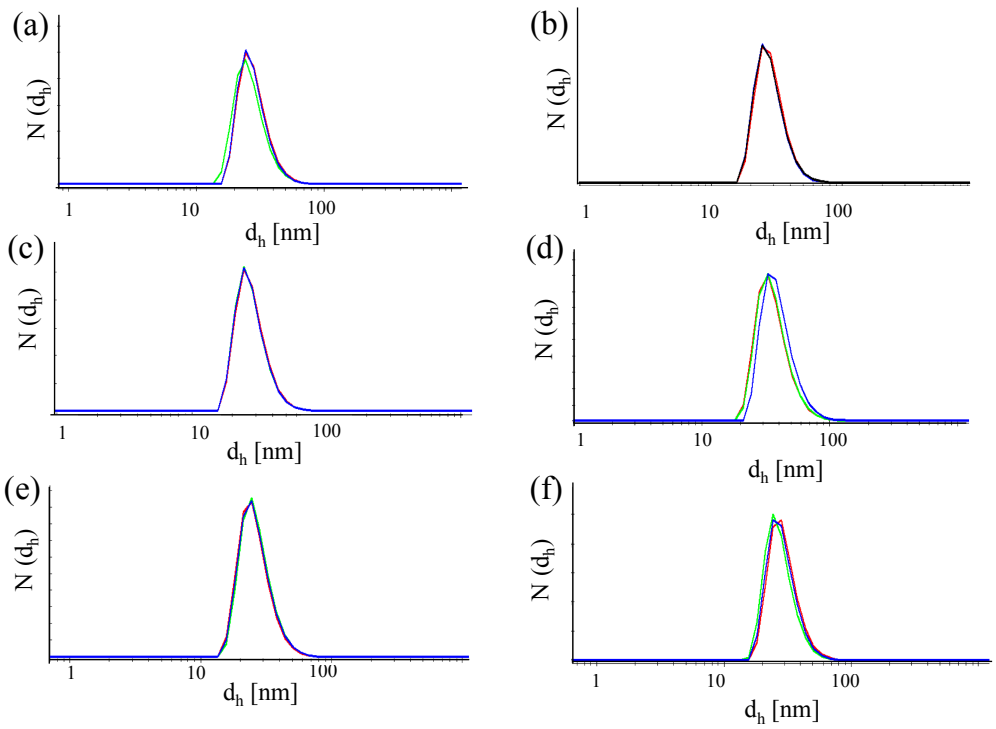


**Figure 9.** Number distribution N ($d_h$) of the hydrodynamic diameter recorded or different NPs. (**a**) Au-PEG NPs, (**b**) Au-PEG-control NPs, (**c**) Au-PEG-anti-HRP* NPs, (**d**) Au-PEG-anti-VEGF* NPs, (**e**) Au-PEG-anti-HRP NPs, and (**f**) Au-PEG-anti-VEGF NPs. The concentration of the NP solutions were $c_{NP} \approx 5$ nM, and the measurements were performed in milliQ water. Each sample was measured at least three times and the mean value of the hydrodynamic diameter was determined.

In the same Malvern Zetasizer set-up, the zeta-potential ζ was also determined based on laser Doppler anemometry, *cf.* Figure 10. The data shown in Table 2 show that despite attachment of antibodies, the NPs retained their negative zeta-potential. In the case of conjugation with antibodies without FITC, the NP-antibody conjugates have a less negative zeta potential than the NPs without attached antibodies.

As proteins can also nonspecifically adsorb to the surface of NPs, the conjugation reactions were repeated but without addition of EDC. In this way, all attached proteins are not covalently attached (as due to the lack of EDC, no amide bonds can be formed), but are nonspecifically attached to the NPs. These samples are termed Au-PEG/control, Au-PEG/anti-HRP, and Au-PEG/anti-VEGF NPs. Hydrodynamic diameters and zeta-potentials as determined with these NPs are enlisted in Table 3. There is less reduction of negative zeta potential upon presence of the antibodies. Thus, less antibodies are present per NP and, in this way, attachment of antibodies under the presence of EDC should be mainly of covalent nature.

**Table 2.** Summary of mean hydrodynamic diameters and zeta-potentials determined in water.

| Sample | Au-PEG NPs | Au-PEG-Control NPs | Au-PEG-anti-HRP* NPs | Au-PEG-anti-VEGF* NPs | Au-PEG-anti-HRP NPs | Au-PEG-anti-VEGF NPs |
|---|---|---|---|---|---|---|
| $d_h$ (nm) | 27.4 ± 0.4 | 27.8 ± 0.8 | 28.0 ± 0.2 | 38.0 ± 1.9 | 27.0 ± 0.6 | 28.9 ± 0.9 |
| ζ (mV) | −32.8 ± 0.6 | −20.0 ± 0.9 | −18.4 ± 1.6 | −24.1± 3.8 | −6.3 ± 0.2 | −11.8 ± 0.7 |

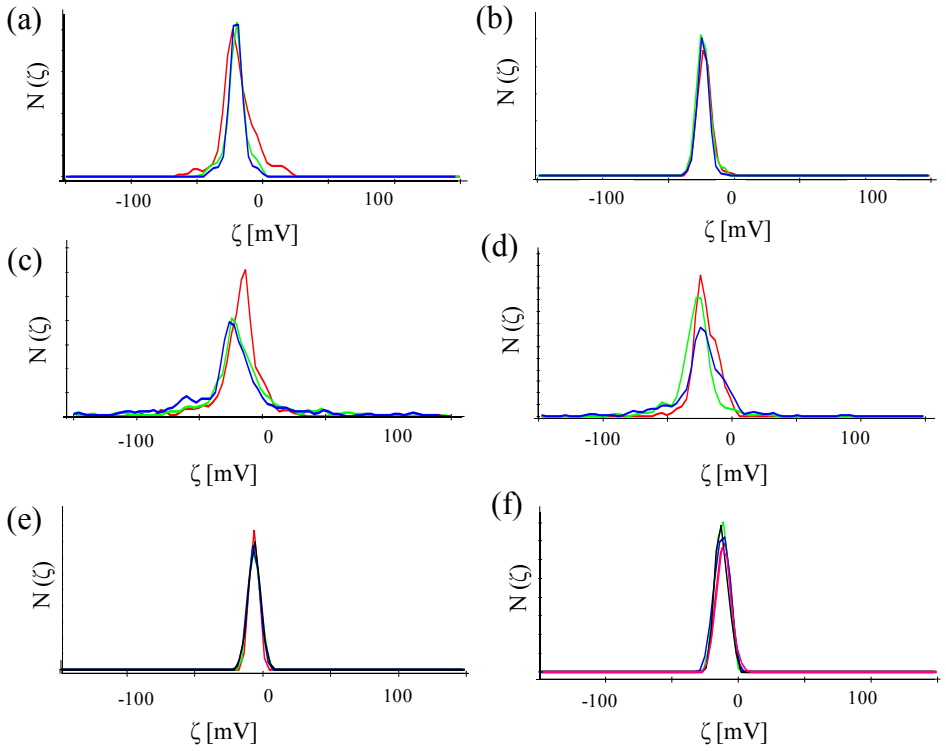


**Figure 10.** Number distribution N (ζ) of the zeta-potential of (**a**) Au-PEG NPs, (**b**) Au-PEG-control NPs, (**c**) Au-PEG-anti-HRP* NPs, (**d**) Au-PEG-anti-VEGF* NPs, (**e**) Au-PEG-anti-HRP NPs, and (**f**) Au-PEG-anti-VEGF NPs. The concentration of the NP solutions were $c_{NP} \approx 5$ nM, and the measurements were performed in milliQ water. Each sample was measured at least three times and the mean value of the zeta-potential was determined.

**Table 3.** Summary of mean hydrodynamic diameters and zeta-potentials determined in water.

| Sample | Au-PEG NPs | Au PEG-Control NPs | Au-PEG-anti-HRP NPs | Au-PEG-anti-VEGF NPs |
|---|---|---|---|---|
| $d_h$ (nm) | 27.4 ± 0.4 | 27.4 ± 1.6 | 26.1 ± 2.1 | 29.3 ± 1.7 |
| ζ (mV) | −32.8 ± 0. 6 | −30.1 ± 1.2 | −24.3± 0.9 | −31.4± 1.3 |

### *2.6. NP Interaction with Cells*

NPs can be internalized by cells via endocytosis, as they may trigger toxic effects. In the following, this is investigated for two different cell lines, human adenocarcinoma alveolar basal epithelial cells (A549) and human umbilical vein endothelial cells (HUVECs). A549 cells, purchased from ATCC, were cultured in Dulbecco's Modified Eagle's Medium (DMEM, Sigma Aldrich) supplemented with 10% fetal bovine serum, 2 mM L-glutamine (Sigma Aldrich), and 100 U/mL penicillin/streptomycin (Sigma Aldrich). HUVECs, purchased fromPromoCell, were cultured in Endothelial Cell Basal Medium (ECBM, PromoCell, Heidelberg, Germany) supplemented with 2% fetal calf serum (PromoCell), 0.4% Endothelial Cell Growth Supplement (PromoCell), Epidermal Growth Factor (0.1 ng/mL, PromoCell), Basic Fibroblast Growth Factor (1 ng/mL, PromoCell), heparin (90 µg/mL, PromoCell) and hydrocortisone (1 µg/mL, PromoCell). The cells were grown at 37 °C in a humidified atmosphere containing 5% $CO_2$.

For uptake experiments, cells were incubated with NPs and after 24 h the amount of incorporated NPs was determined. A549 cells and HUVECs were incubated with Au-PEG NPs of different concentration within medium with or without serum. After 4 h of incubation, the cells were intensively washed and further cultured. Since serum components are known to alter physicochemical characteristics of NPs, we studied their internalization in the presence and absence of serum. Twenty-four hours after adding the NPs, the cells were lysed and the samples were analyzed for their gold content with inductively coupled plasma mass spectrometry (ICP-MS). The protein content of each sample was determined by the Bradford assay (Bio-Rad, Hercules, CA, USA). The results are presented in Figure 11 as ppb of gold per mg of protein.

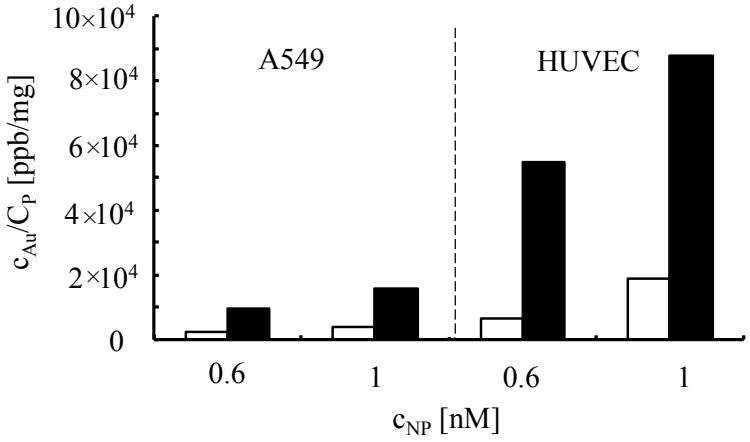


**Figure 11.** Internalization of Au-PEG NPs by A549 cells and HUVECs. A549 cells and HUVECs were incubated with Au-PEG NPs of $c_{NP}$ = 0.6 nM and $c_{NP}$ = 1 nM concentration cells in medium with (white bars) or without (black bars) serum. Twenty-four hours after adding the particles, the gold concentration $c_{Au}$ and the protein concentration $C_P$ was determined.

For all formulations tested, more NPs were taken up if they were incubated with the cells in the absence of serum, which is consistent with previous findings [31]. We speculate that proteins and other constituents of serum that interact with the NPs change their properties in such a way that they are internalized by an endocytic pathway as it has been previously described [32]. Interestingly, the PEGylated NPs were taken up well by cells. This indicates that coating Au NPs with PEG does not completely preclude their internalization. In addition, NP-antibody conjugates were incorporated by cells, as shown in the fluorescence microscopyimages in Figure 12.

The toxic effect of the NPs to the cells was analyzed with a standard viability assay. Ten thousand cells per well were seeded in 96-well-plates one day before planned experiments. A549 cells and HUVECs were incubated for 4 h with Au-PEG NPs at different concentrations $c_{NP}$ ranging from 0.2 to 1 nM. Subsequently, the cells were intensively washed and further cultured. Cell viability was evaluated 24 h after NPs had been added to the cells by the MTT assay (Roche, Germany) according to the manufacturer's instructions, *cf.* Figure 13. The assay is based on conversion of the tetrazolium dye 3-(4,5-dimethylthiazol-2-yl)-2.5-diphenyltetrazoliumbromide to its insoluble formazan, which is purple in color. Data demonstrate that Au-PEG NPs reduce cellular viability in a concentration-dependent manner.

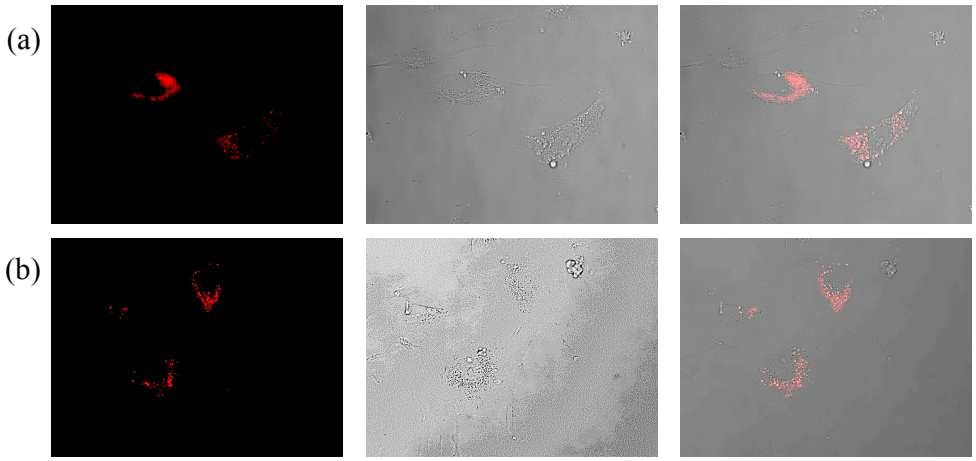


**Figure 12.** Internalization of functionalized Au NPs by human umbilical vein endothelial cells. HUVECs were exposed to TAMRA-labeled Au NPs functionalized with (**a**) anti-VEGF (Au-PEG-antiVEGF NPs), and (**b**) anti-HRP antibodies (Au-PEG-anti-HRP NPs). The NP-antibody conjugates were removed after 2 h and the cells were intensively washed. The images were taken 1 h later by employing a Zeiss fluorescent microscope. Images show the fluorescence and bright field channel, as the overlay of both channels.

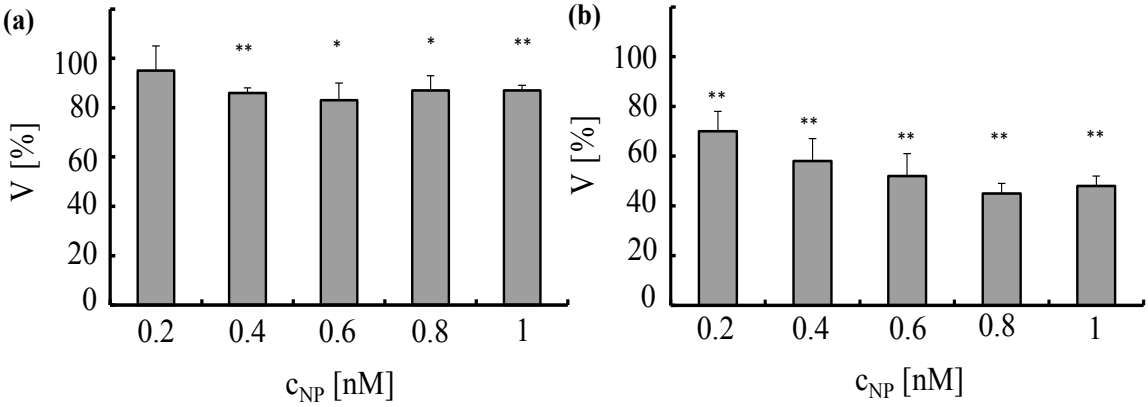


**Figure 13.** Toxicity induced by Au-PEG NPs in A549 cells (**a**) and HUVECs (**b**)Au-PEG NPs, at concentrations ranging from $c_{NP}$ = 0.2 to 1 nM, were incubated for 4 h with A549 cells or HUVECs in media containing serum. Cell viability (V) was determined 24 h after adding the NPs to the cells. The viability was normalized to 100% for untreated control cells, *$p < 0.01$; **$p < 0.001$(versus control value).

### *2.7. Effect of Au NPs with Anti-VEGF on VEGF Stimulation of Cells*

Under physiological conditions VEGF binds to its receptor (VEGFR) present on the membrane of HUVECs, which initiates cascades of signals that stimulate many processes including angiogenesis [33,34]. VEGF receptors convey information to other signal transduction molecules via autophosphorylation of distinct residues in their structure. If VEGF binds to its receptor, HUVECs proliferate. If one blocks the receptor with an antibody [33,35] or NP [36,37], there is reduced proliferation. Antibody-based therapies relay on a sequestering of VEGF molecules by specific antibodies. In this way, VEGF binding to its receptor is prevented [38].

In a first set of experiments, we tested the response of HUVECs to stimulation with VEGF. To that end, the cells were exposed for 24 or 48 h to VEGF at different concentrations ($C_{VEGF}$ = 2–16 ng/mL). As demonstrated in Figure 14, VEGF stimulated proliferation of HUVECs in a dose-dependent manner. At concentrations ≥ 10 ng/mL the number of cells in culture increased by more than 20% after 24 h and by more than 50% after 48 h. Based on these results, we chose to stimulate HUVECs with VEGF at concentrations of 12 and 16 ng/mL in all subsequent experiments.

Next, in order to verify whether proliferation elicited by VEGF can be neutralized by anti-VEGF antibodies, we pre-incubated HUVECs with the antibody, which was followed by stimulation with VEGF. The results presented in Figure 15 demonstrate that soluble anti-VEGF antibodies inhibit proliferation of endothelial cells induced by VEGF in a dose dependent manner. Note that this is not due to blocking of the VEGF receptor but by binding of anti-VEGF to VEGF, which cancels the biological activity of VEGF.

We next assessed whether a similar effect could be achieved by the anti-VEGF antibodies attached to Au NPs (Au-PEG-anti-VEGF NPs). HUVECs were first incubated with Au-PEG-anti-VEGF NPs for 2 h. This was followed by the stimulation with VEGF for 24 and 48 h. To verify whether the observed effects were specific, in this set of experiments, we also tested Au NPs functionalized with the irrelevant antibody anti-HRP (Au-PEG-anti-HRP NPs).

As demonstrated in Figure 16, Au NPs functionalized with anti-VEGF antibody (Au-PEG-anti-VEGF NPs) exhibited some effect on the proliferation of HUVECs upon stimulation with VEGF over a longer period of time. However, the same trend was observed for NP carrying anti-HRP (Au-PEG-anti-HRP NPs). Therefore, it is likely that the recorded decrease in the number of cells in culture was not caused by a specific interaction of the functionalized Au NPs with VEGF but rather was associated with NP induced toxic effects on cells.

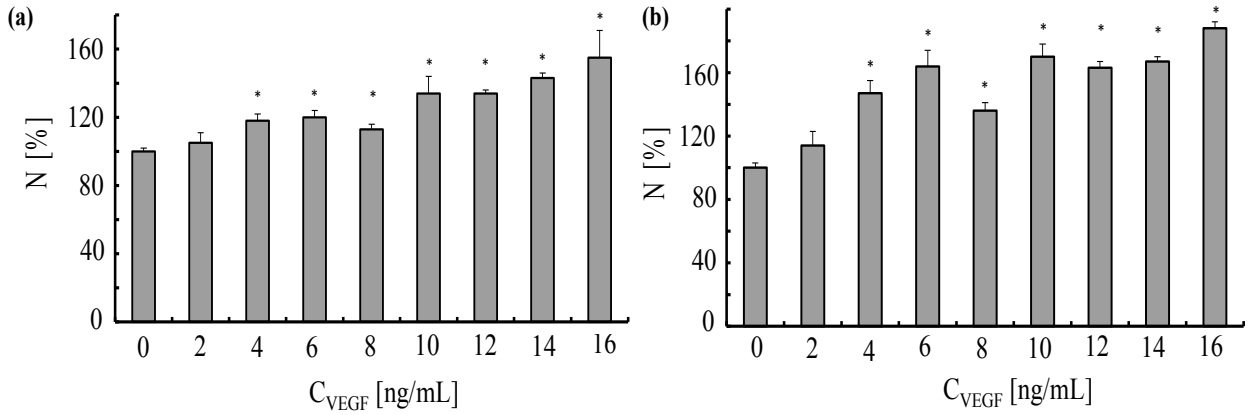


**Figure 14.** Response of human umbilical vein endothelial cells to vascular endothelial growth factor. The endothelial cells were plated in 96-well plates (5000 cells/well) one day before planned experiments. The cells were exposed for 24 h (**a**) and 48 h (**b**) to different concentrations $C_{VEGF}$ of VEGF. The normalized numbers of cells $N$ in culture were evaluated by performing a proliferation test. Data correspond to the mean value ± standard deviation obtained from $n$ = 4 experiments, *$p < 0.001$ (versus control value, no VEGF).

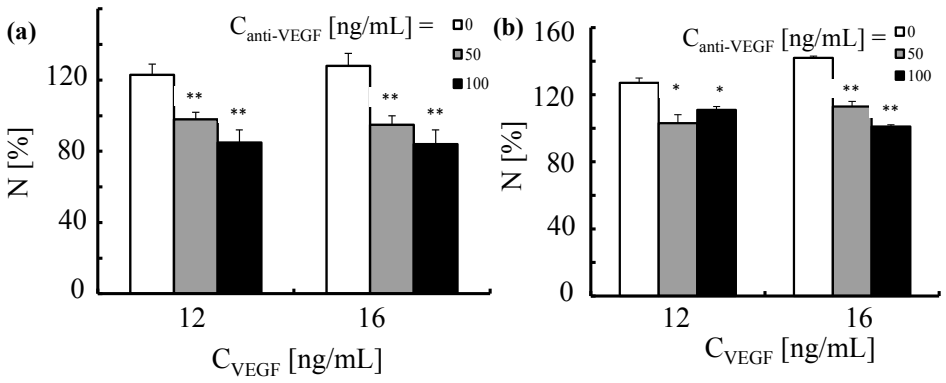


**Figure 15.** Proliferation of human umbilical vein endothelial cells triggered by VEGF and neutralization induced by anti-VEGF antibody. HUVECs were first exposed for 2 h to anti-VEGF antibody at two concentrations ($C_{\text{anti-VEGF}}$ = 50 and 100 ng/mL). This was followed by the incubation with VEGF ($C_{\text{VEGF}}$ = 12 and 16 ng/mL) for (**a**) 24 and (**b**) 48 h. The number of cells was normalized to 100% for untreated control cells. *$p$ < 0.01; **$p$ < 0.001(*versus* cells treated with VEGF only).

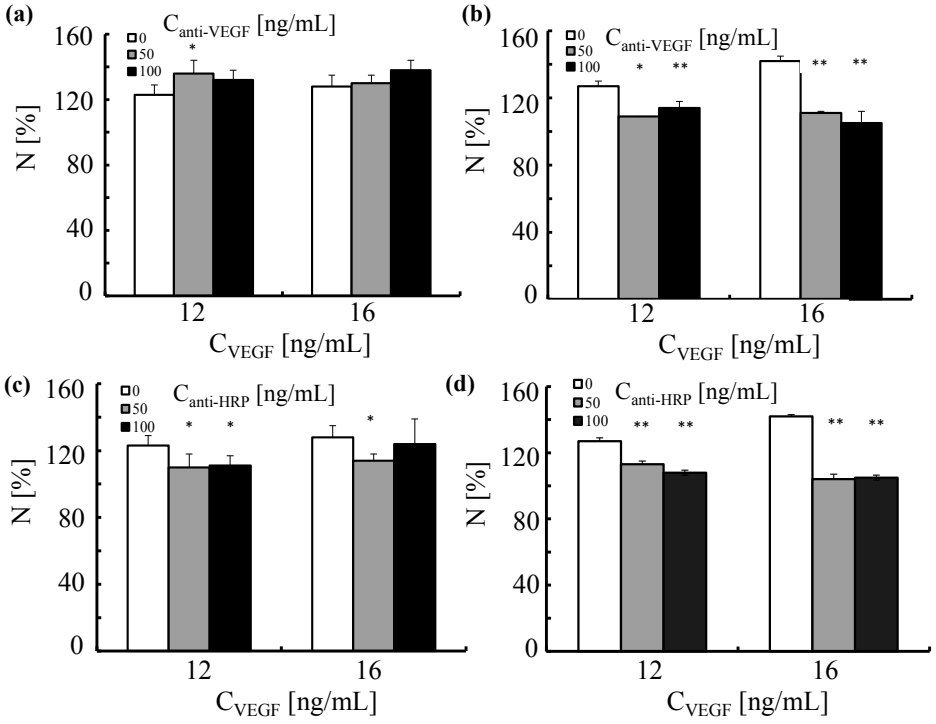


**Figure 16.** The effect of Au NPs functionalized with anti-VEGF or anti-HRP antibody on the proliferation of human umbilical vein endothelial cells triggered by VEGF. HUVECs were first exposed to Au NPs functionalized with (**a**,**b**) anti-VEGF or (**c**,**d**) anti-HRP antibodies. The NPs were added to the cells to reach concentrations of the antibodies equal to $C_{\text{anti-VEGF}}$ and $C_{\text{anti-HRP}}$ of 50 (grey bars) and 100 ng/L (black bars) (adjusted by the NP concentration by knowing the number $R_{P/NP}$ of antibodies per NP as shown in Table 1). This was followed by the incubation with VEGF ($C_{\text{VEGF}}$ = 12 and 16 ng/mL) for (**a**,**c**) 24h and (**b**,**d**) 48 h. The number of cells was normalized to 100% for untreated control cells. *$p$ < 0.01; **$p$ < 0.001 (*versus* cells treated with VEGF only).

## 3. Conclusions

A protocol for functionalizing Au NPs with antibodies has been presented, together with characterization procedures, which quantify the number of antibodies per NP. It is demonstrated that biocojungation did not induce agglomeration. While successful bioconjugation could be demonstrated, this does not provide information about the biological activity of the attached antibodies. For this, profound characterization is also required. With the presented data, a biological effect of the NP-antibodies is demonstrated. However, this example demonstrates that such data can be misleading. As the same effect was observed with NP-antibody conjugates with an irrelevant antibody, the effect can't be ascribed to a specific antibody effect but rather to general NP-induced toxicity. This example points out that antibodies can be deactivated, and that controls with irrelevant antibodies are required to demonstrate specific biological activity of NP-antibody conjugates.

## Acknowledgements

This work was supported by the German Research Foundation (DFG GRK 1782 to Wolfgang J. Parak) and by the European Commission (grant FutureNanoNeeds to Wolfgang J. Parak). Beatriz Pelaz acknowledges a fellowship from the Alexander von Humboldt Foundation. Gamze Tan thanks TUBITAK for financial support through the 2214A-International Research Fellowship Programme. Qian Zhang is grateful to a Chinese Scholarship Council (CSC) for a fellowship. Mahmoud G. Soliman thanks the Youssef Jameel Foundation for a PhD fellowship.

## Author Contributions

Gamze Tan, Daniel Valdeperez, Joanna Rejman and Beatriz Pelaz performed the experiments; Gamze Tan, Mehmet A. Onur, Joanna Rejmanand Beatriz Pelaz analyzed the data. Karsten Kantner, Mahmoud G. Soliman, Daniel Valdeperez, Qian Zhang and Pablo del Pino contributed reagents/materials/analysis tools; Wolfgang J. Parak, Joanna Rejmanand Beatriz Pelaz wrote the paper. Wolfgang J. Parak, Gamze Tan, Mehmet A. Onur, Joanna Rejmanand and Beatriz Pelaz conceived and designed the experiments.

## Conflicts of Interest

The authors declare no conflict of interest.

## References

1. Gonzalez, E.; Arbiol, J.; Puntes, V.F. Carving at the nanoscale: Sequential galvanic exchange and kirkendall growth at room temperature. *Science* **2011**, *334*, 1377–1380.
2. Ye, X.; Jin, L.; Caglayan, H.; Chen, J.; Xing, G.; Zheng, C.; Doan-Nguyen, V.; Kang, Y.; Engheta, N.; Kagan, C.R.; *et al.* Improved size-tunable synthesis of monodisperse gold nanorods through the use of aromatic additives. *ACS Nano* **2012**, *6*, 2804–2817.

3. Osorio-Cantillo, C.; Santiago-Miranda, A.N.; Perales-Perez, O.; Xin, Y. Size-and phase-controlled synthesis of cobalt nanoparticles for potential biomedical applications. *J. Appl. Phys.* **2012**, *111*, doi:10.1063/1.3676620.
4. Pelaz, B.; del Pino, P. Synthesis applications of gold nanoparticles *Front. Nanosci.* **2012**, *4*, 3–33.
5. Li, N.; Zhao, P.; Astruc, D. Anisotropic gold nanoparticles: Synthesis, properties, applications, and toxicity. *Ang. Chem. Int. Ed. Engl.* **2014**, *53*, 1756–1789.
6. Leung, K.C.F.; Xuan, S.H.; Zhu, X.M.; Wang, D.W.; Chak, C.P.; Lee, S.F.; Ho, W.K.W.; Chung, B.C.T. Gold and iron oxide hybrid nanocomposite materials. *Chem. Soc. Rev.* **2012**, *41*, 1911–1928.
7. Parak, W.J. Complex colloidal assembly. *Science* **2011**, *334*, 1359–1360.
8. Wilhelm, S.; Kaiser, M.; Wuerth, C.; Heiland, J.; Carrillo-Carrion, C.; Muhr, V.; Wolfbeis, O.S.; Parak, W.J.; Resch-Genger, U.; Hirsch, T. Water dispersible upconverting nanoparticles: Effects of surface modification on their luminescence and colloidal stability. *Nanoscale* **2015**, *7*, 1403–1410.
9. Rivera-Gil, P.; Jimenez de Aberasturi, D.; Wulf, V.; Pelaz, B.; del Pino, P.; Zhao, Y.; de la Fuente, J.; Ruiz de Larramendi, I.; Rojo, T.; Liang, X.-J.; *et al.* The challenge to relate the physicochemical properties of colloidal nanoparticles to their cytotoxicity. *Acc. Chem. Res.* **2013**, *46*, 743–749.
10. Nazarenus, M.; Zhang, Q.; Soliman, M.G.; del Pino, P.; Pelaz, B.; Carregal_Romero, S.; Rejman, J.; Rothen-Ruthishauser, B.; Clift, M.J.D.; Zellner, R.; *et al. In vitro* interaction of colloidal nanoparticles with mammalian cells: What have we learned thus far? *Beilstein J. Nanotechnol.* **2014**, *5*, 1477–1490.
11. Itano, M.S.; Neumann, A.K.; Liu, P.; Zhang, F.; Gratton, E.; Parak, W.J.; Thompson, N.L.; Jacobson, K. DC-sign and influenza hemagglutinin dynamics in plasma membrane microdomains are markedly different. *Biophys. J.* **2011**, *100*, 2662–2670.
12. Colombo, M.; Mazzucchelli, S.; Montenegro, J.M.; Galbiati, E.; Corsi, F.; Parak, W.J.; Prosperi, D. Protein oriented ligation on nanoparticles exploiting O6-alkylguanine-DNA transferase (SNAP) genetically encoded fusion. *Small* **2012**, *8*, 1492–1497.
13. Montenegro, J.-M.; Grazu, V.; Sukhanova, A.; Agarwal, S.; Fuente, J.M.D.L.; Nabiev, I.; Greiner, A.; Parak, W.J. Controlled antibody/(bio-) conjugation of inorganic nanoparticles for targeted delivery. *Adv. Drug Deliver. Rev.* **2013**, *65*, 677–688.
14. Turkevich, J.; Stevenson, P.C.; Hillier, J. A study of the nucleation and growth processes in the synthesis of colloidal golde. *J. Discuss. Faraday Soc.* **1951**, 55–75.
15. Ojea-Jimenez, I.; Bastus, N.G.; Puntes, V. Influence of the sequence of the reagents addition in the citrate-mediated synthesis of gold nanoparticles. *J. Phys. Chem. C* **2011**, *115*, 15752–15757.
16. Kimling, J.; Maier, M.; Okenve, B.; Kotaidis, V.; Ballot, H.; Plech, A. Turkevich method for gold nanoparticle synthesis revisited. *J. Phys. Chem. B* **2006**, *110*, 15700–15707.
17. Bastus, N.G.; Comenge, J.; Puntes, V. Kinetically controlled seeded growth synthesis of citrate-stabilized gold nanoparticles of up to 200 nm: Size focusing *versus* ostwald ripening. *Langmuir* **2011**, *27*, 11098–11105.
18. Liz-Marzán, L.M. Nanometals: Formation and color. *Mater. Today* **2004**, *7*, 26–31.

19. Haiss, W.; Thanh, N.T.K.; Aveyard, J.; Fernig, D.G. Determination of size and concentration of gold nanoparticles from UV-Vis spectra. *Anal. Chem.* **2007**, *79*, 4215–4221.
20. Kanaras, A.G.; Kamounah, F.S.; Schaumburg, K.; Kiely, C.J.; Brust, M. Thioalkylated tetraethylene glycol: A new ligand for water soluble monolayer protected gold clusters. *Chem. Commun.* **2002**, *2002*, 2294–2295.
21. Pelaz, B.; Grazu, V.; Ibarra, A.; Magen, C.; del Pino, P.; de la Fuente, J.M. Tailoring the synthesis and heating ability of gold nanoprisms for bioapplications. *Langmuir* **2012**, *28*, 8965–8970.
22. Hermanson, G.T. *Bioconjugate Techniques*; Academic Press: San Diego, CA, USA, 2008.
23. Bradford, M.M. A rapid and sensitive method for the quantitation of microgram quantities of protein utilizing the principle of protein-dye binding. *Anal. Biochem.* **1976**, *72*, 248–254.
24. Thermo Scientific Pierce. Available online: http://www.Piercenet.Com/instructions/2160229.pdf (accessed on 1 April 2015).
25. Dai, Q.; Walkey, C.; Chan, W.C. Polyethylene glycol backfilling mitigates the negative impact of the protein corona on nanoparticle cell targeting. *Angew. Chem. Int. Ed.* **2014**, *53*, 5093–5096.
26. Kingshott, P.; Thissen, H.; Griesser, H.J. Effects of cloud-point grafting, chain length, and density of PEG layers on competitive adsorption of ocular proteins. *Biomaterials* **2002**, *23*, 2043–2056.
27. Xie, J.; Xu, C.; Kohler, N.; Hou, Y.; Sun, S. Controlled pegylation of monodisperse $Fe_3O_4$ nanoparticles for reduced non-specific uptake by macrophage cells. *Adv. Mater.* **2007**, *19*, 3163–3166.
28. Puertas, S.; Batalla, P.; Moros, M.; Polo, E.; del Pino, P.; Guisan, J.M.; Grazu, V.; de la Fuente, J.M. Taking advantage of unspecific interactions to produce highly active magnetic nanoparticle-antibody conjugates. *ACS Nano* **2011**, *5*, 4521–4528.
29. Dulkeith, E.; Ringler, M.; Klar, T.A.; Feldmann, J.; Muñoz Javier, A.; Parak, W.J. Gold nanoparticles quench fluorescence by phase induced radiative rate suppression. *Nano Lett.* **2005**, *5*, 585–589.
30. Sperling, R.A.; Liedl, T.; Duhr, S.; Kudera, S.; Zanella, M.; Lin, C.-A.J.; Chang, W.H.; Braun, D.; Parak, W.J. Size determination of (bio-) conjugated water-soluble colloidal nanoparticles: A comparison of different techniques. *J. Phys. Chem. C* **2007**, *111*, 11552–11559.
31. Hühn, D.; Kantner, K.; Geidel, C.; Brandholt, S.; de Cock, I.; Soenen, S.J.H.; Rivera Gil, P.; Montenegro, J.-M.; Braeckmans, K.; Müllen, K.; *et al.* Polymer-coated nanoparticles interacting with proteins and cells: Focusing on the sign of the net charge. *ACS Nano* **2013**, *7*, 3253–3263.
32. Lehmann, A.D.; Parak, W.J.; Zhang, F.; Ali, Z.; Röcker, C.; Nienhaus, G.U.; Gehr, P.; Rothen-Rutishauser, B. Fluorescent-magnetic hybrid nanoparticles induce a dose-dependent increase in proinflammatory response in lung cells *in vitro* correlated with intracellular localization. *Small* **2010**, *6*, 753–762.
33. Neufeld, G.; Cohen, T.; Gengrinovitch, S.; Poltorak, Z. Vascular endothelial growth factor (VEGF) and its receptors. *FASEB J.* **1999**, *13*, 9–22.
34. Hanahan, D. Signaling vascular morphogenesis and maintenance. *Science* **1997**, *277*, 48–50.
35. Sullivan, L.A.; Brekken, R.A. The VEGF family in cancer and antibody-based strategies for their inhibition. *mAbs* **2010**, *2*, 165–175.
36. Bhattacharya, R.; Mukherjee, P.; Xiong, Z.; Atala, A.; Soker, S.; Mukhopadhyay, D. Gold nanoparticles inhibit VEGF165-induced proliferation of huvec cells. *Nano Lett.* **2004**, *4*, 2479–2481.

37. Bartczak, D.; Muskens, O.L.; Nitti, S.; Millar, T.M.; Kanaras, A.G. Nanoparticles for inhibition of *in vitro* tumour angiogenesis: Synergistic actions of ligand function and laser irradiation. *Biomater. Sci.* **2015**, *3*, 733–741.
38. Niu, G.Q.; Castro, C.H.; Nguyen, N.; Sullivan, S.M.; Hughes, J.A. *In vitro* cytotoxic activity of cationic paclitaxel nanoparticles on MDR-3T3 cells. *J. Drug Target.* **2010**, *18*, 468–476.

# Labelling of mesenchymal stromal cells (MSCs) with gold nanoparticles - an initial *in vitro* study towards optimized detection conditions for future *in vivo* tracking of MSCs

Philipp Nold[1,#], Raimo Hartmann[2,#], Karsten Kantner[2], Neus Feliu[3], Mahmoud G Soliman[2], Beatriz Pelaz[2], Mei Lim[3], Sebastian Sjöqvist[3], Philip Jungebluth[3], Pablo del Pino[4], Holger Hackstein[5], Paolo Macchiarini[3,*], Wolfgang J. Parak[2,4,*], Cornelia Brendel[1,*]

[1] Department of Hematology, Oncology and Immunology, Philipps University Marburg, Marburg, Germany.
[2] Department of Physics, Philipps-University of Marburg, Marburg, Germany
[3] Advanced Center for Translational Regenerative Medicine (ACTREM), Department of Clinical Science, Intervention and Technology (CLINTEC), Division of Ear, Nose, Throat, Karolinska Institutet, Stockholm, Sweden
[4] CIC Biomagune, Sand Sebastian, Spain
[5] Institute for Clinical Immunology and Transfusion Medicine, Justus-Liebig University Giessen, Giessen, Germany

[#] equally contributing first authors
[*] corresponding authors: paolo.macchiarini@ki.se, wolfgang.parak@physik.uni-marburg.de, brendelc@staff.uni-marburg.de

## Abstract

The use of inorganic nanoparticles (NP), in particular of Au NPs with a core diameter of 4 nm for labelling mesenchymal stem cells (MSCs) for the purpose of future in vivo MSC tracking was investigated. Time dependent uptake efficiencies of NPs by MSCs at different exposure concentrations and times was investigated. Incorporated NPs were visualized with transmission electron microscopy (TEM). The fate of the MSCs was determined in terms of the amount of excocytosed NPs *versus* the amount of initially endocytosed NPs, demonstrating that at high NP concentrations the internalized NPs are exocytosed over time, leading to a loss of label. While exposure to NPs did not significantly reduce cell viability and expression of MSC-characteristic surface markers, even at concentrations bigger than typically used for cell labelling, at those concentrations MSCs were significantly effected in their proliferation, migration. These results demonstrate that viability assays are not sufficient to claim that labelling of MSCs with NPs does not harm cells, but in fact labelling can alter cells in more subtle ways such as reducing their proliferation or migration. Thus, while labelling of cells with a large amount of NPs improves contrast for imaging, on the other hand the amount of added NPs should be reduced in order to avoid alterations in the MSCs. An estimate about the detection limits of Au NP labelled MSCs within tissue by inductively coupled plasma mass spectrometry (ICP-MS) is provided.

# 1. Introduction

Mesenchymal stromal cells (MSCs) exhibit a high *ex vivo* expansion capacity and have already entered the clinics as cellular products for various applications [1,2]. They possess anti-inflammatory and regenerative potential and migrate into sites of inflammation, tissue repair and neoplasia [3-5]. Due to their properties and safety, they are considered as a promising tool in regenerative medicine and oncology. About 200 clinical phase I/II and III studies revealed no side effects, even in allogenic settings. In oncology new therapeutic concepts envision *e.g.* genetically modified MSCs as a vehicle to selectively deliver anti-tumorigenic proteins or compounds to neoplastic tissue [6]. The efficacy of these approaches as well as the extent of side effects is directly linked to the potential of MSCs to accumulate in tumors after systemic administration. However, the exact mechanism remains unknown. In regenerative medicine MSCs have been used to form transplants.... However, the clinical use of MSCs is still in its infancy steps and thus many details still remain to the unraveled. This involves for example the mechanisms of homing and in particular also the *in vivo* fate of MSCs. This circumstance evokes the necessity for a noninvasive *in vivo* MSC tracking method that does not influence their biological properties and cellular function. Stem cell-tracking methods being currently used are limited in sensitivity and low cell labeling efficiency. Combined with poor stem cell homing efficiency revised labeling considerations are needed.

Noninvasive imaging of MSC after labeling with inorganic colloidal nanoparticles (NPs) is a promising tool is that allows for recording distributions and the long-term tracking of the MSC after systemic application [7-9]. In comparison to organic molecules NPs may allow for higher contrast in certain imaging techniques, such are magnetic resonance imaging (MRI) and computer tomography (CT). In MRI FeOx NPs have been demonstrated to provide good contrast in transversal relaxation time ($T_2$) -based imaging [10,11]. In CT elements with high atomic number obtain best contrast. Thus Au NPs are good candidates [12,13]. NPs are in general readily endocytosed by cells [14,15], and thus labelling of MSCs in principle is straightforward. Upon cell division the NPs are passed to the two daughter cells [16].

However, while in principle easily to carry out labelling of MSCs with NP has to be performed under a delicate balance. From the imaging point of view, more NPs inside each MSC would relate directly to better contrast in imaging. On the other hand it is reasonable to reduce the amount of NPs inside each MSC as much as possible in order to avoid potential cytotoxic effects. Thus labelling conditions need to be optimized. Au NPs are promising candidates, as their biocompatibility at low doses is well-accepted [17]. Gold has been used for example as clinical therapeutic in patients with severe rheumatologic disorder for many years with well known safety profit and limited side effects. Gold is usually not present in living organisms and thus tracing of Au NPs by mass spectrometry benefits from low background signals, in contrast to $FeO_x$ NPs, as there is a significant level of endogenous iron. Recent studies have shown that Au NPs at least partially fulfill basic requirements for efficient long term labeling of MSCs, *i.e.* long term stability, low cytotoxicity and most

importantly, no interference with cellular functioning. Ricles *et al.* have demonstrated that lysine coated Au NPs of hydrodynamic diameters of around 50 nm do not interfere with differentiation [18]. Long term tracking for a period of two weeks seems feasible due to high retention times and low cytotoxicity. In contrast with these findings, some studies revealed a negative effect of Au NPs on certain cellular functions such proliferation [19,20]. In addition the morphology of subcellular structures seems to be disturbed depending on the applied dose [21].

To further assess the biocompatibility and suitability of Au NPs for MSC tracking, we investigated cellular responses to Au NP labelling in mesenchymal stromal cells derived from rats (rMSCs) and humans (hMSCs), such as uptake, cytotoxicity, proliferation, migration, morphology and immunophenotype. For MSC detection *via* mass spectrometry we elucidated the detection sensitivity by quantifying the required number of labeled cells to be able to prove MSC presence in a population of cancer cells.

## 2. Materials and Methods

### 2.1. Synthesis and characterization of NPs

Polymer-coated Au NPs with a core diameter of $d_c$ = 4.25 ± 0.88 nm (as determined by transmission electron microscopy, in the following referred to as "$d_c$ = 4 nm"), a hydrodynamic diameter of $d_h$ = 10.4 ± 0.7 (as determined by dynamic light scattering in water), and a zeta-potential of $\zeta$ = - 25.1 ± 0.36 mV (as determined from laser Doppler anemometry in water) were prepared according to previously published protocols. The experimental protocol is described in detail in the Supporting Information. In addition also bigger spherical Au NPs, rod-shaped Au NPs, and $FeO_x$ NPs were prepared as controls according to previously published protocols [22]t. The NPs were overcoated with an amphiphilic polymer, poly(isobutylene–*alt*–maleic anhydride)–*graft*–dodecylamine (PMA) [23-26]. After synthesis, the NPs were purified by gel electrophoresis and by diafiltration. The concentration of the coated NPs was determined by ICP-MS. Optionally the fluorophore tetramethylrhodamine cadaverine (TAMRA) was integrated in the polymer shell. For detailed characterization of the physicochemical properties of these NPs we refer to previous studies [22,27].

### 2.2. Isolation, expansion and culture of human mesenchymal stem cells (hMSCs)

hMSCs were isolated from bone pieces obtained from hip fragments. The procedure had been approved by local ethic committees (study no. 64/01 and 25/10) and patients had been given written informed consent. 10. Dulbecco's Modified Eagles Medium (DMEM, Sigma-Aldrich, #D5546) was supplemented with 10% fetal bovine serum (FBS), 1% penicillin/streptomycin (P/S, Sigma-Aldrich, #P4333) and 2 mM L-glutamine (Sigma-Aldrich, #G7513). The cells were cultivated in flask at 37 °C and 5 % $CO_2$ until they reached 80% confluence. With every

splitting procedure the passage number was increased. hMSC where used in passages ≤ 5 due to observed adverse effects on MSC functional capabilities for higher passages.

### 2.3. Isolation, expansion and culture of rat mesenchymal stem cells (rMSCs)

Male Lewis rats were utilized use as donors of femurs and tibiae for bone marrow harvest and rMSCs isolation. The animals were treated in fulfilment with the *Principles of laboratory animal care" formulated by the National Society for Medical Research and the "Guide for the care and use of laboratory animal* organized by the Institute of Laboratory Animal Resources, National Research Council, and published by the National Academy Press, revised 1996. The ethical permission was obtained by the Stockholm South Ethical Committee (with registration number S8-11). rMSCs were isolated from rat bone marrow by means of adhesion to cell culture flasks as previously reported [28]. Briefly, rats were euthanized by an intraperitoneal barbiturate before the hind limbs were harvested. Then, the femur and tibia were cleared of soft tissue and the bone marrow was flushed out with containing calcium and magnesium using a needle and syringe. The resulting suspension was collected and after centrifugation the cell pellet was suspended in complete cell culture medium Dulbecco's Modified Eagle Medium (DMEM, Invitrogen, Sweden) with 10% fetal bovine serum (FBS, Invitrogen, Sweden) and 1% antibiotic-antimycotic (Invitrogen, Sweden). rMSCs were then seeded to a 25 $cm^2$ cell culture flask (Corning, New York, USA) and were incubated at 37 °C in 5 % $CO_2$. After 24 h of incubation, the medium was discarded, cells were washed once with phosphate buffered saline (PBS) to remove non-adherent cells, and fresh cell culture medium was added. The cells that adhered to the cell culture flask were defined as MSCs of passage 0. MSCs cultured to passage 12 or below were used for the experiments.

### 2.4. Quantification of Au NP uptake by hMSCs

The labeling efficiency of MSCs with Au NPs ($d_c$ = 4 nm) was examined by inductively coupled plasma mass spectrometry (ICP-MS, Agilent 7700 Series). Cells were seeded into 6-well plates (TPP, Switzerland, #92006) at a density of 5000 hMSCs/cm² and each well with a surface of xx $cm^2$ was filled with $V_{medium}$ = .. mL of medium. In each well there were thus $N_{cell}$ = xx cells. After 24 h Au NPs were added at different concentrations ($c_{NP}$ = 0 – 100 nM) and cells were incubated for 5 h, 24 h and 48 h or 7 days, respectively. After exposure, the cell medium was removed followed by three washing steps with PBS to remove non-internalized NPs. Then, cells were detached with 500 µL trypsin-EDTA (0.05 % trypsin-EDTA, Life Technologies, #25300-054), collected by centrifugation at 280 rcf for 5 min, and washed with PBS followed by an additional centrifugation step. The recovered cell pellets were treated with 100 µL of lysis buffer (Luciferase Cell Culture Lysis Buffer, Promega, #E153A) for 30 min. Finally, the samples were prepared for ICP-MS analysis by digestion in aqua regia. Hereby 50 µL sample was diluted in 150 µL aqua regia, consisting of three parts concentrated (35 wt%) HCl (Fisher Chemical, #7647010) and one part of (67 wt%) $HNO_3$

(Fisher Chemical, #7697372), and left for digestion for at least 3 hours. The sample containing acid was diluted 1:10 in 2 wt% HCl prior to measuring the elemental Au concentration in the sample with ICP-MS. The initial cell number was determined by performing a Lowry protein assay (Sigma-Aldrich, #TP0300) with the lysed cell pellets [29].

### 2.5. Quantification of Au NP uptake by rMSCs

rMSCs were seed at a density of 5 x $10^4$ cells/mL in a 24-well plate with each well filled with $V_{medium}$ = .. mL of medium and exposed to fluorescently labelled Au NPs ($d_c$ = 4 nm, TAMRA) at different concentrations and time points. There were thus $N_{cell}$ = xx cells in each well. Then, cells were washed with phosphate buffered saline (PBS), centrifuged at 280 rcf for 5 min, and the cells pellet was re-suspended with PBS. Flow cytometry (FCM) was performed using a FACSCalibur (Becton Dickinson) operating with CellQuestPro software. Experiments were performed with cells from three independent rat MSC donors.

### 2.6. Imaging of incorporated rMSCs with transmission electron microscopy (TEM)

Internalization of NPs was visualized by TEM analysis. rMSCs were seeded at a density of 5 x$10^4$ cells/mL in a 24-well plate and were exposed to desired concentration NPs for 24 h. At the indicated time-points, cells were harvested and washed three times with PBS and fixed in 2.5% glutaraldehyde in 0.1 M phosphate buffer, pH 7.4. Next cells were rinsed in 0.1 M phosphate buffer and centrifuged. The pellets were post-fixed in 2% osmium tetroxide in 0.1 M phosphate buffer, pH 7.4 at 4 °C for 2 h, and then dehydrated in ethanol followed by acetone and embedded in LX-112 (Ladd, Burlington, VT). Ultrathin sections were cut on a Leica EM UC6 microtome (Leica, Wien, Austria) and contrasted with uranyl acetate followed by lead citrate. Then samples were examined in a Tecnai 12 Spirit Bio TWIN transmission electron microscope (FEI Company, Eindhoven, Netherlands) at 100 kV. Digital images were collected using a Veleta camera (Olympus Soft Imaging Solutions, GmbH, Münster, Germany) as previously reported (Krais et al 2014). While in the main manuscript result for spherical Au NPs of $d_c$ = 4 nm are reported, in the Supporting Information also TEM images of rMSCs with incorporated Au NPs of bigger diameter and of rod-shape are shown. In addition in the Supporting Information also fluorescence microscopy images of fluorescence-labelled $FeO_x$ NPs inside rMSCs are presented.

### 2.7. Assessment of long term labeling efficiency of hMSCs with Au NPs by reporting exocytosis versus endocytosis

For evaluation of the long-term labeling efficiency the fraction of exocytosed NPs was determined after exposure to Au NPs. hMSCs (adherent in 25 cm² culture flasks) were exposed to $c_{NP}$ = 2 – 100 nM of Au NPs for 24 h or 48 h. After labeling, hMSCs were

detached with trypsin-EDTA, washed with PBS and plated into new 25 cm² culture flasks. After 24 h or 48 h, the Au content remaining inside MSCs (*i.e.* the remaining endocytosed NPs) and present in growth medium (*i.e.* the exocytosed NPs) was determined. The intracellular Au was quantified by ICP-MS as described above for the quantitative uptake analysis of Au NPs by hMSCs. The exocytozed fraction of the Au NPs was determined from the Au concentration of the growth medium which was diluted 1:4 in aqua regia first, followed by 1:10 dilution in 2 wt% HCl prior to ICP-MS measurements. Results are represented as Au mass fractions of intracellular *versus* the intracellular + extracellular Au.

### 2.8. Viability/recovery of rMSCs labeled with Au NPs

rMSCs were seeded at a density of 5 x $10^4$ cells/mL in a 24-well plate with each well filled with $V_{medium}$ = .. mL of medium and exposed to Au NPs for 24 h – 72 h. There were thus $N_{cell}$ = xx cells in each well. Then, cells were washed 3 times with PBS and grown for further 48 h. Afterwards, cells were seed at constant density in a 6-well plate and grown for further 7 days. Finally cells were seed at constant into 96-well plates for evaluation of cell viability. Briefly, AlamarBlue® reagent (Invitrogen) was added in each well and incubated for desired time at 37 ºC. The fluorescence was measured at 560 nm excitation and 590 nm emission wavelength using a spectrophotometer (SpectraMax 250, Molecular Devices, USA). Results are expressed as percentage of cell viability V versus control (*i.e.* untreated cells). Experiments were performed in three independent rat MSC donors in triplicates for each time-point and concentration. Data in the main manuscript describe results for $d_c$ = 4 nm Au NPs. Viability data for all other NPs are presented in the Supporting Information.

### 2.9. Proliferation of hMSCs

The effect of exposure of hMSCs to Au NPs on their proliferation rate P was determined with carboxyfluorescein succinimidyl ester (CFSE) and flow cytometry (FCM). Cells were labeled with a certain amount of membrane-impermeable CFSE whose fluorescent intensity decreases upon cell division [30]. $2.5 \cdot 10^5$ cells per sample were labeled with 1 µM CFSE (Molecular Probes, #C34554) for 10 min at 37 °C in 1 mL of PBS. Subsequently, the cells were washed twice with 5 mL of pre-warmed supplemented DMEM and plated in 25 cm² culture flasks. After 24 h NPs ($c_{NP}$ = 0 – 50 nM) were added and a negative control was prepared containing 5 µM of the mitosis inhibitor cholchicine (Sigma-Aldrich, #C9754). After subsequent culturing for additional 6 days, cells were detached with trypsin-EDTA, counter-stained with 1 µM propidium iodide (PI, Sigma-Aldrich, #P4170) and signals were acquired with a BD LSR II FCM device with FACS Diva software (BD Biosciences). Data were analyzed with FlowJo version 9.5.3 (TreeStar Inc.) and GraphPad Prism software. CFSE was excited at 488 nm and emission was detected at 521 nm. Living cell were gated after 4',6-diamidino-2-phenylindole (DAPI) (Sigma-Aldrich, #D9542) staining. Results are normalized to the positive (P = 1, no Au NPs) and negative control (P = 0, cholchicine) and

are representing the mean values ± standard deviations of the median values of the CFSE fluorescent intensity/cell for 3 independent experiments.

### 2.10. Migration of hMSCs

The migration potential of hMSCs was assessed by analyzing cell migration through membrane inserts by fluorescent microscopy [Maijemburg et al 2010]. MSCs were labeled with Au NPs in 25 cm² culture flasks filled with .. mL of medium at $c_{NP}$ = 0 – 25 nM for 2 days. Subsequently, cells were detached with trypsin-EDTA and transferred in serum free medium into the upper chamber of membrane inserts (8 µm, Greiner Bio One, #662638) placed into the wells of a 24 well plate (Greiner Bio One, #622160, xx $cm^2$ surface area per well) at a concentration of X cells/cm² with $V_{medium}$ = xx mL medium in each well. There were thus $N_{cell}$ = xx cells in each well. The lower chambers were filled with growth medium containing 10% humand platelet lysate (HPL, manufactured at the Institute for Clinical Immunology and Transfusion Medicine, Giessen, Germany in a GMP-compliant manner as described in [31]) to stimulate hMSC migration from the upper to the bottom side of the membrane inserts. After 16 h cells were fixed with methanol and nuclei were stained with 50 µM of 4',6-diamidino-2-phenylindole (DAPI, Life Technologies, #D1306) for 5 min. For each sample migrated and non-migrated hMSCs were counted at fixed positions each comprising an area of 0.38 cm². The counting was based on fluorescent images acquired with a confocal laser scanning microscope (CLSM 510 Meta) from Zeiss using a Plan-Apochromat 20x/0.8 M27 objective (pinhole size: 1 airy unit, lateral sampling rate: 0.6 µm/pixel). DAPI (nuclei) was excited with a 405 nm-laser diode an emission was gated with a 420 nm long-pass filter. For imaging the inserts were placed on a microscope slide in a drop of PBS. For 4-6 randomly chosen positions two images were acquired: Non-migrated cells were captured by acquiring an image at a plane above the membrane and migrated cells were imaged below the membrane, *cf.* the Supporting Information for a sketch of the set-up. For each position (A = 0.38 mm²) the number of cells above ($N_{non\text{-}mig}$) and below the membrane ($N_{mig}$) was determined based on their nuclear staining by employing CellProfiler [32] and the ratio $N_{mig}/(N_{mig}+N_{non\text{-}mig})$ was calculated. Results are displayed as mean values ± standard deviations for 3 independent experiments.

## 3. Results and discussion

### 3.1. Au NPs are incorporated by MSCs

As expected MSCs readily incorporate Au NPs in a dose- and time-dependent manner, *cf.* Figure 1. In the present study NP concentrations ranging from $c_{NP}$ = 1 to 100 nM were used for 4 nm core size Au NPs. Uptake was quantified either by determination of elemental Au inside cells *via* ICP-MS (*cf.* Figure 1a), or by recording the cellular fluorescence due to internalized fluorescence-labelled NPs *via* flow cytometry (FCM, *cf.* Figure 1b). In general the amount of internalized NPs increased over time, whereby after long exposure (> 24 h)

and high NP concentrations saturation effects could be observed, *cf.* Figure 1. Hereby it has to be stated that uptake efficiency significantly depended on the individual donor source of the MSCs. The data shown in Figure 1a allow for calculating the number $N_{NP}$ of Au NPs which are internalized by each cell as $N_{NP} = (m_{Au}/M_{Au})\cdot N_A$, with $m_{Au}$ being the mass of elemental Au inside each cell as detected with ICP-MS (*cf.* Figure 1a), $M_{Au}$ = 196 g/mol the molar mass of Au, and Avogadro's constant $N_A = 6.02\cdot 10^{23}$ $mol^{-1}$. In case of exposure to $c_{NP}$ = 10 nM Au NPs for 24 h this results in $N_{NP}$ = xx NPs per cell. This can be compared to the total number of NPs $N_{NP,add}$ to which on cell had been exposed: $N_{NP,add} = c_{NP}\cdot V_{medium}\cdot N_A/N_{cell}$ whereby $V_{medium}$ is the volume of medium in each well and $N_{cell}$ is the number of cells per well. In case of exposure to $c_{NP}$ = 10 nM Au NPs this corresponds to $N_{NP,add}$ = xx per cell. This demonstrates that only a small fraction of NPs present in medium is actually incorporated by cells. There is an agreement in literature that the classical uptake pathway of NPs by cells in endocytosis [15], and thus internalized NPs are located in intracellular vesicles. TEM images showed the presence of NPs inside cells, *cf.* Figure 2a. In the Supporting Information TEM data are presented which demonstrate that also Au NPs with bigger size or with rod shape, as $FeO_x$ NPs are internalized by MSCs. Saturation for extended incubation times may be due to proliferation, as the internalized Au NPs are partitioned to daughter cells, or due to exocytosis. In Figure 2b data are presented in which NP excretion was investigated by measuring the increasing Au content in the extracellular medium 24 or 48 h after labeling. The data demonstrate that with increasing NP concentration the excretion *via* exocytosis is increasing, which is most probably taking place largely within the first 24 h. Thus, the maximum number of NPs with which a cell can be labelled is limited.

## 3.2. Biocompatibility studies

In order to investigate the biocompatibility of the 4 nm Au NPs cell viability of MCS exposed to the NP was assessed using the Alamar blue assay. The data shown in Figure 3 indicate that the cell viability of MCS exposed to NPs for 24, 48 and 72 h was not strongly affected. Still a small trend for a decrease of cell viability was observed at high NP concentration ($c_{NP}$ > 50 nM). Data shown in the Supporting Information also for bigger Au NPs, rod-shaped Au NPs, and $FeO_x$ NPs further demonstrate that MSC labelling with NPs is possible without severely effecting cell viability. Cell viability however is not the most sensitive indicator for probing effects of NPs on MSCs. We thus carried out a NP-concentration dependent proliferation assay, *cf.* Figure 4a. Relative cellular proliferation was significantly reduced for $c_{NP}$ = 50 nM, and in fact already at very low NP doses of 2 nM proliferation was shown to be affected. Another important parameter of MSCs to be maintained is their capacity to migrate. In several studies MSCs were used for homing and tracking experiments. Berlin *et al.* used for example Au NP-labeled neural stem cells (NSCs) to eliminate cancerous tissue *via* light mediated heat generation. For such applications migration of labeled NSCs/MSCs is mandatory. In Figure 4b we demonstrate that cellular migration through a porous membrane is affected in case cells have incorporated NPs. Our data suggest a dose dependent migration capacity of MSCs labeled with Au NPs. High

concentrations of Au NP in MSCs may led to impaired homing. A significant negative effect was already visible for $c_{NP}$ = 50 nM. We note that in one study it is claimed that in contrast labelling of MSCs with $FeO_x$ NPs rather enhanced the migration capability the cells. Based on our data, we identified the least tolerable dose for 24 h exposure with 4 nm Au NPs to be around 10 nM. In order to probe if labeling of MSCs under these conditions affects the immunophenotype of MSC, expression of surface antibodies was determined by flow cytometric analysis. Au NP labeled hMSC proved to express the characteristic antigens CD73, CD90 and CD105, but lacked expression of CD14, CD19, CD34, CD45 and HLA-DR as shown in Figure 5. The immunophenotype of hMSCs labeled under these conditions is in accordance with the consensus criteria for MSCs [33]. This is in line with results obtained by Mailänder *et al.*, who showed no impact on lineage markers and differentiation (Brüstle et al 2015) upon NP labelling of MSCs. Thus, at reasonable Au NP concentrations (*i.e.* 10 nM for 4 nm Au NPs), the NP labeling does not interfere with the immunophenotype and does not cause long-term cytotoxicity. However, our data reveal onset of negative effects on proliferation and migration potential already at these concentrations. This demonstrates that the amount of Au NPs which can be reasonably added as label per cell is clearly limited, which effects the maximum contrast which can be obtained for imaging.

## 3.3. Limits of MSC detection with ICP-MS

Using the above determined parameters for NP labelling of MSCs we wanted to determine the limits of detection of MSCs *via* NP labelling. We chose ICP-MS as detection technique, as it is a frequently used tool for determining of bio-distributions, in particular of Au NPs. With our set-up the detection sensitivity was determined to be around $N_{MSC,limit} \approx 400$ labelled cells. However, upon MSC homing MSCs actually will only form a small fraction of cells on the target site, and there will be many non labelled cells. For this purpose the fraction of labeled hMSCs ($c_{NP}$ = 10 nM, 24 h) in a population of $10^6$ promyelocytic leukemia cells (HL-60) was varied do determine the number of MSCs required for verifying presence of MSCs. According to the data shown in Figure 6 cell numbers down to 400 labeled MSCs/$10^6$ HL-60 cells are resolvable. This corresponds to 0.04% hMSC in a mixture of $1x10^6$ unlabeled HL-60 cells. In addition the ratio between labeled expected cell numbers under optimal conditions and detected hMSC *via* ICP-MSC was linear (*cf.* Figure 6). This allows for some estimation about the minimum tissue volume $V_{min}$ which can be detected *via* homing of MSCs. A mentioned a highly relevant parameter is the amount $N_{MSC}$ of MSCs which can be integrated in tissue with $N_{cell}$ cells, *i.e.* the ration $N_{MSC}/N_{cell}$. In case one assumes a mean value $V_{cell}$ for the volume of one cell, the tissue volume which can be resolved would be $V_{min} = V_{cell} \cdot N_{MSC,limit}/(N_{MSC}/N_{cell})$. In case of tumor homing of MSCs the fraction of MSCs inside the tumor will be relatively low. Using the experimentally determined value $N_{MSC,limit} \approx 400$ and the numbers $N_{MSC}/N_{cell} = 10^{-5}$ and $V_{cell} = 100\ \mu m^3$ as example, the smallest structure which can be detected would be $V_{min} \approx 4 \cdot 10^9\ \mu m^3 = (1.6\ mm)^3$. This would be the minimum size of a tumor which could be detected with ICP-MS upon MSC homing. In case of reseeding decellularized templates for implants all cells in the implant would

be MSCs, and thus $N_{MSC}/N_{cell} = 1$. Thus would result in $V_{min} \approx 4 \cdot 10^4$ μm$^3$ = (34 μm)$^3$. While in this study ICP-MS was used for detection

## 4. Conclusions

On the first glance, the physical properties of Au NPs for MSC labeling seem well suited when looking on the potential perspectives for further applications in diagnosis and therapy. However, due to certain critical impacts on cellular function, their usage requires careful adaption of concentrations and a correct judgment of side effects to avoid a reduction in proliferation or migration. Both are essential parameters for successful application *in vivo.* While in this study we demonstrated that incubation of MSCs with Au NPs can have profound effects on the proliferation and migration the MSCs, the detailed molecular pathways were not investigated so far. In particular one may speculate that part of this impairment could be recovered over time. In fact research in this field is just in its beginnings and a large number of additional effects need to bee considered. MSCs administered intraveneously have shown to be prone to be stuck inside the lungs, while intraaterial administration seems to prevent this 'first-pass' effect [34-36]. Whether this unwanted effect is for example enhanced in Au NP labeled MSCs is subject of future studies.

One potential advantage of using NPs as labels for MSC tracking is the potential of multiplexed detection. Different types of cells can be labelled with different types of NP, thus allowing for parallel imaging of different cells types. NPs of different materials, *e.g.* besides Au NPs also Pt NPs can be distinguished by ICP-MS as well as by CT imaging.

## Acknolwedgments

This work was funded in part by the European Union (grant FutureNanoNeeds to WJP).

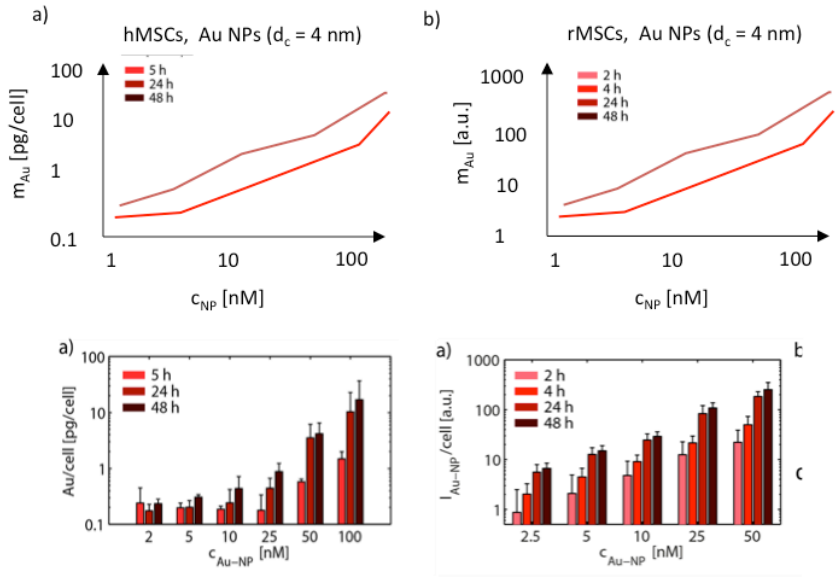


**Figure 1:** Quantitative determination of uptake of Au NPs by a) hMSCs and b) rMSCs. a) hMSCs were incubated with Au NPs ($d_c$ = 4 nm) at varying concentrations ($c_{NP}$ = 2 – 100 nM) for different exposure times (5 h, 24 h, 48 h). After washing the mass $m_{Au}$ of intracellular Au was determined by ICP-MS and was normalized to the initial number of cells. Results are presented as mean value ± standard deviation (SD). b) rMSCs were incubated with fluorescence- labelled Au NPs ($d_c$ = 4 nm; TAMRA in PMA shell) at varying concentrations ($c_{NP}$ = 2.5 – 50 nM) for different exposure times (2 h, 4 h, 24 h, 48 h). The amount of intracellular Au mAu was assumed to be proportional to the TAMRA fluorescence as recorded from each cells as determined by FCM. The results shown correspond to the mean value ± SD from at least three independent experiments using cells from different rats.

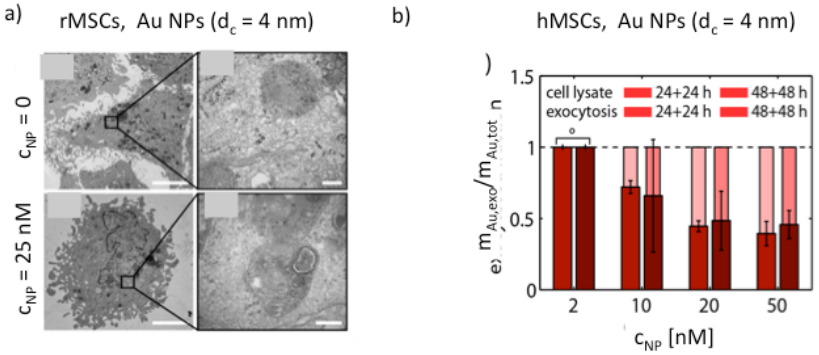


**Figure 2:** Endocytic uptake and exocytosis of Au NPs by MSCs. a) Localization of endocytosed rMSCs. rMSCs were incubated for with Au NP ($d_c$ = 4 nm) for 24 h at a NP concentration of $c_{NP}$ = 25 nM. Control rMSCs were not incubated with NPs. TEM images were recorded. The scale bars in the micrographs correspond to 2 µM (left) and 500 nM (right), whereby images on the right represent enlargements of the black quadrant in the images on the left. Prensence of NPs in intracellular vesicular structures can be seen. b) Exocytosis of hMSCs. hMSCs were exposed to Au NPs ($d_c$ = 4 nm) at the indicated doses $c_{NP}$ for 24 h or 48 h. After washing off residual NPs from the medium and the outer cell membran, i.e. NPs which had not been internalized by the hMSCs, culturing was continued in fresh growth medium for 24 h or 48 h. Then the amount of intracellular Au $m_{Au}$ (*i.e.* Au inside the cell pellet) and exocytozed Au (*i.e.* Au in the medium) $m_{Au,exo}$ was determined by ICP-MS. Then the fraction of exocytosed Au NPs was determined as $m_{Au,exo}/(m_{Au,exo} + m_{Au}) = m_{Au,exo}/(m_{Au,tot})$. For cells labeled with $c_{NP}$ = 2 nM (°) the Au content in the cell medium was below the detection limit.

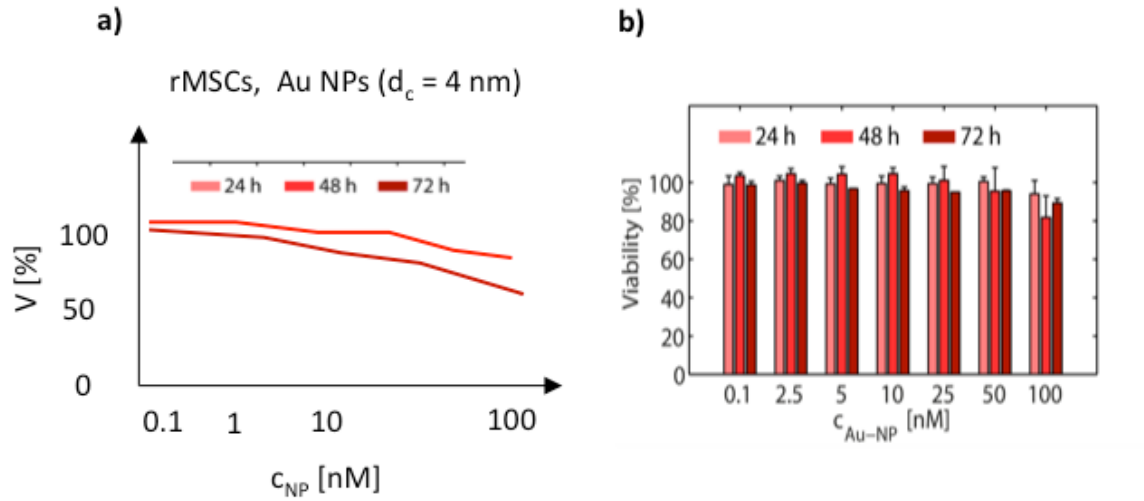


**Figure 3:** Viability of a) hMSCs and b) rMSCs after uptake of Au NPs ($d_c$ = 4 nm). MSCs were exposed to various concentrations $c_{NP}$ of Au NPs different incubation times t. Cell viability V was assessed using the Alarm Blue assay. The viabilities are normalized to the viability of cells which had not been exposed to NPs. Results are presented as mean value ± SD. In the case of rMSCs n = 3 (for 24 h and 48 h exposure) and n = 2 (for 72 h exposure) independent experiments using cells from different rats were carried out. No statistically significant differences were detected using one way ANOVA.

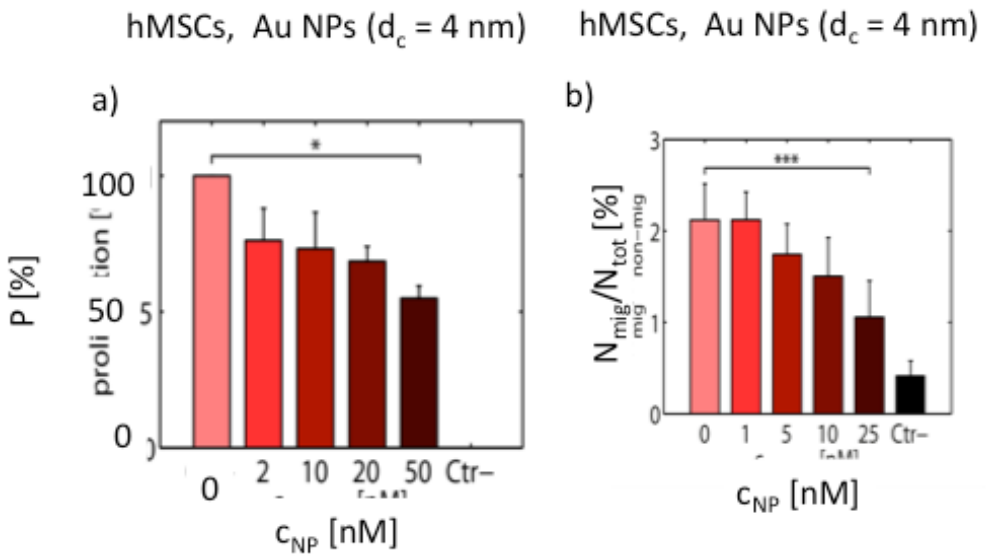


**Figure 1:** a) Effect of Au NP exposure on hMSC proliferation. b) Proliferation ratio P upon exposure to Au NPs normalized to that of untreated cells (= positive control Ctr+ $c_{NP}$ = 0). As negative control Ctr- a mitosis inhibitor was used. Proliferation of hMSCs exposed to $c_{NP}$ = 50 nM was significantly reduced ($p < 0.05$). b) Effect of Au NP exposure on hMSC migration through a membrane. The migration efficiency after exposure to Au NPs is displayed as the ratio of the number of migrated cells $N_{mig}$ divided by the the total cell number, which is the sum of non-migrated cells $N_{non\text{-}mig}$ and migrated cells: $N_{tot} = N_{mig} + N_{non\text{-}mig}$. As negative control Ctr- ... was used. Migration of hMSCs exposed to $c_{NP}$ = 25 nM was significantly reduced ($p < 0.0001$).

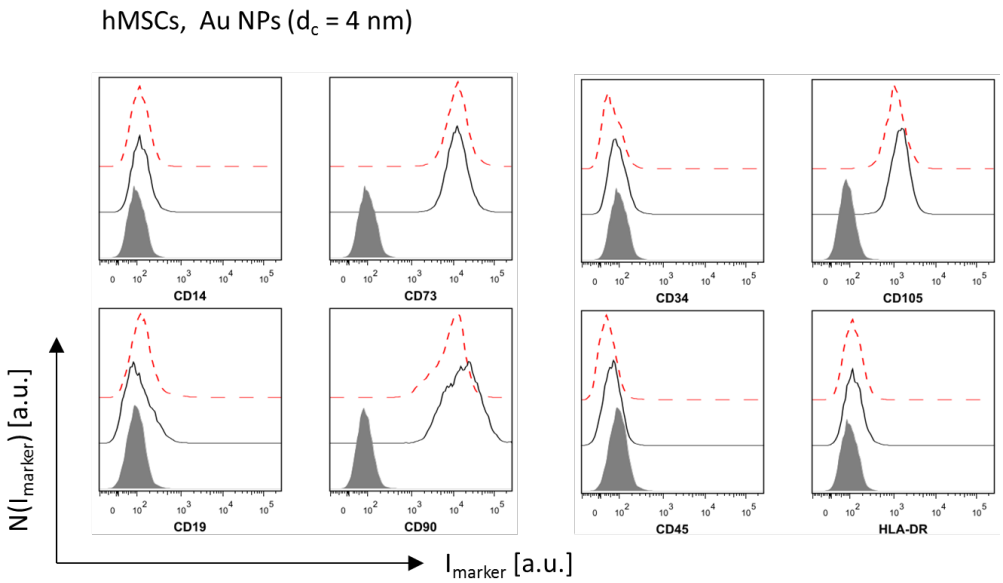


**Figure 5:** Effect of internalized Au NPs on the surface marker expression of hMSCs. Representative histograms of the distribution of the marker fluorescence $N(I_{marker})$ of MSC-defining surface markers of untreated hMSCs (black solid line) and hMSCs exposed to $c_{NP}$ = 10 nM (red dashed line) Au NP for 24 h are shown. The solid grey front curve represents the isotype control.

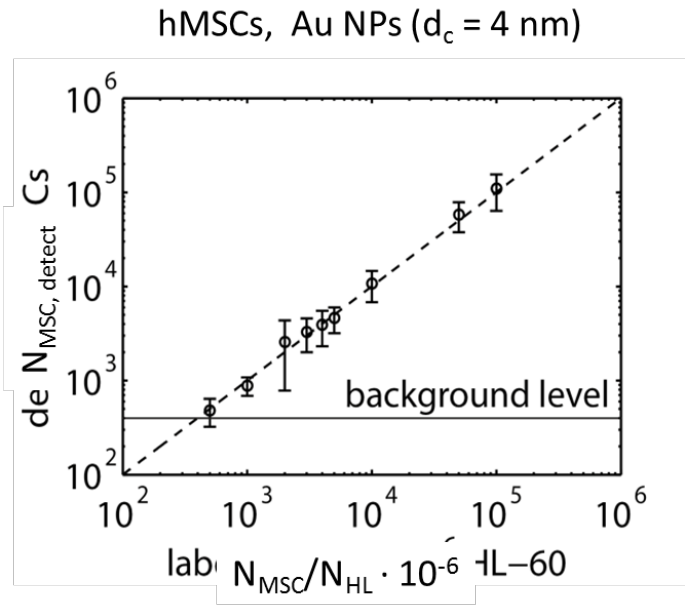


**Figure 6:** Detection of Au NP-labelled hMSCs with ICP-MS. $N_{MSC}$ = 0-100,000 hMSCs labeled with $c_{NP}$ = 10 nM of Au NPs for 24 h were mixed with $N_{HL}$ = 1 x $10^6$ unlabeled HL-60 cells. The then the number $N_{MSC,detect}$ of hMSCs in the mixture was deteted with ICP-MS. The dashed line represents the expected results under optimal conditions. The Au noise background level was corresponding to ~400 labelled cells.

## References


1. Nold P, Brendel C, Neubauer A, Bein G, Hackstein H (2013) Good manufacturing practice-compliant animal-free expansion of human bone marrow derived mesenchymal stroma cells in a closed hollow-fiber-based bioreactor. Biochemical and Biophysical Research Communications 430: 325-330.
2. Menard C, Pacelli L, Bassi G, Dulong J, Bifari F, et al. (2013) Clinical-grade mesenchymal stromal cells produced under various good manufacturing practice processes differ in their immunomodulatory properties: standardization of immune quality controls. Stem cells and development 22: 1789-1801.
3. Chapel A, Bertho JM, Bensidhoum M, Fouillard L, Young RG, et al. (2003) Mesenchymal stem cells home to injured tissues when coâ€ infused with hematopoietic cells to treat a radiationâ€ induced multiâ€ organ failure syndrome. The journal of gene medicine 5: 1028-1038.
4. Kidd S, Spaeth E, Dembinski JL, Dietrich M, Watson K, et al. (2009) Direct evidence of mesenchymal stem cell tropism for tumor and wounding microenvironments using in vivo bioluminescent imaging. Stem cells 27: 2614-2623.
5. Uchibori R, Tsukahara T, Mizuguchi H, Saga Y, Urabe M, et al. NF-κB activity regulates mesenchymal stem cell accumulation at tumor sites. Cancer research 73: 364-372.
6. Uchibori R, Tsukahara T, Ohmine K, Ozawa K (2014) Cancer gene therapy using mesenchymal stem cells. International journal of hematology 99: 377-382.
7. Huang X, Zhang F, Wang Y, Sun X, Choi KY, et al. (2014) Design considerations of iron-based nanoclusters for noninvasive tracking of mesenchymal stem cell homing. ACS nano 8: 4403-4414.
8. Skopalik J, Polakova K, Havrdova M, Justan I, Magro M, et al. (2014) Mesenchymal stromal cell labeling by new uncoated superparamagnetic maghemite nanoparticles in comparison with commercial resovistâ€“an initial in vitro study. International journal of nanomedicine 9: 5355.
9. Schmidtke-Schrezenmeier G, Urban M, Musyanovych A, MailÃ¤nder V, Rojewski M, et al. (2011) Labeling of mesenchymal stromal cells with iron oxid–poly (L-lactide) nanoparticles for magnetic resonance imaging: uptake, persistence, effects on cellular function and magnetic resonance imaging properties. Cytotherapy 13: 962-975.
10. Jacques V, Desreux JF (2002) New classes of MRI contrast agents. Top Curr Chem 221: 123-164.
11. Harisinghani MG, Barentsz J, Hahn PF, Deserno WM, Tabatabaei S, et al. (2003) Noninvasive detection of clinically occult lymph-node metastases in prostate cancer. New England Journal of Medicine 348: 2491-2499.
12. Hainfeld JF, Slatkin DN, Focella TM, Smilowitz HM (2006) Gold nanoparticles: a new X-ray contrast agent. Br J Radiol 79: 248-253.
13. Hainfeld JF, O'Connor MJ, Dilmanian FA, Slatkin DN, Adams DJ, et al. (2011) Micro-CT enables microlocalisation and quantification of Her2-targeted gold nanoparticles within tumour regions. Br J Radiol 84: 526-533.
14. Rothen-Rutishauser B, Kuhn DA, Ali Z, Gasser M, Amin F, et al. (2014) Quantification of gold nanoparticle cell uptake under controlled biological conditions and adequate resolution. Nanomedicine 9: 607-621.
15. Nazarenus M, Zhang Q, Soliman MG, del Pino P, Pelaz B, et al. (2014) In vitro

Interaction of Colloidal Nanoparticles with Mammalian Cells: What Have We Learned Thus Far? Beilstein Journal of Nanotechnology 5: 1477-1490.
16. Parak WJ, Boudreau R, Gros ML, Gerion D, Zanchet D, et al. (2002) Cell Motility and Metastatic Potential Studies Based on Quantum Dot Imaging of Phagokinetic Tracks. Advanced Materials 14: 882-885.
17. Khlebtsov N, Dykman L (2011) Biodistribution and toxicity of engineered gold nanoparticles: a review of in vitro and in vivo studies. CHEMICAL SOCIETY REVIEWS 40: 1647-1671.
18. Ricles LM, Nam SY, Sokolov K, Emelianov SY, Suggs LJ (2011) Function of mesenchymal stem cells following loading of gold nanotracers. Int J Nanomedicine 6: 407-416.
19. Jan E, Byrne SJ, Cuddihy M, Davies AM, Volkov Y, et al. (2008) High-content screening as a universal tool for fingerprinting of cytotoxicity of nanoparticles. ACS nano 2: 928-938.
20. Bhattacharya R, Patra CR, Verma R, Kumar S, Greipp PR, et al. (2007) Gold nanoparticles inhibit the proliferation of multiple myeloma cells. Advanced Materials 19: 711-716.
21. Soenen SJ, Manshian B, Montenegro JM, Amin F, Meermann B, et al. (2012) Cytotoxic Effects of Gold Nanoparticles: A Multiparametric Study. ACS Nano 6: 5767-5783.
22. Soliman MG, Pelaz B, Parak WJ, dP P (2015) Phase transfer and polymer coating methods toward improving the stability of metallic nanoparticles for biological applications. Chemistry of Materials 27: 990-997.
23. Fernández-Argüelles MT, Yakovlev A, Sperling RA, Luccardini C, Gaillard S, et al. Synthesis and Characterization of Polymer-Coated Quantum Dots with Integrated Acceptor Dyes as FRET-based Nanoprobes. Nano Letters 7: 2613-2617.
24. Lin C-AJ, Sperling RA, Li JK, Yang T-Y, Li P-Y, et al. (2008) Design of an Amphiphilic Polymer for Nanoparticle Coating and Functionalization. Small 4: 334-341.
25. Pellegrino T, Manna L, Kudera S, Liedl T, Koktysh D, et al. (2004) Hydrophobic Nanocrystals Coated with an Amphiphilic Polymer Shell: A General Route to Water Soluble Nanocrystals. Nano Letters 4: 703-707.
26. Zhang F, Lees E, Amin F, Rivera_Gil P, Yang F, et al. (2011) Polymer-Coated Nanoparticles: A Universal Tool for Biolabelling Experiments. Small 7: 3113-3127.
27. Hühn D, Kantner K, Geidel C, Brandholt S, De Cock I, et al. (2013) Polymer-Coated Nanoparticles Interacting with Proteins and Cells: Focusing on the Sign of the Net Charge. ACS Nano 7: 3253-3263.
28. Gustafsson Y, Haag J, Jungebluth P, Lundin V, Lim ML, et al. (2012) Viability and proliferation of rat MSCs on adhesion protein-modified PET and PU scaffolds. Biomaterials 33: 8094-8103.
29. Lowry OH, Rosebrough NJ, Farr AL, Randall RJ (1951) Protein measurement with the folin phenol reagent. Journal of Biological Chemistry 193: 265-275.
30. Weston SA, Parish CR (1990) New fluorescent dyes for lymphocyte migration studies: Analysis by flow cytometry and fluorescence microscopy. Journal of Immunological Methods 133: 87.
31. Schallmoser K, Bartmann C, Rohde E, Reinisch A, Kashofer K, et al. (2007) Human platelet lysate can replace fetal bovine serum for clinicalâ€ scale expansion of functional mesenchymal stromal cells. Transfusion 47: 1436-1446.
32. Carpenter A, Jones T, Lamprecht M, Clarke C, Kang I, et al. (2006) CellProfiler: image analysis software for identifying and quantifying cell phenotypes. Genome

Biology 7: R100.
33. Dominici M, Le Blanc K, Mueller I, Slaper-Cortenbach I, Marini FC, et al. (2006) Minimal criteria for defining multipotent mesenchymal stromal cells. The International Society for Cellular Therapy position statement. Cytotherapy 8: 315-317.
34. Eggenhofer E, Benseler V, Kroemer A, Popp FC, Geissler EK, et al. (2012) Mesenchymal stem cells are short-lived and do not migrate beyond the lungs after intravenous infusion. Frontiers in immunology 3.
35. Fischer UM, Harting MT, Jimenez F, Monzon-Posadas WO, Xue H, et al. (2009) Pulmonary passage is a major obstacle for intravenous stem cell delivery: the pulmonary first-pass effect. Stem cells and development 18: 683—692.
36. Nystedt J, Anderson H, Tikkanen J, PietilÃ¤ M, Hirvonen T, et al. (2013) Cell surface structures influence lung clearance rate of systemically infused mesenchymal stromal cells. Stem Cells 31: 317-326.

BEILSTEIN JOURNAL OF NANOTECHNOLOGY

# In vitro interaction of colloidal nanoparticles with mammalian cells: What have we learned thus far?

Moritz Nazarenus[1], Qian Zhang[1], Mahmoud G. Soliman[1], Pablo del Pino[2], Beatriz Pelaz[1], Susana Carregal-Romero[1], Joanna Rejman[1], Barbara Rothen-Rutishauser[3], Martin J. D. Clift[3], Reinhard Zellner[4], G. Ulrich Nienhaus[5,6], James B. Delehanty[7], Igor L. Medintz[7] and Wolfgang J. Parak[*1,2]

Review

Open Access

Address:
[1]Fachbereich Physik, Philipps-Universität Marburg, Renthof 7, 35037 Marburg, Germany, [2]CIC Biomagune, Paseo Miramón 182, 20009 San Sebastian, Spain, [3]BioNanomaterials, Adolphe Merkle Institute, University of Fribourg, Route de L'ancienne Papeterie CP 209, Marly 1, 1723, Fribourg, Switzerland, [4]Institute of Physical Chemistry, University of Duisburg-Essen, Universitätsstraße 5, 45141 Essen, Germany, [5]Institute of Applied Physics and Institute of Toxicology and Genetics, Karlsruhe Institute of Technology (KIT), Wolfgang-Gaede-Straße 1, 76131 Karlsruhe, Germany, [6]Department of Physics, University of Illinois at Urbana-Champaign, 1110 West Green Street, Urbana, IL 61801, USA and [7]Center for Bio/Molecular Science & Engineering, Code 6900, U.S. Naval Research Laboratory, 4555 Overlook Avenue Southwest, Washington D.C., 20375, USA

Email:
Wolfgang J. Parak[*] - wolfgang.parak@physik.uni-marburg.de

* Corresponding author

Keywords:
colloidal stability; intracellular particle distribution; nanoparticles; protein corona; toxicity of nanoparticles

*Beilstein J. Nanotechnol.* **2014,** *5,* 1477–1490.
doi:10.3762/bjnano.5.161

Received: 21 March 2014
Accepted: 12 August 2014
Published: 09 September 2014

This article is part of the Thematic Series "Biological responses to NPs".

Guest Editor: R. Zellner



## Abstract

The interfacing of colloidal nanoparticles with mammalian cells is now well into its second decade. In this review our goal is to highlight the more generally accepted concepts that we have gleaned from nearly twenty years of research. While details of these complex interactions strongly depend, amongst others, upon the specific properties of the nanoparticles used, the cell type, and their environmental conditions, a number of fundamental principles exist, which are outlined in this review.

## Introduction

There is a multitude of reports about the interaction of colloidal nanoparticles (NPs) with mammalian cells [1], as this topic is important for analyzing intended (e.g., medical applications [2-4]) and non-intended (e.g., contamination [5-7]) exposure of NPs to humans. However, there is a great number of available NPs made of many different materials [8-10] with a wide range

of different functionalities, cf. Figure 1. For a classification of NPs according to their composition, functionality, and fields of application we refer to a recent review [11]. To complicate the situation, most NPs do not consist of only one substance, but typically are hybrid materials, involving surface coatings and other modifications [12], cf. Figure 2 [13]. Even a homogeneous NP formed out of only one material will turn effectively into a hybrid NP, when it is brought into contact with any biological system (e.g., biological media) because of an organic coating that will form on the surface of the NPs [14]. This all illustrates that virtually no two types of NPs are the same and their inherent structure, properties, and constituent materials will contribute to the way in which they are taken up by cells. For example, a 20 nm diameter polymeric dendrimer may be very flexible, whereas a 20 nm metal NP may not, which leads to different interaction with cells. Furthermore, all of these different NPs can be exposed to different cells (e.g., macrophages, endothelia, and tumor cells) under different exposure scenarios (in vitro and in vivo), which as a consequence culminates in a large, but diverse body of work reported in the literature [15-17]. Due to this overwhelming amount of data, it is not easy to obtain a comprehensive overview. Many studies focus on the details of particular systems, but those can dramatically vary from case to case, and even conflicting trends are reported [17]. In addition, results will depend on the cellular test model used. In order to simplify the discussion, this review focuses on in vitro interaction of NPs with adherent, mammalian, immortalized cell lines. This avoids for example the problem of having to discuss how NPs reach and penetrate tissue, which makes in vivo scenarios more complicated than in vitro test systems. Despite these issues, it is still possible to discern some general trends, as described within this review. However, a limitation to having general trends equates to being permissive of some specific details, though common agreements reported here are clearly not trivial. It also automatically involves the possibility that studies exist, which under particular experimental conditions claim the opposite to the general statements. The most important of these trends will be discussed. In this regard, the current review will focus on physicochemically defined NPs, i.e., solutions of monodisperse NPs with a defined ligand shell attached, and without residual "left-over" impurities of the NP synthesis [13,18].

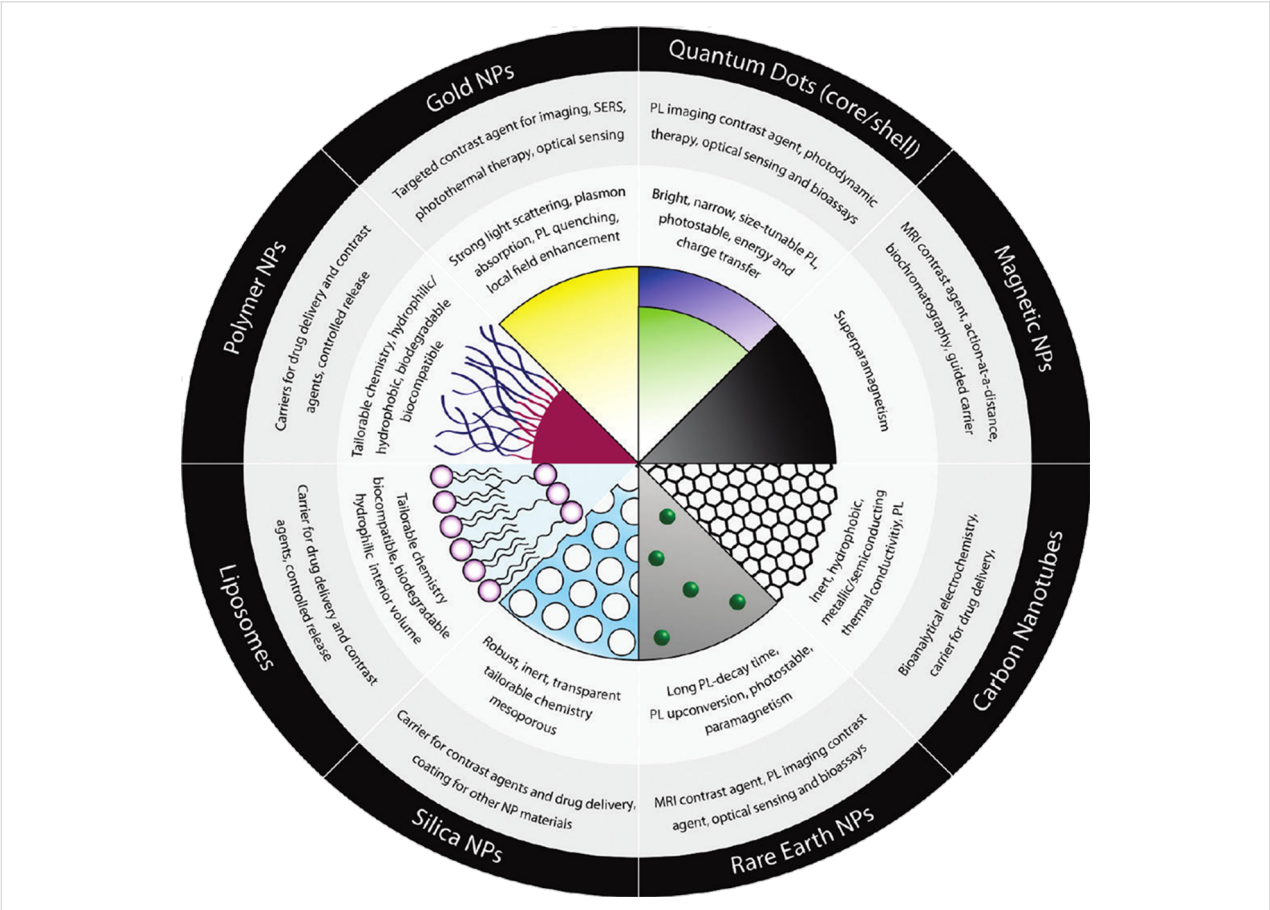


**Figure 1:** An overview of the "zoo" of different NPs concerning their composition, functionality, and fields of application. Reproduced with permission from [11]. Copyright (2011) American Chemical Society.

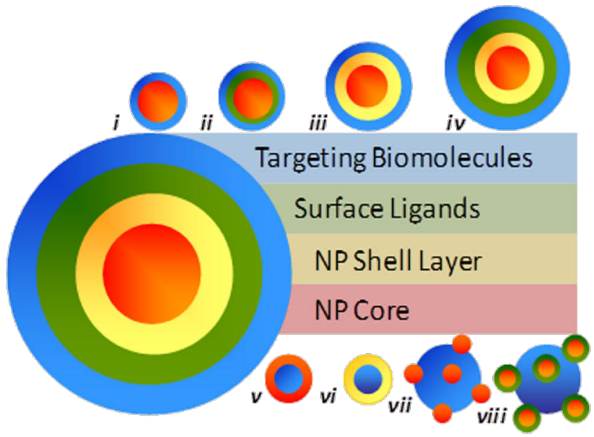


**Figure 2:** Hybrid nature of typical NPs, comprising different structural compartments. Reproduced with permission from [13]. Copyright (2013) American Chemical Society.

# Review

## How do particles enter cells and where do they go?

Virtually all cell lines internalize NPs, which are dispersed in the growth medium [19]. Uptake of different NPs by different cell lines, however, can vary significantly in biological kinetics [20-22] (this is also true for larger microparticles [23]). This is particularly important to keep in mind for specific (i.e., targeted) NP uptake, in which NPs modified by ligands (such as folic acid), which bind to appropriate receptors on the cell surface (such as folate receptors [24]), are specifically internalized [25]. Ligand-mediated uptake (which depends also on the ligand "valence", i.e., the number of ligands per NP, their density, and their orientation [26]) is faster and more efficient than non-specific (i.e., not receptor-mediated) uptake [27,28], although also plain or non-targeted NPs will be incorporated by cells. Thus, an important parameter to compare amongst studies, in which specific uptake is reported, is the time scale used within the experimental approach. While after short times of exposure huge differences in the amount of incorporated NPs can exist (e.g., between ligand-modified and plain NPs), those differences typically become less significant after longer exposure times [29], e.g., by the presence of the protein corona [30], as will be discussed later in more detail. Thus, statements which claim that only specifically modified NPs, but not non-modified NPs are taken up by cells, have to be regarded highly critically and put into the correct context of the reported time-scale. In fact, differences in uptake are not digital (i.e., "yes" or "no"), but rather are based on different kinetics. However, non-adhesive cell lines, i.e., cell suspensions, can be different and examples in which no significant internalization of NPs happened are reported [31]. Coming back to adhesive cell-lines, the first step in NP internalization obviously is the contact of the NP with the cell plasma membrane. This is a concentration-dependent process, which for high NP concentrations no longer scales linearly with concentration (i.e., saturation effects may occur). The first association of a non-targeted NP with a cell surface is usually electrostatic. Positively charged NPs are, for example, believed to interact with surface-displayed heparan sulfate proteoglycans [32,33]. As a rule of thumb, NPs which strongly interact with the cell plasma membrane, be it by ligand–receptor-mediated or by charge-mediated adhesion, are also internalized more efficiently [34]. Non-fouling polyethylene glycol (PEG)-modified NPs, for example, stick less to the cell plasma membrane and are, therefore, incorporated by cells less efficiently than other NPs [35-37] (this is also true in vivo as manifested by enhanced retention times [38]). It is clear that, while there are a number of portals through which NPs can gain entry into the cell, they all have as the common denominator the cell plasma membrane. Thus, the NP either must translocate (diffuse) directly across the cell plasma membrane entering the cytosol, or it must be internalized via any of the several routes of cellular endocytosis. While some evidence exists to support the direct membrane translocation of a select number of NP materials (typically partly hydrophobic and very small, as discussed later) the overwhelming evidence to date supports endocytosis as the common route of NP uptake. Thus, once NPs are associated to the outer cell plasma membrane they are typically internalized by endocytosis [39,40]. While a variety of different endocytotic pathways exist, which can be quite different in detail (to appreciate the complexity of endocytosis, we refer the reader to the review by Iversen et al. [41], cf. Figure 3), all of them have in common that the NPs are surrounded by membrane. Pinching-off of the membrane-surrounded NPs from the cell plasma membrane leaves the NPs incorporated into intracellular vesicles. These vesicles undergo a cascade of intracellular trafficking steps passing the NPs to more and more acidic vesicles [42,43], which also comprise enzymes specialized in digesting nutrition (and thus also parts of the NPs are digested in the lysosome [44,45]). In other words, after incorporation, the majority of NPs is not "free" in the cytosol, but inside intracellular vesicles (cf. Figure 4). Inside those intracellular vesicles the NPs are in an environment (acidic pH, enzymes) completely different from that in the cytosol (cf. Figure 5). Endocytosis and the endosomal escape dilemma have to be taken into account in particular concerning the delivery applications of NPs, in which the goal is to deliver something to the cytosol. Getting stuck inside intracellular vesicles is redundant to the purpose of these applications. However, in contrast to endocytosis as described so far, studies exist in which it is claimed that NPs can directly translocate through the cell membrane, thus indicating alternative pathways for NPs to penetrate the cell plasma membrane [46,47]. Besides other possible mechanisms, passive diffusion through (transient)

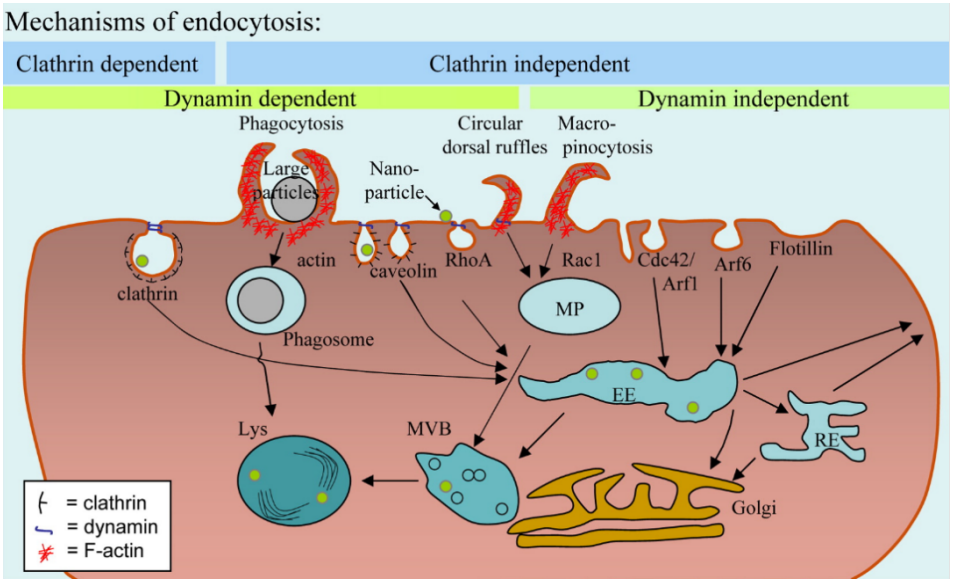


**Figure 3:** Scheme depicting the different mechanisms of cellular endocytosis. Reproduced with permission from [41]. Copyright (2011) Elsevier.

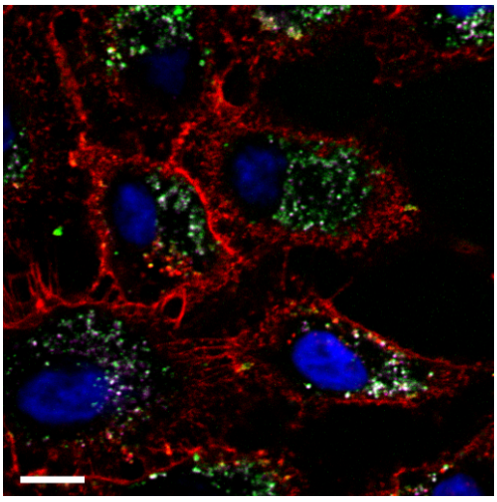

**Figure 4:** Fluorescence microscopy image showing the granular structure of internalized NPs inside A549 lung cancer cells (two types of iron oxide NPs with different surface chemistry, labelled with different fluorophores (green and magenta)) after 24 h of incubation at a concentration of 1 µg/mL, which are located in individual vesicles. Nuclei are stained with DAPI (blue) and the cell membrane with Wheat Germ Agglutinin (red). Note that due to limited lateral resolution of optical microscopy the spots most likely do not correspond to individual NPs, but to several NPs, which are entrapped inside intracellular vesicles. The scale bar represents 5 µm. Adopted with permission from [65] und Creative Commons Attribution 4.0 International Public License.

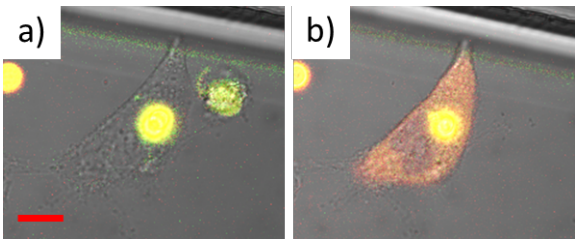


**Figure 5:** a) A microparticle has been internalized by an A549 lung cancer cell into an intracellular vesicle (here the lysosome [165]) and is thus clearly localized. The microparticle is filled with a pH-sensitive fluorophore (SNARF, from Invitrogen, now LifeTech) linked to dextran and the acidic pH of the lysosome is reported by the yellow fluorescence. b) After release of the pH-sensitive fluorophore linked to dextran to the cytosol (by photothermal heating), the fluorophore–dextran conjugates are freely dispersed, without any visible granular structure. Due to the neutral pH in the cytosol the fluorescence of the fluorophore–dextran conjugates has changed to red. The scale bar corresponds to 10 µm. Adopted with permission from [166]. Copyright (2012) Elsevier.

membrane pores and passive uptake by van der Waals or steric interactions (subsumed as adhesive interactions) have been suggested [48]. Still, it is always important to interpret such studies critically [49]. Most of the time studies involve an analysis of intracellular NP distributions, i.e., they rely on images showing NPs distributed in the cytosol. Additionally, these studies often rely on the observation that cellular NP entry still occurs below physiological temperatures (e.g., 4 °C), at which endocytosis and the active transport machinery are abrogated. However, without probing also for vesicular membranes around the NPs it is complicated to claim that the NPs in fact have passed the cell plasma membrane as "naked" NPs, without having ever been inside any intracellular vesicle. Clearly, there are a lot of indications (e.g., simulations) that NPs can enter cells through transient pore formation, in particular very small NPs [50,51]. Still, in many publications experiments do not

unequivocally demonstrate this pathway, though it surely exists. One possibility of experimental modification would involve, for example, pH-sensitive fluorophores (such as SNARF [52,53]) attached to the surface of the NPs, which can distinguish between the neutral cytosol and highly acidic intracellular vesicles [54]. In a similar direction the reductive capacity of glutathione (the cytosolic concentration of which is between 5 and 10 mM) may be used to displace a fluorescence resonance energy transfer (FRET) acceptor on the surface of the NP as confirmation of a successful NP localization to the cytosol [55]. Such experiments are in particular important for distinguishing between direct translocation to the cytosol versus endocytotic uptake followed by endosomal release. In fact, while there is clear experimental proof that NPs can be transported to the cytosol, the most straightforward pathway is uptake through endocytosis followed by release from the intracellular vesicles to the cytosol [56-58] (and not the diffusion through (transient) membrane pores). Endosomal release is, for example, a scenario which has been unraveled in detail for NPs coated with certain cell penetrating peptides (CPPs) [59-62]. Thus, while NPs can be free in the cytosol, this clearly does not automatically involve that they are membrane-permeable and not endocytosed. As pointed out above, observations based on merely measuring intracellular NP distributions are not sufficient for making profound statements about the uptake pathway. On the other hand it is safe to say that different intracellular locations for NPs exist. NPs have been reported in different intracellular organelles such as mitochondria, the nucleus, and free in the cytosol [63,64]. Most of the time such intracellular distributions are analyzed with transmission electron microscopy (TEM), in which also the structure of the intracellular organelles can be resolved (cf. Figure 6), or with fluorescence microscopy, in which the intracellular organelles have been co-stained with a fluorescent marker [65-67]. However, these data have to be interpreted carefully. In particular, such data should always include a quantitative distribution analysis, which is highly time-consuming. Even plain NPs without any particular surface capping can be found free in the cytosol [68], however, only to a very low extent. Thus, images in which NPs are shown in some particular intracellular organelles are only of limited value if the fraction of NPs that resides in these organelles is not quantified. Quantification, however, is not as trivial as it seems, and there is a need for better quantitative techniques for the future. While TEM offers the lateral resolution to visualize individual NPs, typically only a limited amount of cell sections (i.e., thin slices cut from cells) can be observed and thus for an absolute quantification, which is highly time-consuming, stereological tools need to be employed [68,69]. Also in case of TEM studies knowledge and understanding of cells under TEM conditions is essential. Fluorescence, on the other hand, can be recorded quantitatively by assuming that the emission intensity is proportional to the number of NPs. However, fluorescence can be partly quenched in certain organelles (for example at low pH), and it is impossible to resolve individual NPs due to the limited lateral resolution of optical microscopy [70]. In addition, as mentioned before, NPs can be partly degraded after having been internalized [71,72] and thus, in case fluorescently labeled NPs are used, it is required to prove that the fluorescence (or any other) label is still attached to the NPs inside the cells. Otherwise the recorded intracellular distribution of fluorescence may originate from detached labels and thus would not reflect the distribution of the NPs [73]. Summarizing available data suggests that, while translocation from intracellular compartments to the cytosol and from there to other cellular organelles is possible, translocation efficiencies still are moderate at best. In addition, NPs free in the cytosol may later end up again in intracellular vesicles through auto-phagocytosis [74]. Thus, for many applications, such as intracellular sensing or drug delivery, translocation of NPs to the cytosol after spontaneous endocytotic uptake remains a major challenge. External stimuli may be helpful in this direction [75]. In order to close this section it is also important to think about what happens after endocytotic uptake. It is, for instance, often overlooked that there is an eventual loss of the total NP load per cell as a result of mitotic division, NP exocytosis, and NP transcytosis [76]. This is largely due to the fact that in most experimental systems the primary issues addressed are uptake efficiency of the NPs and subsequent intracellular fate. These parameters are typically asked over the time course required for NP internalization and subcellular localization, and are not tracked over long time courses. It is generally accepted that NPs are partitioned during cell division,

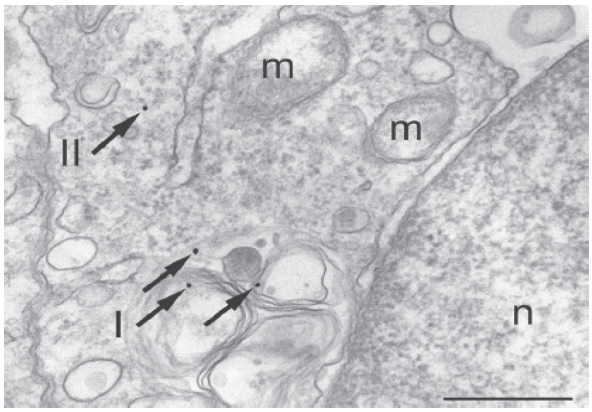


**Figure 6:** Intracellular compartments after internalization of PEG-coated gold NPs as visualized with TEM. The NPs (which are individually resolved due to the high lateral resolution of TEM) are located within a lysosome (arrows I) and in the cytosol (arrow II). *m* and *n* demark the nucleus and mitochondria, respectively. The scale bar corresponds to 500 nm. Adopted from with permission from [68]. Copyright 2010 Wiley-VCH Verlag GmbH & Co. KGaA, Weinheim.

in which they are passed to the daughter cells [76,77]. Such dilution effect of NP labels is in particular important for studies involving NPs as long-term tracers. Here, the relevant question arises whether upon cell division NPs are passed 50/50 to each daughter cell. Summers et al. have done both a theoretical [78] and experimental assessment [79] showing that, while partitioning of endosomes to daughter cells is symmetric, the number of NPs per endosome is a distribution and therefore NP partitioning to daughter cells is asymmetric. Thus, after several division cycles the NP distribution will not necessarily be representative for the fate of the original "mother" cells anymore. NPs also can be excreted to the extracellular medium, which represents an additional source of NP dilution effects. While endocytosis of NPs has been investigated heavily there are only a limited number of reports investigating exocytosis of NPs [80-82]. Excretion of NPs in exosomes (i.e., membrane surrounded vesicles), however, clearly affects the long-term cellular loading with NPs. In addition, for some particular cells, transcytosis has also been reported, i.e., that NPs are passed from one cell to another one [83].

## What are the critical parameters involved in in vitro nanoparticle internalization?

As mentioned before, virtually all NPs are spontaneously internalized by adherent cells, mainly cell lines, that are usually grown on a certain support and covered with cell culture medium under static conditions. In this case, NPs in the medium can directly access cells, and issues like tissue penetration, which need to be considered in in vivo experiments, can be neglected. The kinetics of internalization can depend strongly on the physicochemical properties of the NPs, the type of cells, and other parameters. Cellular uptake studies of NPs require as much characterization of the NP materials as currently possible. Concerning the NPs, this is, unfortunately, hampered by our incapability to synthesize "defined" NPs. For quantitative studies NPs and their bioconjugates should be as monodisperse as possible with regard to all relevant parameters, such as charge and size, well-defined and well-characterized. Moreover, in the case of bioconjugates, the biological molecule, be it protein or drug, should be attached to the NP with control over orientation [84,85], density, affinity, and number or ratio per NP [85]. Although these goals are extremely hard to achieve, the more they can be fulfilled, the less heterogeneity is present in the NP material and the easier the results (i.e., the correlation between the properties of the NPs and the observed interaction of NPs with cells) can be interpreted [13,18,86]. With limitations, a correlation of the spontaneous endocytotic uptake of NPs to the physicochemical properties of the NPs can be found. One, however, has to be aware that many physicochemical properties of NPs, such as size, shape, charge, and colloidal stability are highly entangled [14]. The physicochemical properties are not intrinsically associated with the NPs, but result from the interaction of the NPs with the surrounding particular medium [87]. The colloidal stability is presumably the most influential parameter. NPs with low colloidal stability will agglomerate and thus, originally "small" NPs will transform into agglomerates, resulting in large particles presented to the cells (cf. Figure 7). However, "colloidal stability" is not a defined physicochemical entity such as size, but needs to be put in context with the measurement protocol, such as the tendency to agglomerate. Any correlation to the size of the NPs without any previous demonstration of colloidal stability in the incubation medium has to be seen very critically. Loss of colloidal stability during incubation also complicates dosimetry. If NPs are quantified in numbers, is an agglomerate of NPs considered to be one particle or the number of NPs in the agglomerate [14]? Agglomeration can have direct consequences on cellular uptake [62]. If the cell cultures are turned upside-down, i.e., the cells are hanging in the culture medium, NP agglomerates that have precipitated at the bottom would not reach the cells and thus the effective NP concentration would be dramatically reduced [88]. In contrast, in conventional geometry, in which the culture medium is on top of the cells, a reduced colloidal stability leads to the precipitation of NP agglomerates onto the cells and, thus, to enhanced uptake, which can influence the cell viability negatively [89]. Such different exposure scenarios are highly relevant for the prediction of NP interactions, for instance, in the human body or in ecotoxicology. Some NPs have been mistaken to elicit limited to no adverse effects upon zebrafish assays, as they had precipitated to the bottom, and thus, the fish had not been directly exposed to them. After correct solubilization, however, the same NPs turned out to be highly detrimental to zebrafish health [90]. Colloidal stability does not only interfere with size but also with other parameters such as shape. An agglomerated bundle of sharp NPs may no longer be "sharp". Thus, colloidal stability is the paramount parameter to consider for all correlations between the NP–cell interactions and the physicochemical properties of the NPs.

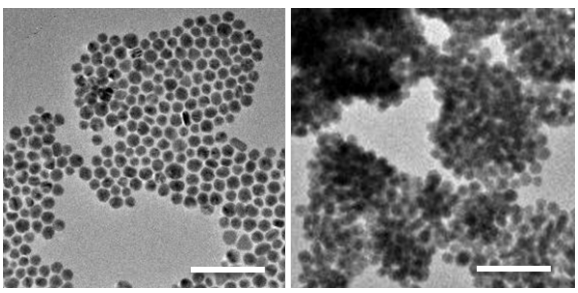

**Figure 7:** TEM images of a) dispersed and b) agglomerated Au NPs. The scale bars correspond to 100 nm. Adopted with permission from [30]. Copyright 2014 Royal Society of Chemistry.

Reports, in which no characterization of colloidal properties has been performed, therefore have to be regarded very critically. Unfortunately, many NPs are not colloidally stable in cell culture media [91]. The reason is that many NPs are stabilized by charge (in contrast to stabilization through steric repulsion). Salt (in particular NaCl, which always is present at high concentration) in the media screens the NP charge and thus can cause agglomeration [92]. Consequently, data which demonstrate that NPs are colloidally stable in water do not provide any proof that the same NPs also will be stable in cell culture media. Besides salt, proteins are another key compound of (serum-containing) cell media. As discussed later in more detail, proteins adsorb to the surface of NPs, forming the so-called protein corona [93,94], which in fact can increase or reduce colloidal stability [95,96]. Thus, characterization of colloidal stability and other physicochemical properties of NPs needs to be carried out under the same conditions under which later on cells are incubated with the NPs (i.e., in the respective cell culture media [86,97,98]). Obviously, NPs also should be appropriately purified [99], as otherwise effects from impurities rather than from the NPs themselves cannot be excluded. Unfortunately, for unstable NPs (e.g., for NPs to which the organic surface capping is only loosely attached) purification can trigger a loss of colloidal stability and thus agglomeration [14]. As lack of colloidal stability can overrule the other parameters, the following discussion about dependencies of other parameters is done assuming colloidally stable NPs. Uptake of NPs into the cells clearly depends on the size of the NPS. In general, smaller NPs are incorporated by cells faster than bigger ones, though there is some kind of size limit, i.e., the trend does not continue down to ultrasmall NPs [40,100]. As mentioned, upon endocytosis NPs are first wrapped by cellular membrane. Due to intrinsic stiffness and other parameters for membrane bending the radii of curvature cannot become infinitely small, and thus, there is an optimal NP size [101,102]. Excluding ultra-small NPs (smaller than 2–3 nm), smaller NP (smaller than 20–25 nm) are internalized readily in endosomes with most rapid kinetics [103]. Larger NPs (smaller than 60–70 nm) are internalized with lower kinetics to the extent that they are largely associated to the cell membrane over the time courses that see an intake of smaller NPS [62]. This has also been shown in fixed, permeabilized cells (to eliminate cell uptake machinery and pathways) to directly assess the size restrictions of plasma and intracellular membrane barriers on NP passage [104]. In contrast, ultrasmall NPs may be small enough to become membrane-permeable and thus bypass endocytotic uptake. Size-dependent uptake has also been reported for in vivo scenarios [105]. However, in particular for statements concerning size-dependent internalization, the experimental size determination of NP is important. Unfortunately, this is not a straightforward task, as different techniques measure different types of sizes. TEM only provides the geometric size of the NP core which has sufficient contrast, but organic surface cappings are typically not included [14]. In solution there is adsorption of counter ions to the NP surface [106,107] and organic surface coatings can swell, which results in hydrodynamic diameters larger than the core diameters as determined with TEM. There are several techniques for determining the hydrodynamic diameters of NPs [108], of which dynamic light scattering (DLS) might be the most common approach. All techniques have their limitations, and it is always helpful to know the measuring principle they are based on. DLS, for example, is based on calculating autocorrelation functions of the light-scattering signal of the solution. In order to obtain quantitative values, these autocorrelation data need to be fitted with a model, which is, for example, often done by assuming free diffusion of three NP species of different size. Thus, the results are based on the model (which is hidden as "black-box" in the software). To give an example, in case three species are assumed one always will obtain three peaks in the size distribution spectra, even though the sample may contain more different NP species. From the model, diffusion coefficients are yielded as fit parameters, which can be converted to hydrodynamic diameters by the Stokes–Einstein relation. As NPs of larger size also scatter light much more than smaller NPs, the results for DLS-derived size distributions also are quite different depending on whether number or intensity distributions are reported. Thus, simply taking the mean hydrodynamic diameter as displayed by commercial set-ups is prone to errors [109]. Calibration standards of NPs of known size are always a good help to benchmark size measurements and it is highly beneficial to apply several techniques in parallel [108-110]. By applying existing techniques correctly, the hydrodynamic diameters of NPs can be determined with remarkable accuracy, in particular if relative size changes are determined. Detection can be sensitive enough to resolve size-changes due to the attachment of individual macromolecules to the NPs [84,85,111,112]. Besides size, also shape has been proven to modulate the NP uptake of cells. In general, elongated, sharp NPs (i.e., NPs with a prolate spheroid shape) enter cells better than flatter NPs (i.e., NPs with an oblate spheroid shape). This however does no longer hold for very long fibers with high aspect ratios [100]. Flattening of NPs has been used, for example, to reduce NP uptake by cells in a way that flat NPs just adhere to the plasma cell membrane like a “backpack”, without being internalized, in contrast to spherical NPs that are readily incorporated [113,114]. Concerning a third parameter, charged NPs usually are internalized more efficiently than neutral ones, presumably due to enhanced charge-mediated adhesion to the outer cell membrane. Note that the charge pattern of the plasma cell membrane is patchy, and thus, while the overall net charge of cells is negative, there are plenty of positively charged domains. However, due to the overall

negative net charge, positively charged NPs are typically incorporated more efficiently by cells than negatively charged ones [65,97,115-119]. Indeed, the current consensus is that positive charges on NPs, such as those provided by the TAT peptide or surface functionalization, interact initially with the negatively charged heparan sulfate proteoglycan groups on the exterior of the cells. This allows them to then be present on the plasma cell membrane as endocytosis starts. Thus, while details may be very complex, clearly some tendencies for which physicochemical parameters enhance the spontaneous endocytosis of NPs can be given. In general, small, elongated, and positively charged NPs are incorporated preferentially to big, flat, and uncharged NPs. Dependency on other physicochemical parameters such as stiffness [120] has not been investigated extensively yet.

## The role of the protein corona

In serum-containing media or inside cells all different types of biologically relevant molecules adsorb to the surface of NPs. i) Ions such as $H^+$, $Na^+$, $K^+$ or $Ca^{2+}$ in the case of negatively charged NPs, or $Cl^-$ in the case of positively charged NPs adsorb to the NPs. As a consequence of counter ion adsorption the local ion concentration around the NPs surface is different from the bulk [54,87,106,107]. ii) Also nucleic acids, such as mRNA or siRNA, which are negatively charged due to their phosphate groups attach to positively charged NPs [121,122]. iii) Lipids present in membranes or second-messenger lipids wrap around NPs driven by hydrophilic/hydrophobic interaction and often result in formation of micelles [123,124]. iv) Thiols, present in glutathione or reduced proteins bind to the surface of noble metal NPs, in particular to Au NPs [125,126]. v) Proteins, in general, tend to adsorb to surfaces, which is also true on the nanometer scale. Adsorption of albumin is, for example, an integral part of opsonization [127,128]. The proteins adsorbed to the surface of NPs are typically termed protein corona [93,94]. The protein corona has a significant impact on how NPs interact with cells and thus will be discussed in the following in more detail. NPs can, in principle, be synthesized in water without any organic surface coating, for example by laser ablation [129-131]. However, also to NPs just stabilized by their surface charge (which can be directly on the inorganic surface) proteins will adsorb in serum-containing cell media and in this way can provide additional colloidal stability [129]. Therefore, there are no "naked" NPs in serum-containing cell culture media and inorganic NP cores are always surrounded by an organic coating [14]. Adsorbed proteins can significantly alter the surface properties of NPs and are of key importance in defining the biological identity of NPs [132,133]. The corona formed around NPs is what the cell will “see” primarily, though certainly also the original properties of the underlying NPs determine interactions with the cells [97]. In general, adsorbed proteins "smear out" differences in the surface chemistry between different NPs. Thus, typically two different types of NPs show more pronounced differences in their interaction with cells in case exposure is done in serum-free media (i.e., without proteins) rather than in serum-containing media [97]. The effect of ligands immobilized on the surface of NPs designated for ligand–receptor-mediated uptake is diminished by the protein corona, which partly overcoats the ligands [134]. However, due to the fact that specific targeting still is possible [84], enough ligands still are biologically active. For highly defined NPs, such as nearly monodisperse NPs overcoated with a shell of an amphiphilic polymer [135], the corona formed by special model proteins can be surprisingly well organized. By using fluorescence correlation spectroscopy (FCS), Röcker et al. investigated the adsorption of human serum albumin onto FePt NPs and found clear evidence that the proteins formed a monolayer on the surface of the NP [136]. Additional FCS studies by using other important serum proteins invariably confirmed the formation of monolayer. The thickness of the monolayer could be related to the molecular dimensions of the adsorbed protein determined by X-ray diffraction. All proteins studied were found to adsorb in a specific orientation determined by local charge distributions on the protein surface [20,137,138]. However, adsorption of proteins to the surface of NPs is not only driven by the basic physicochemical properties of the NP such as size, shape, surface charge, but also by other parameters such as the incubation temperature [139]. While model systems involving only one type of NPs and one type of protein help to analytically quantify protein adsorption, such as by determining binding constants [30,136], the biological reality is more complex. Serum-containing cell culture media comprise hundreds of different proteins. To make it worse to analyze, protein adsorption is also a dynamic process. Thus, proteins which are initially bound to the NP surface can later be replaced by others [140,141], which also is referred to as the Vroman effect [142]. It has been shown, for example, that surfactant lipids bound on multiwall carbon nanotubes are replaced with blood plasma proteins after a subsequent incubation [143]. Mass spectrometry is an invaluable tool for quantifying the amounts of different adsorbed protein species [140,141]. The dynamic exchange of proteins, induced by their different adsorption kinetics and affinities to the NP surface is reflected in the discrimination between "soft" and "hard" corona [144,145]. The initial, soft corona is formed by the most abundant proteins, which are then replaced by the high-affinity proteins to yield the hard corona. It has been suggested that differences for different protein species can be characterized by their dissociation constants [30]. In a simple model the dissociation constant tells which protein concentration is required to saturate half of the NP surface with proteins under equilibrium conditions [30]. With simple treatments such as the Hill Model

[146] one may characterize the protein corona around NPs with only a few parameters, which would be a great help in comparing results obtained with different systems, thus allowing for a more comprehensive understanding. While the protein corona around NPs has been heavily investigated these data ultimately are only relevant for the first interaction of NPs with cells. After spontaneous endocytosis NPs are inside intracellular vesicles. This imposes a completely different environment than that of the extracellular medium, in particular low pH, presence of endo-/lysosomal enzymes, and different reducing agents [147]. Thus, after NP uptake the protein corona around NPs may change significantly. The original proteins can be displaced by other intracellular proteins, and even more severe, part of the original protein corona may be digested enzymatically [44,45,148,149]. Changes of the protein corona in turn may also alter the physicochemical properties (such as colloidal stability) of the NPs [96]. In this manner, for a full understanding of NP interaction with cells along the pathway of NP uptake the physicochemical characterization of NPs should also be done intracellularly, which, however, is complicated. This opens up a window for future research efforts.

## Toxic effects of NPs

NPs clearly can trigger toxic effects in cells such as cytotoxicity, oxidative stress, (pro-)inflammation, and genotoxicity [150-152]. While again the detailed mechanisms are very complex and by far not understood in a comprehensive way, yet again there are certain characteristic features [153]. Toxic effects can result from the NPs themselves (e.g., by their catalytic surface or by their organic coating, such as in the case of cetyltrimethylammonium bromide (CTAB), a surfactant commonly used to synthesize gold nanorods) or by ions released from the NPs [154,155]. Ion release from certain materials such as Ag, ZnO, or CdSe is in particular triggered by the highly acidic pH in endo-/lysosomal compartments [156]. In both cases adverse biological effects are typically correlated with the production of reactive oxygen species (ROS) [157,158]. Also membrane damage plays a decisive role. In case of dissolvable NPs, the extent to which toxicity originates from the NPs themselves and to which extent from released ions is still subject to an intense scientific debate. Unfortunately, it is experimentally complicated to separate both effects. Even if before exposure all free ions were removed from the NP solution, inside cells new ions would be released. Thus, it is virtually impossible to have cells exposed exclusively to NPs without free ions [87]. One may argue that on the other hand cells could be exposed just to the free ions. While this is true, exposure to free ions will result in different intracellular ion distributions than the one obtained by ions which have been released from the NPs intracellularly, which again complicates direct comparison. Physicochemical properties can be, in some way, correlated with NP toxicity. In other words, reporting toxicity without accompanying in-depth NP characterization is not very useful concerning a detailed understanding of the mechanism. Surface coatings and impurities in the NPs can play an important role. Thus, also the coatings alone, as well as potential impurities need to be investigated towards potential toxic effect in control experiments. If only the physicochemical properties of "pure" NPs are considered, NPs with low colloidal stability have bigger effective sizes, thus are internalized to a larger extent, and thus typically have a greater adverse biological impact [154]. In order to account for concentration effects, it is advisable to correlate toxicity with particle internalization by using adequate methods. Enhanced uptake is one major reason (amongst others) why positively charged NPs (which are incorporated to a higher extent) elicit an increased adverse cellular effect compared to negatively charged ones [97,117,118]. This opens a dilemma. While in general, positive charge is better for enhanced uptake, too much positive charge becomes so toxic that it outweighs the added benefit of enhanced uptake. Thus, for delivery applications an optimum between both effects has to be found. This opens up another important point about the biological impact of NPs that merits discussion. There is a big difference between the use of NPs for cellular labeling or biosensing studies in research, as opposed to any therapeutic (in vivo) utility, and the two should never be thought of together or directly compared. It was, for example, recently shown that semiconductor quantum dot NPs (QDs) were unable to elicit a more negative biological effect when used for cellular labeling than a panel of dyes commonly used for the same intrinsic purposes [159]. Along with this, often transformed and immortalized cell lines are used in biological research, meaning that they are essentially cancerous. Thus, what appears to be adverse biological impact in these experiments has to be qualified with this context in mind. For cellular labeling, perhaps, there is the need for a particular experiment that should drive the issue of toxicity. If the use is specifically for in vitro labeling, tracking or sensing, there are multiple studies that have shown that over the time course required to perform such studies, the impact on cellular viability/proliferation at appropriate NP concentrations is minimal and is often comparable to or even less impactful than the use of traditional materials designed for the same purpose [159]. In this case "chronic toxicity" does not play a role, as the experiment is terminated before such an effect may occur. In contrast, for in vivo delivery one has to consider that NPs will remain in the organism over extended periods of time [160], and thus, benefits of treatment have to be weighted with long-term toxic effects [161]. Consequently, toxicity of NPs always has to be seen in the context of the applications the NPs are used for, but furthermore, the potential accidental exposure beyond the application has to be considered and its risk has to be assessed. In the

context of this review we have focused on in vitro studies. The advantage of such studies is the easy screening capability and the possibility to monitor in detail biomolecular pathways and changes in gene expression as a measure of a possible biologically adverse response. In case NP toxicity is investigated in a comprehensive study, however, involvement of in vivo experiments is crucial.

## Conclusion

Due to their interesting functional properties, numerous applications of NPs exist, e.g., plasmonic NPs [2,75], magnetic NPs [162,163] or fluorescent NPs [164]. For optimizing NP properties for biological applications, an understanding of their interaction with mammalian cells needs to be gained. However, the interaction of NPs with cells is complex due to the many different types of NPs, cells, and exposure scenarios being used within the field. Still, one may make an attempt to reduce details to very general statements, in order to highlight some essential elements, which was the motivation for this review.

Endocytosis is the common route of NP uptake. NPs which strongly interact with the cell plasma membrane are also internalized more efficiently. Hereby differences in uptake are not digital (i.e., "yes" or "no"), but rather are based on different concentration-dependent kinetics. After internalization NPs inside intracellular vesicles are in an environment (acidic pH, enzymes) completely different from that in the cytosol and the extracellular space, which can modify their properties. The translocation of the NPs from these vesicles to the cytosol is a current challenge, which is referred to as endosomal escape dilemma. Uptake studies best should involve a quantitative distribution analysis. While endocytotic uptake of NPs has been extensively investigated, the eventual loss of internalized NPs as a result of mitotic division, NP exocytosis, or NP transcytosis on the other hand has not been comprehensively studied yet. Cellular uptake studies of NPs require as much characterization of the NP material as currently possible. However, many physicochemical properties of NPs such as size, shape, charge, and colloidal stability are highly entangled, which complicates analysis. Analysis of physicochemical properties should be always performed in the incubation medium in which the uptake of NPs by cells is studied. The incubation medium can for example modify the colloidal stability of the NPs. Colloidal stability does not only interfere with size but also with other parameters such as shape. In general, small, elongated, and positively charged NPs are incorporated preferentially to big, flat, and uncharged NPs.

## Acknowledgements

This work and a large fraction of quoted work by WJP were supported by the German Research Foundation (DFG, SPP 1313, Project PA794/4-2) and this review represents the final report of this project. The authors are grateful to Dr. Torsten Hotopp from the DFG for managing and guiding the SPP 1313 funding initiative. BP acknowledges a fellowship from the Alexander von Humboldt Foundation. QZ acknowledges a fellowship from the Chinese Scholarship Council (CSC). MGS acknowledges a fellowship from the Youssef Jameel Foundation. JBD and ILM acknowledge the NRL NSI and DTRA for support. GUN acknowledges the DFG for support (DFG grants NI291/7 and NI291/8).

## References

1. Verderio, P.; Avvakumova, S.; Alessio, G.; Bellini, M.; Colombo, M.; Galbiati, E.; Mazzucchelli, S.; Avila, J. P.; Santini, B.; Prosperi, D. *Adv. Healthcare Mater.* **2014,** *3,* 957–976. doi:10.1002/adhm.201300602
2. Sperling, R. A.; Rivera Gil, P.; Zhang, F.; Zanella, M.; Parak, W. J. *Chem. Soc. Rev.* **2008,** *37,* 1896–1908. doi:10.1039/b712170a
3. Rivera Gil, P.; Parak, W. J. *ACS Nano* **2008,** *2,* 2200–2205. doi:10.1021/nn800716j
4. Peteiro-Cartelle, J.; Rodríguez-Pedreira, M.; Zhang, F.; Rivera Gil, P.; del Mercato, L. L.; Parak, W. J. *Nanomedicine* **2009,** *4,* 967–979. doi:10.2217/nnm.09.84
5. Bar-Ilan, O.; Chuang, C. C.; Schwahn, D. J.; Yang, S.; Joshi, S.; Pedersen, J. A.; Hamers, R. J.; Peterson, R. E.; Heideman, W. *Environ. Sci. Technol.* **2013,** *47,* 4726–4733. doi:10.1021/es304514r
6. Borm, P. J. A.; Robbins, D.; Haubold, S.; Kuhlbusch, T.; Fissan, H.; Donaldson, K.; Schins, R.; Stone, V.; Kreyling, W.; Lademann, J.; Krutmann, J.; Warheit, D.; Oberdorster, E. *Part. Fibre Toxicol.* **2006,** *3,* No. 11. doi:10.1186/1743-8977-3-11
7. Lewinski, N.; Colvin, V.; Drezek, R. *Small* **2008,** *4,* 26–49. doi:10.1002/smll.200700595
8. Parak, W. J. *Science* **2011,** *334,* 1359–1360. doi:10.1126/science.1215080
9. Lin, C.-A. J.; Yang, T.-Y.; Lee, C.-H.; Huang, S. H.; Sperling, R. A.; Zanella, M.; Li, J. K.; Shen, J.-L.; Wang, H.-H.; Yeh, H.-I.; Parak, W. J.; Chang, W. H. *ACS Nano* **2009,** *3,* 395–401. doi:10.1021/nn800632j
10. Pandey, A.; Roy, M. K.; Pandey, A.; Zanella, M.; Sperling, R. A.; Parak, W. J.; Samaddar, A. B.; Verma, H. C. *IEEE Trans. NanoBiosci.* **2009,** *8,* 43–50. doi:10.1109/TNB.2009.2017316
11. Algar, W. R.; Prasuhn, D. E.; Stewart, M. H.; Jennings, T. L.; Blanco-Canosa, J. B.; Dawson, P. E.; Medintz, I. L. *Bioconjugate Chem.* **2011,** *22,* 825–858. doi:10.1021/bc200065z
12. Sperling, R. A.; Parak, W. J. *Philos. Trans. R. Soc. London, Ser. A* **2010,** *368,* 1333–1383. doi:10.1098/rsta.2009.0273
13. Sapsford, K. E.; Algar, W. R.; Berti, L.; Gemmill, K. B.; Casey, B. J.; Oh, E.; Stewart, M. H.; Medintz, I. L. *Chem. Rev.* **2013,** *113,* 1904–2074. doi:10.1021/cr300143v
14. Rivera Gil, P.; Jimenez de Aberasturi, D.; Wulf, V.; Pelaz, B.; Del Pino, P.; Zhao, Y.; De La Fuente, J. M.; Ruiz De Larramendi, I.; Rojo, T.; Liang, X.-J.; Parak, W. J. *Acc. Chem. Res.* **2013,** *46,* 743–749. doi:10.1021/ar300039j
15. Auffan, M.; Rose, J.; Bottero, J.-Y.; Lowry, G. V.; Jolivet, J.-P.; Wiesner, M. R. *Nat. Nanotechnol.* **2009,** *4,* 634–641. doi:10.1038/nnano.2009.242
16. Sardar, R.; Funston, A. M.; Mulvaney, P.; Murray, R. W. *Langmuir* **2009,** *25,* 13840–13851. doi:10.1021/la9019475

17. Goesmann, H.; Feldmann, C. *Angew. Chem., Int. Ed.* **2010,** *49,* 1362–1395. doi:10.1002/anie.200903053
18. Medintz, I. *Nat. Mater.* **2006,** *5,* 842. doi:10.1038/nmat1776
19. Treuel, L.; Jiang, X.; Nienhaus, G. U. *J. R. Soc., Interface* **2012,** *10,* 20120939. doi:10.1098/rsif.2012.0939
20. Jiang, X.; Weise, S.; Hafner, M.; Röcker, C.; Zhang, F.; Parak, W. J.; Nienhaus, G. U. *J. R. Soc., Interface* **2010,** *7* (Suppl. 1), S5–S13. doi:10.1098/rsif.2009.0272.focus
21. Doiron, A. L.; Clark, B.; Rinker, K. D. *Biotechnol. Bioeng.* **2011,** *108,* 2988–2998. doi:10.1002/bit.23253
22. Li, Y.; Yue, T.; Yang, K.; Zhang, X. *Biomaterials* **2012,** *33,* 4965–4973. doi:10.1016/j.biomaterials.2012.03.044
23. Muñoz Javier, A.; Kreft, O.; Semmling, M.; Kempter, S.; Skirtach, A. G.; Bruns, O. T.; del Pino, P.; Bedard, M. F.; Rädler, J.; Käs, J.; Plank, C.; Sukhorukov, G. B.; Parak, W. J. *Adv. Mater.* **2008,** *20,* 4281–4287. doi:10.1002/adma.200703190
24. Antony, A. C. *Annu. Rev. Nutr.* **1996,** *16,* 501–521. doi:10.1146/annurev.nu.16.070196.002441
25. Ding, H.-m.; Ma, Y.-q. *Biomaterials* **2012,** *33,* 5798–5802. doi:10.1016/j.biomaterials.2012.04.055
26. Avvakumova, S.; Colombo, M.; Tortora, P.; Prosperi, D. *Trends Biotechnol.* **2014,** *32,* 11–20. doi:10.1016/j.tibtech.2013.09.006
27. Ahrens, E. T.; Feili-Hariri, M.; Xu, H.; Genove, G.; Morel, P. A. *Magn. Reson. Med.* **2003,** *49,* 1006–1013. doi:10.1002/mrm.10465
28. Tassa, C.; Duffner, J. L.; Lewis, T. A.; Weissleder, R.; Schreiber, S. L.; Koehler, A. N.; Shaw, S. Y. *Bioconjugate Chem.* **2010,** *21,* 14–19. doi:10.1021/bc900438a
29. Muñoz Javier, A.; Kreft, O.; Piera Alberola, A.; Kirchner, C.; Zebli, B.; Susha, A. S.; Horn, E.; Kempter, S.; Skirtach, A. G.; Rogach, A. L.; Rädler, J.; Sukhorukov, G. B.; Benoit, M.; Parak, W. J. *Small* **2006,** *2,* 394–400. doi:10.1002/smll.200500282
30. del Pino, P.; Pelaz, B.; Zhang, Q.; Maffre, P.; Nienhaus, G. U.; Parak, W. J. *Mater. Horiz.* **2014,** *1,* 301–313. doi:10.1039/C3MH00106G
31. Lin, J.; Yu, Y.; Li, B.; Huang, H.; Lin, S.; Li, C.; Su, Y.; Feng, S.; Chen, G.; Li, Y.; Huang, Z.; Zeng, H.; Chen, R. *Laser Phys. Lett.* **2012,** *9,* 240–246. doi:10.1002/lapl.201110125
32. Orr, G.; Panther, D. J.; Cassens, K. J.; Phillips, J. L.; Tarasevich, B. J.; Pounds, J. G. *Toxicol. Appl. Pharmacol.* **2009,** *236,* 210–220. doi:10.1016/j.taap.2009.01.022
33. Zhang, H.; Xia, T.; Meng, H.; Xue, M.; George, S.; Ji, Z.; Wang, X.; Liu, R.; Wang, M.; France, B.; Rallo, R.; Damoiseaux, R.; Cohen, Y.; Bradley, K. A.; Zink, J. I.; Nel, A. E. *ACS Nano* **2011,** *5,* 2756–2769. doi:10.1021/nn200328m
34. Verma, A.; Stellacci, F. *Small* **2010,** *6,* 12–21. doi:10.1002/smll.200901158
35. Xiao, Y.; Forry, S. P.; Gao, X.; Holbrook, R. D.; Telford, W. G.; Tona, A. *J. Nanobiotechnol.* **2010,** *8,* No. 13. doi:10.1186/1477-3155-8-13
36. Clift, M. J. D.; Rothen-Rutishauser, B.; Brown, D. M.; Duffin, R.; Donaldson, K.; Proudfoot, L.; Guy, K.; Stone, V. *Toxicol. Appl. Pharmacol.* **2008,** *232,* 418–427. doi:10.1016/j.taap.2008.06.009
37. Soenen, S. J.; Manshian, B. B.; Abdelmonem, A. M.; Montenegro, J.-M.; Tan, S.; Balcaen, L.; Vanhaecke, F.; Brisson, A. R.; Parak, W. J.; De Smedt, S. C.; Braeckmans, K. *Part. Part. Syst. Charact.* **2014,** *31,* 794–800. doi:10.1002/ppsc.201300357
38. Lipka, M.; Semmler-Behnke, M.; Sperling, R. A.; Wenk, A.; Takenaka, S.; Schleh, C.; Kissel, T.; Parak, W. J.; Kreyling, W. G. *Biomaterials* **2010,** *31,* 6574–6581. doi:10.1016/j.biomaterials.2010.05.009
39. Gratton, S. E. A.; Ropp, P. A.; Pohlhaus, P. D.; Luft, J. C.; Madden, V. J.; Napier, M. E.; DeSimone, J. M. *Proc. Natl. Acad. Sci. U. S. A.* **2008,** *105,* 11613–11618. doi:10.1073/pnas.0801763105
40. Chithrani, B. D.; Chan, W. C. W. *Nano Lett.* **2007,** *7,* 1542–1550. doi:10.1021/nl070363y
41. Iversen, T.-G.; Skotland, T.; Sandvig, K. *Nano Today* **2011,** *6,* 176–185. doi:10.1016/j.nantod.2011.02.003
42. Grant, B. D.; Donaldson, J. G. *Nat. Rev. Mol. Cell Biol.* **2009,** *10,* 597–608. doi:10.1038/nrm2755
43. Saftig, P.; Klumperman, J. *Nat. Rev. Mol. Cell Biol.* **2009,** *10,* 623–635. doi:10.1038/nrm2745
44. Rivera-Gil, P.; De Koker, S.; De Geest, B. G.; Parak, W. J. *Nano Lett.* **2009,** *9,* 4398–4402. doi:10.1021/nl902697j
45. Chanana, M.; Rivera Gil, P.; Correa-Duarte, M. A.; Liz-Marzán, L. M.; Parak, W. J. *Angew. Chem., Int. Ed.* **2013,** *52,* 4179–4183. doi:10.1002/anie.201208019
46. Geiser, M.; Rothen-Rutishauser, B.; Kapp, N.; Schürch, S.; Kreyling, W.; Schulz, H.; Semmler, M.; Im Hof, V.; Heyder, J.; Gehr, P. *Environ. Health Perspect.* **2005,** *113,* 1555–1560. doi:10.1289/ehp.8006
47. Rothen-Rutishauser, B. M.; Schürch, S.; Haenni, B.; Kapp, N.; Gehr, P. *Environ. Sci. Technol.* **2006,** *40,* 4353–4359. doi:10.1021/es0522635
48. Rothen-Rutishauser, B.; Blank, F.; Mühlfeld, C.; Gehr, P. *Nanoparticle-Cell Membrane Interactions,* 2nd ed.; Informa Healthcare: New York, USA, 2009; pp 226–242.
49. Luccardini, C.; Yakovlev, A.; Gaillard, S.; van't Hoff, M.; Alberola, A. P.; Mallet, J.-M.; Parak, W. J.; Feltz, A.; Oheim, M. *J. Biomed. Biotechnol.* **2007,** No. 68963. doi:10.1155/2007/68963
50. Lin, J.; Alexander-Katz, A. *ACS Nano* **2013,** *7,* 10799–10808. doi:10.1021/nn4040553
51. Wang, T.; Bai, J.; Jiang, X.; Nienhaus, G. U. *ACS Nano* **2012,** *6,* 1251–1259. doi:10.1021/nn203892h
52. Semmling, M.; Kreft, O.; Muñoz Javier, A.; Sukhorukov, G. B.; Käs, J.; Parak, W. J. *Small* **2008,** *4,* 1763–1768. doi:10.1002/smll.200800596
53. Rivera Gil, P.; Nazarenus, M.; Ashraf, S.; Parak, W. J. *Small* **2012,** *8,* 943–948. doi:10.1002/smll.201101780
54. Zhang, F.; Lees, E.; Amin, F.; Rivera Gil, P.; Yang, F.; Mulvaney, P.; Parak, W. J. *Small* **2011,** *7,* 3113–3127. doi:10.1002/smll.201100608
55. Mitra, R. N.; Doshi, M.; Zhang, X.; Tyus, J. C.; Bengtsson, N.; Fletcher, S.; Page, B. D. G.; Turkson, J.; Gesquiere, A. J.; Gunning, P. T.; Walter, G. A.; Santra, S. *Biomaterials* **2012,** *33,* 1500–1508. doi:10.1016/j.biomaterials.2011.10.068
56. Panyam, J.; Zhou, W.-Z.; Prabha, S.; Sahoo, S. K.; Labhasetwar, V. *FASEB J.* **2002,** *16,* 1217–1226. doi:10.1096/fj.02-0088com
57. Fan, Y.; Li, C.; Cao, H.; Li, F.; Chen, D. *Biomaterials* **2012,** *33,* 4220–4228. doi:10.1016/j.biomaterials.2012.02.038
58. Bayles, A. R.; Chahal, H. S.; Chahal, D. S.; Goldbeck, C. P.; Cohen, B. E.; Helms, B. A. *Nano Lett.* **2012,** *10,* 4086–4092. doi:10.1021/nl102172j

59. Boeneman, K.; Delehanty, J. B.; Blanco-Canosa, J. B.; Susumu, K.; Stewart, M. H.; Oh, E.; Huston, A. L.; Dawson, G.; Ingale, S.; Walters, R.; Domowicz, M.; Deschamps, J. R.; Algar, W. R.; DiMaggio, S.; Manono, J.; Spillmann, C. M.; Thompson, D.; Jennings, T. L.; Dawson, P. E.; Medintz, I. L. *ACS Nano* **2013,** *7,* 3778–3796. doi:10.1021/nn400702r
60. Delehanty, J. B.; Bradburne, C. E.; Boeneman, K.; Susumu, K.; Farrell, D.; Mei, B. C.; Blanco-Canosa, J. B.; Dawson, G.; Dawson, P. E.; Mattoussi, H.; Medintz, I. L. *Integr. Biol.* **2010,** *2,* 265–277. doi:10.1039/c0ib00002g
61. Medintz, I. L.; Pons, T.; Delehanty, J. B.; Susumu, K.; Brunel, F. M.; Dawson, P. E.; Mattoussi, H. *Bioconjugate Chem.* **2008,** *19,* 1785–1795. doi:10.1021/bc800089r
62. Oh, E.; Delehanty, J. B.; Sapsford, K. E.; Susumu, K.; Goswami, R.; Blanco-Canosa, J. B.; Dawson, P. E.; Granek, J.; Shoff, M.; Zhang, Q.; Goering, P. L.; Huston, A.; Medintz, I. L. *ACS Nano* **2011,** *5,* 6434–6448. doi:10.1021/nn201624c
63. Nativo, P.; Prior, I. A.; Brust, M. *ACS Nano* **2008,** *2,* 1639–1644. doi:10.1021/nn800330a
64. Yang, L.; Shang, L.; Nienhaus, G. U. *Nanoscale* **2013,** *5,* 1537–1543. doi:10.1039/c2nr33147k
65. Schweiger, C.; Hartmann, R.; Zhang, F.; Parak, W. J.; Kissel, T. H.; Rivera Gil, P. *J. Nanobiotechnol.* **2012,** *10,* No. 28. doi:10.1186/1477-3155-10-28
66. Delehanty, J. B.; Blanco-Canosa, J. B.; Bradburne, C. E.; Susumu, K.; Stewart, M. H.; Prasuhn, D. E.; Dawson, P. E.; Medintz, I. L. *Chem. Commun.* **2013,** *49,* 7878–7880. doi:10.1039/c3cc42781a
67. Lehmann, A. D.; Parak, W. J.; Zhang, F.; Ali, Z.; Röcker, C.; Nienhaus, G. U.; Gehr, P.; Rothen-Rutishauser, B. *Small* **2010,** *6,* 753–762. doi:10.1002/smll.200901770
68. Brandenberger, C.; Mühlfeld, C.; Ali, Z.; Lenz, A.-G.; Schmid, O.; Parak, W. J.; Gehr, P.; Rothen-Rutishauser, B. *Small* **2010,** *6,* 1669–1678. doi:10.1002/smll.201000528
69. Mühlfeld, C.; Mayhew, T. M.; Gehr, P.; Rothen-Rutishauser, B. *J. Aerosol Med.* **2007,** *20,* 395–407. doi:10.1089/jam.2007.0624
70. Rothen-Rutishauser, B.; Kuhn, D. A.; Ali, Z.; Gasser, M.; Amin, F.; Parak, W. J.; Vanhecke, D.; Fink, A.; Gehr, P.; Brandenberger, C. *Nanomedicine* **2014,** *9,* 607–621. doi:10.2217/nnm.13.24
71. Canton, I.; Battaglia, G. *Chem. Soc. Rev.* **2012,** *41,* 2718–2739. doi:10.1039/c2cs15309b
72. Studer, A. M.; Limbach, L. K.; Van Duc, L.; Krumeich, F.; Athanassiou, E. K.; Gerber, L. C.; Moch, H.; Stark, W. J. *Toxicol. Lett.* **2010,** *197,* 169–174. doi:10.1016/j.toxlet.2010.05.012
73. Ducongé, F.; Pons, T.; Pestourie, C.; Hérin, L.; Thézé, B.; Gombert, K.; Mahler, B.; Hinnen, F.; Kühnast, B.; Dollé, F.; Dubertret, B.; Tavitian, B. *Bioconjugate Chem.* **2008,** *19,* 1921–1926. doi:10.1021/bc800179j
74. Zhao, Y.; Howe, J. L. C.; Yu, Z.; Leong, D. T.; Chu, J. J. H.; Loo, J. S. C.; Ng, K. W. *Small* **2013,** *9,* 387–392. doi:10.1002/smll.201201363
75. Muñoz Javier, A.; del Pino, P.; Bedard, M. F.; Ho, D.; Skirtach, A. G.; Sukhorukov, G. B.; Plank, C.; Parak, W. J. *Langmuir* **2008,** *24,* 12517–12520. doi:10.1021/la802448z
76. Symens, N.; Soenen, S. J.; Rejman, J.; Braeckmans, K.; De Smedt, S. C.; Remaut, K. *Adv. Drug Delivery Rev.* **2012,** *64,* 78–94. doi:10.1016/j.addr.2011.11.012
77. Parak, W. J.; Boudreau, R.; Le Gros, M.; Gerion, D.; Zanchet, D.; Micheel, C. M.; Williams, S. C.; Alivisatos, A. P.; Larabell, C. A. *Adv. Mater.* **2002,** *14,* 882–885. doi:10.1002/1521-4095(20020618)14:12<882::AID-ADMA882>3.0.CO;2-Y
78. Summers, H. D.; Rees, P.; Holton, M. D.; Brown, M. R.; Chappell, S. C.; Smith, P. J.; Errington, R. J. *Nat. Nanotechnol.* **2011,** *6,* 170–174. doi:10.1038/nnano.2010.277
79. Summers, H. D.; Brown, M. R.; Holton, M. D.; Tonkin, J. A.; Hondow, N.; Brown, A. P.; Brydson, R.; Rees, P. *ACS Nano* **2013,** *7,* 6129–6137. doi:10.1021/nn4019619
80. Pi, Q. M.; Zhang, W. J.; Zhou, G. D.; Liu, W.; Cao, Y. *BMC Biotechnol.* **2010,** *10,* No. 36. doi:10.1186/1472-6750-10-36
81. Ruan, G.; Agrawal, A.; Marcus, A. I.; Nie, S. *J. Am. Chem. Soc.* **2007,** *129,* 14759–14766. doi:10.1021/ja074936k
82. Bartczak, D.; Nitti, S.; Millar, T. M.; Kanaras, A. G. *Nanoscale* **2012,** *4,* 4470–4472. doi:10.1039/c2nr31064c
83. Blank, F.; Wehrli, M.; Lehmann, A.; Baum, O.; Gehr, P.; von Garnier, C.; Rothen-Rutishauser, B. M. *Immunobiology* **2011,** *216,* 86–95. doi:10.1016/j.imbio.2010.02.006
84. Colombo, M.; Mazzucchelli, S.; Montenegro, J. M.; Galbiati, E.; Corsi, F.; Parak, W. J.; Prosperi, D. *Small* **2012,** *8,* 1492–1497. doi:10.1002/smll.201102284
85. Montenegro, J.-M.; Grazu, V.; Sukhanova, A.; Agarwal, S.; de la Fuente, J. M.; Nabiev, I.; Greiner, A.; Parak, W. J. *Adv. Drug Delivery Rev.* **2013,** *65,* 677–688. doi:10.1016/j.addr.2012.12.003
86. Sapsford, K. E.; Tyner, K. M.; Dair, B. J.; Deschamps, J. R.; Medintz, I. L. *Anal. Chem.* **2011,** *83,* 4453–4488. doi:10.1021/ac200853a
87. Carrillo-Carrión, C.; Nazarenus, M.; Sánchez Paradinas, S.; Carregal-Romero, S.; Almendral, M. J.; Fuentes, M.; Pelaz, B.; del Pino, P.; Hussain, I.; Clift, M. J. D.; Rothen-Rutishauser, B.; Liang, X.-J.; Parak, W. J. *Curr. Opin. Chem. Eng.* **2014,** *4,* 88–96. doi:10.1016/j.coche.2013.11.006
88. Cho, E. C.; Zhang, Q.; Xia, Y. *Nat. Nanotechnol.* **2011,** *6,* 385–391. doi:10.1038/nnano.2011.58
89. Kirchner, C.; Liedl, T.; Kudera, S.; Pellegrino, T.; Muñoz Javier, A.; Gaub, H. E.; Stölzle, S.; Fertig, N.; Parak, W. J. *Nano Lett.* **2005,** *5,* 331–338. doi:10.1021/nl047996m
90. Kim, K.-T.; Truong, L.; Wehmas, L.; Tanguay, R. L. *Nanotechnology* **2013,** *24,* 115101. doi:10.1088/0957-4484/24/11/115101
91. Izak-Nau, E.; Voetz, M.; Eiden, S.; Duschl, A.; Puntes, V. F. *Part. Fibre Toxicol.* **2013,** *10,* No. 56. doi:10.1186/1743-8977-10-56
92. Pellegrino, T.; Kudera, S.; Liedl, T.; MuñozJavier, A.; Manna, L.; Parak, W. J. *Small* **2005,** *1,* 48–63. doi:10.1002/smll.200400071
93. Cedervall, T.; Lynch, I.; Lindman, S.; Berggård, T.; Thulin, E.; Nilsson, H.; Dawson, K. A.; Linse, S. *Proc. Natl. Acad. Sci. U. S. A.* **2007,** *104,* 2050–2055. doi:10.1073/pnas.0608582104
94. Lynch, I.; Cedervall, T.; Lundqvist, M.; Cabaleiro-Lago, C.; Linse, S.; Dawson, K. A. *Adv. Colloid Interface Sci.* **2007,** *134–135,* 167–174. doi:10.1016/j.cis.2007.04.021
95. Orts-Gil, G.; Natte, K.; Thiermann, R.; Girod, M.; Rades, S.; Kalbe, H.; Thünemann, A. F.; Maskos, M.; Österle, W. *Colloids Surf., B* **2013,** *108,* 110–119. doi:10.1016/j.colsurfb.2013.02.027
96. Gebauer, J. S.; Malissek, M.; Simon, S.; Knauer, S. K.; Maskos, M.; Stauber, R. H.; Peukert, W.; Treuel, L. *Langmuir* **2012,** *28,* 9673–9679. doi:10.1021/la301104a

97. Hühn, D.; Kantner, K.; Geidel, C.; Brandholt, S.; De Cock, I.; Soenen, S. J. H.; Rivera Gil, P.; Montenegro, J.-M.; Braeckmans, K.; Müllen, K.; Nienhaus, G. U.; Klapper, M.; Parak, W. J. *ACS Nano* **2013,** *7,* 3253–3263. doi:10.1021/nn3059295
98. Maiorano, G.; Sabella, S.; Sorce, B.; Brunetti, V.; Malvindi, M. A.; Cingolani, R.; Pompa, P. P. *ACS Nano* **2010,** *4,* 7481–7491. doi:10.1021/nn101557e
99. Kinnear, C.; Dietsch, H.; Clift, M. J. D.; Endes, C.; Rothen-Rutishauser, B.; Petri-Fink, A. *Angew. Chem., Int. Ed.* **2013,** *52,* 1934–1938. doi:10.1002/anie.201208568
100. Chithrani, B. D.; Ghazan, A. A.; Chan, W. C. W. *Nano Lett.* **2006,** *6,* 662–668. doi:10.1021/nl052396o
101. Tzlil, S.; Deserno, M.; Gelbart, W. M.; Ben-Shaul, A. *Biophys. J.* **2004,** *86,* 2037–2048. doi:10.1016/S0006-3495(04)74265-4
102. Deserno, M.; Bickel, T. *Europhys. Lett.* **2003,** *62,* 767–773. doi:10.1209/epl/i2003-00438-4
103. Zhang, S.; Li, J.; Lykotrafitis, G.; Bao, G.; Suresh, S. *Adv. Mater.* **2009,** *21,* 419–424. doi:10.1002/adma.200801393
104. Williams, Y.; Sukhanova, A.; Nowostawska, M.; Davies, A. M.; Mitchell, S.; Oleinikov, V.; Gun'ko, Y.; Nabiev, I.; Kelleher, D.; Volkov, Y. *Small* **2009,** *5,* 2581–2588. doi:10.1002/smll.200900744
105. Kreyling, W. G.; Hirn, S.; Möller, W.; Schleh, C.; Wenk, A.; Celik, G.; Lipka, J.; Schäffler, M.; Haberl, N.; Johnston, B. D.; Sperling, R.; Schmid, G.; Simon, U.; Parak, W. J.; Semmler-Behnke, M. *ACS Nano* **2014,** *8,* 222–233. doi:10.1021/nn403256v
106. Zhang, F.; Ali, Z.; Amin, F.; Feltz, A.; Oheim, M.; Parak, W. J. *ChemPhysChem* **2010,** *11,* 730–735. doi:10.1002/cphc.200900849
107. Riedinger, A.; Zhang, F.; Dommershausen, F.; Röcker, C.; Brandholt, S.; Nienhaus, G. U.; Koert, U.; Parak, W. J. *Small* **2010,** *6,* 2590–2597. doi:10.1002/smll.201000868
108. Sperling, R. A.; Liedl, T.; Duhr, S.; Kudera, S.; Zanella, M.; Lin, C.-A. J.; Chang, W. H.; Braun, D.; Parak, W. J. *J. Phys. Chem. C* **2007,** *111,* 11552–11559. doi:10.1021/jp070999d
109. Hagendorfer, H.; Kaegi, R.; Parlinska, M.; Sinnet, B.; Ludwig, C.; Ulrich, A. *Anal. Chem.* **2012,** *84,* 2678–2685. doi:10.1021/ac202641d
110. Hole, P.; Sillence, K.; Hannell, C.; Maguire, C. M.; Roesslein, M.; Suarez, G.; Capracotta, S.; Magdolenova, Z.; Horev-Azaria, L.; Dybowska, A.; Cooke, L.; Haase, A.; Contal, S.; Manø, S.; Vennemann, A.; Sauvain, J.-J.; Staunton, K. C.; Anguissola, S.; Luch, A.; Dusinska, M.; Korenstein, R.; Gutleb, A. C.; Wiemann, M.; Prina-Mello, A.; Riediker, M.; Wick, P. *J. Nanopart. Res.* **2013,** *15,* No. 2101. doi:10.1007/s11051-013-2101-8
111. Pellegrino, T.; Sperling, R. A.; Alivisatos, A. P.; Parak, W. J. *J. Biomed. Biotechnol.* **2007,** 26796. doi:10.1155/2007/26796
112. Sperling, R. A.; Pellegrino, T.; Li, J. K.; Chang, W. H.; Parak, W. J. *Adv. Funct. Mater.* **2006,** *16,* 943–948. doi:10.1002/adfm.200500589
113. Swiston, A. J.; Gilbert, J. B.; Irvine, D. J.; Cohen, R. E.; Rubner, M. F. *Biomacromolecules* **2010,** *11,* 1826–1832. doi:10.1021/bm100305h
114. Stoehr, L. C.; Gonzalez, E.; Stampfl, A.; Casals, E.; Duschl, A.; Puntes, V.; Oostingh, G. J. *Part. Fibre Toxicol.* **2011,** *8,* No. 36. doi:10.1186/1743-8977-8-36
115. Jiang, X.; Dausend, J.; Hafner, M.; Musyanovych, A.; Röcker, C.; Landfester, K.; Mailänder, V.; Nienhaus, G. U. *Biomacromolecules* **2010,** *11,* 748–753. doi:10.1021/bm901348z
116. Jiang, X.; Musyanovych, A.; Röcker, C.; Landfester, K.; Mailänder, V.; Nienhaus, G. U. *Nanoscale* **2011,** *3,* 2028–2035. doi:10.1039/c0nr00944j
117. Yang, S.-H.; Heo, D.; Park, J.; Na, S.; Suh, J.-S.; Haam, S.; Park, S. W.; Huh, Y.-M.; Yang, J. *Nanotechnology* **2012,** *23,* 505702. doi:10.1088/0957-4484/23/50/505702
118. Kim, S. T.; Saha, K.; Kim, C.; Rotello, V. M. *Acc. Chem. Res.* **2013,** *46,* 681–691. doi:10.1021/ar3000647
119. Albanese, A.; Tang, P. S.; Chan, W. C. W. *The Effect of Nanoparticle Size, Shape, and Surface Chemistry on Biological Systems;* Annual Review Of Biomedical Engineering, Vol. 14; Annual Reviews: Palo Alto, USA, 2012; pp 1–16.
120. Bédard, M. F.; Munoz-Javier, A.; Mueller, R.; del Pino, P.; Fery, A.; Parak, W. J.; Skirtach, A. G.; Sukhorukov, G. B. *Soft Matter* **2009,** *5,* 148–155. doi:10.1039/b812553h
121. Xia, T.; Kovochich, M.; Liong, M.; Meng, H.; Kabehie, S.; George, S.; Zink, J. I.; Nel, A. E. *ACS Nano* **2009,** *3,* 3273–3286. doi:10.1021/nn900918w
122. Su, X.; Fricke, J.; Kavanagh, D. G.; Irvine, D. J. *Mol. Pharmaceutics* **2011,** *8,* 774–787. doi:10.1021/mp100390w
123. Yue, T.; Wang, X.; Huang, F.; Zhang, X. *Nanoscale* **2013,** *5,* 9888–9896. doi:10.1039/c3nr02683c
124. Irvine, D. J. *Nat. Mater.* **2011,** *10,* 342–343. doi:10.1038/nmat3014
125. Larsson, J. A.; Nolan, M.; Greer, J. C. *J. Phys. Chem. B* **2002,** *106,* 5931–5937. doi:10.1021/jp014483k
126. Demers, L. M.; Mirkin, C. A.; Mucic, R. C.; Reynolds, R. A., III; Letsinger, R. L.; Elghanian, R.; Viswanadham, G. *Anal. Chem.* **2000,** *72,* 5535–5541. doi:10.1021/ac0006627
127. Moghimi, S. M.; Hunter, A. C.; Andresen, T. L. *Annu. Rev. Pharmacol. Toxicol.* **2012,** *52,* 481–503. doi:10.1146/annurev-pharmtox-010611-134623
128. Karmali, P. P.; Simberg, D. *Expert Opin. Drug Delivery* **2011,** *8,* 343–357. doi:10.1517/17425247.2011.554818
129. Rehbock, C.; Merk, V.; Gamrad, L.; Streubel, R.; Barcikowski, S. *Phys. Chem. Chem. Phys.* **2013,** *15,* 3057–3067. doi:10.1039/c2cp42641b
130. Menéndez-Manjón, A.; Wagener, P.; Barcikowski, S. *J. Phys. Chem. C* **2011,** *115,* 5108–5114. doi:10.1021/jp109370q
131. Barcikowski, S.; Mafune, F. *J. Phys. Chem. C* **2011,** *115,* 4985. doi:10.1021/jp111036a
132. Fadeel, B.; Feliu, N.; Vogt, C.; Abdelmonem, A. M.; Parak, W. J. *Wiley Interdiscip. Rev.: Nanomed. Nanobiotechnol.* **2013,** *5,* 111–129. doi:10.1002/wnan.1206
133. Kittler, S.; Greulich, C.; Gebauer, J. S.; Diendorf, J.; Treuel, L.; Ruiz, L.; Gonzalez-Calbet, J. M.; Vallet-Regi, M.; Zellner, R.; Köller, M.; Epple, M. *J. Mater. Chem.* **2010,** *20,* 512–518. doi:10.1039/b914875b
134. Monopoli, M. P.; Åberg, C.; Salvati, A.; Dawson, K. A. *Nat. Nanotechnol.* **2012,** *7,* 779–786. doi:10.1038/nnano.2012.207
135. Yakovlev, A. V.; Zhang, F.; Zulqurnain, A.; Azhar-Zahoor, A.; Luccardini, C.; Gaillard, S.; Mallet, J.-M.; Tauc, P.; Brochon, J.-C.; Parak, W. J.; Feltz, A.; Oheim, M. *Langmuir* **2009,** *25,* 3232–3239. doi:10.1021/la8038347
136. Röcker, C.; Pötzl, M.; Zhang, F.; Parak, W. J.; Nienhaus, G. U. *Nat. Nanotechnol.* **2009,** *4,* 577–580. doi:10.1038/nnano.2009.195
137. Maffre, P.; Nienhaus, K.; Amin, F.; Parak, W. J.; Nienhaus, G. U. *Beilstein J. Nanotechnol.* **2011,** *2,* 374–383. doi:10.3762/bjnano.2.43
138. Treuel, L.; Brandholt, S.; Maffre, P.; Wiegele, S.; Shang, L.; Nienhaus, G. U. *ACS Nano* **2014,** *8,* 503–513. doi:10.1021/nn405019v
139. Mahmoudi, M.; Abdelmonem, A. M.; Behzadi, S.; Clement, J. H.; Dutz, S.; Ejtehadi, M. R.; Hartmann, R.; Kantner, K.; Linne, U.; Maffre, P.; Metzler, S.; Moghadam, M. K.; Pfeiffer, C.; Rezaei, M.; Ruiz-Lozano, P.; Serpooshan, V.; Shokrgozar, M. A.; Nienhaus, G. U.; Parak, W. J. *ACS Nano* **2013,** *7,* 6555–6562. doi:10.1021/nn305337c

140. Tenzer, S.; Docter, D.; Rosfa, S.; Wlodarski, A.; Kuharev, J.; Rekik, A.; Knauer, S. K.; Bantz, C.; Nawroth, T.; Bier, C.; Sirirattanapan, J.; Mann, W.; Treuel, L.; Zellner, R.; Maskos, M.; Schild, H.; Stauber, R. H. *ACS Nano* **2011,** *5,* 7155–7167. doi:10.1021/nn201950e
141. Tenzer, S.; Docter, D.; Kuharev, J.; Musyanovych, A.; Fetz, V.; Hecht, R.; Schlenk, F.; Fischer, D.; Kiouptsi, K.; Reinhardt, C.; Landfester, K.; Schild, H.; Maskos, M.; Knauer, S. K.; Stauber, R. H. *Nat. Nanotechnol.* **2013,** *8,* 772–781. doi:10.1038/nnano.2013.181
142. Vroman, L. *Nature* **1962,** *196,* 476–477. doi:10.1038/196476a0
143. Gasser, M.; Rothen-Rutishauser, B.; Krug, H. F.; Gehr, P.; Nelle, M.; Yan, B.; Wick, P. *J. Nanobiotechnol.* **2010,** *8,* No. 31. doi:10.1186/1477-3155-8-31
144. Milani, S.; Bombelli, F. B.; Pitek, A. S.; Dawson, K. A.; Rädler, J. *ACS Nano* **2012,** *6,* 2532–2541. doi:10.1021/nn204951s
145. Liu, W.; Rose, J.; Plantevin, S.; Auffan, M.; Bottero, J.-Y.; Vidaud, C. *Nanoscale* **2013,** *5,* 1658–1668. doi:10.1039/c2nr33611a
146. Hill, A. V. *J. Physiol.* **1910,** *40,* iv–vii.
147. Sasmal, P. K.; Carregal-Romero, S.; Han, A. A.; Streu, C. N.; Lin, Z.; Namikawa, K.; Elliott, S. L.; Köster, R. W.; Parak, W. J.; Meggers, E. *ChemBioChem* **2012,** *13,* 1116–1120. doi:10.1002/cbic.201100719
148. Wang, F.; Yu, L.; Monopoli, M. P.; Sandin, P.; Mahon, E.; Salvati, A.; Dawson, K. A. *Nanomedicine* **2013,** *9,* 1159–1168. doi:10.1016/j.nano.2013.04.010
149. Lunov, O.; Syrovets, T.; Röcker, C.; Tron, K.; Nienhaus, G. U.; Rasche, V.; Mailänder, V.; Landfester, K.; Simmet, T. *Biomaterials* **2010,** *31,* 9015–9022. doi:10.1016/j.biomaterials.2010.08.003
150. Oberdörster, G.; Oberdörster, E.; Oberdörster, J. *Environ. Health Perspect.* **2005,** *113,* 823–839. doi:10.1289/ehp.7339
151. Oberdörster, G.; Stone, V.; Donaldson, K. *Nanotoxicology* **2007,** *1,* 2–25. doi:10.1080/17435390701314761
152. Maynard, A. D.; Aitken, R. J.; Butz, T.; Colvin, V.; Donaldson, K.; Oberdörster, G.; Philbert, M. A.; Ryan, J.; Seaton, A.; Stone, V.; Tinkle, S. S.; Tran, L.; Walker, N. J.; Warheit, D. B. *Nature* **2006,** *444,* 267–269. doi:10.1038/444267a
153. Clift, M. J. D.; Gehr, P.; Rothen-Rutishauser, B. *Arch. Toxicol.* **2011,** *85,* 723–731. doi:10.1007/s00204-010-0560-6
154. Caballero-Díaz, E.; Pfeiffer, C.; Kastl, L.; Rivera-Gil, P.; Simonet, B.; Valcárcel, M.; Jiménez-Lamana, J.; Laborda, F.; Parak, W. J. *Part. Part. Syst. Charact.* **2013,** *30,* 1079–1085. doi:10.1002/ppsc.201300215
155. Karlsson, H. L.; Cronholm, P.; Gustafsson, J.; Möller, L. *Chem. Res. Toxicol.* **2008,** *21,* 1726–1732. doi:10.1021/tx800064j
156. Kittler, S.; Greulich, C.; Diendorf, J.; Köller, M.; Epple, M. *Chem. Mater.* **2010,** *22,* 4548–4554. doi:10.1021/cm100023p
157. Hussain, S. M.; Hess, K. L.; Gearhart, J. M.; Geiss, K. T.; Schlager, J. J. *Toxicol. in Vitro* **2005,** *19,* 975–983. doi:10.1016/j.tiv.2005.06.034
158. AshaRani, P. V.; Low Kah Mun, G.; Hande, M. P.; Valiyaveettil, S. *ACS Nano* **2009,** *3,* 279–290. doi:10.1021/nn800596w
159. Bradburne, C. E.; Delehanty, J. B.; Boeneman Gemmill, K.; Mei, B. C.; Mattoussi, H.; Susumu, K.; Blanco-Canosa, J. B.; Dawson, P. E.; Medintz, I. L. *Bioconjugate Chem.* **2013,** *24,* 1570–1583. doi:10.1021/bc4001917
160. Ballou, B.; Lagerholm, B. C.; Ernst, L. A.; Bruchez, M. P.; Waggoner, A. S. *Bioconjugate Chem.* **2004,** *15,* 79–86. doi:10.1021/bc034153y
161. Liu, J.; Erogbogbo, F.; Yong, K.-T.; Ye, L.; Liu, J.; Hu, R.; Chen, H.; Hu, Y.; Yang, Y.; Yang, J.; Roy, I.; Karker, N. A.; Swihart, M. T.; Prasad, P. N. *ACS Nano* **2013,** *7,* 7303–7310. doi:10.1021/nn4029234
162. Morales, M. P.; Bédard, M. F.; Roca, A. G.; de la Presa, P.; Hernando, A.; Zhang, F.; Zanella, M.; Zahoor, A. A.; Sukhorukov, G. B.; del Mercato, L. L.; Parak, W. J. *J. Mater. Chem.* **2009,** *19,* 6381–6386. doi:10.1039/b906455a
163. Colombo, M.; Carregal-Romero, S.; Casula, M. F.; Gutiérrez, L.; Morales, M. P.; Böhm, I. B.; Heverhagen, J. T.; Prosperi, D.; Parak, W. J. *Chem. Soc. Rev.* **2012,** *41,* 4306–4334. doi:10.1039/c2cs15337h
164. Niebling, T.; Zhang, F.; Ali, Z.; Parak, W. J.; Heimbrodt, W. *J. Appl. Phys.* **2009,** *106,* 104701. doi:10.1063/1.3253762
165. Kastl, L.; Sasse, D.; Wulf, V.; Hartmann, R.; Mircheski, J.; Ranke, C.; Carregal-Romero, S.; Martínez-López, J. A.; Fernández-Chacón, R.; Parak, W. J.; Elsasser, H.-P.; Rivera Gil, P. *ACS Nano* **2013,** *7,* 6605–6618. doi:10.1021/nn306032k
166. Carregal-Romero, S.; Ochs, M.; Rivera Gil, P.; Ganas, C.; Pavlov, A. M.; Sukhorukov, G. B.; Parak, W. J. *J. Controlled Release* **2012,** *159,* 120–127. doi:10.1016/j.jconrel.2011.12.013

## License and Terms

Top Curr Chem (2016) 370: 169–202
DOI: 10.1007/978-3-319-22942-3_6


# Gold-Based Nanomaterials for Applications in Nanomedicine

**Sumaira Ashraf, Beatriz Pelaz, Pablo del Pino, Mónica Carril, Alberto Escudero, Wolfgang J. Parak, Mahmoud G. Soliman, Qian Zhang, and Carolina Carrillo-Carrion**

**Abstract** In this review, an overview of the current state-of-the-art of gold-based nanomaterials (Au NPs) in medical applications is given. The unique properties of Au NPs, such as their tunable size, shape, and surface characteristics, optical properties, biocompatibility, low cytotoxicity, high stability, and multifunctionality potential, among others, make them highly attractive in many aspects of medicine. First, the preparation methods for various Au NPs including functionalization strategies for selective targeting are summarized. Second, recent progresses on their applications, ranging from the diagnostics to therapeutics are highlighted. Finally, the rapidly growing and promising field of gold-based theranostic nanoplatforms is discussed. Considering the great body of existing information and the high speed of its renewal, we chose in this review to generalize the data that have been accumulated during the past few years for the most promising directions in the use of Au NPs in current medical research.

S. Ashraf (✉), B. Pelaz, M.G. Soliman, Q. Zhang, and C. Carrillo-Carrion (✉)
Fachbereich Physik, Philipps Universität Marburg, 35037 Marburg, Germany
e-mail: ashraf@staff.uni-marburg.de; carolina.carrillocarrion@physik.uni-marburg.de

P. del Pino
CIC biomaGUNE, San Sebastian, Spain

M. Carril
CIC biomaGUNE, San Sebastian, Spain

Ikerbasque, Basque Foundation for Science, 48011 Bilbao, Spain

A. Escudero
Fachbereich Physik, Philipps Universität Marburg, 35037 Marburg, Germany

Instituto de Ciencia de Materiales de Sevilla, CSIC-University of Seville, 41092 Seville, Spain

W.J. Parak
Fachbereich Physik, Philipps Universität Marburg, 35037 Marburg, Germany

CIC biomaGUNE, San Sebastian, Spain

**Keywords** Diagnostics • Gold nanoparticles • Nanomedicine • Theranostics • Therapeutics

**Contents**



## 1 Introduction

In recent years, there has been an unprecedented expansion in the field of nanomedicine, which involves the development of novel nanoparticles (NPs) envisaged for the diagnosis and treatment of several diseases, especially cancer. NPs possess extraordinary capabilities to detect, image, and potentially treat diseases at the cellular and molecular levels [1–7]. Although micelle-based NPs (such as formulations loaded with doxorubicin, paclitaxel, or cisplatin) [8] are most advanced towards use in clinical practice, inorganic NPs also offer great potential. Among various inorganic NPs, Au NPs are important examples in the field of nanomedicine, thanks to their chemical, physical, and optical properties [9–13]. Their unique physical and chemical properties, such as inertia, biocompatibility, low cytotoxicity, stability against oxidation and degradation in vivo, and ease of conjugation to biomolecules, provide significant benefits in comparison with other NPs from a medico-biological point of view. The optical properties of Au NPs are determined by the so-called localized surface plasmon resonance band (LSPR) [14], which is associated with a collective excitation of conduction electrons. Depending on the size, shape, structure, and the NPs environment, the LSPR can be localized in a wide region from the visible to the infrared. Implementation of different surface chemistries enables them to have high stability, high carrier capacity, ability to incorporate both hydrophilic and hydrophobic substances, and compatibility with different administration routes. Because of the nano-size, Au NPs have good tumor retention capabilities as they can penetrate the leaky tumor vasculature. These properties make Au NPs interesting materials for sensing,

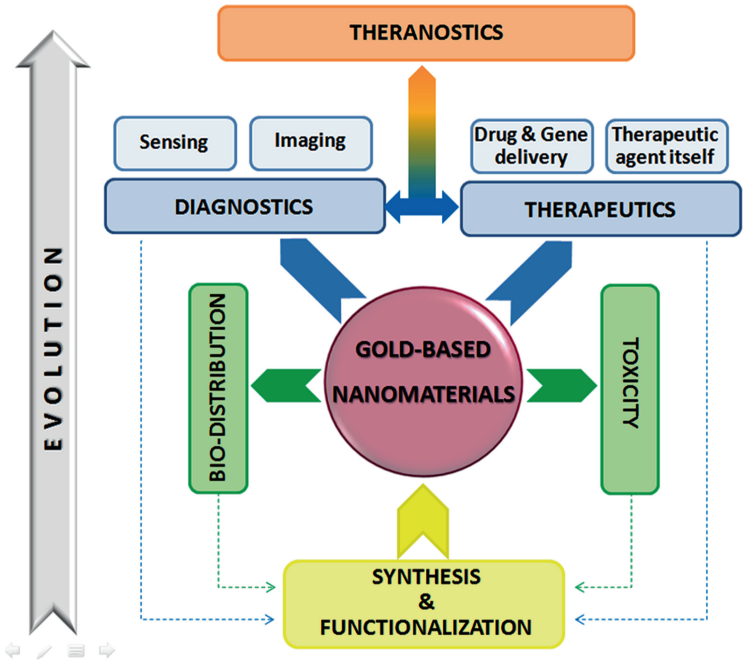


**Fig. 1** Scheme showing different areas of research of Au NPs, involved in the development of their applications in nanomedicine

detection, imaging, targeted delivery of drugs and genes, photo-induced therapies, enhanced radiotherapy, and so on. Furthermore, the multifunctionality potential of Au NPs provides an ideal platform for developing the theranostic modalities combining therapeutic, targeting, and imaging functions, demonstrating synergistic effects of multi-therapies. Figure 1 shows a simplified scheme of different areas of research where Au NPs are involved in the development towards nanomedicine. The evolution of research has progressed from the synthesis and functionalization towards applications. The evolution started with simple and unimodal applications towards more complex multimodal applications (e.g., multimodal imaging, dual-mode therapies, etc.). The latest development is focused on theranostics nanoplatforms, which can diagnose, deliver targeted therapy, and monitor response to therapy. Although the natural evolution is from the bottom to the top (as drawn in the scheme), in parallel (i.e., in transversal mode), studies of toxicity and bio-distribution are key aspects to guarantee the success of their applications. These studies and results of the application performances have a direct feedback in synthesis and functionalization for improvements. These inputs are the reason why new strategies of synthesis are an area of continuous active research.

The following sections describe some recent advances in the different areas of research using Au NPs, mainly focusing on their potential for medical applications and the hurdles to be overcome to translate them into clinical trials. Bio-distribution

and toxicity have been extensively reviewed and discussed in a number of recent publications [15–18], and thus we discuss it in the conclusions section. As the topic of this review involves huge amounts of information with a high speed of renewal, we focus on major ideas and some of the most recent and promising studies performed during the past few years.

## 2 Synthesis and Functionalization of Au NPs

### *2.1 Synthesis*

Before the advent of nanoscience, Au NPs were already attracting interest because of their optical properties. There are many historical examples in which Au NPs were applied even without knowing it (e.g., the Lycurgus Cup or stained-glass windows). In the last few decades, the control in the synthesis of Au NPs has evolved greatly. Nowadays it is possible to produce Au NPs with different sizes and shapes in a highly controlled manner. Many reviews and book chapters have already been published about the state- of- the- art of Au NPs synthesis [13, 19–22]. Thus, here we aim to provide an overview of some of the most recent achievements in the synthesis of Au NPs using wet- chemistry (though also other routes such as laser ablation exist [23]).

Most wet-chemistry-based Au NPs are synthesized in aqueous media, but there are some important examples to produce hydrophobically-capped Au NPs (e.g., the Brust–Schriffin method) [24]. These NPs are typically spherical with a size less than 10 nm. It is well known that most of the applications of Au NPs in nanomedicine are based on their optical properties, i.e., LSPR [25]. The desire for tuning of the LSPR has been a driving force to develop synthesis strategies allowing for Au NPs of different sizes and shapes. Although controlled synthesis of Au NPs has been known since the days of Michael Faraday, most synthetic strategies to produce water soluble spherical Au NPs are based on the Turkevich method [26]. This method has been continuously improved to produce better samples (e.g., with narrow size distribution and more homogeneous NPs). This optimized methodology also allows the growing of Au NPs of sizes up to 200 nm [27]. Yet arguably the most interesting Au NPs for bio-applications are anisotropic Au NPs that exhibit their LSPR in the biological window. This biological window comprises the spectral region of 700–1100 nm, in which the body tissue components absorb less light. This range is therefore the desired region to locate the LSPR of Au NPs intended to be used for bio-applications (e.g., photothermal therapy (PTT) [28, 29] or optoacoustic imaging (OAI) [30]). Recent controls over shape during the synthesis of Au NPs make it possible to tune the position of the LSPR by changing parameters such as the shape (rods, prisms, etc.) [28, 31] or the structure of the NPs (e.g., hollow vs homogeneous) [32]. To induce the growth of anisotropic NPs it is necessary to provoke either a kinetically controlled growth of the NPs or to induce the blocking of some growing facets [33]. The sphere is the most stable

shape in terms of energy. If the NPs synthesis is performed under thermodynamically controlled conditions, the NPs obtained are spherical. In general, to obtain non-spherical NPs the synthetic conditions have to be tuned to induce kinetically controlled NPs growth. This can be performed using surfactants that block some growing facets (e.g., cetyltrimethylammonium bromide (CTAB) or polymers) [34], using halides (e.g., $Br^-$, $I^-$) [35] or weak and mild reductants (e.g., $Na_2S_2O_3$) [28].

To date, Au nanorods remain the most broadly used anisotropic NPs. These rod-shaped NPs were described almost at the same time by the groups of El-Sayed [36, 37] and Murphy [28]. Since then, the synthesis of these NPs has been deeply explored. In general, the synthesis of Au nanorods is performed by using the growth seeding process. First, small spherical Au NPs are synthesized and then added to the growing solution rich in CTAB to induce rod-shaped growth. Because of the cytotoxicity of CTAB [38], Murray et al. have recently developed a modified Au nanorods synthesis method in which the required CTAB concentration is reduced by half (from 0.1 M from El-Sayed and Murphy to 0.05 M) [31, 39]. This synthesis is based on the use of aromatic additives.

Another important type of anisotropic NPs is the Au nanoshells developed by Halas et al. [40]. These structures are built using a silica core in which gold is grown. Their LSPR can be modulated by controlling the relationship between the core size and the thickness of the gold shell. By changing the shape of the core, other similar structures have also been described such as "nanorice" [41]. Halas et al. also described a synthesis for "nanomatryushkas," which are multilayered spheres. The simplest "nanomatryushka" contains a core of a gold sphere of ca. 40 nm coated with a $SiO_2$ shell and a second shell of Au [42]. Several bilayers of $SiO_2$ and Au can be deposited to obtain more complex "nanomatryushkas."

Au nanoprisms also have been described. The synthesis of triangular nanoprisms can often only be achieved with a low yield [43] and by using toxic surfactants (e.g., CTAB or CTAC (cetyltrimethylammonium chloride)) [44]. A synthesis route eliminating the use of toxic surfactants has recently been reported, which allows for tuning the LSPR position by controlling the amount of reductant. This synthesis is based on the reduction of a gold salt by thiosulfate (Fig. 2a) [28].

Au nanostars also exhibit their LSPR in the biological window. Many different synthetic procedures to produce Au nanostars have been reported. For generating Au nanostars, typically the seed-growing method is used. For instance, Liz-Marzán et al. published a method in which gold salt was reduced to metallic gold on top of the 15-nm Au NPs stabilized with poly(vinylpyrrolidone) (PVP) in the presence of dimethylformamide and PVP [45].

Finally, Au nanocages, originally developed by the group of Y. Xia, have been applied extensively with different purposes in nanomedicine [46, 47]. These cages are prepared by using a sacrificial silver nanocube, which then is oxidized to promote the reduction of gold through a galvanic replacement process. Similar approaches have been described using silver nanospheres [48] and silver nanoprisms [49].

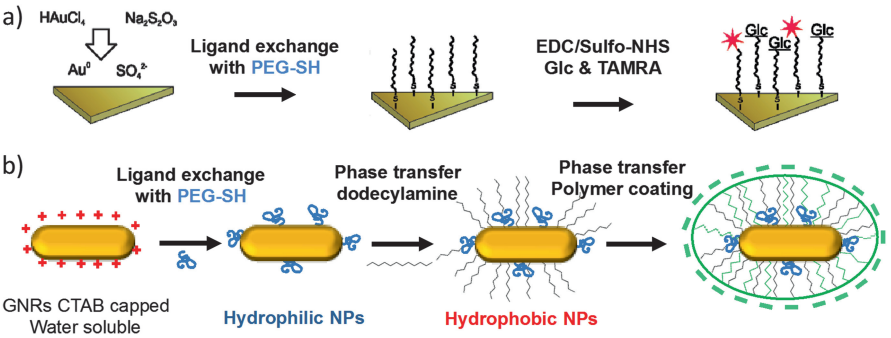


**Fig. 2** Schemes for the synthesis and functionalization of Au NPs. (**a**) Synthesis of Au nanoprisms, PEGylation, and linkage of glucose (Glc) and tetramethylrhodamine (TAMRA) using carbodiimide (EDC) chemistry [28]. (**b**) Strategy of phase transfer to coat Au nanorods (GNRs) with amphiphilic polymers [75]

Aiming to use green chemistry and less toxic reagents, the production of Au NPs using natural extracts from microorganisms (e.g., micro alga [50] or fungi [51]) or plants has been also explored [50, 52]. Nevertheless, the yield and quality of these Au NPs is still far below the quality of the previously described approaches.

Au-based hybrid materials have been developed too, trying to combine the great optical properties of gold with the properties of another material. Several examples of core-shell structures of Au containing iron oxide [53–55] or semiconductors cores [54] or Au cores coated with silver (bimetallic NPs [56]) can be found in the literature. More recently, Au has been combined with more novel materials such as nanodiamonds [57] or graphene [58, 59].

## 2.2 *Functionalization*

After synthesis and before their use in bio-applications, NPs must be provided with stable coatings which should warrant high colloidal stability. Thus, robust organic coatings ensure that the NPs' properties remain intact in biological media [60]. Indeed, the NPs surface determine their biological fate [61]. In addition, any kind of by-product related to the synthesis, including excess of reagents or cytotoxic surfactants, should ideally be washed off to remove potential toxic effects caused by these impurities. To achieve coatings qualifying for these requirements, the NPs' surfaces need to be engineered. One of the biggest advantages of the use of Au is its high reactivity with thiol groups [62]. This reactivity permits stabilizing the NPs with ligands containing a thiol reactive group. Ligand exchange by which original surfactants are replaced by new ones is the most common stabilizing procedure for Au NPs. Ligand exchange can be used to water transfer hydrophobically-capped NPs (e.g., NPs capped with alkanethiol chains) [63] and to replace toxic surfactants (e.g., CTAB) used to produce anisotropic NPs such as Au nanorods [64, 65].

Typically, polyethylene glycol (PEG) chains which provide the NPs with a colloidal high stability in biological media and long in vivo retention times [19, 66] are the most widely used stabilizers for Au NPs. Nowadays, there are many companies which offer an endless number of hetero-functional PEG chains. Using bi-functional PEG allows for future chemical modifications for the attachment of molecules (e.g., dyes, carbohydrates, antibodies, peptides, etc.) and/or to provide charge to the NPs (Fig. 2a) [28, 67, 68]. Not only PEG is used to stabilize Au NPs – other ligands, such as dihydrolipoic acid [69], proteins (e.g., bovine serum albumin) [70], or polymers are used regularly to enhance the NPs' stability in complexes media. Polymers used for this purpose include, for example, polyelectrolytes [71], PVP [72], or amphiphilic polymers [73].

The use of amphiphilic polymers to stabilize NPs and to promote their transfer from organic solvents to aqueous solutions is based on polymer coating of the NPs. This approach can be used for virtually any kind of NPs containing aliphatic chains on the surface (e.g., oleic acid, oleylamine, etc.) [73, 74]. The advantages of this technique are many: (1) coated NPs exhibit a high colloidal stability against media with high salt concentrations and/or proteins; (2) NPs coated with the same polymer have the same surface chemistry; (3) these polymers can be made with reactive groups in their hydrophilic domain (e.g., carboxylic acids), which then can be further modified with biologically relevant molecules. The main limitation of this technique is that it can be only used with NPs soluble in organic solvents. Yet most of the anisotropic Au NPs are synthesized in water. An extension of this method based on phase transfer of the water-soluble Au NPs to organic solvents has recently been reported. This method has been demonstrated for spherical Au NPs (with size up to 15 nm) and Au nanorods (Fig. 2b) [75].

Once Au NPs are sufficiently colloidally stable in biological media, as a function of their surface chemistry, different chemical modifications can be performed. Bioconjugate chemistry protocols developed for modifying proteins, peptides, and/or surfaces can be adapted to NPs [76, 77]. Concerning bio-conjugation, we refer to some recent reviews [11, 78–80]. In summary, currently the synthesis and functionalization of Au NPs has become very versatile. This allows scientists to develop the best customized systems for each application.

## 3 Use of Au NPs Towards Diagnostics

### *3.1 Detection and Sensing*

Different analytical assays involving Au NPs are widely used as sensors, ranging from the detection of ions and elements to more complex molecules, including those of biomedical interest, such as oligonucleotides, proteins, antibodies, and even bacteria and other microorganisms. The methods of designing sensing biomarkers that could be associated with the early stage diagnosis of different diseases

are nowadays attracting special interest. The current challenges consist of designing sensing devices that are able to recognize more specifically different types of analytes, discriminating molecules with similar characteristics, including the use of sensor arrays, which often combine several analytical approaches. Advances in enhancing the sensitivity and reducing the time of analysis are also currently required. The physical and analytical basis of sensing with Au NPs can be summarized in different main areas [81]. They include measurements based on colorimetry and plasmon resonance, fluorescence, electrochemistry, and more recently, surface enhanced Raman spectroscopy (SERS) [82].

Colorimetric assays are based on a visible change of color of functionalized Au NPs suspensions when interacting with the appropriate analyte [83–86]. Colorimetric analyses are normally fast and can often be evaluated with the naked eye. As explained before, Au NPs exhibit plasmonic properties. The position and intensity of this LSPR band depend not only on the metal type, NPs size, shape, structure, composition, and dielectric constant of the surrounding medium [87], but also on the aggregation of the NPs [88]. Colorimetric assays are based on this effect, because analytes that produce a change in the aggregation state of Au NPs give rise to a change in the LSPR absorption band of the NPs dispersion [89]. Such an effect is not only used to sense cations and anions [89–92], but has also been applied to sense molecules of biomedical interest. For example, DNA has been detected by Au NPs wrapped with long genomic single- and double-stranded DNA (ssDNA and dsDNA) molecules [93]. Proteins such as melamine and human carbonic anhydrase II have also been sensed by cyanuric acid derivative grafted Au NPs [94] and polypeptide-functionalized Au NPs [95], respectively. More complex molecules such as folate receptors (FRs), consisting of cysteine-rich cell-surface glycoproteins that can bind folate (FA), can be sensed by FA-modified ssDNA functionalized Au NPs. In the presence of FRs, ssDNA terminally tethered to FA is protected from degradation by exonucleases, and an aggregation of the Au NPs takes place through the formation of cross-linked NPs networks, resulting in a color change of the solution from red to blue [96]. Polyethyleneimine (PEI)-stabilized Au NPs have been used for highly selective and sensitive colorimetric sensing of heparin [97]. Abnormal concentration values of human chorionic gonadotropin (hCG) can be associated with ectopic pregnancy. The concentration of this biomarker can be determined using Au NPs in the presence of positively charged hCG-specific peptides. In this case, hCG inhibits the peptide-induced aggregation of the Au NPs, giving rise to a simple, rapid, and sensitive colorimetric assay [98]. A rapid and low-cost colorimetric analysis of bacteria in drinking water has been designed by using β-galactosidase conjugated Au NPs with a colorimetric substrate (chlorophenol red-β-D-galactopyranoside (CPRG)) deposited on a paper-based test strip [99]. The aggregations of antibody-conjugated oval-shaped Au NPs that selectively target specific sites on the surface of pathogens have been used to sense Salmonella [100]. Although colorimetric assays based on Au NPs involve the large shift of the LSPR band depending on NPs aggregation, a small LSPR peak shift can also be produced when an appropriate analyte binds to the surface-bound receptors of plasmonic NPs, because of a change in the refractive index [101]. In contrast to

agglomeration-based protocols, this shift in the LSPR frequency is not enough to be detected by the naked eye, but can be observed by absorption measurements. Au NPs deposited on several substrates have been used to detect analytes such as DNA [102], human IgG (Immunoglobulin G) [103], and insulin [104] in this way. Recent advances in the detection of microRNAs (miRNAs) by Au nanoprisms without the need for labels [105] and in the sensing of trace oligonucleotides biomarkers [106] have also been reported. Au NPs deposited on the metal sensing surface increase the sensitivity of planar surface plasmon resonance sensors, provided by the high dielectric constants of Au NPs and the electromagnetic coupling with the metal film [107]. This approach has been used for the sensing of different proteins [108] and oligonucleotides [108, 109].

Fluorescence assessments involving Au NPs are widely centered on fluorescence quenching-based methods. Au NPs show an important quenching effect on fluorophores close to their surface caused by their extraordinary high molar extinction coefficients and broad energy bandwidths [83, 110]. Specific interactions with the sensing molecules have been used to detect many different molecules of biomedical interest. Some assays are based on the appearance of fluorescence when the target molecules interact with the Au NP-based-sensors. For example, the quenching of a fluorophore attached to an Au NP through an oligonucleotide chain disappears in the presence of DNA [111], when the fluorophore gets detached from the NPs because of displacement by the DNA strand. Similar strategies have been used to sense proteins [112] and bacteria [113] using Au NPs conjugated with fluorescent polymers. Au NPs functionalized with enzymes have also been used to sense proteins, with an enhanced sensitivity through enzymatic catalysis [114].

Fluorescence quenching assays involving Au NPs are not only restricted to the detection of single analytes. More complicated sensing techniques, focused on the study of the interaction of different analytes, have also been reported. For example, dsDNA-conjugated Au NPs (dsDNA-Au NPs) and water-soluble conjugated polyelectrolytes are used as complementary sensing elements to construct hybrid sensors for detecting protein–DNA interactions [115]. The use of sets of sensors showing different patterns of responses in an array can provide fingerprints that allow for classification and identification of different target molecules [116]. Such an approach is used with DNA–Au NPs conjugates, in which a combination of colorimetric and fluorescence assessments enables better selectivity to distinguish different proteins [117]. Similar combination of colorimetric and fluorometric approaches has been reported for a sensor array consisting of two types of novel blue-emitting collagen-protected Au nanoclusters and macerozyme R-10-protected Au nanoclusters with lower synthetic demands, which has been recently used to sense eight different proteins [118].

The modulation of quenching of fluorescent semiconductor quantum dots (QDs) close to Au NPs in the presence of molecules which inhibit the interaction between QDs- and Au NPs-conjugated biomolecules has been used to sense molecules of biomedical interest such as avidin [119]. Normal, cancerous, and metastatic human breast cells have been distinguished by comparing the fluorescence of different

cationic Au NPs functionalized with poly(*p*-phenyleneethynylene) (PPE), which show different affinities for normal and tumor cells [120].

The conductivity, roughening of the conductive sensing interface, and the catalytic properties of Au NPs have been harnessed for the huge amount of analytical assays based on electrochemical measurements that involve Au and other metal-based NPs [121]. Different immunosensors based on Au NPs have recently been reported to detect cancer biomarkers [122, 123]. Au NPs deposited on electrode surfaces are known to enhance the electrochemical detection of different analytes because of their ability to decrease the overpotentials of many electroanalytical reactions, maintaining the reversibility of redox reactions [124, 125]. This approach has been used to detect several drugs such as isoniazid [126] and hCG [127]. Au nanorods have also been used as sensing interface in pencil graphite electrodes for the electrochemical sensing of deferiprone, an anti-HIV drug, resulting in an amplification of the electrochemical sensing signal [128].

Antibody-functionalized Au NPs, showing target specificity and affinity towards different biomarkers [129], have been used to sense Salmonella by differential pulse voltammetry (DPV) [130]. Cancer circulating cells have been sensed by combining the specific labeling through antibody-modified Au NPs and the sensitivity of the Au NPs-electro-catalyzed hydrogen evolution reaction (HER) detection technique [131]. The reaction of cell surface proteins with specific antibodies conjugated to Au NPs and the catalytic properties of the Au NPs on hydrogen formation from hydrogen ions can be used to quantify the NPs internalized by cancer cells [132, 133].

Raman scattering permits the detection and analysis of many molecules, by giving a unique spectroscopic signature which potentially identifies the species [134]. The Raman scattering signal can be substantially enhanced by the presence of plasmonic NPs, resulting in SERS [135, 136]. This effect is highly influenced by the size, shape, orientation, and aggregation of the NPs [108]. In fact, Au NPs with different morphologies have been used for SERS-based detection [137–139]. Label-free and Raman-dye labeled assays are two different existing SERS-based detection methods. Label-free assays follow vibrational information about the analytes themselves, whereas the dye-labeled methods detect analytes indirectly by monitoring the SERS signal of a Raman label attached to the metallic SERS substrate [140]. Different SERS assays for sensing DNA [141, 142] and proteins [143, 144] using Au NPs can be found in the literature. An extended bi-dimensional array of Au concave nanocubes supported on a polydimethylsiloxane (PDMS) film has recently been proposed for the SERS sensing of proteins that show low intensity Raman signals [145]. The assembly of spherical Au NPs on a highly anisotropic silica-coated substrate has recently been reported for the detection of prostate specific antigen by SERS [146] and the selectively quenching of the SERS signals from the dye molecules adsorbed onto star-shaped Au NPs not internalized by cells has been used to identify intracellular distributions of Au NPs [147].

## *3.2 Imaging*

For the treatment of many diseases and non-invasive evaluation/detection of intracellular and/or intra-subcellular compartments, molecular imaging based on functional nanomaterials is of paramount importance [148, 149]. For molecular imaging, different types of NPs are currently in use. Examples include polymer-based NPs [150–152], dendrimer-based NPs [153, 154], lipid-based NPs [155, 156], magnetic NPs [157–160], QDs [161–163], carbon nanotubes (CNTs) [164, 165], silica NPs [166–168], and Au NPs [169–172]. Among all the above-mentioned NPs, Au NPs possess extraordinary potential for imaging at the cellular and even molecular level. Various Au NPs are currently in use in molecular imaging, based on their different size, shape, and physical properties. Examples include spherical Au NPs [171, 172], nanorods [173–175], nanobipyramids [19], nanoshells [176], nanocages [177–179], core/shell NPs [171, 180], nanostars [181–183], and nanocubes [149], etc.

Au NPs have unique characteristics which enable their use as contrast agents in bio-medical imaging [184, 185]. In this field, they are being used as probes in dark field confocal imaging (DFCI), one- and two- photon fluorescence imaging (OTPFI), optoacoustic imaging (OI), computed tomography (CT), photothermal optical coherence tomography (POCT), positron emission tomography (PET), and imaging based on surface enhanced Raman scattering (SERS) [175, 184]. Different imaging modalities of the Au NPs can be combined, which can provide complementary information. In the following, a description of using Au NPs as contrast agents for the different imaging techniques is given.

DFCI provides contrast enhancement in unstained biological samples, but its main limitation is that it provides low light levels in images. Thus, for better visualization the biological samples should be strongly illuminated, which can, however, damage the samples. The imaging contrast of dark field microscopy can be enhanced by utilizing the high scattering properties of Au NPs [186]. For cellular detection, mostly the light scattering properties of Au NPs are utilized for straightforward image analysis. Light scattered from Au NPs is detected by using high resolution objective lenses of dark field confocal (DFC) microscopes in the form of bright spots, though the size of Au NPs is generally smaller than the diffraction limit of DFC. Using Au nanoshells it was recently possible to observe the binding and antibody mediated specific targeting of cancer cells in in vitro experiments using the dark field scattering properties of the NPs [187]. Similarly, for cancer cells localization, targeting, and real time tracking of Au nanorods-induced DNA damage in cancer cells was visualized using DFCI [188]. Scattering properties of Au NPs are also being utilized for better imaging of breast cancer cells [189]. However, despite the high scattering cross sections of Au NPs for enhancing the contrast in DFCI, their use is limited to in vitro experiments [184].

Photoluminescent properties of sub-nanometer Au nanoclusters made them attractive candidates in OTPFI based on their brightness, non-blinking behavior and stable emission [190, 191]. The luminescence of Au nanoclusters in the near

infrared (NIR) window is used for fluorescence imaging and they have greater photostability than QDs [191]. Not only nanoclusters but also other Au NPs, such as nanoshells and nanostars, can be used in one photon fluorescence imaging (OPFI), after conjugation of the Au NPs with NIR active fluorophores such as indocyanine green or Cy5 [192]. After conjugation with these fluorophores, these structures help in emission enhancement of these dyes for better fluorescence imaging. Presence of a metal surface close to fluorophores does not always quench fluorescence, but can also provide fluorescence enhancement, in particular for very close distances. In OPFI, Au NPs functionalized with fluorophores, offer a suitable platform for in vitro and in vivo cancer imaging and diagnostics [193, 194]. When Au NPs are excited with femtosecond pulsed lasers whose resonance frequency matches with the LSPR band of the Au NPs, two photon absorption occurs which results in two photon luminescence from the Au NPs [182, 193, 195]. For monitoring in vivo biological events, two photon luminescence imaging (TPLI) provides sufficient penetration depth and high three-dimensional (3D) spatial resolution. The signal intensity of TPL (two photon luminescence) can be enhanced three times in magnitude by utilizing the high luminescent properties of Au nanorods and nanocages without the photo-bleaching or blinking that is observed in many fluorophores used in this technique [196]. The contrast of Au nanostars conjugated with wheat germ agglutinin in TPL-based imaging can be utilized for imaging their uptake [182]. Similarly, other Au NP structures, such as nanorods, nanocages, and nanoshells, are also being used as contrast agents in TPL with a resolution at the single NP level inside blood vessels. In this way, in vivo tracking of Au NPs and fluorescence lifetime imaging for visualizing dynamical processes in cell media is possible [197, 198]. After one and two photon luminescence-based imaging, Au nanocages are now also being utilized in three photon luminescence imaging, based on their strong multi-photon absorption capabilities, leading to in vivo detection with diminished background signals and reduced photothermal toxicity [199]. Further studies are still required for using Au NPs in multi-photon luminescence for a better understanding of their role in this imaging technique.

The penetration depth of OI-based imaging, which is typically carried out with NIR pulsed sources, is similar to ultrasound-based imaging, i.e., several centimeters in biological tissues (typically less than 5 cm). This is better compared to simple optical imaging, in which depth resolution is only on the millimeter scale. The photothermal properties of Au NPs provide high contrast in OI [30]. Upon photo-excitation, the non-radiative decay of Au NPs converts light energy into heat, which causes a sharp rise of temperature in the local environment of the NPs, resulting in thermal and acoustic response enhancement in those tissues which contain the photoexcited NPs. The increased thermal response of Au NPs enhances the pressure waves propagating through the surrounding tissues and results in improving the temporal and spatial resolution of tomographic images [200].

In clinical detection of several diseases, CT has received increasing attention because of the high spatial and density resolution. For imaging biological systems using CT, contrast agents are usually required (which can enhance the density of the imaging area) for improving the accuracy in diagnosis. Iodine-based small

molecules such as "Omnipaque" are normally used in clinics, but are associated with certain drawbacks such as short imaging time, non-specificity, and renal toxicity. For overcoming these drawbacks nowadays, Au NP-based suitable contrast agents are being developed. In CT, because of the high atomic number of Au, Au NPs are providing higher spatial and density resolution compared to iodine-based contrast agents. In CT-based imaging, Au NPs attenuate X-rays much more efficiently compared to "Omnipaque," resulting in contrast enhancement by several orders of magnitude [201, 202]. Moreover, by suitable tuning the size and functionalization of the Au NPs, besides improving CT imaging it is also possible to achieve target specificity, long circulation time, and reduced renal toxicity [203].

Optical coherence tomography (OCT) can image cellular and sub-cellular structures 100 times better than CT and magnetic resonance imaging (MRI) and provides 10–25 times better spatial resolution compared to ultrasound-based images [204]. OCT is a non-invasive technique, resembling ultrasound-based imaging but, in this technique, instead of sound, reflections of NIR light are used for imaging. NIR active contrast agents, e.g., Au nanorods, can significantly improve OCT-based imaging because of their large differences in absorption-scattering profiles. Au nanoshells and nanocages, because of their strong scattering properties, can also provide enhanced optical contrast and brightness in OCT for improving the imaging of cancerous cells [205]. In this technique, tissues are illuminated with low coherent light and matching the coherence between incident and reflected beams of light helps in the detection of back-reflected light. This backscattered light thus helps in imaging. Because OCT is much more sensitive towards detection of scattering from the tissues than absorption, the scattered light helps in studying the morphology of tissues [205]. In OCT, Au NPs are being used as exogenous contrast agents based on their ability to produce distinctive backscattered light which is detectable in highly scattering tissues, thereby helping in studying the morphology of tissues [206]. Though OCT is a powerful 3D diagnostic tool in real time imaging, its resolution is low because of intense scattering from some optically dense tissues under investigation. To overcome this limitation nowadays, POCT (photothermal-OCT) imaging techniques using the photothermal properties of Au NPs are being developed [207]. In POCT, when light resonant with the plasmon energy of Au NPs strikes, Au NPs are excited and light is converted into heat and the surface temperature of the tissues is enhanced. The increase in surface temperature results in changes in the local refractive index of the medium which is then optically detected by POCT. Because of active detection of photothermal heating, POCT can identify and separate absorbing targets from scattering background, thereby helping in high resolution imaging compared to OCT [208].

In early stage diagnosis of cancer, PET – with its highly sensitive nuclear imaging modality – is extensively utilized in clinical studies using small doses of radioactive materials. However, these radioactive materials, especially small radioactive molecules, usually have short circulatory life- times in in vivo studies. After radiolabeling, Au NPs (e.g., nanocages, nanoshells, and spherical NPs) can remain inside the bloodstream for longer periods of time. Hence they facilitate long-term

bio-imaging [209]. In PET, radioisotopes undergo positron emission decay or positive beta decay and positrons are emitted. These emitted positrons traverse a short distance inside tissues, lose kinetic energy, and interact with electrons. This union with electrons results in their annihilation and production of gamma photons in the form of light which is used for making images [209]. Sometimes PET is coupled with Cerenkov luminescence (CL)-based imaging for better visualization and cross-checking the imaging results. CL-based imaging is a molecular imaging technique based on Cerenkov radiation, which can originate from the decay of alpha-, beta-, or positron-emitting radionuclides [179]. Recently, a radiolabeled precursor of a gold salt ($H^{198}AuCl_4$) was used for the synthesis of radioactive Au nanocages which gave CL. The CL originating from the decay of radionuclides helps in real-time CL-based imaging and monitoring of tumors over extended periods of time. CL of radionuclides can be increased by using high refractive index materials such as gold in conjugation with higher energy radionuclides. Thus CL imaging based on Au NPs can effectively bridge the gap between nuclear and optical imaging [179]. CL-based imaging can use radionuclides for diagnosis of diseases, which are routinely used for PET based imaging. CL based imaging improves PET-based imaging in terms of resolution. CL imaging signal can be modulated by using smart imaging agents such as NPs, and hence better insight in tumor biology can be obtained [210]. Over the last decade there have been numerous studies for enhancing the efficacy of SERS-based molecular imaging using Au NPs conjugated with Raman active moieties. Au NPs enhance the Raman scattering of vicinal molecules by means of chemical and electromagnetic enhancements. Au NPs enable identification of single molecules spectroscopically at room temperature by amplifying (ca. $10^{15}$-fold) the Raman scattering signals of adsorbed species. The LSPR of Au NPs enhances Raman signals in SERS-based imaging, which helps in better detection of tumor margins during the surgical removal of tumors [211]. The use of Au NPs provides photostability, improved contrast, and higher spectral specificity in SERS-based imaging [184].

Among all enlisted imaging techniques, no single modality can be considered as ideal and sufficient for getting all requisite information for a particular question. Nowadays, multimodal imaging probes based on Au NPs are being designed which possess integrated or complementary functions. For example, SERS-based imaging is highly sensitive and multiplexed imaging is possible with this technique, but it has poor penetration depth. On the other hand, OI has better penetration depth and high spatial resolution, but its sensitivity is limited. For multiplexed imaging, Au nanorod-based SERS/OI can be used for early stage detection of cancer. Similarly, Au NPs having triple modality are being used for MRI/SERS/OI-based imaging [212]. For disease (particularly cancer) intervention, Au NP-based multifunctional/multimodal imaging platforms have enough potential for the development of future contrast agents useful for nanomedicine. One can envision the potential applications of Au NPs for multiplexed detection and imaging of cancer and other such types of diseases by proper tailoring of their functionalization, size, shape, composition, and hybridization with other materials [184].

## 4 Use of Au NPs in Therapeutics

The properties of Au NPs can be exploited in therapy in two ways – as passive carriers for delivery, in which the therapeutic effect arise from active molecules bound to the carrier, or as active therapeutic agents, where the therapeutic effect directly originates from the Au NPs. The first use of Au NPs for therapeutic applications was as delivery vehicles for drugs and genes, because NPs in the size range 2–100 nm can interact with biological systems at the molecular level, and can allow for targeted delivery and passage through biological barriers. Later on, also investigations showing that Au NPs can be intrinsically therapeutic became available. This is because Au NPs can actively mediate molecular processes to regulate cell functions. In this section we summarize the potential of Au NPs in therapy, providing examples of currently investigated strategies.

### *4.1 Au NPs as Passive Carriers in Delivery Systems*

Au NPs are widespread in the field of delivery of different kinds of therapeutic molecules. They are very attractive as nanocarriers because of their colloidal stability, ease of preparation, and their on-demand tunable size and surface modification possibilities. In addition, they are essentially bio-inert, non-toxic and lack immunogenicity. All these features in combination with their ability to enter cells by endocytic pathways naturally make them good vehicles for a plethora of biomolecules and drugs to be delivered inside cells [13, 213]. Normally, the cargoes are loaded onto the Au NPs' surface either by non-covalent binding (via ionic or hydrophobic interactions) or by direct binding on the Au surface by thiolated linkers. Once inside the cells, the cargo may slowly detach from the surface of the Au NPs or its release may be triggered by internal stimuli such as pH [214] or cytosolic glutathione [215], which is able to reduce disulfide bonds, releasing molecules linked to the NPs surface via that kind of linkage. Furthermore, Au NPs are well known for their optical properties which are not only useful in the field of imaging and biosensing, but also serve to detach molecules selectively from the NPs surface when irradiated with light. Upon irradiation of plasmonic Au NPs at their LSPR frequency with a continuous wave laser, they absorb energy and reduce the attraction between the Au surface and non-covalently linked molecules, which eventually produces desorption of the cargo. In contrast, high energy pulse irradiation provokes the reshaping of the nanocarriers and the rupture of Au–S bonds, releasing more strongly linked cargoes. Interestingly, light irradiation of plasmonic nanomaterials allows for spatio-temporal controlled release of drugs and biomolecules because the delivery only takes place during irradiation of the NPs and stops when the laser is off [216–218]. The most commonly used Au NPs for delivery applications are nanospheres, and nanorods.

Au NPs have been used for decades for the purpose of gene delivery, traditionally developed for the transfection of plants using gene guns [219]. Nowadays, Au NPs are also used in gene therapy as non-viral carriers for delivering nucleic acids inside the cells [220]. Gene therapy may include the delivery of DNA inside cells to induce certain protein expression, or the introduction of miRNA able to interfere with the correct translation of messenger RNA inside the cells, avoiding protein production and silencing a particular gene responsible for a cellular malfunction. Gene therapy is increasingly important, particularly in the field of cancer treatment. However, delivery of naked nucleic acids is hampered by their fast degradability inside the body and their polyanionic nature that inhibits the cellular uptake. There are many reports in the literature that have demonstrated that adsorption of nucleic acids onto positively charged Au NPs drastically reduced their degradability and helps their internalization into cells. This could be achieved, for example, by coating Au NPs with positively charged lysine amino acids [221] or with positively charged polymers [222–225]. However, to ensure that the genetic material reaches the nucleus, more sophisticated constructions may be required. Such constructions may involve the use of PEI, a poly-cationic polymer able to escape endosomes because of the "proton sponge" effect causing membrane disruption [226], although it has been shown to be cytotoxic after a certain dose threshold. Hence, several authors have coated Au NPs with PEI to trap DNA or RNA, taking advantage of the endosomal escaping capacity of PEI, and substantially reducing its cytotoxicity [227–232]. Chen et al. have recently described a smart three-layered nanocarrier, based on the layer-by-layer (LBL) deposition of PEI/chitosan-aconitic anhydride (CS-Aco)/PEI/ shRNA (short/small hairpin RNA) onto Au NPs. CS-Aco was introduced as a pH-triggered charge-reversible compound which hydrolyzed into positively charged CS once inside the lysosomes, causing the disassembly of the nanocarrier layers. The as-released Au-PEI NPs facilitated lysosomal membrane disruption and hence the successful delivery of shRNA-PEI into the cytoplasm [214]. Although PEI is particularly attractive for nucleic acids delivery, similar results have been achieved by other poly-cationic polymers adsorbed onto Au NPs [220, 233]. For instance, Lee and co-workers fabricated siRNA-loaded Au NPs using the LBL approach with alternating positively charged poly-L-lysine (PLL) and negatively charged siRNA. They successfully coated the Au NPs with four layers of PLL and three layers of siRNA, which were slowly released inside the cells by protease degradation of PLL and displayed gene silencing capability [234]. As already pointed out, another way of delivering DNA or RNA avoiding normal cell internalization pathways is adsorption onto naked Au NPs or projectiles and direct bombardment inside the cells using gene guns. This strategy is frequently used in plants, but nowadays it has also been explored for mammalian tissues [235, 236].

Drug delivery is also an important field in which Au NPs are utilized. This field is of particular interest in the case of cancer treatment to avoid systemic toxicity during chemotherapy and to facilitate the delivery of hydrophobic drugs [237]. Indeed, the group of Rotello showed how to entrap two different hydrophobic drugs (tamoxifen and β-lapachone) in hydrophobic pockets created within alkanethiol monolayers surrounding Au NPs and their effective delivery

[238]. Some other strategies involve the chemical modifications of drugs to link them covalently onto NPs, which could, in some cases, compromise the drug performance. Gibson et al. covalently functionalized Au NPs with approximately 70 molecules of anticancer drug paclitaxel per NP, but they did not report about the delivery and biological activity of the drug [239]. Nonetheless, most studies are based on systems to deliver doxorubicin (DOX) [240, 241], which is known for its properties for treating cancer, but also for its toxicity and side effects. The group of Li has recently reported high loading of PEGylated hollow Au nanospheres with DOX (up to 63% in weight) and their delivery after NIR light irradiation [242]. Apart from drugs, Au NPs have also been used as carriers for vaccines by decorating their surfaces with appropriate ligands (selected antigens and T-helper peptides) which were able to elicit an immunogenic response [243].

Interestingly, Au NPs have been used not only as carriers but also as smart container openers. Plasmonic Au NPs were embedded in between polyelectrolyte layers in LBL constructed capsules carrying a therapeutic cargo within the capsule cavity. In a similar fashion, as explained before, irradiation of light onto those NPs led to the spatio-temporal controlled disassembly of the polymeric capsules producing the immediate cargo release [244–248].

Nowadays, all these delivery systems are evolving into more sophisticated constructions, which take advantage of the optical properties of Au NPs for combined drug therapy with photothermal ablation (PTA) and imaging [249] and in combination with other materials such as carbon [250, 251]. For instance, some recent reports along this dimension describe the wrapping of Au NPs or nanorods with hydrophilic graphene oxide nanosheets as carriers for gene therapy and improved PTA therapy [252–254].

## *4.2 Au NPs as Active Therapeutic Agents*

When Au NPs act as therapeutic agents per se, several therapies can be distinguished depending on the NPs properties exploited. In the following we illustrate the wide range of potential therapies using Au NPs with some selected recent examples.

One of the most promising groups of therapeutic strategies using Au NPs are light-based therapies. These utilize the application of light to irradiate photosensible materials, whereby this light-activation is directly responsible for the desired therapeutic effects (i.e., destroying tumor cells). This group of light-based therapies includes photothermal therapy (PTT), photodynamic therapy (PDT), and photoimmunotherapy (PIT) [255, 256]. Although PDT and PIT use a photosensitizer (i.e., light-activated drugs) for the release of reactive oxygen species (ROS) and the activation of immune responses, PTT is based on the use of photosensible materials (e.g., Au NPs) to generate local heat after being irradiated with electromagnetic radiation. The main difference between PIT and PDT is that in PIT monoclonal antibodies are associated with photosensitizers to improve the

selective binding to the target tissues [255]. PTT has lately received more interest because it does not require oxygen to interact with the target cells or tissues and is able to use longer wavelength light, which is less energetic and therefore less harmful to other cells and tissues. PTT using Au NPs, also called plasmonic photothermal therapy (PPTT), exploits the unique LSPR properties of Au NPs. When an energy source such as electromagnetic radiation is applied, conversion to heat energy efficiently occurs in Au NPs because of electron excitation and subsequent non-radiative relaxation through electron–phonon and phonon–phonon coupling. This generated thermal energy can induce temperature increases of more than 20 °C (i.e., hyperthermia), which can thereby induce tumor tissue ablation [255, 256].

There are several advantages of using Au NPs for PTT: (1) Au NPs have high absorption cross sections, and thus only minimal irradiation energy is required, (2) the conversion of light into heat is very fast (about 1 ps), (3) Au NPs are biocompatible, and (4) the ability of tuning the LSPR absorption (changing the size and shape of Au NPs) to absorb light in the visible up to the NIR region. Although visible light is successful in destroying cells labeled with spherical Au NPs, the NIR region is especially crucial to penetrate deep into tissues, with minimal attenuation by water and hemoglobin. The light can penetrate up to 10 cm in soft tissues in the "biological window" (650–900 nm), a region ideal for the LSPR absorption of Au nanoshells, nanorods, nanoprisms, and nanocages [28, 257]. When comparing the different NPs structures in terms of their applications in PTT, Au nanorods exhibit the best efficient NIR photothermal heat conversion. Although nanoshells have a larger absorption cross-section because of their larger size, and as a result they produce more heat, the nanorod shape has been shown to be twice as efficient in converting light radiation into thermal energy (photothermal efficiency) [258]. El-Sayed et al. determined the most effective Au nanorods size for PTT heat generation [259]. In this context, $28 \times 8$ nm Au nanorods were found to be the most effective, both in theoretical calculations and in in vitro experiments with human oral squamous cell carcinoma. Au nanorods in this dimension were the best compromise between the total light absorbed and the fraction that is converted into heat. Additionally, nanorods in this size led to an intense electromagnetic field that extends far enough from the NPs surface to allow for field coupling between NPs aggregates, resulting in enhanced experimental photothermal heating in solution. For example, Lin et al. [260] synthesized PEG-coated Au nanorods that showed enhanced PTT when used in the soft tissues of a genetically engineered mouse model (GEMM) of sarcoma. This model recapitulates the human disease more accurately in terms of structure and biology than subcutaneous xenograft models. This study represented a nice demonstration of a therapeutic, NPs-mediated thermal ablation protocol in a GEMM. Untargeted PEG-Au nanorods accumulated in the sarcomas at levels comparable to those in subcutaneous xenografts, providing evidence that passive targeting is indeed sufficient for PEG-Au nanorods to accumulate in a physiologic tumor microenvironment. Significant delays in tumor growth with no progression in some instances demonstrated the success of this method. A similar approach was used by Chen et al. [261], where PEG- Au

nanocages could be passively delivered and accumulated into animal tumors, causing irreversible damage to tumor cells after exposure to NIR laser. Interestingly, PEG-Au nanocages were found not only on the surface but also in the core of the tumor.

There are increasing efforts to enhance therapeutic treatments by combining therapy methods that show synergistic effects, as in the case of PTT and PDT. For example, Choi et al. have reported a method which combines both phototherapies using Au nanorods-photosensitizer complexes and two different light sources to excite the photosensitizers and photothermal NPs separately because of their absorption mismatch [262]. In this work, the negatively charged photosensitizer Al(III) phthalocyanine chloride tetrasulfonic acid (AlPcS4) was attached onto the positively charged surface of Au nanorods by electrostatic interaction, and the photodynamic effect of the AlPcS4 photosensitizer was temporarily suppressed after complex formation with Au nanorods. In the intracellular environment the photosensitizer was released and it could finally be optically activated for phototherapeutic effect. Two different light sources were used to excite Au nanorods (810 nm laser) and AlPcS4 photosensitizer (675 nm laser) separately. Tumor growth was suppressed by 95% with PTT/PDT dual therapy, whereas the suppression was only 79% with PDT alone.

These examples successfully demonstrate the potential of NIR-active Au NPs for use in light-based therapies. The current challenge in these phototherapies is to increase the level of selectivity to act on tumor tissues with minimum damage to the surrounding healthy tissue. Furthermore, better control over bio-distribution and clearance are critical issues to be addressed.

Au NPs are also used for enhanced X-ray radiotherapy. A challenge of X-ray radiation therapy in general is that high-dose X-rays under therapeutic conditions damage normal cells. Au NPs, upon X-ray irradiation, can act as dose enhancers and/or generate radicals that damage cancer cells and induce cell apoptosis. There are two main features of Au NPs which make them very good candidates for acting as X-ray radiosensitizers. First, Au has high number of protons ($Z = 79$) and neutrons, compared with the previous elements evaluated for dose enhancing such as iodine ($Z = 53$) and gadolinium ($Z = 64$). This translates into an increased photoelectric cross-section. Second, the size of Au NPs is critical for escaping the tumor vasculature using the enhanced permeability and retention (EPR) phenomena. Thus, Au NPs have been proposed as potential radiosensitizers for X-rays mediated cancer therapy, allowing for a reduction in X-ray dose with improved therapeutic results [263–266]. Yang et al. have recently demonstrated the potential effects of radiation-induced killing of melanoma cells as mediated by amphiphilic Au NPs embedded within the walls of lipid nanocapsules. Interestingly, the membrane-penetrating properties of these amphiphilic Au NPs allowed for significant enhancement of the radiotherapy efficiency, which opens a path for improving the efficacy of frontline radiotherapy treatments [264]. An additional way to improve the radiotherapeutic enhancement effects has been reported by using Au NPs with glucose (Glc) and PEG as ligands (PEG-Glc-Au NPs) [265]. The enormous reduction in tumor size after 47 days of treatment was also because of the role

of PEG and Glc in improving uptake and bio-distribution, which led to a concentration of PEG-Glc-Au NPs in tumor tissue 20 times higher than in healthy cells 48 h after injection. Alternatively, the potential of Au NPs to aggregate within tumors can be exploited in this direction [266]. In addition, 15 nm Au NPs have been designed to aggregate and remain largely in the tumor, after direct intratumoral infusion, thus changing from NIR-transparent to NIR-absorbent, enabling tumor-specific heating upon NIR illumination. Aggregation within tumors seems to be induced by the lower pH of the tumor milieu and endosomes/lysosomes or other mechanisms, such as by labile ligand bonds and lysosomal enzymes. This aggregation effect, and subsequent heating by NIR followed by X-ray treatment, was able to reduce the X-ray dose needed for tumor control by a factor $>3$. Because of the limited penetration of NIR, certain superficial or accessible tumors (e.g., a subset of head, neck, and melanoma) would be immediate candidates to evaluate the potential of this strategy. These examples illustrate the huge potential of Au NPs to enhance radiotherapy treatments, providing useful insights for further clinical studies.

It is important to note that the mechanism by which Au NPs can lead to dose enhancements in radiation therapy differs when comparing photon and proton radiations for NPs excitation. The dose enhancement using protons can be up to 14% and is independent of proton energy, in contrast to photon excitation where the dose enhancement is highly dependent on the photon energy used. A theoretical Monte Carlo simulation study [267] concluded that the potential of Au NPs to enhance radiation therapy depends on the type of radiation source, and proton therapy can be enhanced significantly only if the Au NPs are in close proximity to target tissues.

Radioactive Au NPs are being used to make radiation therapy more effective. The radioactive properties of $^{198}$Au ($\beta_{max} = 0.96$ MeV; half-life 2.7 days) make it an ideal candidate for use in radiotherapeutic applications [268]. A major challenge in cancer therapy has been delivery and retention, as it is necessary to increase the therapeutic payload to get an effective tumor treatment. In this regard, NPs containing radioactive isotopes can concentrate within the tumor and provide an opportunity to tune the radioactive therapeutic dose delivered to tumor cells. Furthermore, $^{198}$Au NPs have extraordinary tumor retention capabilities because of their natural affinity to leaky tumor vasculature. In this area, relevant advances have been achieved [268–270]. Khan et al. developed a method for the encapsulation of radioactive Au within a dendrimeric composite and demonstrated that radioactive Au NPs could deliver therapeutic doses to tumors [269]. More recently, gum arabic glycoprotein (GA)-functionalized Au NPs, consisting of beta-emitting $^{198}$Au, were used for reducing the sizes of inoperable prostate tumors [268, 270]. Interestingly, the optimum hydrophobicity of the GA matrix allowed for effective penetration across tumor membranes. The therapeutic efficacy of GA-$^{198}$Au NPs was demonstrated in prostate tumor-bearing severely compromised immunodeficient (SCID) mice models, reaching an unprecedented 82%, 3 weeks after single-dose intratumoral administration of GA-$^{198}$Au NPs (408 μCi). The findings of significant therapeutic efficacy, good in vivo tolerance, and

non-toxic features make these NPs potentially ideal candidates for future human applications.

Radiofrequency (RF) fields can be used to induce Au NP-mediated thermal ablation in a similar manner to that of photothermal and radio-sensitization therapies. The efficiency of RF-based therapy is significantly enhanced by using Au NPs, which are accumulated in the tumor area and then absorb main RF radiation power to heat cancer cells and thus cause their selective destruction. In particular, an intense source of RF radiation with frequency of 13.6 MHz and the power of 600 W induced the heating of suspensions of Au NPs with a heating rate of ~20 K/s, which resulted in considerable cell necrosis [271]. The NPs heating mechanism in an RF field is a very complex phenomenon. Glazer et al. have demonstrated that Au NPs heat primarily via Joule heating [271, 272]. Briefly, the Au NPs are hypothesized to function as tiny resistors, where free electrons on the surface have restricted movements. Therefore the friction created at the individual NP level releases heat into the surrounding aqueous solution [273].

The potential use of Au NPs coupled to RF waves was evaluated for the treatment of human hepatocellular and pancreatic cancer cells [274]. Direct injection of citrate-Au NPs into the tumor allowed focusing of the RF waves (13.56 MHz RF field) for selective heating of cancer cells. The resulting induced heat was lethal to these cancer cells bearing Au NPs in vitro. It was also demonstrated that the Au NPs had no intrinsic cytotoxicity or antiproliferative effects in the two human cancer cell lines studied. In another example, Curley et al. designed a method using Au NPs functionalized with the epidermal growth factor receptor (EGFR) inhibitor cetuximab in Panc-1 (pancreatic adenocarcinoma) and Difi (colorectal adenocarcinoma) cells which express high levels of EGFR [275]. This method proved to be cytotoxic to nearly 100% of the pancreatic and colorectal cells, but hardly any of the cells from the control group were damaged. The advantages of this therapy are that shortwave (megahertz range) RF energy is non-ionizing, penetrates deeply into biological tissues with no adverse side effects, and heats Au NPs efficiently. Thus, this technique may represent an effective treatment for numerous human malignant diseases using non-invasive RF hyperthermia.

The finding that Au NPs are able to inhibit angiogenesis (i.e., the formation of new vessels in organs or tissues) has also opened a new path to control the growth and spread of cancerous tissues via angiogenesis therapy. One method to inhibit angiogenesis in vivo is to block the function of pro-angiogenic heparin-binding growth factors (HB-GFs) such as vascular endothelial growth factor 165 (VEGF165) and basic fibroblast growth factor (bFGF). Mukherjee et al. demonstrated that Au NPs inhibit VEGF165-induced proliferation of endothelial cells in a dose-dependent manner [276]. This inhibition effect was tested in vivo using a nude mouse ear model, showing that after a week of daily intraperitoneal injections, the ascites volume had reduced in the NPs treated mice compared to the non-treated tumor-bearing mice. More recently, detailed studies of the antiangiogenic properties of Au NPs concluded that Au NPs not only inhibit VEGF165-induced HUVEC (Human Umbilical Vein Endothelial Cells) proliferation but also repress endothelial cell migration and tube formation [277]. Using Au NPs of different sizes and

surface charges, it was demonstrated that a naked Au NPs surface is required and that the core size plays an important role to inhibit the function of heparin-binding growth factors (HB-GFs) and subsequent intracellular signaling events. Furthermore, the inhibitory effect of Au NPs was produced by the change in HB-GFs conformation/configuration (denaturation) by the NPs, whereas the conformations of non-HB-GFs remained unaffected [278]. The antiangiogenic properties of Au NPs have also been exploited for the treatment of chronic inflammatory diseases such as rheumatoid arthritis. Intra-articular delivery of Au NPs has been demonstrated to be an effective treatment strategy for collagen-induced arthritis [279].

## 5 Use of Au NPs Towards Theranostics

Recent research has paved the way for multimodal 'theranostic' (i.e., a combination of therapy and diagnosis) nanocarriers designed for carrying out simultaneous detection/diagnosis and treatment of the disease following administration [184, 280–282]. Au NPs are suitable for developing theranostic NPs thanks to their unique characteristics that enable their use as contrast agents, as therapeutic entities, and as scaffolds to adhere functional molecules, therapeutic cargoes (e.g., drugs/genes), and targeting ligands [184, 281]. Several examples of Au-based theranostic NPs are illustrated in Fig. 3, which are explained below.

Au-based theranostic NPs that utilize light-based techniques for monitoring and treating diseases are of special interest as they allow for spatially and temporally controllable drug release, localized therapy, and minimally invasive treatment modalities that reduce patients discomfort [282]. An interesting photo-triggered theranostic system has been developed by Khlebtsov et al. [283], consisting of a silver/gold (Ag/Au) nanocage core surrounded by a silica shell containing the NIR photosensitizer Yb–2,4-dimethoxyhematoporphyrin (Yb–HP) for monitoring tumors and simultaneous dual therapy, i.e., PTT/PDT (Fig. 3a). A significant higher death rate of HeLa cervical cancer cells was observed in vitro when they were incubated with the composite NPs and irradiated by 630-nm light because of PTT by the Ag/Au NPs as well as PDT using the presence of Yb-HP. Furthermore, the IR luminescence of Yb-HP (900–1060 nm, originating from $Yb^{3+}$ ions, and located in the tissue transparency window) could be used for diagnostic purposes and for controlling the accumulation and bio-distribution of the composite NPs in tumors. Another example of theranostic NPs for simultaneous X-rays/ CT dual-imaging and dual-mode enhanced radiation therapy (RT) and PTT was reported by Huan et al. [284]. Folic acid-conjugated and silica-modified Au nanorods were synthesized and showed highly selective targeting, excellent X-ray/CT imaging ability, and enhanced RT and PTT effects (Fig. 3b). These multifunctional NPs could specifically bind to folate receptors on the surface of MGC803 gastric cancer cells and were imaged in vivo using both X-ray and CT imaging followed by treatment via RT or PTT. Alternatively, activatable theranostic NPs were developed by using

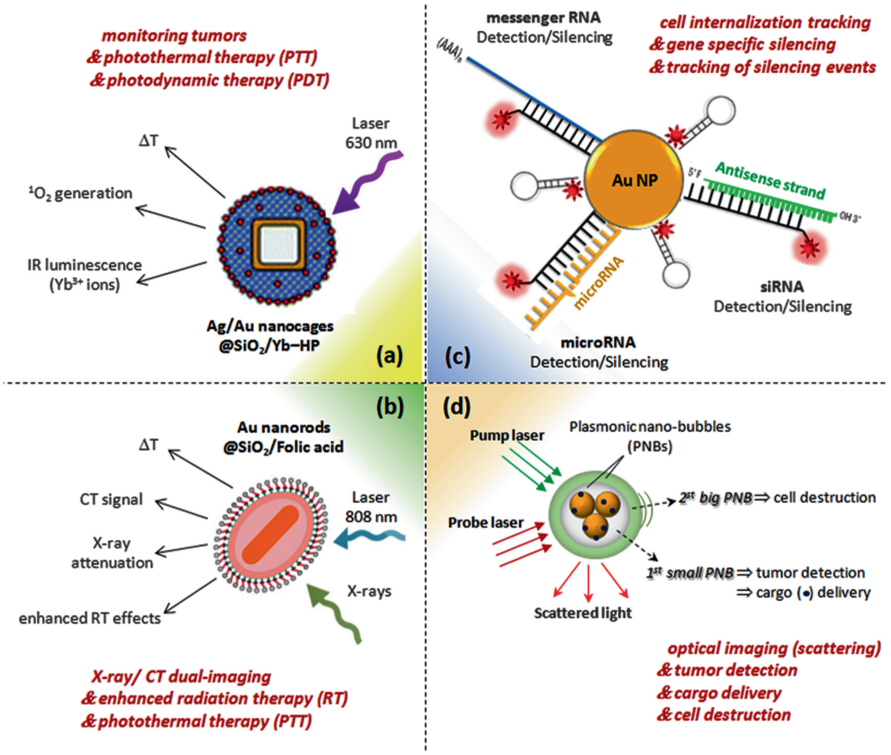


**Fig. 3** Simplified examples of diverse Au-based theranostic NPs. (**a**) Silver/gold (Ag/Au) nanocages surrounded by a silica shell containing the NIR photosensitizer Yb–2,4-dimethoxyhematoporphyrin (Yb–HP) for monitoring tumors *via* IR luminescence and simultaneous dual-therapy PTT/PDT [283]. (**b**) Au nanorods conjugated with folic acid for selective targeting, cancer cells X-ray/CT dual-imaging and treatment *via* enhanced-RT or PTT [284]. (**c**) Au NPs functionalized with a fluorophore labeled hairpin-DNA for simultaneous gene specific silencing and intracellular tracking of the silencing events [285]. (**d**) Use of Au NPs, either alone or with linked cargo molecules, for generating plasmonic nano-bubbles (PNBs) which allow tumor detection *via* light scattering, cargo delivery *via* creation of transient holes on the cell membrane and finally cell destruction *via* mechanical impact [286]

Au@Ag/Au NPs assembled with activatable aptamer probes, which provided high-contrast image-guided site-specific PTT therapy [287]. The Au@Ag/Au NPs simultaneously serve as an optical heater and a fluorescence quencher. The activatable aptamer probes comprised a thiolated aptamer and a fluorophore-labeled complementary DNA. Thus, the activatable theranostic NPs with quenched fluorescence in the free state could undergo signal activation through target binding-induced conformational change of the activatable aptamer probes in specific tumor tissues, and then achieve on-demand treatment under image-guided irradiation. By using S6 aptamer as a model, in vitro and in vivo studies of A549 lung cancer cells verified

that these NPs greatly improved imaging contrast and specific destruction. This strategy might be explored as a versatile platform for simultaneous detection and treatment of multiple kinds of cancer cells with the use of specific aptamers for varying cancer targets.

Conde et al. [285] recently developed an interesting Au-based theranostic system capable of intersecting all RNA pathways: from gene specific downregulation to silencing the silencers, i.e., siRNA and miRNA pathways (Fig. 3c). The system consists of Au NPs functionalized with a fluorophore labeled hairpin-DNA, which allows one to downregulate a specific gene directly and also to silence single gene expression, exogenous siRNA, and endogenous miRNAs, simultaneously tracking cell internalization and identifying the cells where silence is occurring (i.e., the fluorescence signal is directly proportional to the level of silencing). The usefulness of this approach was demonstrated for silencing an endogenous miRNA (miR-21) commonly upregulated in cancer, such as in colorectal carcinoma cells (HCT-116). The photothermal properties of Au NPs can also be used to generate transient vapor nano-bubbles to produce a tunable nanoscale theranostic agent, described as PNBs [286]. These PNBs are generated when Au NPs are locally overheated with short laser pulses because of the evaporation of a very thin volume of the surrounding medium, which in turn creates a vapor nanobubble that expands and collapses within nanoseconds. The bubble scatters the light, thus acting as an optical probe which allows for tumor detection, and the fast expansion of the PNB produces a localized mechanical impact which damages cell membranes, resulting in cell death, and therefore acting as a therapeutic agent. This novel theranostic system has been successfully applied as an in vivo tunable theranostic cellular agent in zebrafish hosting prostate cancer xenografts, presenting higher therapeutic selectivity when compared with Au NPs alone [288]. Au NPs conjugated with anti-EGFR antibody C225 could actively target EGFR-positive A549 lung carcinoma cells. Following cellular uptake, single human prostate cancer cells could be detected and ablated under optical guidance in vivo by tunable PNBs in a single theranostic procedure. By varying the energy of the laser pulse, the PNBs size could be dynamically tuned in a theranostic sequence of two PNBs: an initial small PNB detected a cancer cell through optical scattering, followed by a second bigger PNB, which mechanically ablated this cell without damaging the surrounding tissues, and its optical scattering confirmed the destruction of the cells. This innovative and promising theranostic strategy concept of a ‘cell theranostics’ approach that unites diagnosis, therapy, and confirmation (guidance) of the results of therapy in a single process at cellular level principally can help to improve both the rapidity and the precision of treatment [288]. Recently, the same group has used this concept for both, localized delivery of molecular cargo as well as mechanical destruction of cells by generation of a transient PNB around the Au NPs with a single incident laser pulse. Small PNBs can create a transient hole on the cell membrane to ‘inject’ molecular cargo without damage to the cells. Large PNBs, on the other hand, can cause mechanical destruction of the cells of interest [289] (Fig. 3d).

Based on these examples, it is apparent that theranostic Au NPs have opened the door to novel and advanced treatment strategies that combine therapeutics with diagnostics, aiming to monitor the response to treatment and increase drug efficacy and safety, which would be a key part of personalized medicine.

## 6 Applications of Au NPs in Clinical Trials

Some of the above-mentioned medical applications using Au NPs are already in the stage of pre-clinical or clinical trials.

The diagnostics company "Nanosphere" has developed the so-called Nanosphere's Verigene® System, which utilizes advanced automation and Au NPs to enable rapid direct detection of nucleic acids and high-sensitivity protein detection on the same platform. This technology has already received food and drug administration (FDA) approval in the United States. It is based on Au NPs of 13–20 nm diameter functionalized with either a defined number of oligonucleotides (i.e., short pieces of DNA or RNA) or a defined number of antibodies specific to a particular protein of interest.

One therapy using Au NPs which has reached clinical trials is CYT-6091, 27 nm citrate-coated Au NPs conjugated with thiolated-PEG and tumor necrosis factor-α (TNF-α) (Aurimmune; CytImmune Sciences). The NPs have the dual effect of increasing tumor targeting and tumor toxicity in comparison with the use of TNF-α alone [290]. In this trial the side effects and best dose of CYT-6091 in treating patients with advanced solid tumors by intravenous administration have been studied [291]. Future clinical studies should focus on combining CYT-6091 with approved chemotherapies for the systemic treatment of non-resectable cancers.

Using the same CYT-6091 NPs, another clinical trial has been carried out to evaluate the tissue distribution and the selective tumor trafficking of CYT-6091 in patients with primary and metastatic cancers [292]. Patients, stratified according to cancer type, received CYT-6091 and then underwent standard-care surgery. Tumor and normal tissues were removed during surgery for analysis of antitumor effects and tissue distribution of CYT-6091 by electron microscopy.

Au nanoshells (AuroShells®, Nanospectra Biosciences), which consist of a silica core of 120 nm diameter with a 15-nm gold shell, were used in clinical trials to treat head and neck cancers using PPTT. This therapy, called AuroLase® Therapy, consisted of an injection of Au nanoshell NPs into the patient's bloodstream. After 12–24 h (enough time for the NPs to accumulate inside the tumor), an 808 nm IR laser was used to heat the NPs and destroy tumor cells [293]. These NPs are currently under clinical trials in patients with primary and/or metastatic lung cancer where there is airway obstruction. In this study, patients are given a systemic infusion of NPs and a subsequently escalating dose of laser radiation delivered by an optical fiber via bronchoscopy.

In the treatment of atherosclerotic lesions, two delivery techniques for NPs and PPTT are under clinical trials (NANOM FIM) [294]. Patients underwent nano-

intervention either with the delivery of silica-Au NPs in a mini-surgery implanted bioengineered on-artery patch, or with the delivery of silica-Au iron-bearing NPs with targeted micro-bubbles or stem cells by means of magnetic navigation system vs stent implantation. The primary results showed a similar degree of regression of total atheroma volume after 12 months for both approaches of delivery.

Another technique being tested in pre-clinical trials works is on validating polyvalent Au NPs functionalized with RNAi (RNA interference) as anti-glioma therapeutics [295]. This nano-RNAi platform can be used to target signature lesions of glioblastoma, which play an important role in driving glioma pathogenesis, mediating therapeutic resistance, and instigating neurologically debilitating necrogenesis. RNAi-Au NPs are being validated on multiple levels, using glioma stem cell cultures, derived xenografts, and genetically engineered glioma mouse models.

Despite these examples, the full clinical impact of Au NP-based therapies is not yet known. There is clearly a need to translate already developed applications to clinical trials in a timely but safe manner.

## 7 Concluding Remarks and Future Outlook

We have discussed novel strategies for the synthesis and functionalization of Au NPs to evaluate their potential use in nanomedicine. In addition, their detection and sensing properties have been explored for diagnosing some diseases. Au NPs either alone or in hybrid form can also improve the performance of practically used imaging techniques. Moreover, Au NP-based therapies are generally superior in terms of specificity, selectivity, efficiency, and cytotoxicity compared to the same methods without Au NPs. Additionally, Au composite NPs have recently been evaluated for their theranostic potential both in vitro and in vivo. Nowadays, the main focus is the transition of Au NPs from laboratories to the clinics. Though the initial theranostic efficacy of Au NPs shows promising results, there are still many challenges which need to be addressed before their use in clinical practice. The first challenge involves the long-term retention, cytotoxicity, and ultimate renal clearance of the NPs. Though the biodistribution and toxicity of Au NPs have been extensively studied, reliable predictions based on these results are rare. Therefore, more studies need to be performed to ensure their safety before use in humans. The biodistribution of Au NPs is dependent on their size, geometry and surface chemistry. Dissimilarities of reported results dealing with Au NPs of the same size and shape have been attributed to the type of coating or stabilizing agents used. In order to overcome this problem, strategies to improve comparability and standardization of nanotoxicological studies are needed. Moreover, there should be a shift of the focus of toxicological experiments from ‘live–dead’ assays to the assessment of cell function, allowing observation of bioresponses at lower doses, which are more relevant for in vivo scenarios. Second, detection and sensing of analytes in complex biological fluids (such as urine, blood, etc.) are still complicated to achieve. Third, non-invasive clinical trials at the molecular level need to be better explored. Fourth,

the development of personalized medicines for the treatment of individual patients according to their genetic profiles is so far merely a vision described in scientific papers. Last, but not least, vaccinations based on Au NPs for humans and/or animals against biologically active factors or diseases still remain a dream to be fulfilled. Addressing these and other such types of challenges may help in the future to shift Au NP-based nanomedicines further into clinics.

**Acknowledgments** This work was supported by the European Commission (project Futurenanoneeds to WJP). SA, BP, and CCC acknowledge the Alexander von Humboldt Foundation for a PostDoc fellowship. QZ acknowledges CSC for funding. MGS acknowledges the Youssef Jameel Foundation for a PhD fellowship. AE acknowledges Junta de Andalucia for a Talentia Postdoc Fellowship, co-financed by the European Union's Seventh Framework Programme, grant agreement no 267226. MC acknowledges a Research Fellow Grant from Ikerbasque, Basque Foundation for Science.

## References

1. Patra CR, Bhattacharya R, Mukhopadhyay D, Mukherjee P (2010) Adv Drug Deliv Rev 62:346
2. Jain KK (2008) Nanomedicine 17:89
3. Chakraborty M, Jain S, Rani V (2011) Appl Biochem Biotechnol 165:1178
4. Shi J, Votruba AR, Farokhzad OC, Langer R (2010) Nano Lett 10:3223
5. Parveen S, Misra R, Sahoo SK (2012) Nanomed Nanotechnol Biol Med 8:147
6. Hauert S, Bhatia SN (2014) Trends Biotechnol 32:448
7. Steichen SD, Caldorera-Moore M, Peppas NA (2013) Eur J Pharm Sci 48:416
8. Nishiyama N, Okazaki S, Cabral H, Miyamoto M, Kato Y, Sugiyama Y, Nishio K, Matsumura Y, Kataoka K (2003) Cancer Res 63:8977
9. Cai W, Gao T, Hong H, Sun J (2008) Nanotechnol Sci Appl 1:17
10. Arvizo R, Bhattacharya R, Mukherjee P (2010) Expert Opin Drug Deliv 7:753
11. Giljohann DA, Seferos DS, Daniel WL, Massich MD, Patel PC, Mirkin CA (2010) Angew Chem Int Ed 49:3280
12. Dykman L, Khlebtsov N (2012) Chem Soc Rev 41:2256
13. Sperling RA, Rivera-Gil P, Zhang F, Zanella M, Parak WJ (2008) Chem Soc Rev 37:1896
14. Myroshnychenko V, Rodriguez-Fernandez J, Pastoriza-Santos I, Funston AM, Novo C, Mulvaney P, Liz-Marzan LM, Abajo FJG (2008) Chem Soc Rev 37:1792
15. Khlebtsov N, Dykman L (2011) Chem Soc Rev 40:1647
16. Fraga S, Brandão A, Soares ME, Morais T, Duarte JA, Pereira L, Soares L, Neves C, Pereira E, de Lourdes BM (2014) Nanomed Nanotechnol Biol Med 10:1757
17. Simpson CA, Salleng KJ, Cliffel DE, Feldheim DL (2013) Nanomed Nanotechnol Biol Med 9:257
18. Bednarski M, Dudek M, Knutelska J, Nowiński L, Sapa J, Zygmunt M, Nowak G, Luty-Błocho M, Wojnicki M, Fitzner K (2014) Pharmacol Rep 67:405
19. Dreaden EC, Alkilany AM, Huang X, Murphy CJ, El-Sayed MA (2012) Chem Soc Rev 41:2740
20. Pelaz B, del Pino P (2012) Front Nanosci 4:3
21. Bao C, Conde J, Polo E, del Pino P, Moros M, Baptista PV, Grazu V, Cui D, de la Fuente JM (2014) Nanomedicine 9:2353
22. Li N, Zhao P, Astruc D (2014) Angew Chem Int Ed 53:1756
23. Petersen S, Barcikowski S (2009) J Phys Chem C 113:19830

24. Brust M, Walker M, Bethell D, Schiffrin DJ, Whyman R (1994) J Chem Soc Chem Commun 1994:801
25. Liz-Marzán LM (2004) Mater Today 7:26
26. Turkevich J, Stevenson PC, Hillier J (1951) Discuss Faraday Soc 11:55
27. Bastús NG, Comenge J, Puntes V (2011) Langmuir 27:11098
28. Pelaz B, Grazu V, Ibarra A, Magen C, del Pino P, de la Fuente JM (2012) Langmuir 28:8965
29. Perez-Hernandez M, del Pino P, Mitchell SG, Moros M, Stepien G, Pelaz B, Parak WJ, Galvez EM, Pardo J, De La Fuente JM (2014) ACS Nano 9:52
30. Bao C, Beziere N, del Pino P, Pelaz B, Estrada G, Tian F, Ntziachristos V, de la Fuente JM, Cui D (2013) Small 9:68
31. Ye X, Zheng C, Chen J, Gao Y, Murray CB (2013) Nano Lett 13:765
32. Skrabalak SE, Chen J, Sun Y, Lu X, Au L, Cobley CM, Xia Y (2008) Acc Chem Res 41:1587
33. Personick ML, Mirkin CA (2013) J Am Chem Soc 135:18238
34. Perez-Juste J, Pastoriza-Santos I, Liz-Marzan LM, Mulvaney P (2005) Coord Chem Rev 249:1870
35. DuChene JS, Niu W, Abendroth JM, Sun Q, Zhao W, Huo F, Wei WD (2012) Chem Mater 25:1392
36. Nikoobakht B, El-Sayed MA (2003) Chem Mater 15:1957
37. Jana NR, Gearheart L, Murphy CJ (2001) J Phys Chem B 105:4065
38. Alkilany AM, Nagaria PK, Hexel CR, Shaw TJ, Murphy CJ, Wyatt MD (2009) Small 5:701
39. Ye X, Jin L, Caglayan H, Chen J, Xing G, Zheng C, Doan-Nguyen V, Kang Y, Engheta N, Kagan CR (2012) ACS Nano 6:2804
40. Pham T, Jackson JB, Halas NJ, Lee TR (2002) Langmuir 18:4915
41. Wang H, Brandl DW, Le F, Nordlander P, Halas NJ (2006) Nano Lett 6:827
42. Bardhan R, Mukherjee S, Mirin NA, Levit SD, Nordlander P, Halas NJ (2009) J Phys Chem C 114:7378
43. Ha TH, Koo H-J, Chung BH (2007) J Phys Chem C 111:1123
44. Chen L, Ji F, Xu Y, He L, Mi Y, Bao F, Sun B, Zhang X, Zhang Q (2014) Nano Lett 14:7201
45. Kumar PS, Pastoriza-Santos I, Rodriguez-Gonzalez B, de Abajo FJG, Liz-Marzan LM (2008) Nanotechnology 19:015606
46. Chen J, Wiley B, Li ZY, Campbell D, Saeki F, Cang H, Au L, Lee J, Li X, Xia Y (2005) Adv Mater 17:2255
47. Cobley CM, Chen J, Cho EC, Wang LV, Xia Y (2011) Chem Soc Rev 40:44
48. Goodman AM, Cao Y, Urban C, Neumann O, Ayala-Orozco C, Knight MW, Joshi A, Nordlander P, Halas NJ (2014) ACS Nano 8:3222
49. Aherne D, Charles DE, Brennan-Fournet ME, Kelly JM, Gun'ko YK (2009) Langmuir 25:10165
50. Luangpipat T, Beattie IR, Chisti Y, Haverkamp RG (2011) J Nanopart Res 13:6439
51. Gericke M, Pinches A (2006) Hydrometallurgy 83:132
52. Mittal AK, Chisti Y, Banerjee UC (2013) Biotechnol Adv 31:346
53. Levin CS, Hofmann C, Ali TA, Kelly AT, Morosan E, Nordlander P, Whitmire KH, Halas NJ (2009) ACS Nano 3:1379
54. Bardhan R, Grady NK, Ali T, Halas NJ (2010) ACS Nano 4:6169
55. Salado J, Insausti M, Lezama L, de Muro IG, Moros M, Pelaz B, Grazu V, de la Fuente J, Rojo T (2012) Nanotechnology 23:315102
56. Cardinal MF, Rodriguez-Gonzalez B, Alvarez-Puebla RA, Perez-Juste J, Liz-Marzan LM (2010) J Phys Chem C 114:10417
57. Cheng L-C, Chen HM, Lai T-C, Chan Y-C, Liu R-S, Sung JC, Hsiao M, Chen C-H, Her L-J, Tsai DP (2013) Nanoscale 5:3931
58. Tan C, Huang X, Zhang H (2013) Mater Today 16:29
59. Moon H, Kumar D, Kim H, Sim C, Chang J-H, Kim J-M, Kim H, Lim D-K (2015) ACS Nano 9:2711
60. Rivera-Gil P, Jimenez De Aberasturi D, Wulf V, Pelaz B, Del Pino P, Zhao Y, De La Fuente JM, Ruiz De Larramendi I, Rojo T, Liang X-J (2012) Acc Chem Res 46:743

61. Pelaz B, Charron G, Pfeiffer C, Zhao Y, de la Fuente JM, Liang X-J, Parak WJ, del Pino P (2013) Small 9:1573
62. Love JC, Estroff LA, Kriebel JK, Nuzzo RG, Whitesides GM (2005) Chem Rev 105:1103
63. Yang J, Lee JY, Ying JY (2011) Chem Soc Rev 40:1672
64. Indrasekara A, Wadams RC, Fabris L (2014) Part Part Syst Charact 31:819
65. Kinnear C, Dietsch H, Clift MJ, Endes C, Rothen-Rutishauser B, Petri-Fink A (2013) Angew Chem 125:1988
66. Flynn NT, Tran TNT, Cima MJ, Langer R (2003) Langmuir 19:10909
67. Pino P, de la Fuente JM (2013) Chem Commun 49:3676
68. Puertas S, Batalla P, Moros M, Polo E, del Pino P, Guisan JM, Grazu V, de la Fuente JM (2011) ACS Nano 5:4521
69. Roux S, Garcia B, Bridot J-L, Salomé M, Marquette C, Lemelle L, Gillet P, Blum L, Perriat P, Tillement O (2005) Langmuir 21:2526
70. Brewer SH, Glomm WR, Johnson MC, Knag MK, Franzen S (2005) Langmuir 21:9303
71. Mayya KS, Schoeler B, Caruso F (2003) Adv Funct Mater 13:183
72. Mahl D, Greulich C, Meyer-Zaika W, Köller M, Epple M (2010) J Mater Chem 20:6176
73. Lin C-AJ, Sperling RA, Li JK, Yang T-Y, Li P-Y, Zanella M, Chang WH, Parak WJ (2008) Small 4:334
74. Pellegrino T, Kudera S, Liedl T, Muñoz Javier A, Manna L, Parak WJ (2005) Small 1:48
75. Soliman MG, Pelaz B, Parak WJ, del Pino P (2015) Chem Mater 27:990
76. Fuentes M, Mateo C, Guisán J, Fernández-Lafuente R (2005) Biosens Bioelectron 20:1380
77. Tang W, Becker ML (2014) Chem Soc Rev 43:7013
78. Sperling RA, Parak WJ (2010) Phil Trans R Soc A 368:1333
79. Montenegro J-M, Grazu V, Sukhanova A, Agarwal S, Jesus M, Nabiev I, Greiner A, Parak WJ (2013) Adv Drug Deliv Rev 65:677
80. Avvakumova S, Colombo M, Tortora P, Prosperi D (2014) Trends Biotechnol 32:11
81. Jimenez de Aberasturi D, Montenegro J-M, Ruiz de Larramendi I, Rojo T, Klar TA, Alvarez-Puebla R, Liz-Marzán LM, Parak WJ (2012) Chem Mater 24:738
82. Saha K, Agasti SS, Kim C, Li X, Rotello VM (2012) Chem Rev 112:2739
83. Sapsford KE, Berti L, Medintz IL (2006) Angew Chem Int Ed 45:4562
84. Leuvering J, Thal P, Waart M, Schuurs A (1980) Fresenius J Anal Chem 301:132
85. Leuvering JH, Thal PJ, Van der Waart M, Schuurs AH (1981) J Immunol Methods 45:183
86. Elghanian R, Storhoff JJ, Mucic RC, Letsinger RL, Mirkin CA (1997) Science 277:1078
87. Mie G (1976) Ann Phys 25:377
88. Srivastava S, Frankamp BL, Rotello VM (2005) Chem Mater 17:487
89. Lin S-Y, Liu S-W, Lin C-M, Chen C-H (2002) Anal Chem 74:330
90. Reynolds AJ, Haines AH, Russell DA (2006) Langmuir 22:1156
91. Watanabe S, Seguchi H, Yoshida K, Kifune K, Tadaki T, Shiozaki H (2005) Tetrahedron Lett 46:8827
92. Daniel WL, Han MS, Lee J-S, Mirkin CA (2009) J Am Chem Soc 131:6362
93. Deng H, Zhang X, Kumar A, Zou G, Zhang X, Liang X-J (2012) Chem Commun 49:51
94. Ai K, Liu Y, Lu L (2009) J Am Chem Soc 131:9496
95. Aili D, Selegård R, Baltzer L, Enander K, Liedberg B (2009) Small 5:2445
96. Zhu Y, Wang G, Sha L, Qiu Y, Jiang H, Zhang X (2015) Analyst 140:1260
97. Wen S, Zheng F, Shen M, Shi X (2013) Colloids Surf A 419:80
98. Chang C-C, Chen C-Y, Chen C-P, Lin C-W (2015) Anal Methods 7:29
99. Creran B, Li X, Duncan B, Kim CS, Moyano DF, Rotello VM (2014) ACS Appl Mater Interfaces 6:19525
100. Wang S, Singh AK, Senapati D, Neely A, Yu H, Ray PC (2010) Chem Eur J 16:5600
101. Malinsky MD, Kelly KL, Schatz GC, Duyne RPV (2001) J Am Chem Soc 123:1471
102. Moon S, Kim DJ, Kim K, Kim D, Lee H, Lee K, Haam S (2010) Appl Opt 49:484
103. Wang J, Wang L, Sun Y, Zhu X, Cao Y, Wang X, Zhang H, Song D (2010) Colloids Surf B 75:520
104. Frasconi M, Tortolini C, Botre F, Mazzei F (2010) Anal Chem 82:7335
105. Joshi GK, Deitz-McElyea S, Johnson M, Mali S, Korc M, Sardar R (2014) Nano Lett 14:6955

106. Hu Y, Zhang L, Ying Z, Wang B, Wang Y, Fan Q, Huang W, Wang L (2015) ACS Appl Mater Interfaces 7:2459
107. Wang J (2005) Small 1:1036
108. Mitchell JS, Lowe TE (2009) Biosens Bioelectron 24:2177
109. He L, Musick MD, Nicewarner SR, Salinas FG, Benkovic SJ, Natan MJ, Keating CD (2000) J Am Chem Soc 122:9071
110. Jain PK, El-Sayed IH, El-Sayed MA (2007) Nano Today 2:18
111. Dubertret B, Calame M, Libchaber AJ (2001) Nat Biotechnol 19:365
112. You C-C, Miranda OR, Gider B, Ghosh PS, Kim I-B, Erdogan B, Krovi SA, Bunz UH, Rotello VM (2007) Nat Nanotechnol 2:318
113. Phillips RL, Miranda OR, You CC, Rotello VM, Bunz UH (2008) Angew Chem Int Ed 47:2590
114. Miranda OR, Chen H-T, You C-C, Mortenson DE, Yang X-C, Bunz UH, Rotello VM (2010) J Am Chem Soc 132:5285
115. Lukman S, Aung KMM, Liu J, Liu B, Su X (2013) ACS Appl Mater Interfaces 5:12725
116. Albert KJ, Lewis NS, Schauer CL, Sotzing GA, Stitzel SE, Vaid TP, Walt DR (2000) Chem Rev 100:2595
117. Sun W, Lu Y, Mao J, Chang N, Yang J, Liu Y (2015) Anal Chem 87:3354
118. Xu S, Lu X, Yao C, Huang F, Jiang H, Hua W, Na N, Liu H, Ouyang J (2014) Anal Chem 86:11634
119. Oh E, Hong M-Y, Lee D, Nam S-H, Yoon HC, Kim H-S (2005) J Am Chem Soc 127:3270
120. Bajaj A, Miranda OR, Kim I-B, Phillips RL, Jerry DJ, Bunz UH, Rotello VM (2009) Proc Natl Acad Sci 106:10912
121. Katz E, Willner I, Wang J (2004) Electroanal 16:19
122. Munge BS, Coffey AL, Doucette JM, Somba BK, Malhotra R, Patel V, Gutkind JS, Rusling JF (2011) Angew Chem 123:8061
123. Jensen GC, Krause CE, Sotzing GA, Rusling JF (2011) Phys Chem Chem Phys 13:4888
124. Li Y, Schluesener HJ, Xu S (2010) Gold Bull 43:29
125. Chen A, Chatterjee S (2013) Chem Soc Rev 42:5425
126. Jena BK, Raj CR (2010) Talanta 80:1653
127. Chai R, Yuan R, Chai Y, Ou C, Cao S, Li X (2008) Talanta 74:1330
128. Narang J, Malhotra N, Singh G, Pundir C (2015) Biosens Bioelectron 66:332
129. Omidfar K, Khorsand F, Azizi MD (2013) Biosens Bioelectron 43:336
130. Afonso AS, Pérez-López B, Faria RC, Mattoso LH, Hernández-Herrero M, Roig-Sagués AX, Maltez-da Costa M, Merkoçi A (2013) Biosens Bioelectron 40:121
131. Maltez-da Costa M, de la Escosura-Muñiz A, Nogués C, Barrios L, Ibáñez E, Merkoçi A (2012) Nano Lett 12:4164
132. de la Escosura-Muñiz A, Sánchez-Espinel C, Díaz-Freitas B, González-Fernández A, Maltez-da Costa M, Merkoçi A (2009) Anal Chem 81:10268
133. Maltez-da Costa M, de la Escosura-Muñiz A, Nogués C, Barrios L, Ibáñez E, Merkoçi A (2012) Small 8:3605
134. Kneipp K, Kneipp H, Itzkan I, Dasari RR, Feld MS (1999) Chem Rev 99:2957
135. Willets KA (2009) Anal Bioanal Chem 394:85
136. Cialla D, März A, Böhme R, Theil F, Weber K, Schmitt M, Popp J (2012) Anal Bioanal Chem 403:27
137. La Porta A, Grzelczak M, Liz-Marzán LM (2014) ChemistryOpen 3:146
138. Scarabelli L, Coronado-Puchau M, Giner-Casares JJ, Langer J, Liz-Marzán LM (2014) ACS Nano 8:5833
139. Quaresma P, Osório I, Dória G, Carvalho PA, Pereira A, Langer J, Araújo JP, Pastoriza-Santos I, Liz-Marzán LM, Franco R (2014) RSC Adv 4:3659
140. Hughes J, Izake EL, Lott WB, Ayoko GA, Sillence M (2014) Talanta 130:20
141. Thuy NT, Yokogawa R, Yoshimura Y, Fujimoto K, Koyano M, Maenosono S (2010) Analyst 135:595

142. Harpster MH, Zhang H, Sankara-Warrier AK, Ray BH, Ward TR, Kollmar JP, Carron KT, Mecham JO, Corcoran RC, Wilson WC (2009) Biosens Bioelectron 25:674
143. Wang Y, Lee K, Irudayaraj J (2010) Chem Commun 46:613
144. Da P, Li W, Lin X, Wang Y, Tang J, Zheng G (2014) Anal Chem 86:6633
145. Matteini P, de Angelis M, Ulivi L, Centi S, Pini R (2015) Nanoscale 7:3474
146. Panikkanvalappil SR, El-Sayed MA (2014) J Phys Chem B 118:14085
147. Xie H-N, Lin Y, Mazo M, Chiappini C, Sánchez-Iglesias A, Liz-Marzán LM, Stevens MM (2014) Nanoscale 6:12403
148. Liu G, Swierczewska M, Lee S, Chen X (2010) Nano Today 5:524
149. Doane TL, Burda C (2012) Chem Soc Rev 41:2885
150. Sun X, Zhang N (2010) Mini Rev Med Chem 10:108
151. Koo H, Jin G-W, Kang H, Lee Y, Nam K, Bai CZ, Park J-S (2010) Biomaterials 31:988
152. Danhier F, Ansorena E, Silva JM, Coco R, Le Breton A, Préat V (2012) J Control Release 161:505
153. Menjoge AR, Kannan RM, Tomalia DA (2010) Drug Discov Today 15:171
154. Zhang L, Gu FX, Chan JM, Wang AZ, Langer RS, Farokhzad OC (2008) Clin Pharmacol Ther 83:761
155. Mulder WJ, Strijkers GJ, van Tilborg GA, Griffioen AW, Nicolay K (2006) NMR Biomed 19:142
156. Puri A, Loomis K, Smith B, Lee J-H, Yavlovich A, Heldman E, Blumenthal R (2009) Crit Rev Ther Drug Carrier Syst 26:523
157. Talelli M, Rijcken CJ, Lammers T, Seevinck PR, Storm G, van Nostrum CF, Hennink WE (2009) Langmuir 25:2060
158. Gupta AK, Naregalkar RR, Vaidya VD, Gupta M (2007) Future Med Chem 2:23
159. Figuerola A, Di Corato R, Manna L, Pellegrino T (2010) Pharmacol Res 62:126
160. Singh SP (2011) J Biomed Nanotechnol 7:95
161. Wang Y, Chen L (2011) Nanomed Nanotechnol Biol Med 7:385
162. Smith AM, Duan H, Mohs AM, Nie S (2008) Adv Drug Deliv Rev 60:1226
163. Bentolila LA, Ebenstein Y, Weiss S (2009) J Nucl Med 50:493
164. Kostarelos K, Bianco A, Prato M (2009) Nat Nanotechnol 4:627
165. Son SJ, Bai X, Lee S (2007) Drug Discov Today 12:657
166. Jokerst JV, Lobovkina T, Zare RN, Gambhir SS (2011) Nanomedicine 6:715
167. Lee D-E, Koo H, Sun I-C, Ryu JH, Kim K, Kwon IC (2012) Chem Soc Rev 41:2656
168. Tasciotti E, Liu XW, Bhavane R, Plant K, Leonard AD, Price BK, Cheng MMC, Decuzzi P, Tour JM, Robertson F, Ferrari M (2008) Nat Nanotechnol 3:151
169. Huang X, Jain PK, El-Sayed IH, El-Sayed MA (2007) Nanomedicine 2:681
170. Qian X, Peng X-H, Ansari DO, Yin-Goen Q, Chen GZ, Shin DM, Yang L, Young AN, Wang MD, Nie S (2008) Nat Biotechnol 26:83
171. Boisselier E, Astruc D (2009) Chem Soc Rev 38:1759
172. Murphy CJ, Gole AM, Stone JW, Sisco PN, Alkilany AM, Goldsmith EC, Baxter SC (2008) Acc Chem Res 41:1721
173. Huff TB, Tong L, Zhao Y, Hansen MN, Cheng JX, Wei A (2007) Nanomedicine 2:125
174. Tong L, Wei Q, Wei A, Cheng JX (2009) Photochem Photobiol 85:21
175. Ye S, Marston G, McLaughlan JR, Sigle DO, Ingram N, Freear S, Baumberg JJ, Bushby RJ, Markham AF, Critchley K (2015) Adv Funct Mater. doi:10.1002/adfm.201404358:1-11
176. Bardhan R, Lal S, Joshi A, Halas NJ (2011) Acc Chem Res 44:936
177. Xia X, Xia Y (2014) Front Phys 9:378
178. Moon GD, Choi S-W, Cai X, Li W, Cho EC, Jeong U, Wang LV, Xia Y (2011) J Am Chem Soc 133:4762
179. Wang Y, Liu Y, Luehmann H, Xia X, Wan D, Cutler C, Xia Y (2013) Nano Lett 13:581
180. Salgueiriño-Maceira V, Correa-Duarte MA (2007) Adv Mater 19:4131
181. Yuan H, Fales AM, Vo-Dinh T (2012) J Am Chem Soc 134:11358
182. Yuan H, Khoury CG, Hwang H, Wilson CM, Grant GA, Vo-Dinh T (2012) Nanotechnology 23:075102

183. Yuan H, Khoury CG, Wilson CM, Grant GA, Bennett AJ, Vo-Dinh T (2012) Nanomed Nanotechnol Biol Med 8:1355
184. Webb JA, Bardhan R (2014) Nanoscale 6:2502
185. Latterini L, Tarpani L (2014) Bio Bioinspir Nanomater 7:173
186. Wang Z (2013) Sci China Phys Mech Astron 56:506
187. Melancon MP, Lu W, Yang Z, Zhang R, Cheng Z, Elliot AM, Stafford J, Olson T, Zhang JZ, Li C (2008) Mol Cancer Ther 7:1730
188. Kang B, Mackey MA, El-Sayed MA (2010) J Am Chem Soc 132:1517
189. Rosman C, Pierrat S, Henkel A, Tarantola M, Schneider D, Sunnick E, Janshoff A, Sönnichsen C (2012) Small 8:3683
190. Wu Z, Jin R (2010) Nano Lett 10:2568
191. Wu X, He X, Wang K, Xie C, Zhou B, Qing Z (2010) Nanoscale 2:2244
192. Dam DHM, Lee JH, Sisco PN, Co DT, Zhang M, Wasielewski MR, Odom TW (2012) ACS Nano 6:3318
193. Zhu J, Yong K-T, Roy I, Hu R, Ding H, Zhao L, Swihart MT, He GS, Cui Y, Prasad PN (2010) Nanotechnology 21:285106
194. Hong G, Tabakman SM, Welsher K, Chen Z, Robinson JT, Wang H, Zhang B, Dai H (2011) Angew Chem Int Ed 50:4644
195. Li J-L, Gu M (2010) Biomaterials 31:9492
196. Durr NJ, Larson T, Smith DK, Korgel BA, Sokolov K, Ben-Yakar A (2007) Nano Lett 7:941
197. Gao L, Vadakkan TJ, Nammalvar V (2011) Nanotechnology 22:365102
198. Au L, Zhang Q, Cobley CM, Gidding M, Schwartz AG, Chen J, Xia Y (2009) ACS Nano 4:35
199. Tong L, Cobley CM, Chen J, Xia Y, Cheng J-X (2010) Angew Chem Int Ed 49:3485
200. Wang LV, Hu S (2012) Science 335:1458
201. Hainfeld JF, Slatkin DN, Focella TM, Smilowitz HM (2006) Br J Radiol 79:248
202. Ahn S, Jung SY, Lee SJ (2013) Molecules 18:5858
203. Peng C, Qin J, Zhou B, Chen Q, Shen M, Zhu M, Lu X, Shi X (2013) Polym Chem 4:4412
204. Fujimoto JG (2003) Nat Biotechnol 21:1361
205. Zagaynova E, Shirmanova M, Kirillin MY, Khlebtsov B, Orlova A, Balalaeva I, Sirotkina M, Bugrova M, Agrba P, Kamensky V (2008) Phys Med Biol 53:4995
206. Ntziachristos V (2010) Nat Methods 7:603
207. Sebastián V, Lee S-K, Zhou C, Kraus MF, Fujimoto JG, Jensen KF (2012) Chem Commun 48:6654
208. Boyer D, Tamarat P, Maali A, Lounis B, Orrit M (2002) Science 297:1160
209. Karmani L, Labar D, Valembois V, Bouchat V, Nagaswaran PG, Bol A, Gillart J, Levêque P, Bouzin C, Bonifazi D (2013) Contrast Media Mol Imaging 8:402
210. Das S, Grimm J, Thorek DL (2014) Emerg Appl Mol Imaging Oncol 124:213
211. Singhal S, Nie S, Wang MD (2010) Annu Rev Med 61:359
212. Li J, Gupta S, Li C (2013) Quant Imaging Med Surg 3:284
213. Ghosh P, Han G, De M, Kim CK, Rotello VM (2008) Adv Drug Deliv Rev 60:1307
214. Chen Z, Zhang L, He Y, Shen Y, Li Y (2014) Small 11:952
215. Kong WH, Bae KH, Hong CA, Lee Y, Hahn SK, Park TG (2011) Bioconjug Chem 22:1962
216. Bansal A, Zhang Y (2014) Acc Chem Res 47:3052
217. Braun GB, Pallaoro A, Wu G, Missirlis D, Zasadzinski JA, Tirrell M, Reich NO (2009) ACS Nano 3:2007
218. Huschka R, Zuloaga J, Knight MW, Brown LV, Nordlander P, Halas NJ (2011) J Am Chem Soc 133:12247
219. Yang N, Burkholder J, Roberts B, Martinell B, McCabe D (1990) Proc Natl Acad Sci 87:9568
220. Park J, Kim WJ (2012) J Drug Target 20:648
221. Ghosh PS, Kim C-K, Han G, Forbes NS, Rotello VM (2008) ACS Nano 2:2213
222. YoungáChoi S, YeongáLee S (2011) J Mater Chem 21:13853
223. Yan X, Blacklock J, Li J, Möhwald H (2011) ACS Nano 6:111
224. Ramos J, Rege K (2013) Mol Pharm 10:4107

225. Ramos J, Rege K (2012) Biotechnol Bioeng 109:1336
226. Wagner E (2011) Acc Chem Res 45:1005
227. Hu C, Peng Q, Chen F, Zhong Z, Zhuo R (2010) Bioconjug Chem 21:836
228. Elbakry A, Zaky A, Liebl R, Rachel R, Goepferich A, Breunig M (2009) Nano Lett 9:2059
229. Song W-J, Du J-Z, Sun T-M, Zhang P-Z, Wang J (2010) Small 6:239
230. Guo S, Huang Y, Jiang Q, Sun Y, Deng L, Liang Z, Du Q, Xing J, Zhao Y, Wang PC (2010) ACS Nano 4:5505
231. Wang F, Shen Y, Zhang W, Li M, Wang Y, Zhou D, Guo S (2014) J Control Release 196:37
232. Lee M-Y, Park S-J, Park K, Kim KS, Lee H, Hahn SK (2011) ACS Nano 5:6138
233. Bonoiu AC, Bergey EJ, Ding H, Hu R, Kumar R, Yong K-T, Prasad PN, Mahajan S, Picchione KE, Bhattacharjee A (2011) Nanomedicine 6:617
234. Lee SK, Han MS, Asokan S, Tung CH (2011) Small 7:364
235. Uchida M, Li XW, Mertens P, Alpar HO (2009) Biochim Biophys Acta 1790:754
236. Martin-Ortigosa S, Wang K (2014) Transgenic Res 23:743
237. Zhu Y, Liao L (2015) J Nanosci Nanotechnol 15:4753
238. Kim CK, Ghosh P, Pagliuca C, Zhu ZJ, Menichetti S, Rotello VM (2009) J Am Chem Soc 131:1360
239. Gibson JD, Khanal BP, Zubarev ER (2007) J Am Chem Soc 129:11653
240. Mohammad F, Yusof NA (2014) J Colloid Interface Sci 434:89
241. You J, Zhang R, Zhang G, Zhong M, Liu Y, Van Pelt CS, Liang D, Wei W, Sood AK, Li C (2012) J Control Release 158:319
242. You J, Zhang G, Li C (2010) ACS Nano 4:1033
243. Hartwell BL, Antunez L, Sullivan BP, Thati S, Sestak JO, Berkland C (2015) J Pharm Sci 104:346
244. Skirtach AG, Javier AM, Kreft O, Köhler K, Alberola AP, Möhwald H, Parak WJ, Sukhorukov GB (2006) Angew Chem Int Ed 45:4612
245. del Mercato LL, Rivera-Gil P, Abbasi AZ, Ochs M, Ganas C, Zins I, Sönnichsen C, Parak WJ (2010) Nanoscale 2:458
246. Carregal-Romero S, Ochs M, Parak WJ (2012) Nanophotonics 1:171
247. Muñoz Javier A, Pino P, Bedard M, Skirtach AG, Ho D, Sukhorukov G, Plank C, Parak WJ (2009) Langmuir 24:12517
248. De Geest BG, De Koker S, Sukhorukov GB, Kreft O, Parak WJ, Skirtach AG, Demeester J, De Smedt SC, Hennink WE (2009) Soft Matter 5:282
249. Choi KY, Liu G, Lee S, Chen X (2012) Nanoscale 4:330
250. Wang C, Li J, Amatore C, Chen Y, Jiang H, Wang X-M (2011) Angew Chem Int Ed 50:11644
251. Modugno G, Ménard-Moyon C, Prato M, Bianco A (2015) Br J Pharmacol 172:975
252. Xu C, Yang D, Mei L, Lu B, Chen L, Li Q, Zhu H, Wang T (2013) ACS Appl Mater Interfaces 5:2715
253. Xu C, Yang D, Mei L, Li Q, Zhu H, Wang T (2013) ACS Appl Mater Interfaces 5:12911
254. Ma X, Qu Q, Zhao Y, Luo Z, Zhao Y, Ng KW, Zhao Y (2013) J Mater Chem B 1:6495
255. Sanchez-Barcelo EJ, Mediavilla MD (2014) Recent Pat Endocr Metab Immune Drug Discovery 8:1
256. Menon JU, Jadeja P, Tambe P, Vu K, Yuan B, Nguyen KT (2013) Theranostics 3:152
257. Huang X, Jain P, El-Sayed I, El-Sayed M (2008) Lasers Med Sci 23:217
258. Pattani VP, Tunnell JW (2012) Lasers Surg Med 44:675
259. Mackey MA, Ali MR, Austin LA, Near RD, El-Sayed MA (2014) J Phys Chem B 118:1319
260. Lin KY, Bagley AF, Zhang AY, Karl DL, Yoon SS, Bhatia SN (2010) Nano Life 1:277
261. Chen J, Glaus C, Laforest R, Zhang Q, Yang M, Gidding M, Welch MJ, Xia Y (2010) Small 6:811
262. Jang B, Park J-Y, Tung C-H, Kim I-H, Choi Y (2011) ACS Nano 5:1086
263. Kong T, Zeng J, Wang X, Yang X, Yang J, McQuarrie S, McEwan A, Roa W, Chen J, Xing JZ (2008) Small 4:1537
264. Yang Y-S, Carney RP, Stellacci F, Irvine DJ (2014) ACS Nano 8:8992

265. Geng F, Xing JZ, Chen J, Yang R, Hao Y, Song K, Kong B (2014) J Biomed Nanotechnol 10:1205
266. Hainfeld JF, Lin L, Slatkin DN, Dilmanian FA, Vadas TM, Smilowitz HM (2014) Nanomed Nanotechnol Biol Med 10:1609–1617
267. Lin Y, McMahon SJ, Scarpelli M, Paganetti H, Schuemann J (2014) Phys Med Biol 59:7675
268. Chanda N, Kan P, Watkinson LD, Shukla R, Zambre A, Carmack TL, Engelbrecht H, Lever JR, Katti K, Fent GM (2010) Nanomed Nanotechnol Biol Med 6:201
269. Khan MK, Minc LD, Nigavekar SS, Kariapper MS, Nair BM, Schipper M, Cook AC, Lesniak WG, Balogh LP (2008) Nanomed Nanotechnol Biol Med 4:57
270. Kannan R, Zambre A, Chanda N, Kulkarni R, Shukla R, Katti K, Upendran A, Cutler C, Boote E, Katti KV (2012) Wiley Interdiscip Rev Nanomed Nanobiotechnol 4:42
271. Moran CH, Wainerdi SM, Cherukuri TK, Kittrell C, Wiley BJ, Nicholas NW, Curley SA, Kanzius JS, Cherukuri P (2009) Nano Res 2:400
272. Glazer ES, Curley SA (2010) Cancer 116:3285
273. Glazer ES, Curley SA (2011) Ther Deliv 2:1325
274. Gannon CJ, Patra CR, Bhattacharya R, Mukherjee P, Curley SA (2008) J Nanobiotechnol 6:1
275. Curley SA, Cherukuri P, Briggs K, Patra CR, Upton M, Dolson E, Mukherjee P (2007) J Exp Ther Oncol 7:313
276. Mukherjee P, Bhattacharya R, Wang P, Wang L, Basu S, Nagy JA, Atala A, Mukhopadhyay D, Soker S (2005) Clin Cancer Res 11:3530
277. Pan Y, Wu Q, Qin L, Cai J, Du B (2014) BioMed Res Int 2014:1
278. Arvizo RR, Rana S, Miranda OR, Bhattacharya R, Rotello VM, Mukherjee P (2011) Nanomed Nanotechnol Biol Med 7:580
279. Tsai C-Y, Shiau A-L, Chen S-Y, Chen Y-H, Cheng P-C, Chang M-Y, Chen D-H, Chou C-H, Wang C-R, Wu C-L (2007) Arthritis Rheum 56:544
280. Muthu MS, Leong DT, Mei L, Feng S-S (2014) Theranostics 4:660
281. Akhter S, Ahmad MZ, Ahmad FJ, Storm G, Kok RJ (2012) Expert Opin Drug Deliv 9:1225
282. Rai P, Mallidi S, Zheng X, Rahmanzadeh R, Mir Y, Elrington S, Khurshid A, Hasan T (2010) Adv Drug Deliv Rev 62:1094
283. Khlebtsov B, Panfilova E, Khanadeev V, Bibikova O, Terentyuk G, Ivanov A, Rumyantseva V, Shilov I, Ryabova A, Loshchenov V (2011) ACS Nano 5:7077
284. Huang P, Bao L, Zhang C, Lin J, Luo T, Yang D, He M, Li Z, Gao G, Gao B (2011) Biomaterials 32:9796
285. Conde J, Rosa J, Jesús M, Baptista PV (2013) Biomaterials 34:2516
286. Lukianova-Hleb EY, Oginsky AO, Samaniego AP, Shenefelt DL, Wagner DS, Hafner JH, Farach-Carson MC, Lapotko DO (2011) Theranostics 1:3
287. Shi H, Ye X, He X, Wang K, Cui W, He D, Li D, Jia X (2014) Nanoscale 6:8754
288. Wagner DS, Delk NA, Lukianova-Hleb EY, Hafner JH, Farach-Carson MC, Lapotko DO (2010) Biomaterials 31:7567
289. Lukianova-Hleb EY, Mutonga MB, Lapotko DO (2012) ACS Nano 6:10973
290. National Institutes of Health Clinical Center (CC), National Cancer Institute (NCI) (2012) http://www.clinicaltrials.gov; identifier: NCT00356980
291. Libutti S, Paciotti G, Myer L, Haynes R, Gannon W, Walker M, Seidel G, Byrnes A, Yuldasheva N, Tamarkin L (2009) ASCO annual meeting proceedings 27:3586
292. National Institutes of Health Clinical Center (CC), National Cancer Institute (NCI) (2012) http://www.clinicaltrials.gov; identifier: NCT00436410
293. Nanospectra Biosciences (2014) http://www.clinicaltrials.gov; identifier: NCT00848042
294. Nanospectra Biosciences (2012–to date) http://www.clinicaltrials.gov; identifier: NCT01679470
295. Stegh AH (2012–to date) http://www.nu-ccne.org/Research_project4.htm

Available online at www.sciencedirect.com

ScienceDirect

Current Opinion in Pharmacology

# Fluorescence-based ion-sensing with colloidal particles

Sumaira Ashraf[1], Carolina Carrillo-Carrion[1], Qian Zhang[1], Mahmoud G Soliman[1], Raimo Hartmann[1], Beatriz Pelaz[1], Pablo del Pino[2] and Wolfgang J Parak[1,2]

Particle-based fluorescence sensors for the quantification of specific ions can be made by coupling ion-sensitive fluorophores to carrier particles, or by using intrinsically fluorescent particles whose fluorescence properties depend on the concentration of the ions. Despite the advantages of such particle-based sensors for the quantitative detection of ions, such as the possibility to tune the surface chemistry and thus entry portal of the sensor particles to cells, they have also some associated problems. Problems involve for example crosstalk of the ion-sensitive fluorescence read-out with pH, or spectral overlap of the emission spectra of different fluorescent particles in multiplexing formats. Here the benefits of using particle-based fluorescence sensors, their limitations and strategies to overcome these limitations will be described and exemplified with selected examples.

**Addresses**
[1] Fachbereich Physik, Philipps Universität Marburg, Marburg, Germany
[2] CIC BiomaGUNE, San Sebastian, Spain

Corresponding author: Parak, Wolfgang J (wolfgang.parak@physik.uni-marburg.de)

**Current Opinion in Pharmacology** 2014, **18**:98–103

This review comes from a themed issue on **New technologies**

Edited by **Gleb B Sukhorukov**

For a complete overview see the Issue and the Editorial

Available online 30th September 2014

http://dx.doi.org/10.1016/j.coph.2014.09.011



## Introduction

Ions play an important role in cells, such as $Na^+$, $K^+$, $Cl^-$, and $Ca^{2+}$ for electric signaling. Irregularities in ion distributions can be associated with medical diseases, such as reduction of $Cl^-$-channels in the case of cystic fibrosis [1,2]. Observation of ion concentrations in cells thus can be relevant in medical diagnosis. Besides *in vivo* diagnosis also cellular *in vitro* models are of interest. Here response in ion concentrations upon pharmacological treatment may help to screen different pharmaceutical agents concerning their biological activity [3••]. For such *in vitro* models particle-based ion sensors with fluorescence-read-out are a helpful tool.

## Potential of particles-based ion-sensitive fluorescence sensors

Particle-based fluorescence sensing of specific ions is an interesting methodology as it offers important technical features [4–7,8•,9,10]: firstly, fluorescence-based detection is a very convenient method in the field of sensing in life science applications because of its high sensitivity, simplicity, and diversity of fluorescent materials available. In contrast to electronic detection fluorescence can also be recorded conveniently from the interior of cells, making this technique suitable in particular for *in vitro* sensing. Secondly, besides acting as mere carrier for ion-sensitive organic fluorophores, there is an increasing number of intrinsically fluorescent particles, such as quantum dots, carbon dots, lanthanide nanoparticles, or metal nanoclusters. These particles can exhibit different fluorescence properties than classical organic fluorophores (i.e. (depending on the particle material) continuous absorption spectra, longer fluorescence lifetimes, reduced photobleaching, etc.), and are thus complementary to organic fluorescence dyes [11]. The size of the particles hereby can reach from the nanometer to the micrometer range. Thirdly, particle-based sensors always involve the particle as carrier, which allows for addition of other compounds, such as other fluorophores (e.g. for fluorescence resonance energy transfer, FRET) [12], ligands for colloidal stability or for targeting, or therapeutic compounds [13,14], and thus permits an exceptional tailoring in the design of these systems. In case magnetic nanoparticles are used as carriers the same system could act magnetically guided as drug delivery carrier, which simultaneously monitors the delivered drug [15]. Also polyelectrolyte capsules are a very universal system toward the integration of many different functional units into one particle [16], in addition to the actual ion-sensitive fluorophores [17]. Fourthly, working with a particle-based system offers the possibility of having a universal interaction with cells, as the interaction of particles with the cell environment is predominantly governed by the physico-chemical properties of the particle surface, and thus can be made similar for particles responsive to different ions [18]. Cellular uptake and intracellular distribution is thus predominantly determined by the particle carrier. Different ion-sensitive fluorophores on the other hand typically have very different chemical structure and thus may interact in a different way (i.e. being cell-permeable, incorporated by endocytotic pathways, no cellular entry). Finally, it is important to point out that particle-based sensors detect

ion concentrations at their surface, which can be quite different from bulk concentrations [19]. This however can be turned into an advantage as presence of the particle surface helps tuning the working-point by adjusting the surface chemistry [20]. While these points illustrate the huge potential of such sensors, unfortunately there are also problems associated with particle-based fluorescence sensing, which will be highlighted in the following sections, together with some potential solutions to address them.

## Crosstalk with pH

The crosstalk of ion-sensitive fluorophores with pH is a major problem, that is fluorescence readout does not only response to changes in concentrations of the ion species which are to be quantified, but also to changes in pH. This is very critical and difficult to solve in the case of intracellular sensing applications, in case particle sensors are administered via cellular internalization. Spontaneous internalization of particles predominantly is via endocytotic pathways, and thus involves massive changes in pH, in which the particles are translocated from neutral to slightly alkaline extracellular medium to highly acidic intracellular vesicles [3••,21]. Thus, in case of a particulate ion-sensitive fluorophore, which does not only respond to its target ion, but also to pH, it is not straightforward to interpret changes in fluorescence readout, as they may reflect changes in target ion concentration or in pH. An illustration of this problem is shown in Figure 1, where quantum dots (QDs) bar-coded polyelectrolyte

**Figure 1**

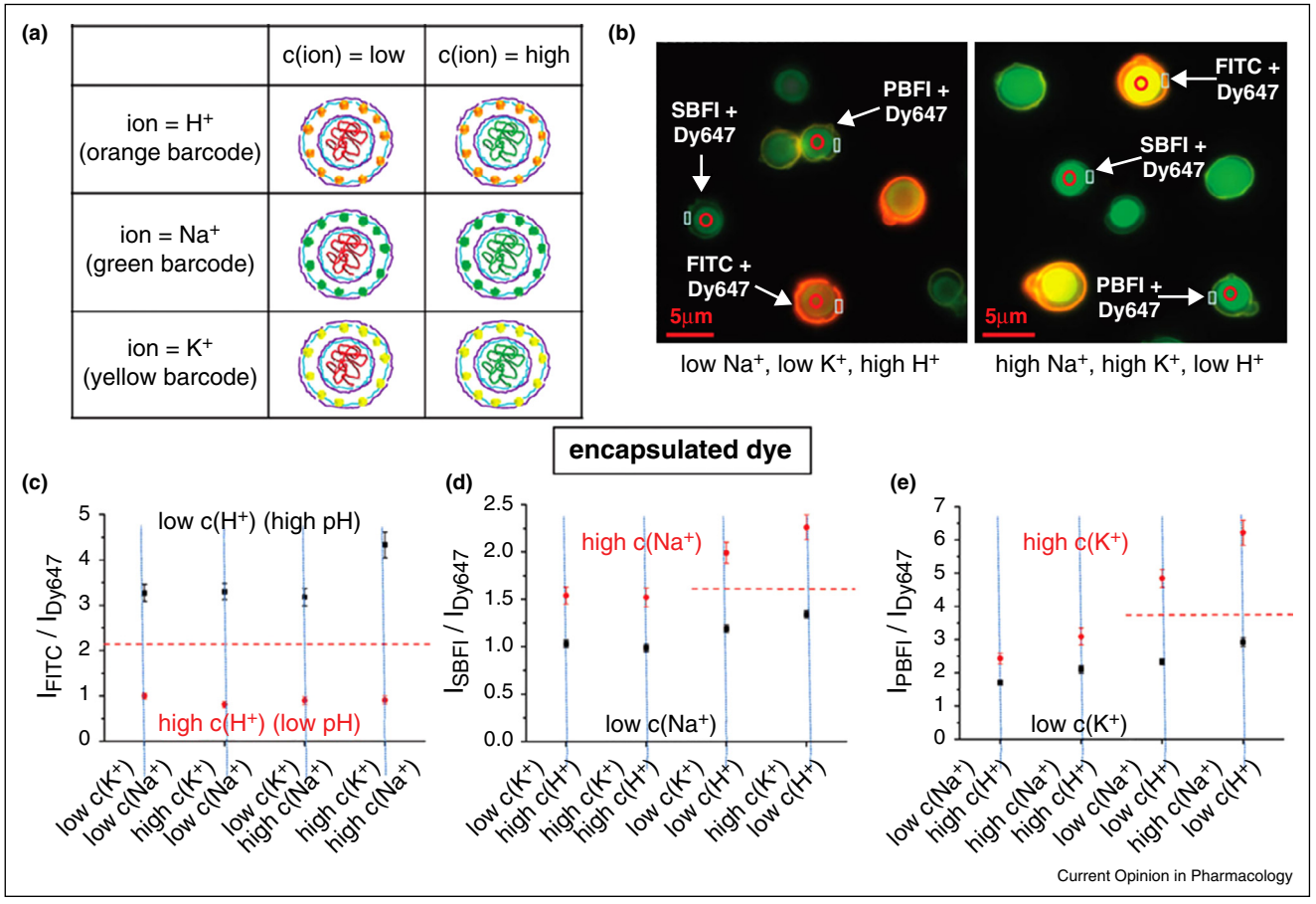


QDs barcoded polyelectrolyte capsules with ion-sensitive fluorophores embedded in their cavity were used for multiplexed measurements of several ions simultaneously. **(a)** Different sensor fluorophores such as FITC (fluorescein 5(6)-isothiocyanate; sensitive toward pH), SBFI (sodium-binding benzofuran isophthalate in the form of tetra-ammonium salt; sensitive toward $Na^+$), and PBFI (potassium binding bezofuran isophthalate in the form of tetra-ammonium salt; sensitive toward $K^+$) and a reference fluorophore Dy647 (Dy647 as N-hydroxysuccinimidyl-ester; Dy647 is not sensitive to the cellular environment) conjugated with dextran were loaded inside the cavities of these porous capsules. To distinguish the different capsule species barcodes made by mixtures of QDs with different color were embedded inside the outer shell of these capsules. **(b)** Fluorescence microscopic images of a mixture of all the capsules at low and high concentrations of sodium, potassium and protons are shown from left to right. Changes in fluorescence could be observed upon changes in ion concentrations. **(c–e)** The pH sensitive capsules were able to sense low and high pH even in the presence of other ions. On the other hand, the $Na^+$ and $K^+$ sensors were not able to sense their respective ions at all pH values. Due to crosstalk with pH it was not possible to determine $Na^+$ and $K^+$ concentrations at low pH, and in this way these capsules would not have been able to distinguish $Na^+$ and $K^+$ in highly acidic lysosomes.Adapted from Ref [8•].

capsules with different ion-sensitive fluorophores embedded in their cavity were used for multiplexed measurements of several ions [8•]. While this system has been demonstrated being able to detect $Na^+$ and $K^+$ ions simultaneously, this was only possible at controlled pH. In this way this sensor system could not be used for reporting local $Na^+$ and $K^+$ concentrations upon the internalization pathway of the particles, upon which severe changes in pH are involved. This problem could be resolved by integrating a pH sensor, which then would be based on a calibration curve to deconvolute pH effects.

## Uncertainty in fluorescence intensity-based detection

According to the signal-output mode, particle-based fluorescent probes can work in different sensing mechanisms, in which upon presence of the target ions intensity, wavelength, lifetime, and polarization of fluorescence is changed. To date, most of the proposed particle-based fluorescent sensors are based on fluorescence-intensity changes. Unfortunately they suffer from uncertainties in the calibration of the responses, particularly when these systems are applied as intracellular probes (i.e. fluctuations in intracellular particle densities), which can produce misleading readouts. One solution to partially overcome this problem is by means of ratiometric approaches [6,22–25], which only require relative determination of fluorescence intensities to a reference, instead of absolute intensity measurements. As mentioned, particles allow for easy incorporation of reference fluorophores [20]. Alternatively fluorescence wavelength-shift and lifetime detection are recently used approaches to overcome this limitation. However, there are relatively few ion-sensitive fluorophores involving wavelength-shift modes available. One demonstrated example involves an alteration in the band-gap energy of QDs upon the presence of target ions, causing shift of the emission wavelength [26]. Fluorescence lifetime-based sensing approaches are more universal. The combination of time-resolved fluorescence with QDs is of particular interest due to the longer fluorescence lifetime of QDs (typically five to hundreds of nanoseconds) as compared to that of most organic fluorophores and cell autofluorescence. The potential of these systems for quantifying ions, such as $Cl^-$ or $H^+$ in bulk solutions mimicking the intracellular environment has recently been demonstrated [27,28,29••]. A novel step in this direction is the use of fluorescence lifetime imaging microscopy (FLIM) for sensing purposes, which is based on using the fluorescence lifetime of QD probes collected from FLIM images as analytical signal for determining the concentration of the target ions. The example illustrated in Figure 2 clearly shows the great potential of FLIM for intracellular imaging and sensing [29••].

## Spectral overlap in multiplexing formats

Nowadays there is an increasing demand for multiparameter chemical and biological sensing. However, unfortunately the emission spectra of many ion-sensitive fluorophores show overlap, and thus the number of fluorophores that can be spectrally resolved and independently detected in parallel is limited [30,31]. To solve this major problem of spectral crosstalk the use of particle-based fluorescence systems plays an important role. There are several ways of discrimination between different fluorescence signals: spectral resolution (i.e. fluorescence signals of different wavelength), spatial resolution (i.e. fluorescence originating from different locations), and temporal resolution (i.e. fluorescence with different lifetimes) [30]. In this direction, two very promising strategies of realizing multiplexing without spectral overlap problems are the use of temporal resolution (distinguishing the emission of different fluorophores with time-dependent fluorescence spectroscopy), the interaction of different fluorophores in FRET, or the combination of both strategies. While organic fluorophores have similar lifetimes of a few ns, QDs have much longer fluorescence lifetimes, reaching even ms by doping. By using QDs as donor and several (ion-sensitive) fluorophores as acceptors, successful FRET systems based on lifetime measurements have been developed [32–34,35•]. The combination of QDs (as donors and/or acceptors) with organic dyes (as acceptors) and lanthanide complexes (as donors) allows for the use of different FRET pathways and spectral candidates for the design of time-resolved fluorescence multiplexing formats due to their long photoluminescence lifetimes (ms) [36,37•]. This advantage has been used for time-resolved immunoassays based on FRET from luminescent terbium complexes (LTC) to different quantum dots or five different organic fluorophores [38,39], allowing the simultaneous determination of several tumor markers from a single sample. These examples show how the problem of spectral overlap, which has blocked the advance in multiplexing platforms during years, can be solved via FRET and fluorescence lifetime based spectrotemporal approaches.

## Intracellular delivery

Delivery of particle sensors to specific intracellular locations is not trivial, and in fact one of the biggest challenges nowadays. Endocytosis is the classical natural entry of particles into cells [21], consequently leading to a localization of the particles inside acidic intracellular vesicles (endosomes and lysosomes) [40]. Delivery routes to different cellular regions such as the cytosol, mitochondria, and the nucleus can be divided in two main groups, physical and biochemical strategies. Physical strategies include microinjection, electroporation, and photothermal heating [41], which allow (optionally in the context with receptor-specific ligands on their surface) for the delivery of the particles to intracellular targets. In contrast, biochemical strategies involve specific surface ligands of the particles. In this way particles are released from the intracellular vesicles after

**Figure 2**

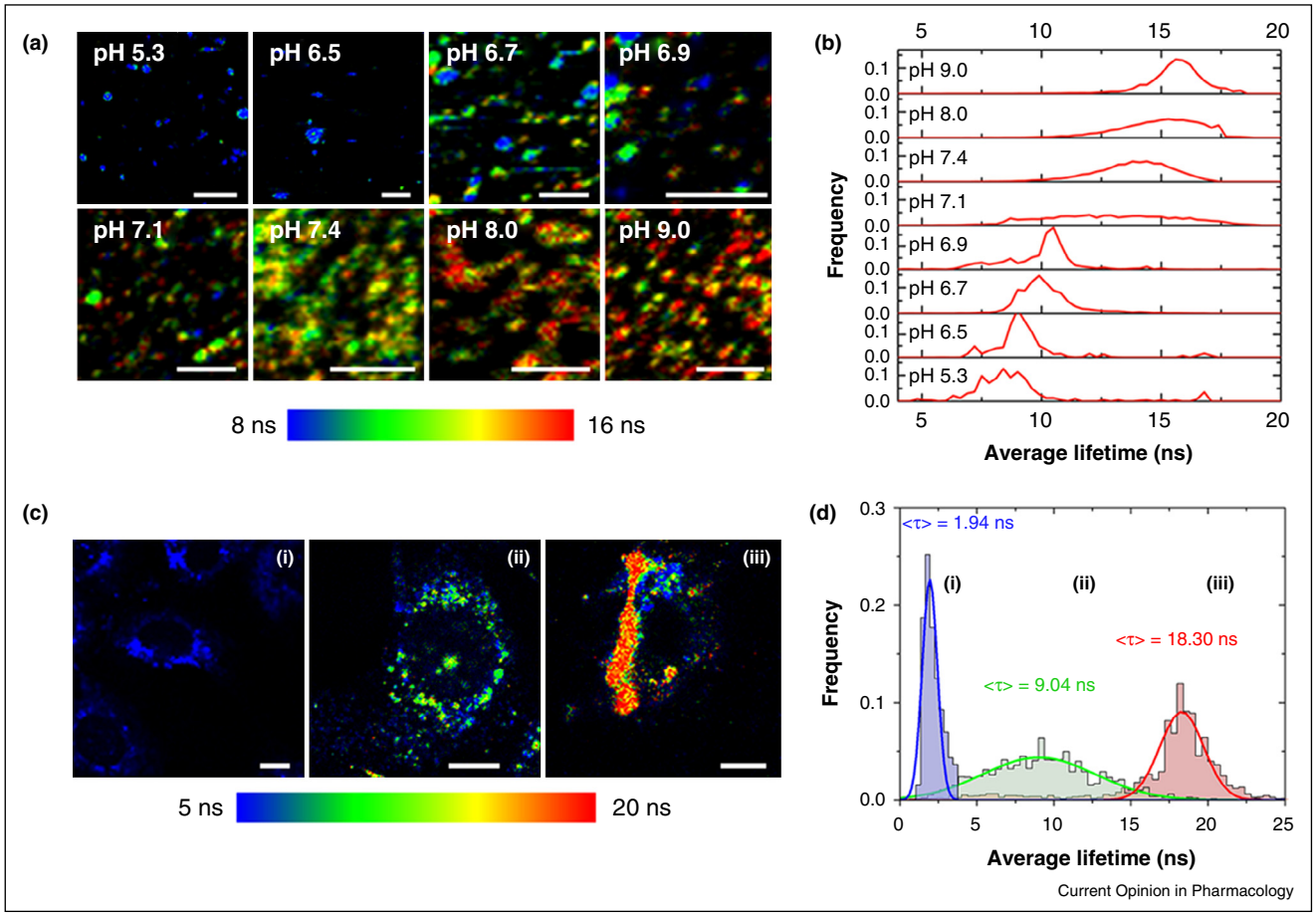


Example for the use of FLIM in combination with pH-sensitive CdSe/ZnS QDs for sensing of intracellular pH. **(a)** FLIM images of QDs suspended in solutions mimicking the intracellular environment at different pH values. The scale bars (white lines) represent 10 μm. **(b)** Fluorescence lifetime histograms collected from the images in (a). **(c)** FLIM images of MC3T3-E1 cells before (i) and after incubation with QDs (ii and iii). Image (i) shows the autofluorescence of the cells. MC3T3-E1 cells were incubated with nigericin and buffers mimicking the extracellular medium at pH 4.87 (ii) and 8.14 (iii). The scale bars (white lines) represent 10 μm. **(d)** Fluorescence lifetime histograms collected from the images in (c).
Adapted from Ref [29••].

endocytosis to the cytolsol ('endosomal escape') [42,43]. Several functionalizations of the particle surface with specific ligands are used in this direction, such as cell penetrating peptides (CCPs) [44], transferrin [45], nuclear-localization sequence (NLS) peptides [46], endoplasmic reticulum (ER) signal peptides [47], triphenylphosphonium derivates (TPP) [48], and polyethyleneimine (PEI) [49]. It even has been suggested that under certain conditions very small particles can directly traverse the cell membrane (i.e. by transient poration) [50] and thus bypass the endocytotic uptake. However, the details of such mechanisms are still under scientific discussion and controversial results can be found in the literature. In spite of all the studies carried out in this topic, there are not yet reliable general methods for delivering particles into the cytosol, and even less for sub-cellular organelles [51]. Thus, successful delivery strategies still must be determined for each particle-based system on a case-by-case basis.

## Calibration

The performance of most of the reported sensing systems for intracellular applications are based on the interpolation of the intracellular readouts using corresponding extracellular calibration plots [27,28]. It is well-known that the intracellular environment can alter the behavior of the response of the sensor, as consequence for example of the fact of 'protein corona' formation [52]. Even working with solutions mimicking the intracellular environment, one never can be sure that the scenario is exactly the same as inside the cells. Therefore a proper way to face this problem may be by carrying out a calibration inside cells, in order to introduce all the factors of uncertainty in the calibration model. In addition one has to take

into account that particles can be also partially disintegrated inside cells (e.g. by proteolytic enzymes), which obviously may impact fluorescence readout [53].

## Outlook

Particle-based ion-sensitive fluorescence sensing is an interesting methodology, in particular for the development of *in vitro* assays. Due to the particular nature these sensors (in case they are big enough) can be easily localized and could be introduced as artificial 'cellular organelles', allowing for spatially resolved online monitoring of intracellular ion concentrations. In particular the possibility of measuring the changes in intracellular ion concentration upon exposure of cells to specific pharmaceutical agents would offer a convenient way to measure dose-response curve and pharmacokinetics on the level of individual cells [54]. Thus, these platforms could provide significant advances in drug screening, also in the direction of 'personalized medicine', in which cellular response to treatment can be detected.

## Conflict of interest statement

The authors do not have any conflicting interests.

## Acknowledgements

This project was funded by LOEWE (project SynChemBio to WJP). SA, CCC, and BP are grateful to the Alexander von Humboldt Foundation for a postdoctoral fellowship. QZ and MGS are grateful to the Chinese Scholarship Council (CSC) and the Yousef Jameel Scholarship Fund, respectively, for a fellowship working toward their PhD thesis.

## References and recommended reading

Papers of particular interest, published within the period of review, have been highlighted as:

- • of special interest
- •• of outstanding interest

1. Linsdell P: **Cystic fibrosis transmembrane conductance regulator chloride channel blockers: pharmacological, biophysical and physiological relevance**. *World J Biol Chem* 2014, **5**:26-39.

2. Matsui H, Grubb BR, Tarran R, Randell SH, Gatzy JT, Davis CW, Boucher RC: **Evidence for periciliary liquid layer depletion, not abnormal ion composition, in the pathogenesis of cystic fibrosis airways disease**. *Cell* 1998, **95**:1005-1015.

3. •• Rivera Gil P, Nazarenus M, Ashraf S, Parak WJ: **pH sensitive capsules as intracellular optical reporters for monitoring lysosomal pH changes upon stimulation**. *Small* 2012, **8**: 943-948.

An example on how response to pharmaceutical treatment can be monitored *in vitro* based on fluorescent ion-sensitive particles.

4. Lee YEK, Smith R, Kopelman R: **Nanoparticle PEBBLE sensors in live cells and in vivo**. *Annu Rev Anal Chem* 2009, **2**:57-76.

5. Kreft O, Muñoz Javier A, Sukhorukov GB, Parak WJ: **Polymer microcapsules as mobile local pH-sensors**. *J Mater Chem* 2007, **17**:4471-4476.

6. Si D, Epstein T, Lee Y-EK, Kopelman R: **Nanoparticle PEBBLE sensors for quantitative nanomolar imaging of intracellular free calcium ions**. *Anal Chem* 2012, **84**:978-986.

7. Carregal-Romero S, Montenegro J-M, Parak WJ, Rivera Gil P: **Subcellular carrier-based optical ion-selective nanosensors**. *Front Pharmacol* 2012, **3**:70-76.

8. • del Mercato LL, Abbasi AZ, Ochs M, Parak WJ: **Multiplexed sensing of ions with barcoded polyelectrolyte capsules**. *ACS Nano* 2011, **5**:9668-9674.

An example for multiplexed measurements using spatial instead of spectral discrimination of different fluorescent particles.

9. Rana S, Singla AK, Bajaj A, Elci SG, Miranda OR, Mout R, Yan B, Jirik FR, Rotello VM: **Array-based sensing of metastatic cells and tissues using nanoparticle-fluorescent protein conjugates**. *ACS Nano* 2012, **6**:8233-8240.

10. Dennis AM, Rhee WJ, Sotto D, Dublin SN, Bao G: **Quantum dot-fluorescent protein FRET probes for sensing intracellular pH**. *ACS Nano* 2012, **6**:2917-2924.

11. Hötzer B, Medintz IL, Hildebrandt N: **Fluorescence in nanobiotechnology: sophisticated fluorophores for novel applications**. *Small* 2012, **8**:2297-2326.

12. Jin Z, Hildebrandt N: **Semiconductor quantum dots for *in vitro* diagnostics and cellular imaging**. *Trends Biotechnol* 2012, **30**:394-403.

13. del Mercato LL, Ferraro MM, Baldassarre F, Mancarella S, Greco V, Rinaldi R, Leporatti S: **Biological applications of LbL multilayer capsules: from drug delivery to sensing**. *Adv Colloid Interface Sci* 2014, **207**:139-154.

14. Xiong R, Soenen SJ, Braeckmans K, Skirtach AG: **Towards theranostic multicompartment microcapsules: in-situ diagnostics and laser-induced treatment**. *Theranostics* 2013, **3**:141-151.

15. Mitra RN, Doshi M, Zhang X, Tyus JC, Bengtsson N, Fletcher S, Page BD, Turkson J, Gesquiere AJ, Gunning PT *et al.*: **An activatable multimodal/multifunctional nanoprobe for direct imaging of intracellular drug delivery**. *Biomaterials* 2012, **33**:1500-1508.

16. Sukhorukov GB, Rogach AL, Garstka M, Springer S, Parak WJ, Muñoz-Javier A, Oliver Kreft, Skirtach AG, Susha AS, Ramaye Y *et al.*: **Multifunctionalized polymer microcapsules: novel tools for biological and pharmacological applications**. *Small* 2007, **3**:944-955.

17. Reibetanz U, Halozan D, Brumen M, Donath E: **Flow cytometry of HEK 293T cells interacting with polyelectrolyte multilayer capsules containing fluorescein-labeled poly(acrylic acid) as a pH sensor**. *Biomacromolecules* 2007, **8**:1928-1933.

18. Sapsford KE, Algar WR, Berti L, Gemmill KB, Casey BJ, Oh E, Stewart MH, Medintz IL: **Functionalizing nanoparticles with biological molecules: developing chemistries that facilitate nanotechnology**. *Chem Rev* 2013, **113**:1904-2074.

19. Zhang F, Ali Z, Amin F, Feltz A, Oheim M, Parak WJ: **Ion and pH sensing with colloidal nanoparticles: influence of surface charge on sensing and colloidal properties**. *ChemPhysChem* 2010, **11**:730-735.

20. Zhang F, Lees E, Amin F, Rivera Gil P, Yang F, Mulvaney P, Parak WJ: **Polymer-coated nanoparticles: a universal tool for biolabelling experiments**. *Small* 2011, **7**:3113-3127.

21. Kastl L, Sasse D, Wulf V, Hartmann R, Mircheski J, Ranke C, Carregal-Romero S, Martínez-López JA, Fernández-Chacón R, Parak WJ *et al.*: **Multiple internalization pathways of polyelectrolyte multilayer capsules into mammalian cells**. *ACS Nano* 2013, **7**:6605-6618.

22. del Mercato LL, Abbasi AZ, Parak WJ: **Synthesis and characterization of ratiometric ion-sensitive polyelectrolyte capsules**. *Small* 2011, **7**:351-363.

23. Chen T, Hu Y, Cen Y, Chu X, Lu Y: **A dual-emission fluorescent nanocomplex of gold-cluster-decorated silica particles for live cell imaging of highly reactive oxygen species**. *J Am Chem Soc* 2013, **135**:11595-11602.

24. Zong C, Ai K, Zhang G, Li H, Lu L: **Dual-emission fluorescent silica nanoparticle-based probe for ultrasensitive detection of $Cu^{2+}$**. *Anal Chem* 2011, **83**:3126-3132.

25. Ju E, Liu Z, Du Y, Tao Y, Ren J, Qu X: **Heterogeneous assembled nanocomplexes for ratiometric detection of highly reactive**

**oxygen species *in vitro* and *in vivo***. *ACS Nano* 2014, **8**: 6014-6023.

26. Gui M, Bao L, Xia Y, Wei C, Zhang S, Zhu C: **Indication of intracellular physiological pH changes by L-cysteine-coated CdTe quantum dots with an acute alteration in emission color**. *Biosens Bioelectron* 2011, **30**:324-327.

27. Ruedas-Rama MJ, Orte A, Hall EAH, Alvarez-Pez JM, Talavera EM: **A chloride ion nanosensor for time-resolved fluorimetry and fluorescence lifetime imaging**. *Analyst* 2012, **137**:1500-1508.

28. Ruedas-Rama MJ, Orte A, Hall EAH, Alvarez-Pez JM, Talavera EM: **Quantum dot photoluminescence lifetime-based pH nanosensor**. *Chem Commun* 2011, **47**:2898-2900.

29. •• Orte A, Alvarez-Pez JM, Ruedas-Rama MJ: **Fluorescence lifetime imaging microscopy for the detection of intracellular pH with quantum dot nanosensors**. *ACS Nano* 2013, **7**:6387-6395.

An excellent example in which detection of fluorophores by their lifetimes is demonstrated *in vivo*.

30. Abbasi AZ, Amin F, Niebling T, Friede S, Ochs M, Carregal-Romero S, Martos JMM, Rivera Gil P, Heimbrodt W, Parak WJ: **How colloidal nanoparticles could facilitate multiplexed measurements of different analytes with analyte-sensitive organic fluorophores**. *ACS Nano* 2011, **5**:21-25.

31. Wan X, Yao S, Liu H, Yao Y: **Selective fluorescence sensing of $Hg^{2+}$ and $Zn^{2+}$ ions through dual independent channels based on the site-specific functionalization of mesoporous silica nanoparticles**. *J Mater Chem A* 2013, **1**:10505-10512.

32. Kaiser U, Aberasturi DJd, Malinowski R, Amin F, Parak WJ, Heimbrodt W: **Multiplexed measurements by time resolved spectroscopy using colloidal CdSe/ZnS quantum dots**. *Appl Phys Lett* 2014, **104**:041901-041904.

33. Algar WR, Ancona MG, Malanoski AP, Susumu K, Medintz IL: **Assembly of a concentric Förster resonance energy transfer relay on a quantum dot scaffold: characterization and application to multiplexed protease sensing**. *ACS Nano* 2012, **6**:11044-11058.

34. Algar WR, Wegner D, Huston AL, Blanco-Canosa JB, Stewart MH, Armstrong A, Dawson PE, Hildebrandt N, Medintz IL: **Quantum dots as simultaneous acceptors and donors in time-gated forster resonance energy transfer relays: characterization and biosensing**. *J Am Chem Soc* 2012, **134**:1876-1891.

35. • Algar WR, Kim H, Medintz IL, Hildebrandt N: **Emerging non-traditional Förster resonance energy transfer configurations with semiconductor quantum dots: investigations and applications**. *Coord Chem Rev* 2014, **263**:65-85.

An example for spectro-temporal multiplexing based on simultaneous FRET from LTC-to-QD (QD acceptor) and QD-to-dye (QD donor).

36. Hildebrandt N, Wegner KD, Algar WR: **Luminescent terbium complexes: superior Förster resonance energy transfer donors for flexible and sensitive multiplexed biosensing**. *Coord Chem Rev* 2014, **273**:125-138.

37. • Geißler D, Charbonnière LJ, Ziessel RF, Butlin NG, Löhmannsröben H-G, Hildebrandt N: **Quantum dot biosensors for ultrasensitive multiplexed diagnostics**. *Angew Chem Int Ed* 2010, **49**:1396-1401.

An example for FRET-based multiplexing, in which five different QDs are used as acceptor with one LTC donor.

38. Wegner KD, Jin Z, Lindén S, Jennings TL, Hildebrandt N: **Quantum-dot-based Förster resonance energy transfer immunoassay for sensitive clinical diagnostics of low-volume serum samples**. *ACS Nano* 2013, **7**:7411-7419.

39. Geißler D, Stufler S, Löhmannsröben H-G, Hildebrandt N: **Six-color time-resolved Förster resonance energy transfer for ultrasensitive multiplexed biosensing**. *J Am Chem Soc* 2012, **135**:1102-1109.

40. Wang X, Boschetti C, Ruedas-Rama MJ, Tunnacliffe A, Hall EAH: **Ratiometric pH-dot ANSors**. *Analyst* 2010, **135**:1585-1591.

41. Carregal-Romero S, Ochs M, Rivera Gil P, Ganas C, Pavlov AM, Sukhorukov GB, Parak WJ: **NIR-light triggered delivery of macromolecules into the cytosol**. *J Control Release* 2012, **159**:120-127.

42. Verma A, Uzun O, Hu YH, Hu Y, Han HS, Watson N, Chen SL, Irvine DJ, Stellacci F: **Surface-structure-regulated cell-membrane penetration by monolayer-protected nanoparticles**. *Nat Mater* 2008, **7**:588-595.

43. Guo S, Huang L: **Nanoparticles escaping RES and endosome: challenges for siRNA delivery for cancer therapy**. *J Nanomater* 2011, **2011**:11-22.

44. Liu BR, Huang Y-W, Chiang H-J, Lee H-J: **Cell-penetrating peptide-functionized quantum dots for intracellular delivery**. *J Nanosci Nanotechnol* 2010, **10**:7897-7905.

45. Wang J, Tian S, Petros RA, Napier ME, DeSimone JM: **The complex role of multivalency in nanoparticles targeting the transferrin receptor for cancer therapies**. *J Am Chem Soc* 2010, **132**:11306-11313.

46. Chen FQ, Gerion D: **Fluorescent CdSe/ZnS nanocrystal-peptide conjugates for long-term, nontoxic imaging and nuclear targeting in living cells**. *Nano Lett* 2004, **4**:1827-1832.

47. Mukai Y, Yoshinaga T, Yoshikawa M, Matsuo K, Yoshikawa T, Matsuo K, Niki K, Yoshioka Y, Okada N, Nakagawa S: **Induction of endoplasmic reticulum-endosome fusion for antigen cross-presentation induced by poly (γ-glutamic acid) nanoparticles**. *J Immunol* 2011, **187**:6249-6255.

48. Biswas S, Dodwadkar NS, Piroyan A, Torchilin VP: **Surface conjugation of triphenylphosphonium to target poly (amidoamine) dendrimers to mitochondria**. *Biomaterials* 2012, **33**:4773-4782.

49. Shim MS, Kwon YJ: **Controlled cytoplasmic and nuclear localization of plasmid DNA and siRNA by differentially tailored polyethylenimine**. *J Control Release* 2009, **133**:206-213.

50. Patil ML, Zhang M, Taratula O, Garbuzenko OB, He H, Minko T: **Internally cationic polyamidoamine PAMAM-OH dendrimers for siRNA delivery: effect of the degree of quaternization and cancer targeting**. *Biomacromolecules* 2009, **10**:258-266.

51. Huang JG, Leshuk T, Gu FX: **Emerging nanomaterials for targeting subcellular organelles**. *Nano Today* 2011, **6**:478-492.

52. del Pino P, Pelaz B, Zhang Q, Maffre P, Nienhaus GU, Parak WJ: **Protein corona formation around nanoparticles — from the past to the future**. *Mater Horiz* 2014, **1**:301-313.

53. Chanana M, Rivera Gil P, Correa-Duarte MA, Parak WJ, Liz-Marzán LM: **Physicochemical properties of protein-coated gold nanoparticles in biological fluids and cells before and after proteolytic digestion**. *Angew Chem Int Ed* 2013, **52**:4179-4183.

54. Zhang Y, Chan HF, Leong KW: **Advanced materials and processing for drug delivery: the past and the future**. *Adv Drug Deliv Rev* 2013, **65**:104-120.